The Institute of Paper Chemistry

Appleton, Wisconsin

Doctor's Dissertation

An Investigation of the Mechanisms of Heat Transfer to Multicomponent Solutions Under Convective Boiling Conditions

Hugh P. Lavery

June, 1981

AN INVESTIGATION OF THE MECHANISMS OF HEAT TRANSFER TO MULTICOMPONENT SOLUTIONS UNDER CONVECTIVE BOILING CONDITIONS

A thesis submitted by

Hugh P. Lavery

B.S.Ch.E., June, 1973, Massachusetts Institute of Technology

M.S., June, 1976, Lawrence University

in partial fulfillment of the requirements
of The Institute of Paper Chemistry
for the degree of Doctor of Philosophy
from Lawrence University,
Appleton, Wisconsin

June, 1981

TABLE OF CONTENTS

ABSTRACT

Although the overall heat transfer performance of long-tube vertical evaporators has been extensively studied in the past, little is known about the mechanisms of heat transfer from the tube walls to the liquor inside the tubes. The purpose of this study was to evaluate several possible heat transfer mechanisms. Black liquor flow in these evaporators is known to be unstable and pulsating, with irregularly repeated backflows. The transport of heat might, therefore, be dominated by purely convective mechanisms controlled by either the net upflow or by the backflow of liquor, by the nucleate boiling mechanism, by some combination of these mechanisms, or by mass transfer controlled heat transfer superimposed on a combination of these mechanisms.

An experimental program was carried out using an electrically heated pilot evaporator with dimensions and operating conditions consistent with kraft recovery practice. Heat transfer coefficients were measured for evaporating black liquor model solutions and black liquor.

A computer program was written which uses numerical methods to simulate the deposition, flow, and heat transfer behavior of downward flowing films in an evaporator tube. Models for the other alternative mechanisms were available in the literature. Special attention was given to the Chen (1) correlation model.

The results show that the purely convective mechanism based on backflow is the dominant heat transfer mechanism under typical black liquor evaporator conditions. The nucleate boiling contribution is minor, as is the net-upward-flow convective mechanism. No mass transfer control of heat transfer was observed. The predictions of the computer simulation of purely convective backflow heat transfer gave reasonable agreement with much of the data.

The agreement between the model and the data was poor whenever foaming occurred in the tubes. The heat transfer coefficients observed during foaming flow were much

higher than those for nonfoaming flow. This appears to be a convective effect arising from the higher mixture velocities caused by reduced slip between the phases in foaming flow. Foam stability is probably a controlling factor. No model for the foam flow regime is proposed, since foam stability under high shear conditions is not predictable from current knowledge.

INTRODUCTION

The kraft pulping process produces large quantities of dilute black liquor. This spent pulping liquor, initially at 10 to 20 percent solids, must be concentrated to at least 60 percent solids so that it may be burned for reclamation of its inorganic chemicals and heat content. The first part of this concentration is usually done in a series of five or six long-tube vertical (LTV) black liquor evaporators, which brings the concentration of the liquor to about 50 percent solids. A LTV evaporator is basically a vertical bundle of stainless steel tubes inside a steam shell. Liquor enters the bottom of the tubes and flows upward inside them. Steam condensing on the outside of the tubes heats the liquor. These evaporators represent a substantial capital expense and consume large amounts of energy.

Despite the importance of the long-tube vertical black liquor evaporator, very little is known about the mechanisms by which heat is moved from the tube walls into the liquor, ultimately resulting in evaporation. Knowing which mechanism controls heat transfer inside the evaporator tubes would help in the rational design and operation of black liquor evaporators.

An obstacle in studying black liquor evaporator heat transfer is that the evaporators generally operate under conditions which produce unstable and pulsating flows. Considerable backflow of liquor occurs in this type of flow. This "slug" or "churn" behavior is very complicated and does not permit an elegant analysis of its flow and heat transfer characteristics. Slug flow behavior has been avoided in vertical boiling heat transfer studies in the past in favor of "annular flow," which can be induced with vapor flow rates somewhat greater than those typical of black liquor evaporators. Annular flow is important in many industrial processes, including power boilers, and is more easily modeled than slug and churn flow.

The objective of the present study was to find out what the major mechanism of heat transfer is under the pulsating "slug" and "churn" conditions of long-tube vertical black liquor evaporation.

Work toward this goal included a survey of the literature on evaporation and boiling heat transfer mechanisms, summarized here in the Literature Survey, a computer simulation based on a simple model of slug and churn flow discussed in "A Numerical Model for Slug and Churn Flow," the design and construction of an electrically heated pilot evaporator described in Experimental, and the implementation of an experimental program on black liquor model solutions and black liquor, the results of which are presented in Results and Discussion. The Conclusions section explores some of the implications of the major result of this work, which is that black liquor evaporator heat transfer is dominated by convective heat transfer across falling films of liquor on the tube walls. However, when the liquor has a great tendency to foam, the foaming flow substantially increases the heat transfer coefficient above its slug and churn flow value.

LITERATURE SURVEY

INTRODUCTION

Thousands of papers have been published over the past fifty years on the subject of two-phase flow. The literature review in this chapter will be concerned with the relatively narrow topic of heat transfer in saturated boiling, two-phase, vertical, net-upward-flow systems. There are a number of textbooks available which contain discussions of this and other important two-phase flow topics. These references include the texts by Butterworth and Hewitt (2), Collier (3), Hewitt and Hall-Taylor (4), Hsu and Graham (5), Wallis (6), Soo (7), and Tong (8).

This chapter is in three parts. The first section presents some classic experiments which form the basis of what we know about the overall performance of long-tube vertical evaporators. In particular, the sequence of flow regimes found in an evaporator tube will be discussed. In the second section, boiling heat transfer experiments of a specifically mechanistic orientation will be reviewed, leading up to a presentation of the Chen (1) correlation, the most widely accepted two-phase flow heat transfer model. In the third section, material pertinent to heat transfer in the slug and churn flow regimes will be presented to provide background for the slug/churn flow computer simulation model presented in "A Numerical Model for Slug and Churn Flow."

NONMECHANISTIC EVAPORATOR STUDIES

INTRODUCTION

Long-tube vertical evaporators have been extensively studied in the past. An excellent summary of this work is given by Wills and Hedström (9,10). McKee (11) provides an informative literature survey about a close relative of the long-tube vertical evaporator, the thermosiphon reboiler. All this past work provides

invaluable information on the effect of various operational variables on overall heat transfer performance. Unfortunately, very little of this work is useful in understanding the mechanisms of heat transfer, that is, how heat moves from the tube walls to the liquor. The problem with many of these older studies from a mechanistic point of view is that they concentrated on overall heat transfer coefficients defined in several different ways rather than the local inside film heat transfer coefficient (h). Thus, they give us no information on how the nature of the heat transfer may be changing along the length of the tube. The various heat transfer coefficients used in the literature are defined in Fig. 1. Most of the older pilot evaporators were steam-heated and of the natural-circulation variety, features which complicate the problem of interpreting the data even when film heat transfer coefficients were measured. Steam-heated evaporators have rather poor heat flux control and always involve measurement of average heat fluxes by condensate flow rates over a finite (and usually large) length of tube; thus, it is not possible to measure truly local heat transfer coefficients. Natural circulation couples the flow rate with the heat flux and makes it difficult to control either. In summary, too much is happening at once in this sort of apparatus to allow us to extract information about heat transfer mechanisms with any degree of confidence.

The most important concept from these studies is probably that there is a sequence of flow regimes in the evaporator tubes which has a major effect on the heat transfer behavior of the evaporator. In this section, a definition of some flow regimes is presented, and then several evaporator studies are reviewed with special emphasis on the effects of the various flow regimes on heat transfer.

FLOW REGIMES

The distribution of the gas and liquid phases in an evaporator tube may take a number of different forms. Discussing almost any work on evaporators requires some

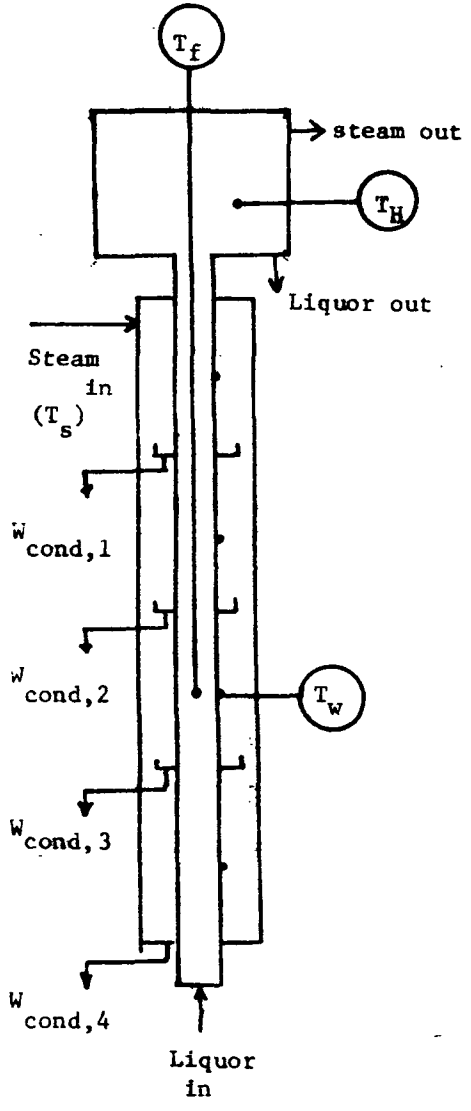

For typical steam heated designs (left):

$$Q = \sum_{i=1}^{n} W_{cond,i}\, h_{fg}$$

$$Q_{local} = W_{cond,i} h_{fg}$$

$$U = Q/(T_s - T_H)A$$

$$U_{local} = Q_{local}/(T_s - T_f)A_{local}$$

$$\bar{h} = Q/\left(\left(\frac{1}{n} \sum_{i=1}^{n} T_{w,i}\right) - \left(\frac{1}{n} \sum_{i=1}^{n} T_{f,i}\right) A \right)$$

For a tube with inside wall radius a and outside wall radius b,

$$\bar{h}_{local} = \frac{a}{b}\left(\frac{1}{U}_{loc.} - \left(\frac{b \ln(b/a)}{k_{ss}}\right) - \frac{1}{h}_{condensate}\right)$$

where $h_{condensate}$ is the condensate-side heat transfer coefficient.

For typical electrically heated design (right):

$$h = (Q/A)/(T_w - T_f)$$

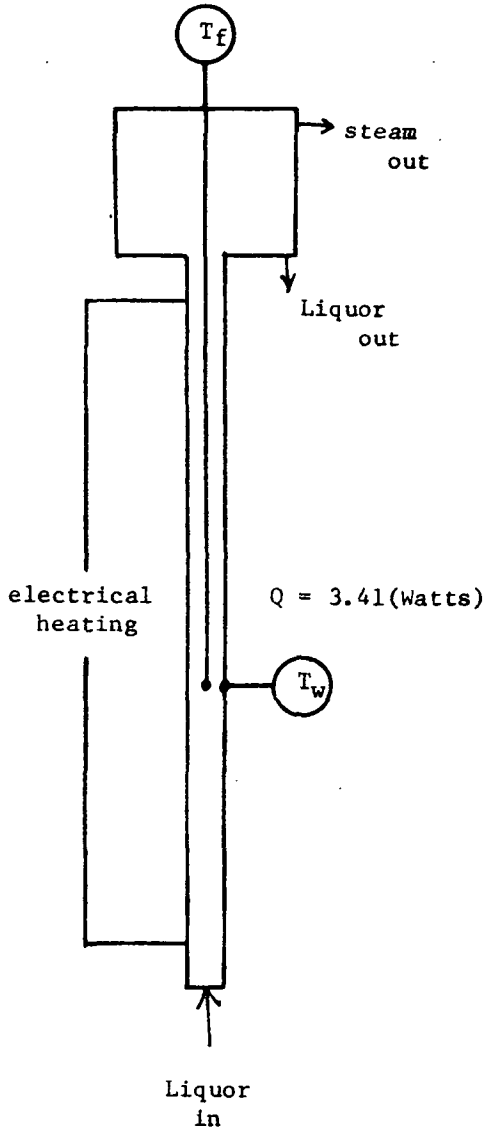

Figure 1. Definition of several types of evaporator heat transfer coefficients.

definition of these distributions, or flow regimes. A succession of flow regimes in evaporator tubes was recognized in the early evaporator study of Brooks and Badger (12), who identified the major regimes of bubble, slug, and annular flow. Since then, flow regime studies have identified a large number of regimes and subregimes which may be important under various conditions. The four-regime system of Taitel, Bornea, and Dukler (13) will be followed here. These four regimes are defined below and are illustrated in Fig. 2.

- Bubble flow: The gas phase is distributed throughout the liquid phase in the form of small bubbles. The bubbles themselves originate from nucleation sites on the tube walls.
- Slug flow: Most of the gas phase is in large, bullet-shaped bubbles surrounded by thin, falling liquid films. Liquid is transported upward in large lumps which bridge the tube between successive gas slugs.
- Churn flow: At a sufficiently high gas rate, the films surrounding the slug flow gas bubble will flood. This means that part of the liquid in the film will be entrained by the gas and carried upward. This process distorts the bubble shape and causes the entrainment of gas bubbles in the liquid lump. This regime is sometimes known as "froth flow" because of the appearance of the gas inclusions in the liquid lump.
- Annular flow: At very high gas velocities, the bulk of the liquid is drawn up the tube walls in a thin film by the action of interfacial shear. The remaining liquid is entrained as small droplets in the gas phase.

Gudmundson and coworkers (14) have shown that the largest part of the tubes in a black liquor evaporator should be operating in the first three regimes.

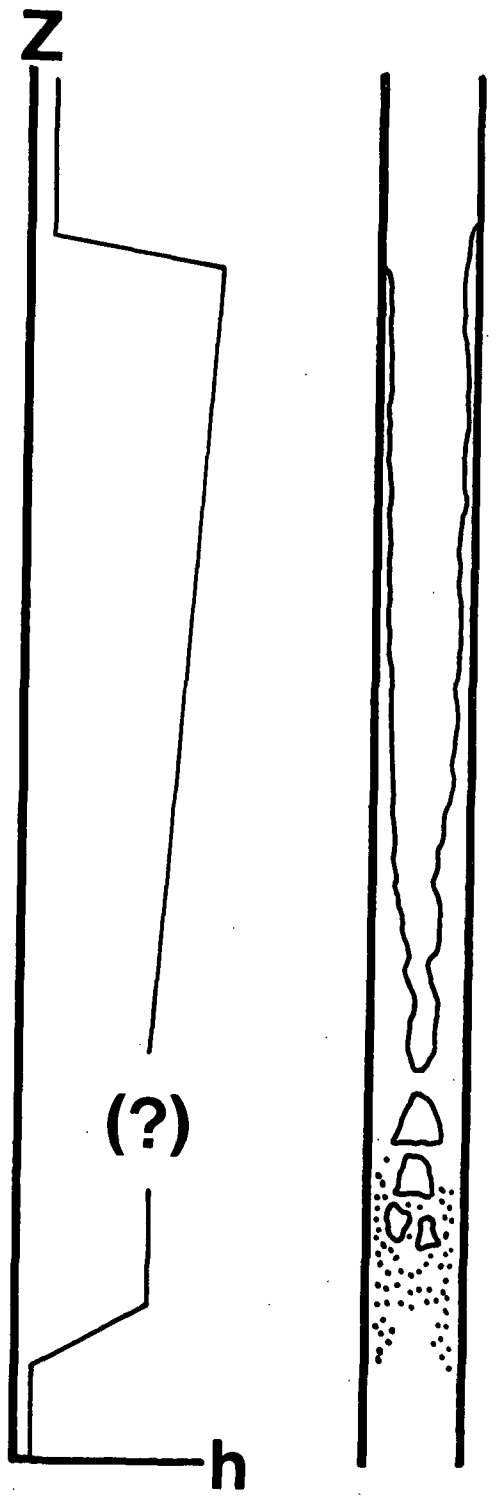

FLOW REGIME

Dry Wall

High vapor quality
Annular

Low vapor quality
Annular
Churn
Slug

Bubble

Subcooled

Figure 2. Flow regimes in vertical upflow boiling.

The transition between the bubble and slug regime is governed by the rate of coalescence of small bubbles to form large vapor slugs. The slug-to-churn transition is determined by the onset of flooding. Finally, the churn-annular transition occurs when gas velocities are great enough to support the film. The last two transitions will be discussed in greater detail in "Flooding and Churn Flow."

One further regime, called foam flow, may occur when the liquid has a tendency to foam. The foam flow regime will end when the gas velocity becomes great enough to break the foam, and the flow will probably assume the regime characteristic of that gas velocity.

NONMECHANISTIC EVAPORATOR STUDIES

General Effects of Flow Regimes on Heat Transfer

Some of the earliest work on evaporator heat transfer was done by Badger and coworkers (12,15-17) in a series of papers intended to give a complete picture of the performance of long-tube vertical evaporators. Their pilot evaporator was of close to industrial scale, a steam-heated 1.76-inch inner diameter copper tube twenty feet long. Flow rates were between 250 and 1000 lbs/hr of distilled water and sucrose solutions. Brooks and Badger (12) divided the tube into boiling and nonboiling sections using the readings from a traveling thermocouple and noted the much higher heat transfer coefficients of the boiling section. Badger (15) identified five flow regimes - nonboiling, bubble flow, slug flow, annular flow, and drywall - by visual observation of the flow conditions at the tube exit. He observed that as the apparent temperature drop (steam shell side to vapor head) decreased, the flow regimes regressed from drywall to annular flow to slug flow, and the overall boiling section heat transfer coefficient (U_B) increased. In the next paper in the series, Stroebe, Baker, and Badger (16) attached thermocouples to the tube walls at one-foot intervals. Only tube-average inside film heat transfer coefficients

($\overline{h_B}$) based on averaged wall temperatures could be calculated, since only the overall heat flux from the condensate flow rate was known. The feed was preheated to eliminate any subcooled length in these experiments. The tube-average inside film heat transfer coefficients ($\overline{h_B}$) for water and sucrose solutions could be correlated by

$$\overline{h_B} = (7.8 \times 10^6)\ U^{0.1}/Pr\ \sigma^2\ \Delta T_B^{0.13} \qquad (1)$$

The observed exit conditions ranged from slug flow to a slightly unstable annular flow. The inverse thermal driving force dependence suggests the same sort of flow regime effect observed by Badger with overall heat transfer coefficients is operating on $\overline{h_B}$ as well. Cessna, Lientz, and Badger (17) studied overall heat transfer coefficients (U_B) in a slightly smaller, 1.25-inch outer diameter copper tube 18.5 feet long, and again observed an increase in U_B with decreasing ΔT_B.

This increase in U_B or $\overline{h_B}$ with decreases in ΔT is not always observed in evaporator heat transfer. For example, Kirschbaum (18) used a 30-mm-diameter, steam-heated copper tube 1.5 meters long for boiling water and observed an increase in $\overline{h_B}$ with increasing ΔT, although the rate of increase was falling with increasing ΔT. Coulson and Mehta (19) noted the same effect in their 0.5-inch-diameter, 5.25-foot-long, steam-heated copper tube using water, sucrose solutions, surfactant solutions, and isopropanol. The reasons for these contradictory data are not clear from the experiments, but we might speculate that the greater superficial velocities in the smaller tubes result in a faster transition to annular flow, greatly reducing the importance of the slug flow regime contribution to the observed overall or tube-average inside film heat transfer coefficient. The overall data then reflect only the steady increase of the heat transfer coefficient with vapor velocity characteristic of annular flow which will be discussed in the next section. If there was a local maximum in heat transfer in the slug flow regime, it would pass unobserved under these circumstances. As Badger's equipment should have produced flow

conditions similar to those in industrial equipment of the same dimensions (black liquor evaporators), his observations deserve special emphasis.

Black Liquor Evaporator Studies

There have been several studies directed specifically at the performance of black liquor evaporators. The most comprehensive study was by Gudmundson and coworkers (14,20), who used both a large pilot evaporator and process data from on-line industrial equipment. The pilot evaporator contained four stainless steel tubes of 44 mm (1.81 inch) inner diameter, 10 meters (32.8 feet) long. Two tubes were equipped with condensate collection trays to permit measurement of sectional heat fluxes. Seven sections were available. The same tubes contained thermocouple wells in thirteen locations to measure the temperature of the liquid inside the tubes. Thus, Gudmundson's equipment could measure only overall sectional heat transfer coefficients (U_{Local}). Water and sugar solutions with and without the addition of a surfactant were tested in the pilot evaporator, and a large amount of process data on black liquor evaporation was available from three kraft pulp mills.

Gudmundson noted that the only flow regimes commonly observed in black liquor evaporators are bubble, slug, and "froth," the latter being another name for churn flow. Foaming flow does occur under some circumstances. Gudmundson's study of foaming flow is very interesting and will be reviewed together with several other foam flow papers in "Foam Flow in the Evaporator." True annular flow is found only occasionally in black liquor evaporators. Gudmundson did not pursue a mechanistic approach to the problem but instead developed multiple regression equations for the separate effects of heat flux, liquid boiling point, feed rate, liquid feed temperature, liquid viscosity, and liquid surface tension on the overall heat transfer coefficient (U). Most of the effects observed occur via changes in the nonboiling length in the tubes.

An interesting feature of Gudmundson's pilot evaporator data is that many of the water runs show a local maximum in the sectional local overall heat transfer coefficient (U_{Local}) about halfway along the length of the tube. Gudmundson offers no explanation for this phenomenon.

The Institute of Paper Chemistry has built a steam-heated pilot evaporator which has been used for several heat transfer studies. The apparatus is described in detail in Grace and Andrews (21). The pilot evaporator is a 1.87-inch-diameter tube of type 304 stainless steel. It has a 19-foot steam-heated length divided into five sections with separate condensate collection trays. Again, this type of apparatus measures sectional overall heat transfer coefficients (U_{Local}).

Black liquor heat transfer data reported by Grace and Andrews (21) and by Olsen (22) showed local maxima in the sectional overall heat transfer coefficients (U_{Local}). These maxima were most frequently located in the third section from the bottom of the evaporator. The drop-off in heat transfer between the third section and the last (fifth) section was often large. The fifth section overall heat transfer coefficient in some of Olsen's data is approximately half the value for the third section. Olsen also tried to separate the sectional condensing film coefficient from the sectional inside film coefficient using a condensation heat transfer correlation from McAdams (23). The sectional inside film heat transfer coefficient ($\overline{h}_{local}$) followed the same trends as U_{Local}. Using the concepts of the Chen (1) heat transfer model which will be presented in "The Chen Correlation," Olsen attributed this drop-off in $\overline{h}_{local}$ to the suppression of nucleate boiling by the high velocities and extreme turbulence toward the top of the evaporator tube. He did not test this hypothesis.

Pozzuto (24) used the same apparatus to test the effects of nitrogen gas injection on boiling heat transfer to water. Too many variables were changing at once in

this study to draw definite conclusions. However, the heat transfer data to water alone show no significant change in heat transfer after the third section in most of the experiments. This leveling-off of U_{local} is not as striking as the drop-offs reported above, but it is still not readily explained.

Foam Flow in the Evaporator

Foam flow produces substantial increases in heat transfer in evaporators. Stroebe, Baker, and Badger (16) reported tube average inside film heat transfer coefficients ($\overline{h_B}$) which were two to four times higher with surfactant solutions than with pure water. Their empirical correlation, Eq. (1), indicates that $\overline{h_B}$ is inversely proportional to the square of the surface tension. Both Kirschbaum (18) and Coulson and Mehta (19) reported similar effects. However, Coulson and Mehta's study included tests on isopropyl alcohol, which has a surface tension of 21.7 dynes/cm, much less than the 33 dynes/cm of their lowest surface tension surfactant solution. The isopropyl alcohol did not foam and had heat transfer coefficients much lower than the highly foaming surfactant solutions. Coulson and Mehta suggested, therefore, that the heat transfer increases with surfactant addition are the effect of increased foaming rather than decreased surface tension. They also suggested that the foam gradually broke down as it rose up the tube.

Gudmundson and coworkers (14) added a high foaming detergent to water and sugar solutions and observed substantial increases in U and U_{Local}. They noted the importance of foam stability on the heat transfer behavior of foaming flows. In particular, Gudmundson found that increases in viscosity destabilized foams and reduced U_{Local}. Foam was completely suppressed in sugar solutions with viscosities above 4 x 10^{-3} kg/m sec (9.6 lb/hr ft). The heat transfer coefficients U and U_{Local} were the same for sugar solutions with and without added surfactant for these higher viscosity trials. Thus, it is the foaming flow and not the surface tension which produces the improvement in heat transfer. In addition, Gudmundson observed that

decreasing the system pressure destabilizes foams, presumably due to the increase in the vapor specific volume which results in higher vapor volumetric flow rates. The foam would be torn apart by the higher vapor velocities. The same effects of viscosity and pressure could be found in the black liquor evaporator process data.

Foaming flow has been proposed as a technically and economically practical means to improve heat transfer in seawater desalinization evaporators by Sephton (25). Improvements of one hundred percent and more were reported in the overall heat transfer coefficients for this application.

CONCLUSIONS

The preceding discussion has shown that black liquor evaporators operate principally in the slug and churn flow regimes, with occasional excursions into annular flow. Foam flow will be present whenever viscosity, pressure, and the presence of foam-promoting materials make it possible.

Virtually nothing is known about foam flow. The problem is extremely complex, since it includes the difficult question of predicting the stability of foams under a wide range of conditions. This stability behavior is likely to change from material to material and to depend on a number of surface properties which would be very difficult to measure at high temperatures.

In addition, foam is not desirable in black liquor evaporators, whatever positive effects it may have on heat transfer. Black liquor foams are difficult to break, and carryover of foam into the contaminated condensate causes material losses and a serious environmental protection problem.

Foaming flows, therefore, were treated as a side issue in the present thesis work. The problem we do wish to address is the prediction of slug and churn flow heat transfer behavior. This will be explored in the following two sections.

ANNULAR CLIMBING FILM STUDIES

INTRODUCTION

In the preceding section, we noted that the normal operation of black liquor evaporators is in the slug and churn flow regimes. A review of annular climbing film heat transfer studies may therefore seem somewhat irrelevant to the present problem. The reason that it is relevant to review annular flow research is that this work led to the development of the Chen (1) correlation. The Chen correlation is known to be correct for the annular flow regime and to be substantially correct for subcooled boiling and bubble flow. Attempts have been made to apply it generally, without regard for flow regimes. There was no a priori reason to think that the Chen correlation would not be correct, at least in form, for the slug and churn flow regimes.

There has been an enormous number of studies concerned with annular flow. The work reviewed here is at least slightly similar in geometry and conditions to black liquor evaporators. For other topics, such as high pressure annular flow or horizontal annular flow, please consult the major references listed in the Chapter introduction. A list of the studies which will be discussed in this section, together with the conditions used in each study, may be found in Table I.

In this section, the two mechanisms which govern heat transfer in annular flow will be reviewed. The mechanisms are, first, the convective transport of heat across the annular film by the same means as in single-phase flow and, second, the transport of heat which results from the growth and departure of vapor bubbles at the heated wall, which is known as nucleate boiling. The successful Chen (1) correlation, which is based on consideration of these two mechanisms, will then be discussed, together with some possible modifications which might extend the

TABLE I

ANNULAR CLIMBING FILM HEAT TRANSFER STUDIES

Reference	Geometry	Test Liquid	Pressure, psia	Mass Flux, lb/hr ft^2	Heat Flux, Btu/hr ft^2
Anderson et al. (26)	0.530-inch ID copper tube electric heat	Water	20 - 120	42000 - 1126000	3600 - 97000
Bennet et al. (27), Collier et al. (28)	Vertical annulus, electrical heating	Water	15 - 35	52000 - 217000	32000 - 160000
Dengler and Addoms (29)	1-inch ID vertical copper tube, steam heat in five sections	Water	8 - 40	44000 - 1000000	28000 - 200000
Guerrieri and Talty (30)	0.748-inch ID vertical tube	Misc. organics	15	22000 - 650000	3000 - 17000
Penman and Tait (31)	0.375-inch, 0.500-inch, 0.747-inch, 0.999-inch ID electric heat	Water, methanol, ethanol, other organics	15	14000 - 1000000	3000 - 90000
Piret and Isbin (32)	1.068-inch ID copper tube, electric heat, nat. circulation	Water, water - K_2CO_3, other organics	15	166000 - 762000	1000 - 53000
Schrock and Grossman (33)	0.118-inch, 0.237-inch, 0.432-inch ID stainless steel	Water	45 - 505	176000 - 3280000	60000 - 1450000
Shock (34-5), Toral, Kenning, and Shock (36)	1.25-inch ID, nickel plated copper, electrical heat	Water, water - ethanol, misc. organics	15	70000 - 161000	5200 - 40600

correlation's usefulness. Finally, the mechanistic concepts of the Chen correlation are not universally accepted, and we will briefly review this controversy.

PURELY CONVECTIVE CORRELATIONS

Definition of the Convective Mechanism

The annular climbing film regime is defined by the presence of a thin film of liquid on the tube walls which is pulled up the walls of the tube by the cocurrent vapor flow. This is almost always a highly turbulent flow pattern in both the vapor core and the liquid film. The convective heat transfer mechanism in this regime is completely analogous to the mechanism in single-phase flow. For conceptual purposes, the convective mechanism may be pictured as the result of the transport of heated liquid "particles" from the neighborhood of the heated wall into the cooler bulk liquid by turbulent eddies. Evaporation occurs from the liquid/vapor interface. This mechanism is the major mechanism in high vapor mass quality annular flow, although in general there will be some contribution from nucleate boiling, which is discussed in "Empirical Convective Correlations Using Lockhart-Martinelli Methods."

Analytical Treatments

It is possible, at least in principle, to extend the methods for calculating single-phase full-tube turbulent flow heat transfer to the case of climbing films. Anderson (26) attempted to extend the von Kármán (37) universal velocity profile approach, and Hewitt (38) worked with the eddy viscosity relationships of Deissler (39) and von Kármán (40), assuming the identity of eddy viscosity and eddy thermal diffusivity. In both these analyses, the film has to be considered smooth, whereas, in reality, it is covered with waves. The critical assumption is that the profiles in the film, whether velocity or eddy viscosity profiles, are exactly the same in a film as in a full tube. This assumption will not be very good at the liquid-vapor interface. Collier and Pulling (41) found that Hewitt's (38) method overpredicted

heat transfer coefficients by over thirty percent. Thus, the analytical treatment of climbing film flow and heat transfer awaits further improvements.

Empirical Convective Boiling Correlations Using Lockhart-Martinelli Methods

Dengler and Addoms (29) introduced the use of the Lockhart-Martinelli parameter (X_{tt}) as a dimensionless group for correlating convective heat transfer coefficients in climbing film annular flow. Lockhart and Martinelli (42) suggested the parameter X_{tt}^2 is defined as the pressure drop of the liquid phase part of the flow calculated as if it were flowing by itself in the tube divided by the pressure drop of the vapor phase flow calculated on the same basis, that is

$$X_{tt}^2 = \left(\frac{dp}{dz}\right)_f / \left(\frac{dp}{dz}\right)_g \tag{2}$$

By introducing a Blasius-type friction factor relationship and performing the indicated pressure drop calculations for turbulent flow, it turns out that

$$X_{tt}^2 = \left(\frac{1-x}{x}\right)^{1.8} \left(\frac{\rho_g}{\Delta_f}\right) \left(\frac{\mu_f}{\mu_\lambda}\right)^{0.2} \tag{3}$$

This parameter is useful in correlating both pressure drop and void fraction. The reason that it is also useful in correlating heat transfer coefficients is that the void fraction relates directly to the liquid film thickness, which in turn relates to the flow rates in and Reynolds number of the film. The Reynolds number, of course, is usually important in convective heat transfer. This circuitous relationship is discussed in detail in Shock (43).

Dengler and Addoms (29) found that eighty-five percent of their purely convective data could be correlated to within twenty percent by

$$\frac{h}{h_{10}} = A \left(\frac{1}{X_{tt}}\right)^n \tag{4}$$

with A = 3.5 and n = 0.5, where h_{10} is the heat transfer coefficient calculated from the Dittus-Boelter equation by assuming that the entire mass flow has liquid phase properties.

$$h_{10} = 0.023 \frac{k}{D} \left(\frac{4W}{\pi D \mu_f}\right)^{0.8} Pr_f^{0.4} \tag{5}$$

The "purely convective data" is that part of the data which shows a strong dependence on the weight fraction of vapor and, thus, on velocity; nucleate boiling heat transfer data, on the other hand, are characterized by a dependence on the temperature driving force rather than the flow velocity.

Correlations of the form of Eq. (4) have been used by other workers. Schrock and Grossman (33) found that A = 2.17 and n = 0.70 in smaller tubes at higher pressures. Collier, Lacey, and Pulling (28) used A = 2.17 and n = 0.70 to correlate data from their electrically heated annulus. Guerrieri and Talty (30) found that A = 3.4 and n = 0.45 in their study of various organic liquids.

Empirical Convective Boiling Correlations Which Rely on Definitions of Characteristic Velocities

Since the two-phase flow convective heat transfer mechanism is analogous to the single-phase mechanisms, it should be possible to extend the familiar Dittus-Boelter equation

$$Nu = A\, Re^b\, Pr^c \tag{6}$$

to the two-phase case. Several authors have taken this approach. Since in the annular flow regime we are concerned with heat transfer to and through the liquid

phase, it seems reasonable to use liquid phase physical properties for all the physical properties called for in the Dittus-Boelter equation. This leaves the problem of defining the characteristic velocity term in the Reynolds number. There is no unambiguously correct definition for this velocity.

Davis and David (44) chose to define the average superficial liquid velocity ($\overline{u_f}$) as the characteristic velocity in the Dittus-Boelter equation. They related this hard-to-measure quantity to the more easily measurable total superficial mass flow rate by means of a slip model. The slip ratio is defined as the ratio of the superficial vapor and liquid velocities

$$\alpha_{fg} = \overline{u}_g/\overline{u}_f \tag{7}$$

The Reynolds number may then be rewritten as

$$Re = \left(\frac{D\rho_f\overline{u}_f}{\mu_f}\right) = \left(\frac{D\rho_f}{\mu_f}\frac{\overline{u}_g}{\alpha_{fg}}\right) \tag{8}$$

by using the definition of the superficial mass flux

$$G_g = \rho_g\overline{u}_g \tag{9}$$

and assuming that the liquid phase occupies a negligible fraction of the tube cross section so that the vapor superficial mass flux is simply the product of the vapor mass quality and the total mass flux,

$$G_g = xG_t \tag{10}$$

we find that

$$\overline{u}_g = \frac{xG_t}{\rho_g} \tag{11}$$

Thus, the Reynolds number becomes

$$Re = \left(\frac{D\rho_f}{\mu_f}\frac{\overline{ug}}{\alpha_{fg}}\right) = \left(\frac{D\rho_f}{\mu_f}\frac{1}{\alpha_{fg}}\frac{xG_t}{\rho_g}\right) \tag{12}$$

Introducing this result into the Dittus-Boelter equation, we find that

$$Nu = \frac{A}{\alpha_{fg}{}^a}\left(\frac{xG_t\ D}{\mu_f}\right)^a\left(\frac{\rho_f}{\rho_g}\right)^a Pr_f \tag{13}$$

Davis and David (45) empirically fitted the parameter (A/α_{fg}^a) as a function of the ratio of liquid and vapor density.

$$\frac{A}{\alpha_{fg}{}^a} = B\left(\frac{\rho_f}{\rho_g}\right)^{-0.59} \tag{14}$$

whence

$$Nu = B\left(\frac{\rho_f}{\rho_g}\right)^{a-0.59}\left(\frac{xG_t\ D}{\mu_f}\right)^a Pr \tag{15}$$

The data of Dengler and Addoms (29) and of Anderson and coworkers (46-48) fit this equation to within seventeen percent using the constants

$$Nu = 0.060\left(\frac{\rho_f}{\rho_g}\right)^{0.28}\left(\frac{xG_t\ D}{\mu_f}\right)^{0.87} Pr_f{}^{0.4} \tag{16}$$

This equation also worked well for the horizontal duct heat transfer data of Davis and David (45). This analysis is only valid in the absence of nucleate boiling.

Piret and Isbin (32) correlated their measurements of tube-average inside film coefficients $(\overline{h}_b)$ by using a Dittus-Boelter type equation with a log mean superficial velocity (u_m) substituted in the Reynolds number.

$$u_m = \frac{u_{exit} - u_{in}}{\ln(u_{exit}/u_{in})} \tag{17}$$

In this equation, u_{in} is the liquid velocity at the entrance to the test section and u_{exit} is the liquid-vapor mixture velocity at the tube outlet. The correlation for $\overline{h}_b$ is

$$Nu = \frac{h_b D}{k_f} = 0.0086 \left(\frac{\rho f u_m D}{\mu f}\right)^{0.8} Pr_f^{0.6} \left(\frac{\sigma_w}{\sigma}\right) \tag{18}$$

where the surface tension ratio term is the surface tension of water (σ_w) divided by that of the test liquid (σ).

Penman and Tait (31) used a different set of dimensionless groups in an analysis which relies on a definition of a characteristic velocity. They chose groups to represent the ratios

$$\left(\frac{\text{Thermal forces causing surface expansion}}{\text{Momentum forces resisting surface expansion}}\right) = f\left(\frac{\text{Momentum forces causing surface expansion}}{\text{Surface forces resisting surface expansion}}\right) \tag{19}$$

or,

$$\frac{h}{c_p}\sqrt{\frac{D}{\rho_f \sigma g_c}} = f\left[u_b \sqrt{\frac{D \rho_f}{\sigma g_c}}\right] \tag{20}$$

where u_b is a "bulk velocity" defined as the sum of the liquid and vapor superficial velocities. Fitting the data to this form yields the equation

$$\frac{h}{c_p} \frac{D}{\rho_f \sigma g_c} = 0.012 \left[u_b \sqrt{\frac{D \rho_f}{\sigma g_c}}\right]^{0.5} \tag{21}$$

This equation is, again, only applicable to purely convective annular flow without any nucleate boiling.

NUCLEATE BOILING IN ANNULAR CLIMBING FILM STUDIES

Definition of the Nucleate Boiling Heat Transfer Mechanism

The nucleate boiling heat transfer mechanism is connected with the growth and departure of bubbles from nucleation sites on the heated surface. Nucleation sites

may be scratches, pits, grain boundaries, or any other gas-filled surface defects. The nucleate boiling mechanism moves heat largely by disturbing the thermal boundary layer which would otherwise develop near the wall. A growing bubble pushes liquid away from the wall. When the bubble leaves, cooler bulk liquid rushes in behind it. As the cooler liquid is heated at the wall, another bubble forms and the cycle is repeated.

The first necessity of the nucleate boiling mechanism is a layer of liquid near the wall hot enough and thick enough to permit bubble growth. Some critical degree of superheat throughout this layer will be required for bubble growth due to surface tension effects. The entire superheated layer must be at or above the critical temperature or the bubble will not grow. This leads to the important phenomenon of nucleation suppression: increasing turbulence in the fluid decreases the thickness of the boundary layer making bubble growth increasingly difficult. Eventually, bubbles cannot grow at all.

In this subsection, some basic information about nucleate boiling will be reviewed. Then, some of the attempts to correct annular flow convective boiling correlations for the effects of nucleate boiling will be presented.

Basic Phenomena Behind the Nucleate Boiling Heat Transfer Mechanism

Nucleate boiling is a complex phenomenon which has been the subject of hundreds of papers. The present discussion is restricted to a few key concepts which are necessary to understand the Chen (1) correlation. A much more detailed treatment may be found in any of the textbooks listed in the chapter introduction; Hsu and Graham (5) has an especially good review of the subject.

Let us first develop the concept that bubble growth requires a superheated liquid layer near the wall. Consider a bubble situated in the rather idealized

conical pit drawn in Fig. 3. To begin with, let us assume that the wall, liquid, and bubble are all uniformly heated to T_b, a temperature greater than the saturation temperature at the local pressure (T_{sat}). From the Young-Laplace equation, we can state that the difference between the pressure of the vapor in the bubble (p_g) and the pressure in the surrounding liquid (p_f) is

$$p_g - p_f = \frac{2\sigma}{r^*} \tag{22}$$

where r^* is the equilibrium bubble radius. The pressure and temperature in the bubble are related by the Clausius-Clapeyron equation,

$$\frac{dp}{dt} = \frac{h_{fg}}{T(v_g - v_f)} \tag{23}$$

which may be simplified if we assume that the vapor specific volume (v_g) is much greater than the liquid specific volume (v_f) and that the gas is ideal. The equation then becomes

$$\frac{1}{p}\, d\, p = \frac{h_{fg}\, M}{R\, T^2}\, dT \tag{24}$$

Integrating the pressure over p_f to p_g and the temperature from the liquid saturation temperature at p_f (T_{sat}) to the temperature of the vapor in the bubble (T_g) gives

$$\ln\left(\frac{p_g}{p_f}\right) = \frac{h_{fg}M}{R}\left(\frac{1}{T_g} - \frac{1}{T_{sat}}\right) \tag{25}$$

or

$$\ln\left(\frac{p_f}{p_g}\right) = \frac{h_{fg}\, M}{R\, T_g\, T_{sat}}\,(T_g - T_{sat}) \tag{26}$$

Now, taking the Young-Laplace Eq. (22), dividing through by p_f, rearranging, and taking the natural logarithm results in

$$\ln\left(\frac{p_f}{p_g}\right) = \ln\left(1 + \frac{2\sigma}{p_f r^*}\right) \tag{27}$$

Combining Eq. (26)-(27), we obtain the result

$$T_g - T_{sat} = \frac{R\, T_g\, T_{sat}}{h_{fg}\, M} \ln\left(1 + \frac{2\sigma}{p_f r^*}\right) \tag{28}$$

When $2\sigma/p_f r^*$ is small, the natural logarithm term may be approximated by a power series. Taking the first term of the series and assuming that the bubble and liquid temperatures are approximately equal leads to

$$T_g - T_{sat} = \frac{RT_{sat}^2}{h_{fg}\, M} \frac{2\sigma}{p_f r^*} = \frac{T_{sat}}{h_{fg}} \frac{2\sigma}{r^* p_g} \tag{29}$$

This represents the superheat $(T_g - T_{sat})$ required for the stability of a bubble of radius r^*.

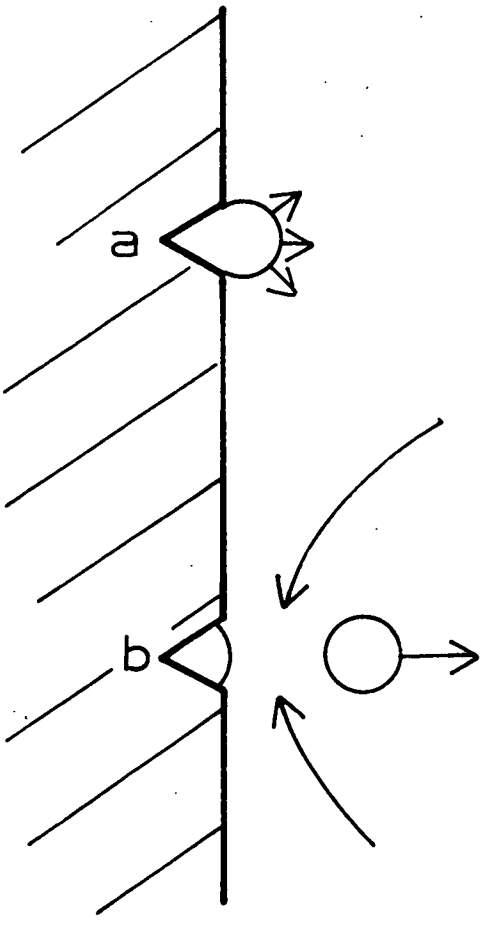

Figure 3. Growth and departure of bubbles at a cavity on a heated wall.

This derivation should be modified to account for the presence of a noncondensable gas, since nucleation sites are normally activated by gas entrapped in the cavities as liquid covers the surface, or by dissolved gas coming out of solution at the heated surface. For this case, the Young-Laplace equation becomes

$$p_g + p_a - p_f = \frac{2\sigma}{r^*} \tag{30}$$

where p_a is the partial pressure of the noncondensable gas in the bubble. Repeating the preceding derivation with this change gives

$$T_g - T_{sat} = \frac{RT_gT_{sat}}{h_{fg}\,M} \ln\left(1 - \left(\frac{2\sigma}{p_f r^*} - \frac{p_a}{p_f}\right)\right) \tag{31}$$

The effect of a noncondensable gas is to reduce the superheat required for nucleation.

The uniformly superheated liquid case just developed is of little practical importance. We are usually concerned with bubbles growing in a boundary layer near a heated wall. There will be a temperature drop across this boundary layer, as shown in Fig. 4. If we assume that the temperature drop is linear across the boundary layer thickness (δ), we can form the proportion

$$\frac{T_w - T_\infty}{\delta} = \frac{T_b - T_\infty}{\delta - y_b} \tag{32}$$

where y_b is the height of the bubble in a coordinate system having $y = 0$ at the wall. Referring to the idealized bubble geometry of Fig. 5, we see that

$$y_b = (1 + \cos\,\theta)\, r_c \tag{33}$$

and

$$r_b = \frac{r_c}{\sin\,\theta} \tag{34}$$

where r_c is the radius of the cavity mouth and θ is the contact angle between the liquid and the wall. Thus, Eq. (32) and (29) can be rewritten as:

$$\frac{T_b - T_\infty}{T_w - T_\infty} = \frac{\delta - (1 + \cos\ \theta)r_c}{\delta} \tag{35}$$

and

$$T_b - T_{sat} = \frac{T_{sat}\ 2\sigma}{(r_c/\sin\ \theta)\ h_{fg}P_v} \tag{36}$$

These two equations define the range of cavity sizes which could contain growing bubbles under the given temperature conditions.

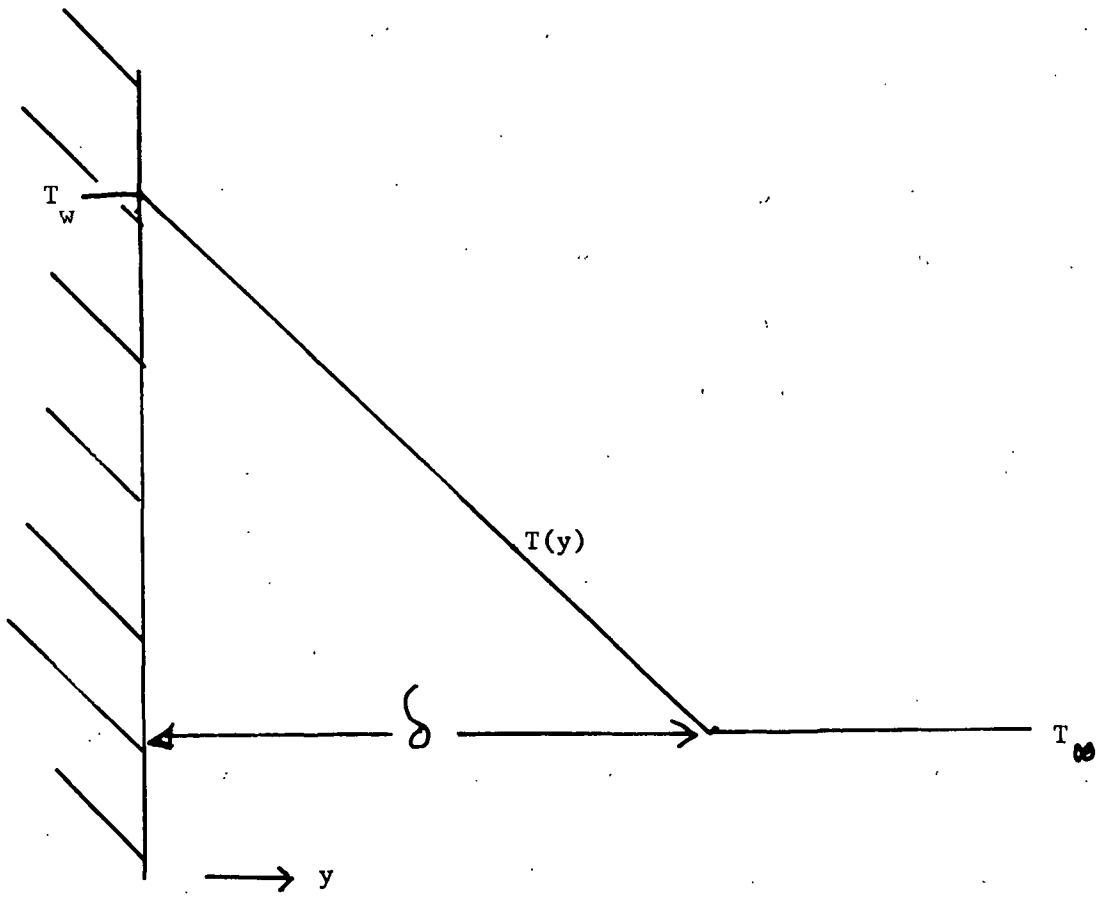

Figure 4. Temperature drop across the boundary layer near a heated wall.

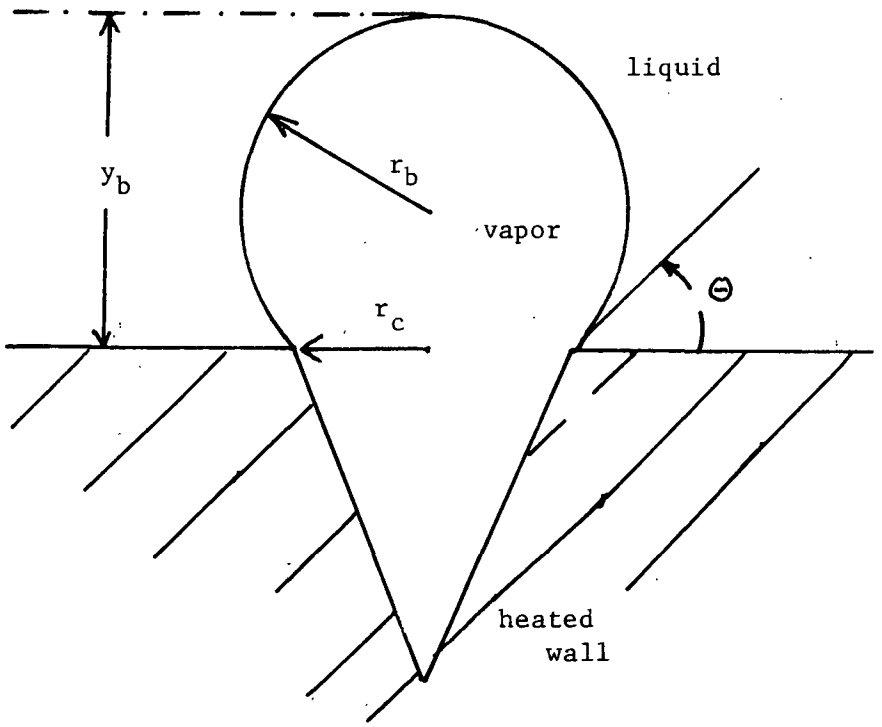

Figure 5. Idealized bubble geometry.

This brings us to the object of this discussion, Fig. 6 (a), which is a sketch of the last two equations above plotted on $(T - T_\infty)$ vs. y coordinates. A system corresponding to this sketch could have active nucleation sites with sizes between $r_{c,min}$ and $r_{c,max}$. Now, consider what happens if the boundary layer is thinned by increasing turbulence in the flow past the wall. Figure 6 (b) shows that as the boundary layer thins, the range of cavity sizes which could be active decreases, until finally the superheated boundary layer is so thin that the curve for the temperature profile does not intersect the bubble growth curve at all, and bubble growth is not possible from cavities of any size. This is what is meant by the term suppression of nucleate boiling. In annular flow convective boiling studies, the nucleate boiling contribution to the total heat transfer declines as evaporation progresses along the tube because the increasing velocities result in the suppression of nucleate boiling.

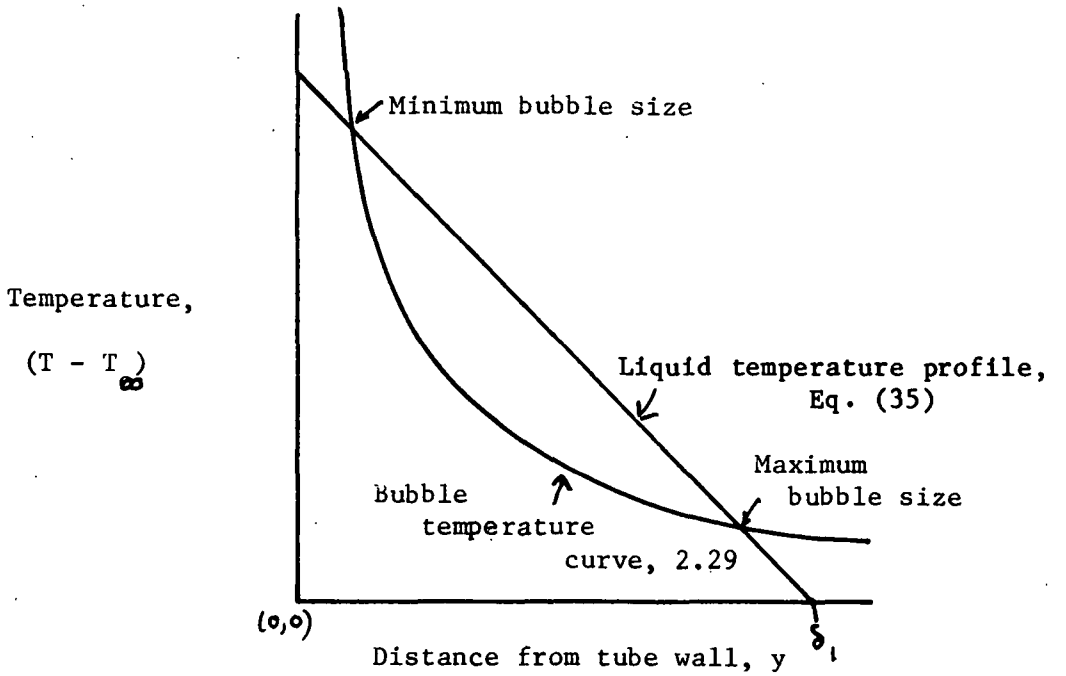

Figure 6 (a). Bubble nucleation criterion.

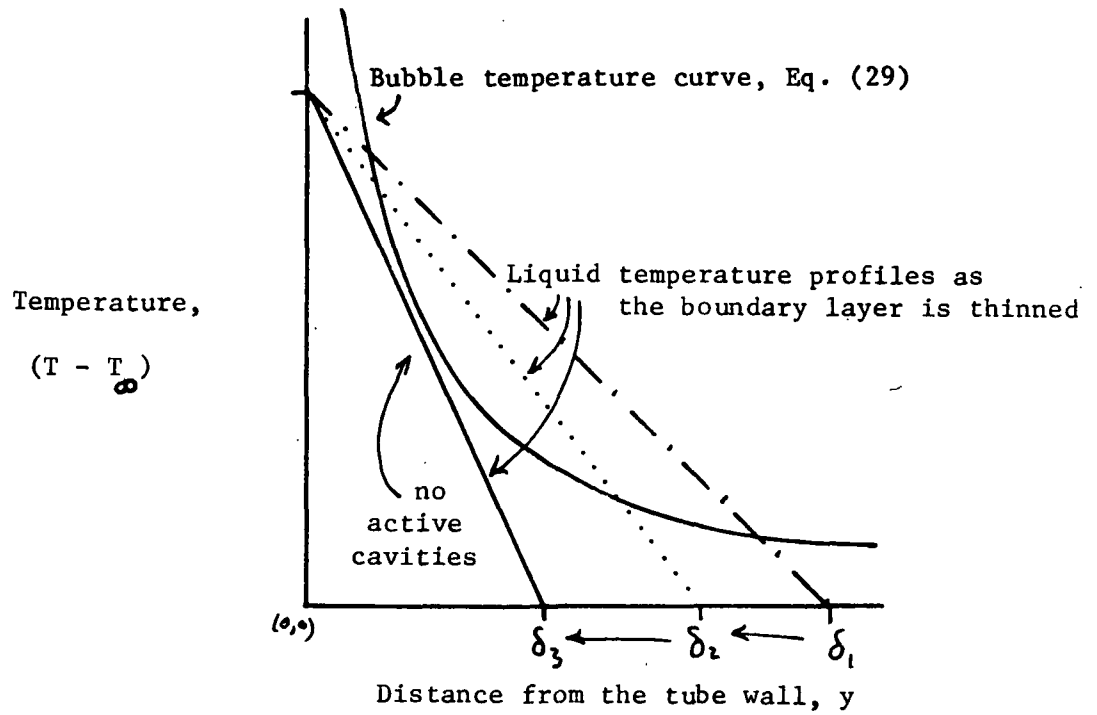

Figure 6 (b). Illustration of the suppression of nucleation by a thinning boundary layer.

Let us now consider the question of how bubble growth effects heat transfer. Kenning (49) summarizes the nucleate boiling heat transfer mechanisms which have been proposed as follows:

(a) Latent heat transport, in which heat is transported via the latent heat of vaporization of the vapor in the bubbles. This mechanism includes the case of simultaneous evaporation at the base of the bubble and condensation at its tip.

(b) Microconvection, which is the result of bubble growth agitating the boundary layer near the wall.

(c) Vapor-liquid exchange, which is a pumping model. Bubble growth and departure causes an interchange of liquid between the wall and bulk fluid regions.

The difference between (b) and (c) is the scale of the phenomena, (b) involving a very thin layer of liquid of about the same dimensions as the bubble diameter.

(d) Surface quenching, which is a submechanism of (c) involving transient conduction of heat to the cooler bulk liquid which "fills in" behind the departing bubble.

(e) Wake flow, for which the liquid motion behind a departing bubble causes convection from the wall.

(f) Enhanced natural convection, which occurs when the columns of bubbles leaving a nucleation site produce a cellular flow pattern analogous to natural convection above a horizontal plate.

(g) Thermocapillary flow, which would be caused by the Marangoni effect of flow caused by small differences in surface tension due to temperature variations

around a bubble. This can be an important mechanism, for example, in the case of boiling heat transfer from a downward facing surface, but is usually negligible.

Kenning (49) notes that not one of the above models can adequately explain the heat transfer observed in nucleate boiling. There are probably several simultaneous mechanisms of heat transfer in nucleate boiling.

Mechanisms (b) through (f) all depend in one way or another on the growth rate of the bubbles and on their departure diameter. In "The Chen Correlation," we will discuss how Chen (1) uses this more general concept of the importance of growth rate and diameter to construct a nucleate boiling heat transfer correlation by using expressions for these two parameters derived from consideration of bubble dynamics in a dimensionless group treatment similar to the Dittus-Boelter equation for forced convection.

Empirical Correlations for Nucleate Boiling in Annular Flow

The studies which were discussed in "Empirical Convective Correlations Using Lockhart-Martinelli Methods" all included a quantity of heat transfer data at lower velocities which could not be correlated by equations based on a purely convective model. This discrepancy was interpreted as the result of a nucleate boiling mechanism acting simultaneously with the convective mechanism. In this section, we will review how these nucleate boiling results were correlated using simple corrections to the convective model equations.

Dengler and Addoms (29) observed that the heat flux contributions of the nucleate boiling and convective mechanisms appeared to add together to account for the total heat flux. For simplicity's sake, however, they chose to correct for nucleate boiling by including a multiplier (F) in their correlation.

$$\frac{h}{h_{10}} = F \left\{ 3.5 \left(\frac{1}{X_{tt}}\right)^{0.5} \right\} \tag{37}$$

where F was determined empirically to be

$$F = 0.67 \left[\left((T_w - T_{sat}) - (T_w - T_{sat})_{ONB}\right) \left(\frac{\partial p}{\partial T_{sat}} \frac{D}{\sigma}\right)_{T_w} \right]^{0.1} \tag{38}$$

The temperature driving force term represents the driving force in excess of that required to initiate nucleate boiling. The empirical equation for this term was

$$(T_w - T_{sat})_{ONB} = 10 \ (u_{ave})^{0.3} \tag{39}$$

The u_{ave} term is the average stream velocity,

$$u_{ave} = \frac{G \ (1 - x)}{\rho_f \ (1 - \alpha)} \tag{40}$$

This average velocity term was included to account for the suppression of nucleate boiling.

A similar approach by Guerrieri and Talty (30) introduced a multiplier (E).

$$\frac{h}{h_l} = E \left\{ 3.4 \left(\frac{1}{X_{tt}}\right)^{0.45} \right\} \tag{41}$$

where

$$E = 0.187 \left(\frac{r^*}{\delta}\right)^{-5/9} \tag{42}$$

The critical bubble radius r^* is the same one defined by Eq. (29), while the boundary layer thickness δ is calculated from

$$\delta = \frac{10\ \mu_f}{\rho_f}\left[\frac{4\ \rho_f}{(dp/dz)\ D}\right]^{0.5} \tag{43}$$

If the value of E calculated from Eq. (42) is less than unity, E should be set equal to one. The ratio of critical bubble radius to the boundary layer thickness may again be interpreted as a nucleation suppression correction.

Schrock and Grossman (33,50) expanded their Martinelli parameter correlation by incorporating an additional dimensionless group, the boiling number (Bo) to give

$$\frac{h}{h_L} = C_1 \left\{ Bo + C_2 \left(\frac{1}{X_{tt}}\right)^n \right\} \tag{44}$$

This form has the advantage that the nucleate boiling contribution is presented in its observed additive form. The boiling number

$$Bo = \frac{(Q/A)}{G\ h_{fg}} \tag{45}$$

may be interpreted as the ratio of the mass flux arising from evaporation, which is perpendicular to the wall, to the total mass flux in the tube which is parallel to the wall. Schrock and Grossman used the constants $C_1 = 7390$, $C_2 = 0.00015$, and $n = 0.66$. Collier and coworkers (41) used Eq. (44) but found that the constants $C_1 = 6700$, $C_2 = 0.00035$ and $n = 0.66$ gave better agreement with their data.

Convective correlations in the Dittus-Boelter form discussed in "Empirical Convective Boiling Correlations which Rely on Definitions of Characteristic Velocities" have also been extended to account for nucleate boiling effects. Piret and Isbin (32) used a combination of the Dittus-Boelter equation and the Rohsenow (51) pool boiling (zero net flow) correlation to correlate their data as an alternative to the

purely convective form of Eq. (18). The Rohsenow (51) correlation was derived using the dimensionless equation

$$Nu = A\ Re^{b}\ Pr^{c} \tag{46}$$

with the characteristic diameter defined by the bubble departure diameter (D_b), which may be represented by a ratio of surface tension and buoyancy forces.

$$D_b = f\left(\frac{\sigma}{g_c\ (\rho_f - \rho_g)}\right) \tag{47}$$

The characteristic velocity is scaled by

$$u_b = f\left(\frac{(Q/A)}{h_{fg}\ \rho_f}\right) \tag{48}$$

The final form of the Rohsenow correlation, after fitting constants and rearranging, is

$$(T_w - T_{sat})\left(\frac{Cp}{h_{fg}}\right) = C_{sf}\left[\frac{(Q/A)}{\mu_f\ h_{fg}}\left(\frac{\sigma}{g_c\ (\rho_f - \rho_g)}\right)^{0.5}\right]^{0.33} Pr_f^{1.7} \tag{49}$$

where C_{sf} is a surface effect constant with a different value for each combination of wall surface and liquid chosen.

Piret and Isbin (32) found that by subtracting the convective heat flux component calculated by the Dittus-Boelter equation from the total heat flux of an experiment, they obtained a nucleate boiling heat flux component which could be correlated by the Rohsenow correlation, Eq. (49). This method does not account for the suppression of nucleation.

THE CHEN CORRELATION

The Rationale Behind the Chen Correlation

Chen (1,52) compared the predictions of the correlations of Dengler and Addoms (29), Guerrieri and Talty (30), Bennett et al. (27), and Schrock and Grossman (50) for heat transfer in vertical upward annular flow with the combined data from all these papers. He found that although each correlation worked well with its own author's data, the disagreement with the other data was often substantial. Chen, therefore, developed his own correlation, which could predict the values of the over six hundred data points available, with an average deviation of only twelve percent. Chen restricted this correlation to the conditions of

(a) saturated, two-phase, convective boiling flow,

(b) vertical flow,

(c) stable flow,

(d) no slug flow,

(e) no liquid deficiency (dry wall), and

(f) heat flux less than its burnout value.

The Chen correlation is an extension of the Rohsenow (51) superposition principle, which states that the total heat flux is the sum of convective ("macroconvective") components.

$$q = q_{mac} + q_{mic} \tag{50}$$

The microconvective and macroconvective heat transfer coefficients are defined by

$$q_{mac} = h_{mac} (T_w - T_b) \tag{51}$$

and

$$q_{mic} = h_{mic} (T_w - T_{sat}) \tag{52}$$

In saturated boiling, the bulk liquid temperature is equal to its saturation temperature, T_{sat}. For this case, the heat transfer coefficients may also be added together.

$$h = h_{mac} + h_{mic} \tag{53}$$

Chen (1) proposed that the macroconvective heat transfer coefficient (h_{mac}) would behave according to a Dittus-Boelter type relationship.

$$h_{mac} = 0.023 \frac{k_{TP}}{D} Re_{TP}^{0.8} Pr_{TP}^{0.4} \tag{54}$$

Since the main resistance to heat transfer will be in the liquid layer near the wall, Chen suggested that the two-phase thermal conductivity (k_{TP}) and Prandtl number (Pr_{TP}) should be assigned their liquid phase values. This leaves the problem of defining the two-phase Reynolds number. Chen proposed that the two-phase Reynolds number (Re_{TP}) could be related to the Reynolds number of the liquid flowing by itself in the tube (Re_f) by

$$\left(\frac{Re_{TP}}{Re_f}\right)^{0.8} = F \tag{55}$$

where

$$Re_f = \frac{(1 - x)\ G\ D}{\mu_f} \tag{56}$$

The unknown correction function F is purely hydrodynamic and, as such, should be a function of the reciprocal of the Martinelli parameter ($1/X_{tt}$), where

$$\left(\frac{1}{X_{tt}}\right) = \left(\frac{1 - x}{x}\right)^{0.9} \left(\frac{\rho v}{\rho_f}\right)^{0.5} \left(\frac{\mu f}{\mu v}\right)^{0.1} \tag{57}$$

The resulting equation

$$h_{mac} = 0.023 \frac{k_f}{D} Re_f^{0.8} Pr_f^{0.4} F\left(\frac{1}{X_{tt}}\right) \tag{58}$$

may be rearranged to the form introduced by Dengler and Addoms (29)

$$\frac{h_{mac}}{h_{Lo}} = F \left(\frac{1}{X_{tt}}\right) \tag{59}$$

which will be familiar from the discussion in "Purely Convective Correlations."

For the microconvective or nucleate boiling heat transfer component (h_{mic}), Chen (1) adapted a pool boiling heat transfer correlation proposed by Forster and Zuber (53). In this correlation, the Dittus-Boelter equation is invoked again,

$$Nu = A\, Re^b\, Pr^c \tag{60}$$

this time with the characteristic length and velocity defined as the bubble departure radius and radial growth rate.

The equations for bubble growth which Forster and Zuber incorporated into their correlation were derived by Plesset and Zwick (54). Considering the mechanical energy and continuity equations for the case of a spherical bubble growing in an infinite, superheated liquid leads to the Raleigh equation.

$$R\ddot{R} + \frac{3}{2}\dot{R}^2 = \frac{\Delta p}{\rho_f} \tag{61}$$

The Plesset and Zwick solution to this equation assumes that bubble growth is limited by the conduction of heat to the interface. The bubble radius as a function of bubble growth time, t, is given by

$$R = \frac{\Delta T_{sat}}{h_{fg}\ \rho v}\ (\pi\ k_f\ \rho_f\ c_{pf})^{0.5}\ t^{0.5} \tag{62}$$

The time at bubble departure was calculated from considerations of bubble dynamics. This critical time value is

$$t^{0.5} = \left(\frac{2\sigma}{\Delta p_{sat}}\right)^{0.5} \left(\frac{\rho_f}{\Delta p_{sat}}\right)^{0.25} \tag{63}$$

whence

$$R = \frac{\Delta T_{sat}}{h_{fg}\ \rho v} \left(\frac{2\pi\ k_f\ \rho_f\ c_{pf}\ \sigma}{\Delta p_{sat}}\right)^{0.5} \left(\frac{\rho_f}{\Delta p_{sat}}\right)^{0.25} \tag{64}$$

The bubble Reynolds number Re_b

$$Re_b = \frac{R\dot{R}\ \rho_f}{\mu_f} \tag{65}$$

may be found by differentiating Eq. (62) with respect to time. The product $(R\dot{R})$ is independent of t, and the Reynolds number is given by

$$Re_b = \frac{\pi\ k_f\ c_{pf}}{\mu_f} \left(\frac{\rho_f\ \Delta T_{sat}}{\rho v\ h_{fg}}\right) \tag{66}$$

The final form of the Forster and Zuber (53) correlation is

$$h_{mic}^{\circ} = 0.00122\ \frac{k_f^{0.79}\ c_{pf}^{0.45}\ \rho_f^{0.49}\ g_c^{0.25}}{\sigma^{0.5}\ \mu_f^{0.29}\ h_{fg}^{0.24}\ \rho_v^{0.24}}\ (\Delta T)^{0.24}\ (\Delta p)^{0.75} \tag{67}$$

Again, this is a derivation for a bubble growing in an infinite, uniformly superheated liquid which has been empirically corrected to the case of a bubble growing from a heated wall in a zero-net-flow environment. The superscript in h_{mic}° indicates that this is a pool boiling heat transfer coefficient. Chen, in

applying Forster and Zuber's work to the convective boiling case, found it necessary to introduce a 'suppression factor' S into the above equation to correct for the difference between the wall superheat and the mean superheat of the fluid in the boundary layer in which the bubble is growing. The factor S is defined as the ratio of the effective superheat (ΔT_e) to the wall superheat (ΔT).

$$S = \left(\frac{\Delta T_e}{\Delta T}\right)^{0.99} \tag{68}$$

The exponent is arbitrary and is used so that S appears to the first power in the final equations. By using the Clausius-Clapeyron equation and assuming that the ratio ($\Delta T/T$) is much less than one, Chen found that

$$S = \left(\frac{\Delta T_e}{\Delta T}\right)^{0.24} \left(\frac{\Delta p_e}{\Delta p}\right)^{0.75} \tag{69}$$

Thus,

$$h_{mic} = h_{mic}^{\circ}\, S = 0.00122 \frac{k_f^{0.79}\, c_{pf}^{0.45}\, \rho_f^{0.49}\, g_c^{0.25}}{\sigma^{0.5}\, \mu_f^{0.29}\, h_{fg}^{0.24}\, \rho_v^{0.24}} (\Delta T)^{0.24}\, (\Delta p)^{0.75}\, S \tag{70}$$

The suppression factor S should be a function of the two-phase Reynolds number (Re_{TP}) and will have the properties

$$S \longrightarrow 1 \text{ at zero flow,}$$

$$\text{and } S \longrightarrow 0 \text{ at infinite flow.}$$

The two correction functions S and F were determined empirically from the experimental data. A sketch of these two functions is given in Fig. 7.

To calculate the heat transfer coefficient at a given heat flux, mass velocity, and vapor mass quality using the Chen correlation, the following procedure is followed:

1. Calculate X_{tt}
2. Find the appropriate value of F from the graph of F vs. $(1/X_{tt})$
3. Calculate h_{mac} from Eq. (58)
4. Calculate Re_{TP} from Eq. (55) and (56)
5. Find the value of S from the graph of S vs. Re_{TP} (Fig. 7)
6. Calculate h_{mic} from Eq. (70) for a first guess of ΔT_{sat}
7. Calculate h; $h = h_{mic} + h_{mac}$
8. Calculate the heat flux $(Q/A) = h(\Delta T_{sat})$
9. If the calculated heat flux is not equal to the experimental heat flux, guess a new value for (ΔT_{sat}) and return to step 6. Repeat this process until the calculated heat flux converges on the experimental value.

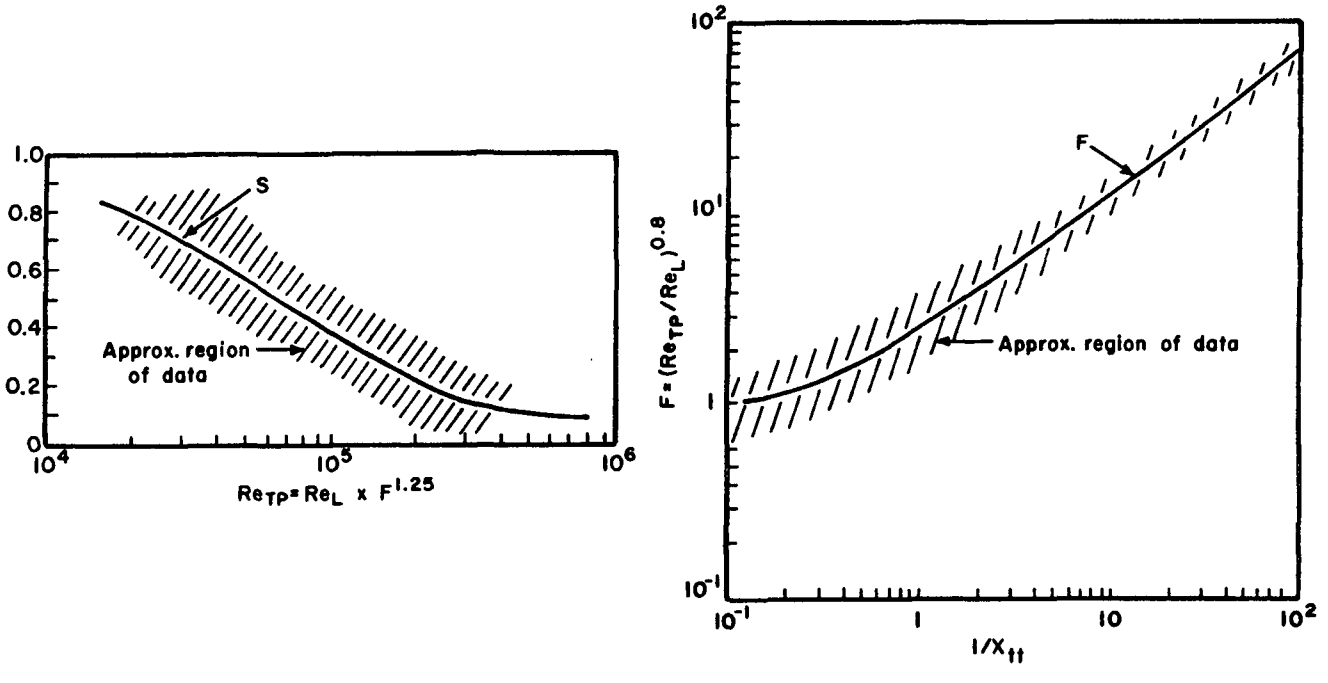

Figure 7. The two-phase Reynolds number correction (F), and the nucleate boiling suppression factor (S) used in the Chen (1) correlation.

Modifications to the Chen Correlation to Correct for Mass Diffusion Effects in Multicomponent Systems

The original Chen (1) correlation was based on data for boiling pure liquids only. In practice, we are much more often concerned with solutions of two or more components. Kraft black liquor contains an enormous variety of different compounds.

Adding a second component to a system in which nucleate boiling is an important heat transfer mechanism effects a significant reduction in the heat transfer coefficient. Evaporation from the bubble wall will result in an excess or deficiency of one component in the bubble wall. Bubble growth is then controlled by the diffusion of the limiting material to or from the interface. The reduction in the bubble growth rate leads to a reduction in the amount of heat transferred by the nucleate boiling mechanism. In this section, we will discuss modifications to the Chen correlation which correct for the effects of diffusion control of nucleate boiling.

Shock (34) studied the evaporation of water and ethanol/water mixtures in a vertical, electrically heated, nickel-plated copper tube. He modified the Chen correlation to account for possible diffusion effects in the water-ethanol system by correcting the temperature driving force, using an empirical method developed by Stephan and Körner (55) for the pool boiling case:

$$\frac{\Delta T_{sat}}{\Delta T_{sat,ideal}} = 1 + \theta \tag{71}$$

where

$$\Delta T_{sat,ideal} = x_\infty \ \Delta T_{sat,A} + (1 - x_\infty) \ \Delta T_{sat,B} \tag{72}$$

and

$$\theta = A \left| y_{A,\infty}^* - x_{A,\infty} \right| \tag{73}$$

The ideal temperature driving force ($\Delta T_{sat,ideal}$) is simply a weighted average of the temperature driving force which would be observed in boiling pure components A and B at the same heat flux. The mole fraction of component A far from the wall (x_∞) is used as the weighting factor. The expression for θ represents the deviation from the ideal due to mass transfer resistance where y_∞^* is the equilibrium mole

fraction of A in the vapor phase corresponding to the concentration of A, x_∞, at the local pressure. The factor A is a dimensionless, empirical function of pressure (the units of pressure taken as N m^{-2})

$$A = A_o \ (0.88 + 0.12 \times 10^{-5} \ p) \tag{74}$$

where A_o is a constant which depends only on the combination of liquids in question. For ethanol/water, $A_o = 1.21$.

Combining these equations and using the definition of the heat transfer coefficient,

$$h_{mic,mixture} = \frac{1}{(1 + A \left| y_{A,\infty}^* - x_{A,\infty} \right|) \left[(x_{A,\infty}/Sh_{mic,A}^\circ) + (x_{B,\infty}/Sh_{mic,B}^\circ) \right]} \tag{75}$$

where the microconvective pool boiling heat transfer coefficient for each component (h_{mic}°) is calculated as usual from Eq. (67). The suppression factor S is identical to that normally used in the Chen correlation to correct pool boiling heat transfer coefficients to convective boiling ones. Shock's modification reduces to the usual $h_{mic} = h_{mic}^\circ S$ if only one component is present.

This method did not give good agreement with Shock's experimental data. Shock pointed out, however, that the nickel plating inside his test section produced a very smooth surface with very few defects to serve as nucleation sites. Therefore, these experiments probably did not provide an adequate test of this modification of the Chen correlation, as the data base underlying the Chen correlation was all taken on surfaces which had a wide distribution of nucleation sites.

Chen has recently supervised a major modification in his correlation which accounts for mass diffusion effects. In Bennett and Chen (56), the suppression factor S has been adjusted using the Florshuetz and Khan (57) expression for the thermal driving force in a bubble growing in a binary mixture under pool boiling conditions.

$$\Delta T_b = \frac{\Delta T_{sat}}{1 - \frac{c_{pf}\left(F_v - F_f\right)}{h_{fg}} \frac{\partial T_{sat}}{\partial F_f} \left(\frac{\alpha}{D}\right)^{1/2}} \tag{76}$$

where F_v and F_f are the local vapor and liquid mass fractions, respectively. This may be extended to forced convective boiling conditions by the usual Chen correlation method, where ΔT_b has replaced ΔT_{sat} as the pool-boiling driving force.

$$\frac{\Delta T_{TE}}{\Delta T_b} = \left\{ S\ (Re_{TP}) \right\}^{1/0.99} \tag{77}$$

Defining S_{binary} in terms of the usual, easily measured driving force $(T_w - T_{sat})$

$$S_{binary} = \left[\frac{\Delta T_{TE}}{\Delta T_{sat}}\right]^{0.99} \tag{78}$$

where S_{binary} is the suppression factor corrected for the effects of mass diffusion on the temperature driving force, we can derive

$$S_{binary} = \frac{1}{1 - \left(\frac{c_{pf}\left[F_v - F_f\right]}{h_{fg}}\right) \frac{\partial T_{sat}}{\partial F_f} \left(\frac{\alpha}{D}\right)^{1/2}} S\ (Re_{TP}) , \tag{79}$$

which may be substituted for S in the microconvective heat transfer coefficient Eq. (69) to yield the modified correlation for the nucleate boiling heat transfer component (h_{mic}) of a binary mixture.

Bennett and Chen (56) have also corrected the Chen correlation for the possibility of mass transfer effects on the convective heat transfer mechanism. This effect would arise because of excesses or deficiencies of a component at the annular gas-liquid interface. Shock (34) has shown that such effects are not likely to be important. However, if there were an excess of one component at the surface, the thermal driving force would become the difference between the wall and interface temperatures.

$$q_{mac,binary} = h_{mac}\ (T_w = T_i) = h_{mac}\ \tilde{\Delta T} \tag{80}$$

rather than the usual difference between the wall and saturation temperature. Defining the ratio of the thermal driving force in this case to the single component driving force (ΔT_{sat}),

$$\left[\frac{\tilde{\Delta T}}{\Delta T_{sat}}\right] = \frac{T_w - T_i}{T_w - T_{sat}} \tag{81}$$

the following equation for the binary mixture convective heat transfer coefficient may be derived.

$$h_{mac,binary} = h_{mac}\left[\frac{\tilde{\Delta T}}{\Delta T_{sat}}\right]_{mac} \tag{82}$$

If we now define a mass transfer coefficient (h_m)

$$j = \rho_{avg}\ h_m\ (F_{interface} - F_f) \tag{83}$$

and assume that the vapor composition and liquid composition are at equilibrium and that all the heat flux results in evaporation,

$$j = \frac{(1 - Fv)\ q}{h_{fg}} \tag{84}$$

Solving for the mass fraction of the less volatile component at the interface

$$F_{interface} = F_f + \frac{(1 - Fv)\ q}{h_{fg}\ h_m} \tag{85}$$

Thus,

$$\left[\frac{\tilde{\Delta T}}{\Delta T_{sat}}\right]_{mac} = 1 - \frac{(1 - Fv)\ q}{\rho_{avg}\ h_{fg}\ h_m\ \Delta T_{sat}} \left.\frac{\Delta T_{sat}}{\partial F_f}\right|_{P_B} \tag{86}$$

The mass transfer coefficient was empirically fit to

$$h_m = 0.023\ (Re_{TP})^{0.8}\ (Sc)^{0.4}\ \frac{D}{d} \tag{87}$$

where D is the diffusion coefficient and Sc is the Schmidt number ($\mu_f/\rho_f\ D$). The macroconvective heat transfer coefficient expression thus becomes

$$h_{mac} = \left[0.023\ \left(\frac{k_f}{D}\right)\ Re_f^{0.8}\ Pr_f^{0.4}\right]\ F\left(\frac{1}{X_{tt}}\right)\left[\frac{\Delta T}{\Delta T_{sat}}\right] f(Pr) \tag{88}$$

The last term in this equation is a Prandtl number correction,

$$f(Pr) = Pr_f^{0.296} \tag{89}$$

This new Chen correlation was tested on over one thousand data points taken in a one-inch ID copper tube with electrical heat. The mean deviation of the correlation with respect to these data was 14.9 percent. The data and the validity of the correlation were again limited to the annular flow regime.

Modifications to the Chen Correlation to Extend the Correlation to Subannular Flow Regimes

Although Chen emphatically restricts his correlation to the annular flow regime, other workers have attempted to extend it to the bubble, slug, and churn regimes as well. Moles and Shaw (58) estimated subcooled boiling heat transfer coefficients by calculating h_{mac} with F set equal to one and h_{mic} with s evaluated using the single phase Reynolds number (GD/μ_f). For this case,

$$q = h_{mic}\ (T_w - T_{sat}) + h_{mac}\ (T_w - T_f) \tag{90}$$

since the thermal driving forces governing the two mechanisms are not the same for both mechanisms in subcooled boiling. The Chen correlation modified in this way

underestimates the heat flux somewhat when subcooled voids and a net vapor mass quality exist, increasing the velocity of the liquid so that the F equals one assumption no longer is true.

Shock (34) used his modification of the Chen correlation on water and ethanol/water mixtures at outlet qualities from near-zero to 16.6 percent. A large amount of his data should be in the slug or churn regime, hence, an implicit extension of the Chen correlation to the slug flow regime. Agreement between the data and the predictions was poor, however. As was mentioned above, the nickel plating on Shock's experimental equipment gave very atypical conditions for nucleate boiling, and so the lack of agreement is not conclusive. There is no obvious reason why such an extension of the Chen correlation would not be possible.

THE CONVECTIVE VS. NUCLEATE BOILING CONTROVERSY

Thin Film Pool Boiling and its Possible Implications with Respect to Convective Heat Transfer

Recently, Mesler (59) has challenged the concept that the nucleate boiling contribution to convective boiling heat transfer declines as the annular flow regime develops. A number of pool boiling studies have shown that there is a dramatic increase in the pool boiling heat transfer coefficient (h°) when the thickness of the liquid pool is reduced. Nishikawa et al. (60), for example, reported increasing h° with decreasing depth for pools thinner than 5 mm (0.19 inch). Mesler (61) studied this phenomenon and observed that the bubble lifetimes from nucleation to departure were much shorter in thin liquid films than in normal pool boiling. The short lifetimes were due to a special method of bubble departure which is possible in thin films. The wall of the bubble contacts the interface, ruptures, and a new liquid film is quickly established. Because the bubble lifetime is short, latent heat transport by way of evaporation from the thin layer of liquid beneath the

bubble is the important nucleate boiling heat transfer mechanism, rather than the microconvective mechanisms which predominate in deeper pools. This "microlayer" beneath the bubble exists for only a small part of the lifetime of the relatively long-lived bubbles of normal pool boiling; thus, its contribution to the total nucleate boiling heat transfer is proportionally less in that case. In short, as the liquid depth in a pool boiling apparatus is reduced, there is a mechanism change, and the latent heat transport mechanism which takes over from the microconvective mechanisms is more effective in moving heat.

Extending this reasoning to annular flow convective boiling, Mesler (59) points out that as the velocities in the tube increase, the liquid film thins. As the film thins, the nucleate boiling mechanism may become more effective, just as it does in thin film pool boiling. This is exactly the opposite of the argument behind the Dengler and Addoms (29) concept of nucleation suppression due to a steadily growing convective heat transfer mechanism.

Mesler (59) also attacked the custom of graphing (h_{TP}/h_l) or (h_{TP}/h_{lo}) against the reciprocal of the Martinelli parameter $(1/X_{tt})$, which was introduced by Dengler and Addoms (29) and subsequently used by many other authors, including Chen (1). Mesler suggests that the correlations developed using this method are an artifact of the method, as the two quantities which are plotted against each other contain many of the same variables. The use of log-log coordinates and the exclusion of "rogue points" may have contributed to an illusory correlation. In particular, the break in the correlation line from the initial region where (h_{TP}/h_l) is independent of $(1/X_{tt})$ to the developed region where (h_{TP}/h_l) is a function of $(1/X_{tt})$, which is often interpreted as indicating the change in mechanism from nucleate boiling to purely convective heat transfer, can be accounted for by considering the effects of plotting groups containing the same variable against one another on log-log paper.

Mesler (59) therefore rejects the hypothesis that there is a change in mechanism from nucleate boiling to purely convective boiling in high velocity annular flows.

As an alternative to the Dengler and Addoms correlation method, Mesler (59) suggests working with data graphed as heat flux (Q/A) versus thermal driving force (ΔT_{sat}) on linear coordinates. Mesler shows that Dengler and Addoms data, when plotted in this manner, follow the same trends as pool boiling data. The scatter of the points in the plot is rather great; however, Mesler is not optimistic about the accuracy of the Dengler and Addoms data and so considers the agreement to be significant.

Mesler's proposal has not received wide acceptance. The phenomenon of nucleation suppression is well documented; indeed, anyone with a stove, a pot of boiling water, and a spoon can observe that increased velocity (stirring the pot) reduces the nucleate boiling. The Mesler hypothesis is an extrapolation from a zero-net-flow case to the violently agitated conditions in an evaporator tube. This extrapolation is in itself questionable. No experiments to directly test this hypothesis have been published yet.

CONCLUSIONS

In this section, we have developed the Chen (1) correlation against the background of the correlations which preceded it and which it has largely supplanted. We have also seen that the Chen correlation may be modified to account for the likely mass diffusion effects in evaporating mixtures. Despite the objections of Mesler (59) to part of its underlying concepts, the Chen correlation still seems to be the best available model to predict heat transfer in annular flow convective boiling.

Unfortunately, we are not greatly concerned with annular flow in black liquor evaporators. The possibility of extending the Chen correlation to the conditions which dominate black liquors has not been tested in the literature. Although we could not be certain that the Chen correlation could not be extended to the slug/churn flow regimes, it was desirable to develop an alternative method for estimating heat transfer in these regimes. The remaining section of this chapter, together with "A Numerical Model for Slug and Churn Flow," provide such an alternative.

SLUG AND CHURN FLOW AND THE BEHAVIOR OF FALLING FILMS

INTRODUCTION

Vertical slug and churn flow boiling heat transfer has not received much attention in the literature. Gudmundson and coworkers (20) noted in their literature review that no attempt had yet been made to model this regime, despite its probable importance in black liquor evaporators. In "A Numerical Model for Slug and Churn Flow," I will piece together a simple model for slug/churn flow heat transfer by considering slug flow as an intermittent falling film system. To do this, I will have recourse to a large amount of previous work on simpler systems. First, we need to be able to predict slug rise velocities in order to predict the thickness of the liquid film left behind a slug. Then, we need to evaluate whether or not this film thickness could be in stable downflow against the local upflow of vapor and, if it could not, to be able to estimate the maximum film thickness that could fall smoothly under those conditions. Finally, we need to be able to relate the thickness of the falling film to its heat transfer behavior. This section briefly reviews the work which has been published on these topics.

SLUG FLOW

Introduction

The slug flow regime is characterized by a pattern of alternating vapor bubbles and slugs of liquid. Griffith and Wallis (62) have noted that the slug flow regime is a very persistent regime; vestiges of slug flow structure can persist well into the annular flow regime. There are, however, a number of subregimes within the slug flow regime. At low vapor velocities, a slugging flow may approximate the ideal case of rising spherical gas bubbles surrounded by smoothly falling films. This subregime ends when the vapor velocities become high enough to cause flooding in the films. The neat spherical cap is lost, and the liquid slug may begin to resemble a foam more than a lump of liquid because of the entrainment of vapor bubbles by the flooding films. At very high vapor velocities, the films on the wall will begin to climb, and the flow will have entered the wispy-annular regime. Vertical slug flow studies have generally been limited to the fully developed constant vapor and liquid rate case. Almost no information is available on slug flow in nonsteady-state systems.

In this section, the methods for calculating slug rise velocities and equilibrium film thicknesses for the ideal case will be briefly reviewed. A more detailed discussion of these topics may be found in Wallis (6).

Rise Velocity of a Slug

The rise velocity of a slug is that velocity with which a gas bubble would ascend in a tube full of stagnant liquid. Wallis (6) presents three dimensionless groups which represent the balance between buoyancy and either inertia, viscosity, or surface tension. The groups are

$$\frac{\rho_f V_\infty^2}{D g (\rho_f - \rho_g)} \tag{91}$$

for inertia-dominated systems,

$$\frac{\mu_f V_\infty}{D^2 g (\rho_f - \rho_g)} \tag{92}$$

for viscosity-dominated systems, and

$$\frac{\sigma}{D^2 g (\rho_f - \rho_g)} \tag{93}$$

for systems in which surface tension is important. The first group is of the greatest practical importance, and for this case Davies and Taylor (63) found that

$$V_\infty = k_1 \rho_f^{-1/2} [g D (\rho_f - \rho_g)]^{1/2} \tag{94}$$

where $k_1 = 0.328$, from an approximate analytical solution to the problem. Wallis (6) recommends the value of $k_1 = 0.345$ determined in the experiments of White and Beardmore (64). Equation (94) is valid for systems where the dimensionless inverse viscosity

$$N_f = [D^3 g (\rho_f - \rho_g) \rho_f]^{1/2} / \mu_f \tag{95}$$

is greater than 300.

Drift Velocity of a Slug

In the ideal case, the drift velocity, or velocity of the bubble moving relative to the average volumetric flux j, would be given by

$$V_{gj} = V_\infty = V_b - j \tag{96}$$

or,

$$V_b = j + V_\infty \tag{97}$$

However, in reality, the drift velocity will be influenced by the velocity profile in the liquid slug. Nicklin and coworkers (65) found that this influence could be accounted for by introducing constants into Eq. (97) to give

$$V_b = C_1 \, j + C_2 \, V_\infty \tag{98}$$

For tubes where the Reynolds number based on the total volumetric flux, Re_j, is greater than 8000, the values of the constants are $C_1 = 1.2$ and $C_2 = 1.0$. For boiling flows, Griffith (66) suggested that C_2 should equal 1.6.

The Asymptotic Film Thickness Behind a Slug

For the ideal, spherical cap bubble, the velocity of the liquid film relative to the bubble will be

$$V = \sqrt{2 \, g_c \, h_z} \tag{99}$$

at a distance h_z below the tip of the bubble nose. Ideal bubble or not, at some point the falling film will reach a terminal velocity at which the film's weight is exactly balanced by the shear stress at the wall. Wallis (6) shows how this asymptotic film thickness and velocity may be calculated from continuity considerations. From Eq. (98), the bubble velocity - which is, of course, also the gas velocity - is

$$V_b = V_g = 1.2j - V_\infty \tag{100}$$

Continuity indicates that the total volumetric flux across any cross section will be constant, and therefore

$$Q'_g - Q'_f = Q = \frac{\pi D^2}{4} \, j \tag{101}$$

where the true (not superficial) vapor volumetric rate Q'_g is

$$Q'_g = \frac{\pi}{4} (D - 2\delta)^2 V_g \tag{102}$$

Combining these equations and rearranging, the liquid flux downward is given by

$$j'_f = \frac{4 Q'_f}{\pi D^2} = (1.2 j + V_\infty) \left(1 - 2 \frac{\delta}{D}\right)^2 - j \tag{103}$$

The true liquid volumetric flow rate Q'_f may be related to the film thickness δ by the falling film theories which are discussed in "Falling Films: Hydrodynamics and Heat Transfer." The results are, for laminar films,

$$\frac{j'_f}{V_\infty} = 3.85 N_f \left(\frac{\delta}{D}\right)^3; \quad Re_\Gamma \leq 3500 \tag{104}$$

and for turbulent films,

$$\frac{j'_f}{V_\infty} = 190 \left(\frac{\delta}{D}\right)^{3/2}; \quad Re_\Gamma > 3500 \tag{105}$$

where

$$Re_\Gamma = \frac{4\Gamma}{\mu_f} = \frac{j'_f}{V_\infty} (0.345) N_f \tag{106}$$

The film thickness is found by solving simultaneously Eq. (103) and the appropriate film flow equation, either (104) or (105).

FLOODING AND CHURN FLOW

Introduction

If a liquid film is falling against a given countercurrent flow of gas, there will be some critical liquid flow rate, and thus critical film thickness, above

which the flow is unstable and will flood. This means that if a slug, for example, deposits an excessively thick film, part of the liquid will be lifted by the countercurrent gas flow until the film thickness is reduced below its critical value. This is the characteristic process of churn flow. There is evidence, summarized by Hewitt and Wallis (67), that there is no gas flow rate effect on the flow of films thinner than their critical flooding value. Thus, if we calculate film deposition thicknesses such that they are always just less than the critical thickness for flooding, we should not have to be concerned with the complicated question of interfacial friction factors.

Mechanisms of Flooding

Dukler and coworkers (68,69) have done a great deal of work on the mechanisms of flooding in connection with the problem of emergency core cooling in nuclear reactors. They note three possible mechanisms: wave motion, droplet entrainment, and flow reversal within the film. The following paragraphs will review these mechanisms.

The wave motion flooding mechanism was proposed by Hewitt and Wallis (67) to account for the fact that flooding is always accompanied by the growth of large waves on the surface of the film. These waves can result in flooding either by growing until they bridge the tube and are ejected as slugs, or by being propagated upward under the influence of shear and/or form drag. The bridging mechanism seems unlikely in tubes of large diameter. The second mechanism has not yet been worked out theoretically or even been tested experimentally. Dukler (69) concludes that the evidence for this mechanism is entirely circumstantial.

Flooding by droplet entrainment could occur when the gas rate is sufficient to form large waves on the film surface, and then tear droplets from the crests of the waves and lift the droplets out of the tube. Dukler and Smith (70) assumed that the

last step is the controlling one, which reduces the problem to one of drop mechanics rather than of wave mechanics. To develop this concept into a predictive correlation, we need to be able to predict the minimum vapor velocity which will support the largest droplet torn from the waves. The balance between the drag forces and gravity may be expressed by the equation

$$\frac{1}{2} C_d \left(\frac{\pi d^2}{4}\right) \rho_g V_g{}^{t2} = \left(\frac{\pi d^3}{6}\right) g_c (\rho_f - \rho_g) \tag{107}$$

which may be rearranged to give

$$V_g{}^t = \frac{2}{\sqrt{3}} \left(\frac{g_c (\rho_f - \rho_g) d}{\rho_g C_d}\right)^{1/2} \tag{108}$$

The unknown drop size, d, may be estimated by the methods of Hinze (71)

$$d = \frac{We_c \sigma}{\rho_g V_g{}^{t2}} \tag{109}$$

where We_c is a critical Weber number, approximately 20 for a fast acceleration from a slowly moving surface. Using a drop coefficient of $C_d = 0.44$ for large spheres in turbulent flow, the equation becomes

$$V_g{}^s = 2.8 \frac{(\sigma g_c (\rho_f - \rho_g))^{1/4}}{\rho_g{}^{1/2}} (1 - \alpha) \tag{110}$$

This equation gives good agreement with the data of Dukler and Smith (70), but it does not appear to work equally well under all conditions. The predicted velocities are in better agreement with the onset of the annular climbing film regime than with the onset of flooding. Dukler and coworkers (69) conclude that the droplet entrainment mechanism is not a fully general model of the flooding mechanism.

The film flow mechanism for flooding was proposed by Dukler and coworkers (69). The basic concept of this mechanism is that near the critical flooding conditions, the wave action on the surface of the film increases dramatically. The roughened interface which results from the waves causes an increase in the interfacial shear stress. The increased shear stress causes flow reversal over the entire section of film covered by the waves. Note that the film itself moves, not just a few large waves on its surface. The film may be either in a true upflow condition or may be in a state of split flow, with upflow at the interface but downflow near the wall. Dukler and coworkers (69) calculated the required interfacial shear stresses to produce various states of flow in a laminar film and found reasonable agreement between their calculations and the experimental data. The much more difficult turbulent flow case was not worked out in their study.

A useful concept from this model is that a film of a given thickness falling against a given counterflow of gas can have two accessible states: a smooth surfaced condition in which the film falls freely and a wavy surfaced condition which can result in upflow or split flow. There is, therefore, the possibility of a limit cycle in which the film switches between these two states and so experiences an alternation of upward and downward flows. This is just a hypothesis, but it offers an attractive explanation for the flooding hysteresis loops observed by Hewitt and Wallis (67). Flooding hysteresis is the phenomenon in which a flooding system will continue to flood as the gas or liquid flow rates are reduced below the values at which flooding began, but once flooding has stopped, the rates must again be increased to the original critical level to produce flooding.

Empirical Flooding Correlations

The mechanisms of flooding discussed above are valuable concepts, but they do not provide us with usable correlations for the onset of flooding in the general

turbulent film case. The most widely accepted empirical flooding correlation is that of Hewitt and Wallis (67). This correlation uses two dimensionless groups,

$$j_g^* = j_g \rho_g^{1/2} [g D (\rho_f - \rho_g)]^{-1/2} \quad (111)$$

and

$$j_f^* = j_f \rho_f^{1/2} [g D (\rho_f - \rho_g)]^{-1/2} \quad (112)$$

The correlation takes the form

$$j_f^{*1/2} + j_g^{*1/2} = C \quad (113)$$

In the experiments of Hewitt and Wallis, a film of liquid was introduced into a tube through a section of porous sinter. At a given gas rate, the liquid flow rate was increased until flooding was observed visually. This onset of flooding can be correlated by Eq. (113) with the constant C = 1.0. If the liquid rate was then decreased, flooding would continue until a lower critical flow rate was reached, which could be correlated by setting C = 0.88. Above a dimensionless gas velocity of $j_g^{*1/2} = 0.50$, this flooding hysteresis loop disappeared, and both the onset and cessation of flooding could be correlated by using Eq. (113) with C = 1.0. This velocity is the hanging film point at which the film is just supported by the counterflow of gas and moves neither up nor down on the average.

FALLING FILMS: HYDRODYNAMICS AND HEAT TRANSFER

Introduction

Falling liquid films are in general very complex flows. The classic analysis of Nusselt (72) for laminar flow film thickness and heat transfer holds true for only very low film Reynolds numbers. Above $Re_\Gamma = 30$, as determined by Tailby and Portalski (73), a complex system of waves forms on the surface of the films. Recent studies of these waves by Dukler (74), Chu and Dukler (75,76), Chu (77), and Dukler

(68) have shown how these waves may be simulated mathematically. There appear to be two families of waves: large waves which control film thickness and surface renewal and very small waves which act principally as surface roughness. The formation of eddies behind the large waves has a major effect on heat and mass transfer in falling film systems, as shown by Portalski (78). An analysis which can account for the effects of these waves and eddies has yet to be performed. We are left with the choice between highly idealized smooth film analyses which generally are not very successful, and successful empirical correlations of limited applicability.

Analytical Models

The flow of a laminar falling film can be treated by a straightforward mathematical analysis, summarized by Wallis (6). The force balance

$$\tau = \mu_f \frac{dv}{dy} = g_c \, (\rho_f - \rho_g) \, (\delta - y) \tag{114}$$

may be integrated over the thickness of the film. Then, using the definitions of the film Reynolds number and dimensionless film thickness

$$Re_\Gamma = \frac{4\Gamma}{\mu} \tag{115}$$

$$\delta^* = \frac{\delta}{D} N_f^{2/3} \tag{116}$$

the final result

$$\delta^* = 0.909 \, Re_\Gamma^{2/3} \tag{117}$$

is obtained. This theoretical equation is in good agreement with the experimental data of Belkin (79) below about $Re_\Gamma = 1.00$.

The turbulent flow problem is much more difficult. Dukler (80) developed a smooth film model that extends the Deissler (39) and von Kármán expressions for eddy viscosity in single-phase full pipe flow to falling films.

Deissler:
$$E = n^2 uy \left[1 - e^{\frac{-n^2 uy}{\mu_f \rho_f}} \right] \tag{118}$$

von Kármán:
$$E = K \left(\frac{du}{dy}\right)^3 / \left(\frac{d2u}{dy2}\right)^2 \tag{119}$$

This model assumes that the eddy viscosity profile in a film is identical to that in a full pipe, an assumption which is particularly questionable at the liquid-gas interface. These two equations for eddy viscosity are substituted in the basic equations

$$\tau = \frac{1}{g} \left(\mu_f + E\rho_f\right) \frac{du}{dy} \tag{120}$$

$$Re_{Lx} = \frac{4\rho_f}{\mu_f} \int_0^\delta u dy$$

Heat transfer may also be treated, if we assume the identity of eddy thermal conductivity with eddy viscosity. In that case,

$$q = -\left(k_f + E\, C_{pf}\, \rho_f\right) \frac{dT}{dy} \tag{121}$$

From these relationships, the velocity profiles, film thicknesses, and heat transfer coefficients may be calculated using computerized numerical methods.

The film thicknesses predicted by this model are in reasonable agreement with the data of Belkin (79), but, unfortunately, the heat transfer coefficient predictions are inaccurate in the case of evaporating films. Both Collier and Pulling

(41) and Chun and Seban (81) found that Dukler's model overpredicts the heat transfer coefficients by about thirty percent. Similarly, the agreement of the model with the data of Abou and Huyghe (82) is quite poor. The disagreement is probably due to the suppression of turbulent eddies at the gas-liquid interface, which is not accounted for in the model.

Variations on this theme were proposed by Kunz and Yerazunis (83) and Narayana-Murthy and Sarma (84,85), who substituted alternative expressions for the eddy viscosity. The development and results of these models are similar to those of Dukler (80).

A related treatment discussed by Butterworth (86) and extensively developed by Anderson, Haseldon and Mantzouranis (48) uses the universal velocity profiles of von Kármán (37), again assuming the identity of the film profile with the full pipe profile. The results of this model are almost identical with Dukler's (80) and suffer the same problems.

Empirical Flow Correlations

The empirical film thickness correlation recommended by Wallis (6) and Perry's handbook (87) was developed by Belkin (79).

$$\delta^* = 0.315 \left[Re_\Gamma \sqrt{C_f} \right]^{2/3} \tag{123}$$

Wallis (6) suggests using $C_f = 0.008$, which reduces this equation to the convenient form

$$\delta^* = 0.063 \, Re_\Gamma^{2/3} \tag{124}$$

Perry's handbook uses the friction factor expression of Walker et al. (88):

$$C_f = 0.079 \, Re^{-0.25} \tag{125}$$

to give

$$\delta = 0.304 \left(\frac{\Gamma^{1.75} \mu_f^{0.25}}{g_c \rho_f^2}\right)^{1/3} \tag{126}$$

The laminar-turbulent transition is at about $Re_\Gamma = 1000$. Below the transition, Eq. (117) may be used.

Empirical Heat Transfer Correlations

The theoretical models discussed in the previous section are all inadequate as predictors of the heat transfer behavior of falling films. The empirical correlations presented in this section all have the virtue of good agreement with the experimental data, but extrapolating them to conditions other than those tested is risky. Only recent work on evaporating falling film heat transfer will be considered here; for a review of nonevaporating film heat transfer see Narayana-Murthy and Sarma (84,85) and for condensations, Collier, Chapter 10 (3).

Chun and Seban (81) studied heat transfer to evaporating films falling outside a vertical tube of 1.13 inches outside diameter. Their data fit the following equations

$$\text{laminar flow} \qquad h = 0.606 \left(\frac{k^3 g_c}{\nu^2}\right)^{1/3} \left(\frac{Re_\Gamma}{4}\right)^{-0.22} \tag{127}$$

$$\text{turbulent flow} \qquad h = 0.00383 \left(\frac{k^3 g_c}{\nu^2}\right)^{1/3} Re^{0.4} Pr^{0.65} \tag{128}$$

with the laminar-turbulent transition at

$$Re_\Gamma = 5800 \, Pr_f^{-1.06} \tag{129}$$

A similar set of experiments was performed by Fujita and Ueda (89,90) using a tube of 16 mm (0.63 inch) outside diameter. They studied a wider range of heat

fluxes than Chun and Seban (81), whose maximum flux was about 8500 Btu/hr ft^2. Below 25,000 Btu/hr ft^2, Fujita and Ueda found no heat flux effect, which they interpreted as the absence of a significant nucleate boiling mechanism. The data in this range could be correlated with the equations

$$h = \left(\frac{k^3 g_c}{\nu}\right)^{1/3} 0.90 \, Re_\Gamma^{0.22} \quad Re_\Gamma \leq 3200 \tag{130}$$

and

$$h = \left(\frac{k^3 g_c}{\nu}\right)^{1/3} 0.006 \, Re_\Gamma^{0.4} \quad Re_\Gamma > 3200 \tag{131}$$

Nucleate boiling became important for heat fluxes in excess of 51,000 Btu/hr ft^2 for which

$$h = 1.24 \, q^{0.741} \tag{132}$$

The low heat flux data were compared with the predictions of the Chun and Seban (81) correlation. This correlation followed the trends, but was about ten percent too low.

Abou and Huyghe (82) studied evaporating films falling inside 1.12- and 1.4-inch ID tubes. Their data correlated with the following equations:

$$Nu = 0.004 \, Re_\Gamma^{0.8} \, Pr^{0.9} \qquad Re_v \leq 25{,}000 \tag{133}$$

$$Nu = 0.004 \, Re_\Gamma^{0.8} \, Pr^{0.9} \left(\frac{Re_v}{25{,}000}\right)^2 \qquad Re_v > 25{,}000 \tag{134}$$

where Re_v is the Reynolds number of the gas phase. This, obviously, contains a correction for vapor velocity which would be unnecessary in the case of the Chun and Seban or Fujita and Ueda experiments. Abou and Huyghe observed no nucleate boiling effects at fluxes up to 61 kW/m^2 (19,400 Btu/hr ft^2).

CONCLUSION: MAKING A SLUG/CHURN FLOW MODEL

In attempting to assemble a slug/churn flow model from the information discussed above, the worst area of uncertainty is the flooding process. We have no information that would allow us to estimate film thicknesses or heat transfer coefficients if flooding is in progress. The best policy seems to be to assume that flooding occurs instantaneously and completely, leaving a film thinner than its critical value and so immune to the upflow of vapor. In doing this, we have deliberately overlooked the effect of flooding hysteresis loops, which are very likely present, and which would tend to reduce the total amount of downflow. However, ignoring the effects of the counterflow of vapor permits us to use the Belkin and Chun and Seban correlations, which are simple and reasonably accurate. The accuracy of the theoretical models does not justify their use, considering the complexity of the computer program which would result.

A NUMERICAL MODEL FOR SLUG AND CHURN FLOW

SLUG FLOW AND CHURN FLOW BOILING OF MIXTURES: A SIMPLE MODEL

INTRODUCTION

A computer program was written which calculates heat transfer coefficients in boiling slug and churn flow using a simple model of these regimes. The model is a combination of several of the empirical correlations discussed in "Slug and Churn Flow and the Behavior of Falling Films." The basic function of this model is to estimate the thickness of a film left on the tube walls by a rising slug or lump of liquid and then to calculate the drainage of the film over time. The Reynolds number of the draining film can then be used to estimate the heat transfer coefficient. The correlations used in the model are as follows:

- The method of Wallis (6) is used to estimate the asymptotic film thickness behind a rising slug.

- The Hewitt and Wallis (67) correlation is used to estimate the maximum film thickness not subject to flooding at a given vapor flow rate.

The lesser of these two film thicknesses at any point is taken as the film thickness left on the tube walls by the rising slug. The transition between the two correlations is the slug flow/churn flow regime boundary.

- The Belkin (79) correlation is used to find the relationship between a film's thickness and its Reynolds number.

- The evaporating falling film heat transfer coefficient correlation of Chun and Seban (81) is used to predict the heat transfer coefficient from the calculated Reynolds number.

This section describes the scheme which was used to combine these correlations into a computer simulation model of slug and churn flow. To avoid computer jargon, the model will be presented as though the calculations were to be done by hand. An annotated copy of the computer program printout is available in Appendix I.

DESCRIPTION OF THE SLUG AND CHURN FLOW MODEL

Introduction

The slug and churn flow model works by dividing the tube into small increments of length (Fig. 8) and then following the history of the liquid films in each increment of length over many small increments of time. To generate this history, the model has to be able to:

1. simulate the formation of slugs at the bottom of the tube;

2. predict the rise velocity of each slug wherever it may be located in the tube, and then move the slug the appropriate distance during the current increment of time;

3. predict the thickness of the films deposited by the slug on the tube walls during its movement over the time increment;

4. calculate the film flow rate in each increment of length from the thickness of the film in the increment, and then follow the drainage and evaporation of the film over time;

and

5. calculate the heat transfer coefficient in each length increment from the film flow rate in the increment.

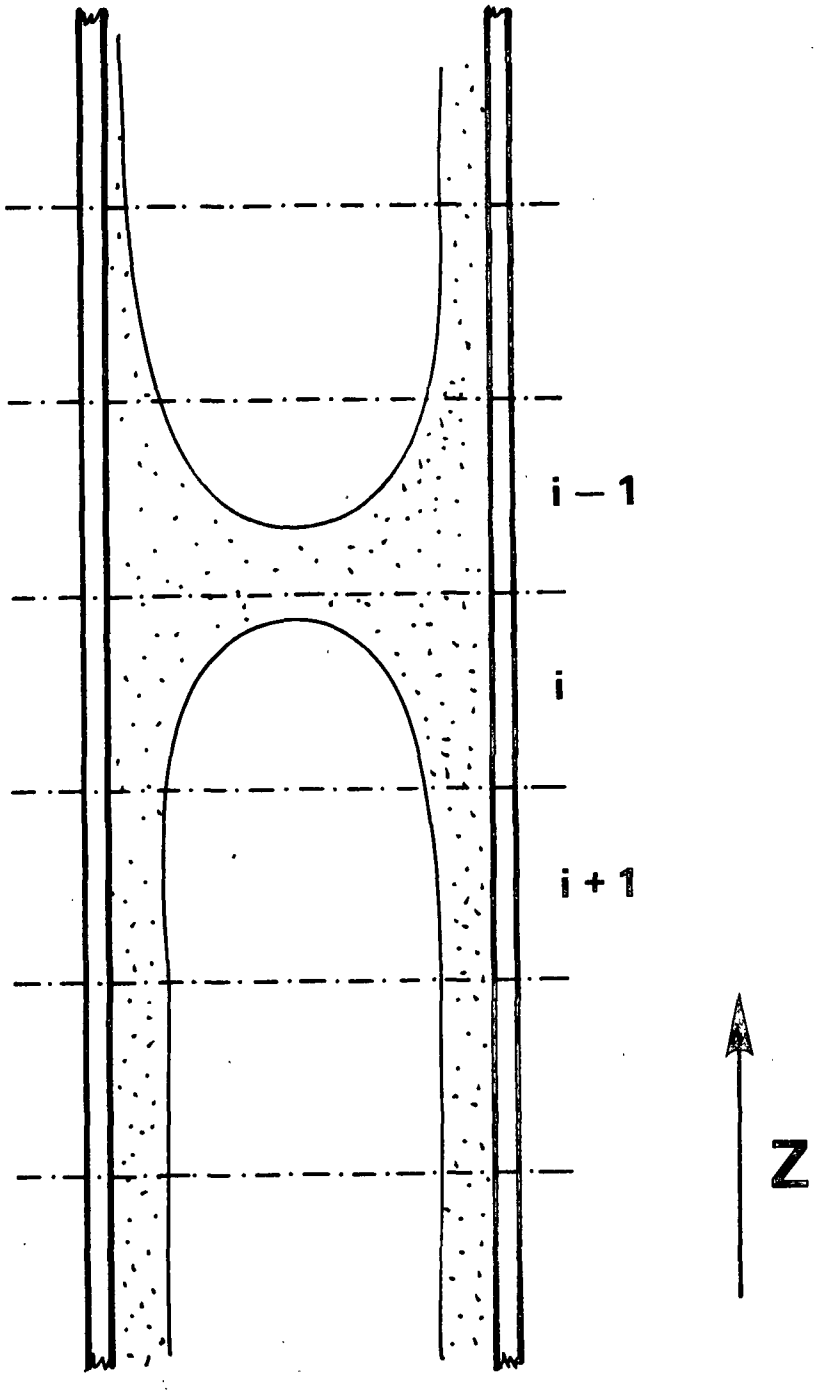

Figure 8. An evaporator tube divided into small increments of length.

The assumptions made in developing the model are as follows:

a. saturated, two-phase convective boiling flow;

b. vertical, net-upflow conditions;

c. maximum vapor velocity less than the critical value for the transition to annular flow;

d. no nucleate boiling;

e. no mass transfer control of heat transfer;

f. no interaction between the deposited falling films and the counterflow of vapor;

g. the pressure drop along the tube is small enough that its effects on the boiling point and on other physical properties can be neglected.

In addition, the model assumes that the empirical equations for slug movement and film deposition which were obtained from nonboiling systems may be extended to a boiling system.

Slug Formation

In an evaporator tube, slugs are produced by the coalescence of smaller vapor bubbles. Small bubbles are continuously produced from nucleation sites on the heated wall while the volume of the liquid at the bottom of the tube increases as liquid flows down in the films and fresh feed enters the tube. In time, the small bubbles agglomerate into a large vapor slug which begins to rise, pushing part of the liquid ahead of it in a "lump." This process is sketched in Fig. 9. The agglomeration of the bubbles will be strongly influenced by pressure fluctuations in

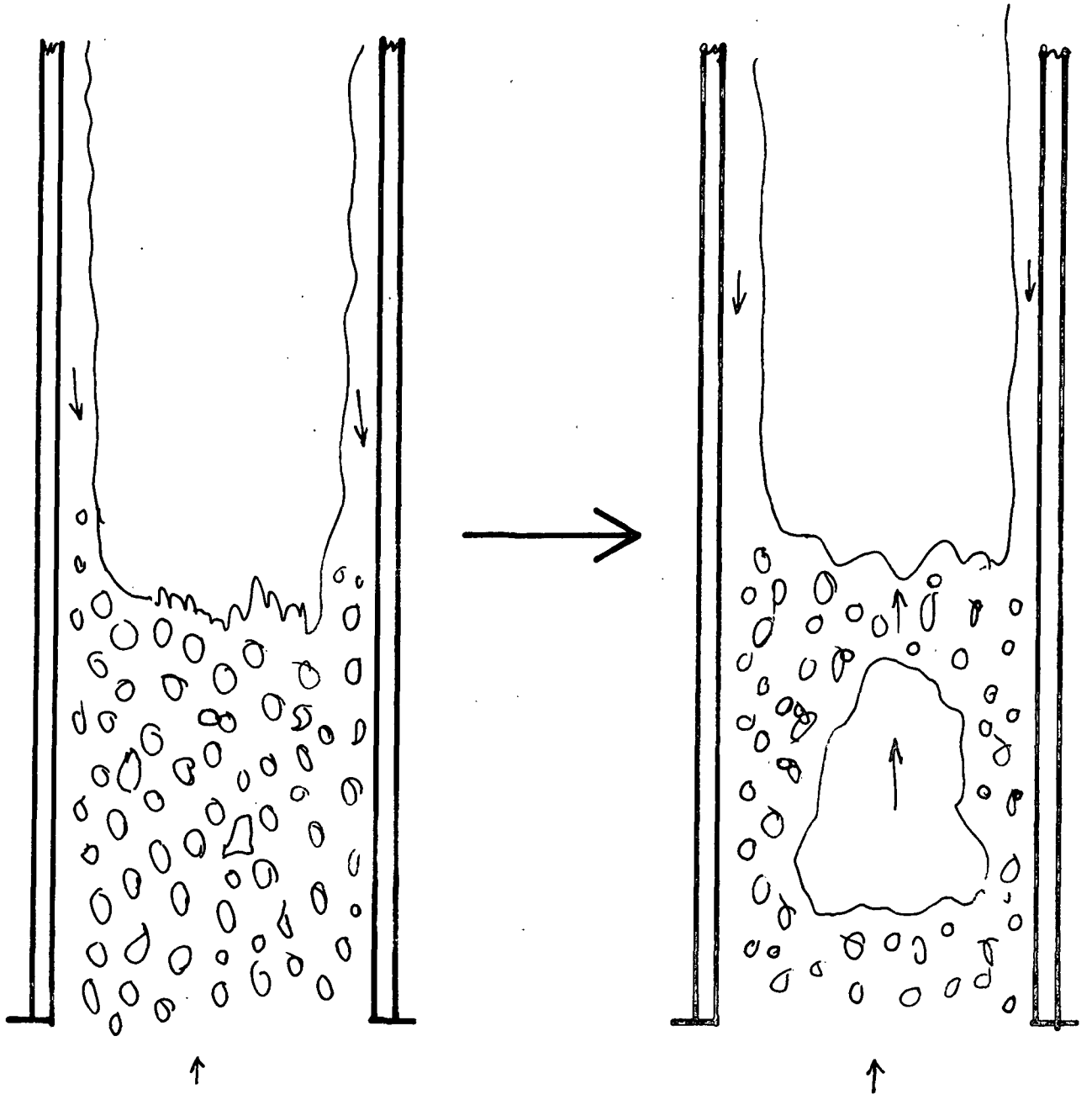

Figure 9. The formation of a vapor slug by the coalescence of small vapor bubbles.

the evaporator system. An evaporator system resonant frequency would thus interact with the slug-forming process, since the low-pressure part of the cycle would lead to rapid bubble expansion and coalescence. Assuming that the slugging frequency is fixed by a characteristic of the evaporator system rather than by the physics of

bubble collision and coalescence, the slugging rate can best be treated as an experimentally measured variable, "known" for a given evaporator system. Figure 10 illustrates how slugs are introduced in the model. Over the succession of time intervals between slugs, the backflow from the films and the inflow of fresh feed are added together as though they were accumulating below the entrance to the tube. Then, when the time comes to start a slug, the accumulated backflow and fresh feed are introduced as a lump which then rises in the tube as vapor forms beneath it. The initial quantity of vapor beneath the liquid lump which sets the slug in motion is simulated by assuming that the bottom increment of tube length is initially full of vapor, with the liquid lump filling the appropriate number of length increments above the bottom, vapor-filled increment.

The Rise Velocity of a Slug

At any time increment, several slugs may be present in the tube at different positions along its length. To calculate the location of each slug at the start of the next time increment, its velocity during the current time increment must be known. Since the heat flux and the physical properties of the liquid at its local concentration are known, the local average volumetric flux, j, is easily calculated. Then, the rise velocity of the slug may be estimated using the methods of Wallis (6) in which the vapor slug rise velocity in a stagnant liquid

$$V_\infty = 0.345\ (g_c\ D\ (\rho_f - \rho_g))^{1/2}\ \rho_f^{-1/2} \tag{135}$$

is empirically corrected for the net upward flow to give

$$j_b = 1.2j + V_\infty \tag{136}$$

as was discussed in "Drift Velocity of a Slug." This equation is multiplied by the duration of an increment of time to give the distance traveled by the slug over the increment of time. The increments of length and time were chosen by trial and error

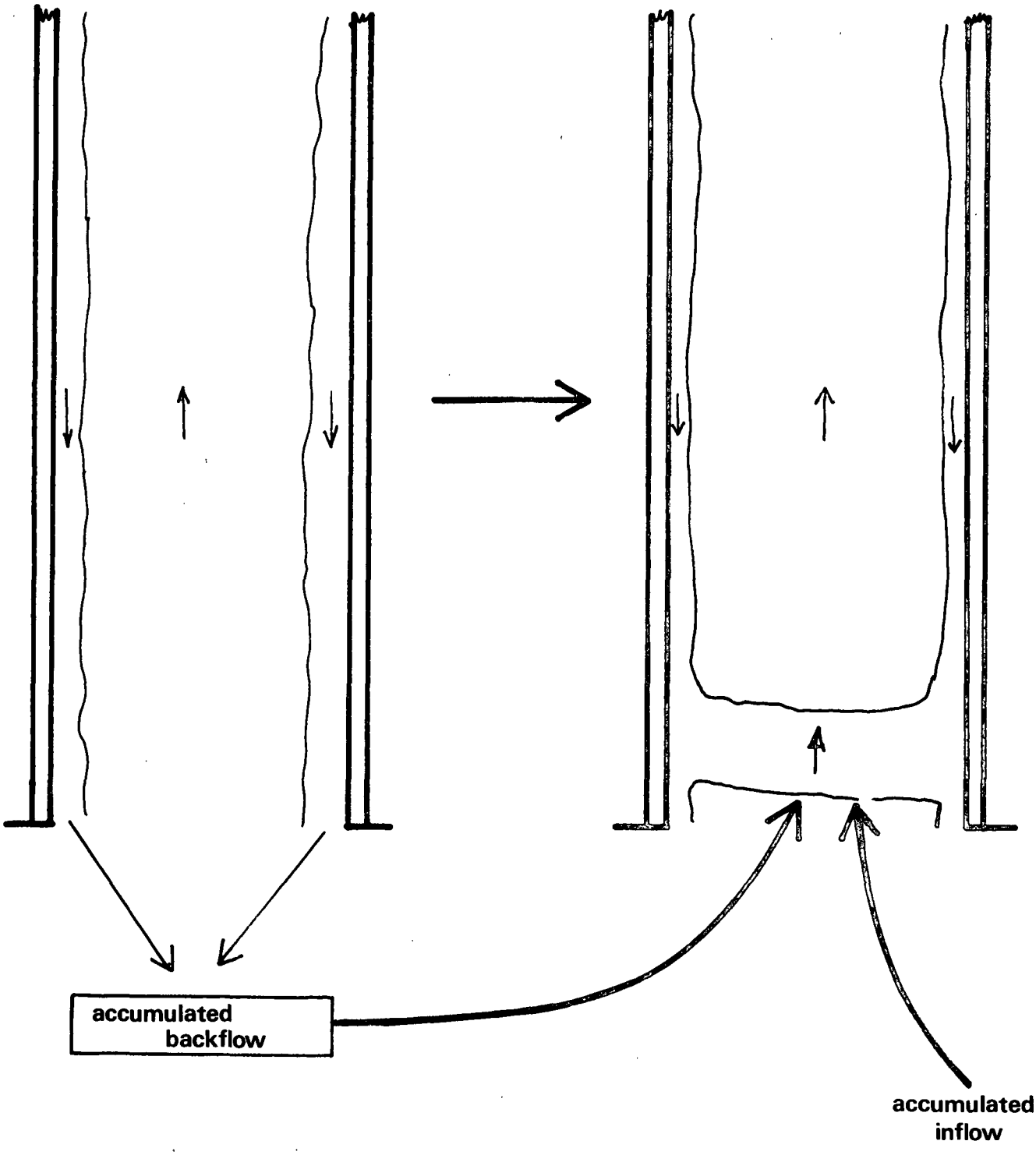

Figure 10. The model treatment of slug formation. Liquid lumps are introduced into the tube at equal intervals of time.

to be small enough (one inch and five milliseconds, respectively) that making them smaller makes no difference in the slug transit time and film deposition predictions. Thus, the procedure closely approximates the acceleration of the slug as the vapor velocity increases along the tube. When a slug leaves the top of the tube, the weight and concentration of the liquid lump are recorded and the validity of the mass balance over the tube is checked. The slug location is taken as the bottom of the liquid lump. The length of the lump is recomputed at each increment of time from a mass balance over the films engulfed and deposited by the slug. A slug is considered to have broken if its length becomes zero.

Film Deposition Behind a Slug

The thickness of the films left behind a slug is first estimated using the methods of Wallis (6). This calculation requires the simultaneous solution of an equation derived from continuity considerations

$$\frac{j_f'}{V_\infty} = \left(1.2\,\frac{j}{V_\infty} + 1\right)\left(1 - 2\,\frac{\delta}{D}\right) - \frac{j}{V_\infty} \qquad (137)$$

and the appropriate laminar or turbulent equation for film thickness as a function of film flow rate taken from the data of Belkin (76):

$$\frac{j_f'}{V_\infty} = 190\,\left(\frac{\delta}{D}\right)^{1.5}\ \mathrm{Re}_\Gamma \geq 3500 \qquad (138)$$

$$\frac{j_f'}{V_\infty} = 3.85\,N_f\,\left(\frac{\delta}{D}\right)^3 \qquad \mathrm{Re}_\Gamma < 3500 \qquad (139)$$

Solving these equations by hand is best accomplished using the graphical method illustrated in Fig. 11. The intersection of Eq. (137) with Eq. (138) or (139) yields both

the superficial film velocity, j_f', and the asymptotic film thickness δ. The computer program uses a guess-and-step routine to get this same result. Figure 12 shows how this model of slug motion and film deposition compares with the real situation. The rise velocity of the slug at any starting point "z" is computed from the known volumetric flow rate at "z." The slug is moved the appropriate distance over the current interval of time and its asymptotic film thickness is calculated. This process effectively squares off the slug by ignoring the shape of the slug nose and assuming that the region of accelerating films immediately below the slug nose is negligible.

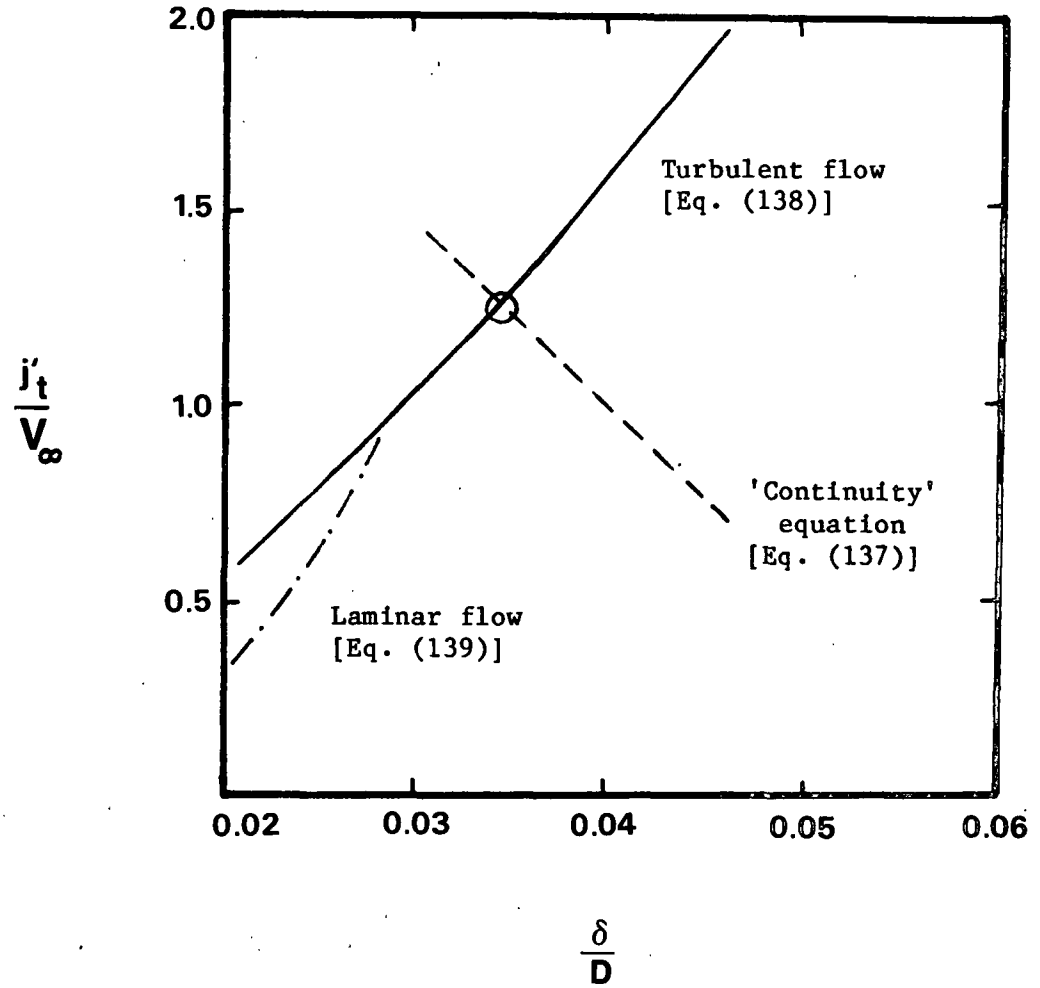

Figure 11. Graphical method for estimating film deposition thickness and flow rate behind a rising slug [Wallis (6)]. The intersection of the "continuity" equation and the laminar or turbulent film flow equation yields the film thickness and superficial velocity.

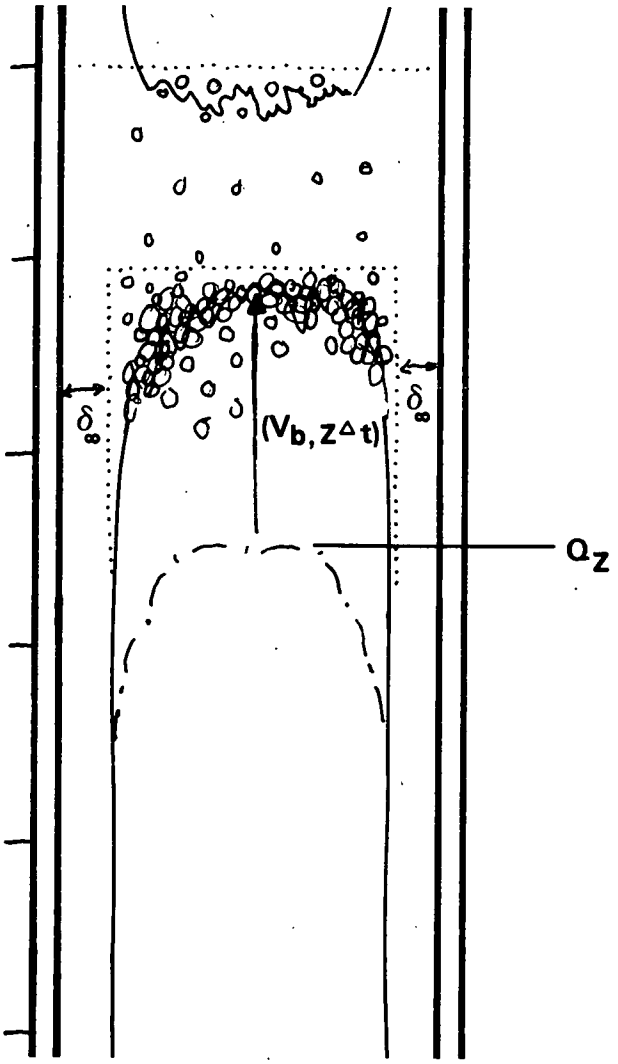

Figure 12. The model squares off the slug nose by ignoring the shape of the slug nose and the region of accelerating films below the slug nose.

The film thickness calculated in this manner is only valid at low vapor flow rates (Fig. 13). At higher vapor flow rates, the film thickness is limited by the effects of the counterflow of vapor. If the film is too thick, part of the film will be entrained upward by the vapor, leaving a much thinner film on the wall. This process is known as flooding, and flooded slug flow may be called "churn flow." According to the Wallis (91) empirical correlation, flooding will occur when

$$j_f^{*1/2} + j_g^{*1/2} > C \tag{140}$$

where

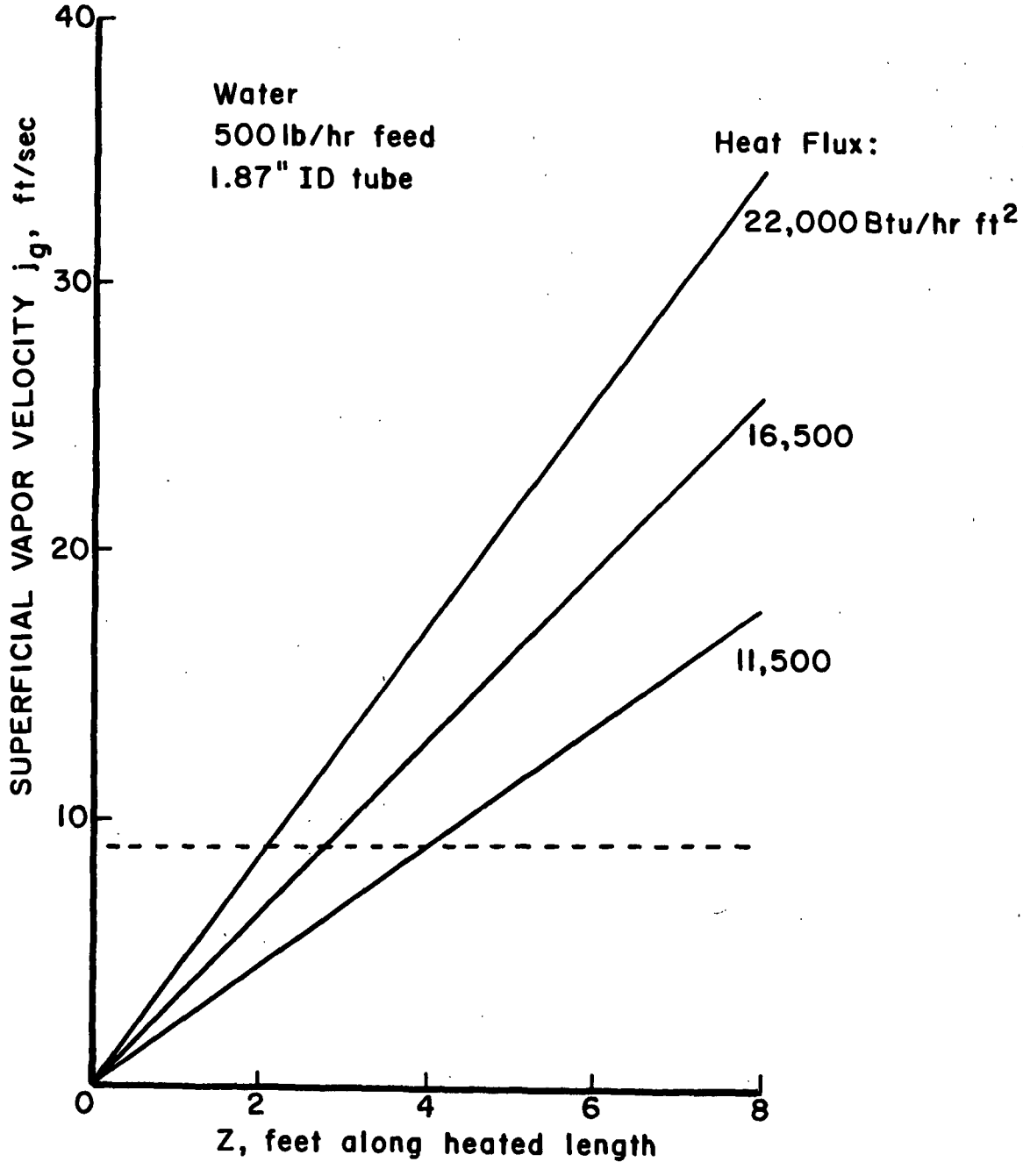

Figure 13. The vapor flow rate at the flooding point compared with the superficial vapor velocities obtained along an electrically heated tube (1.87-inch ID) at several heat flux conditions. Water fed at 500 lb/hr entering the tube at its saturation temperature.

$$j_f^* = j_f \rho_f^{1/2} [g_c D (\rho_f - \rho_g)]^{-1/2} \quad (141)$$

and

$$j_g^* = j_g \rho_g^{1/2} [g_c D (\rho_f - \rho_g)]^{-1/2} \quad (142)$$

The constant C is between 0.88 and 1.0 (Fig. 14). Flooding begins when C = 1.0, but to stop flooding in a flooded system, the liquid flow rate must be reduced until C = 0.88. Thus, the maximum film flow rate which will fall without flooding in a system which has been flooding may be calculated from the following series of equations:

$$j_f^* = (C - j_g^*)^2 \quad ; \quad C = 0.88 \tag{143}$$

$$j_f = j_f^* \, V_\infty / 0.345 \tag{144}$$

$$\Gamma = j_f \, \rho_f \, (\pi \, D^2/4) / \pi \, D = j_f \, \rho_f \, D \tag{145}$$

$$Re_\Gamma = 4\Gamma/\mu_f \tag{146}$$

and

$$\delta/D = 0.909 \, Re_\Gamma^{1/3} \, N_f^{-2/3} \quad , \; Re_\Gamma < 1000 \tag{147}$$

or

$$\delta/D = 0.063 \, Re_\Gamma^{2/3} \, N_f^{-2/3} \quad , \; Re_\Gamma > 1000 \tag{148}$$

where

$$N_f = [D^3 \, g_c \, (\rho_f - \rho_g) \, \rho_f]^{1/2} \, \mu_g^{-1/2} \tag{149}$$

In churn flow, flooding probably looks like the sketch in Fig. 15(a). The slug deposits an excessively thick film, part of which is blown back into the nose of the slug. The flooding process probably takes a finite amount of time, during which the films jiggle up and down with a net upflow. Eventually, the film emerges at less than its critical flooding thickness calculated from Eq. (147) and (148) and falls freely without interference from the counterflow of vapor. In the model [Fig. 15(b)], the flooding process is assumed to occur instantaneously immediately behind the slug so that the film is deposited at its critical flooding thickness. Ignoring the time the films spend in a jiggling film state leads to overestimation of the amount of backflow in the films and is the most serious flaw in the model. Unfortunately, there is no reliable method to account for the fact that flooding is not completed instantaneously.

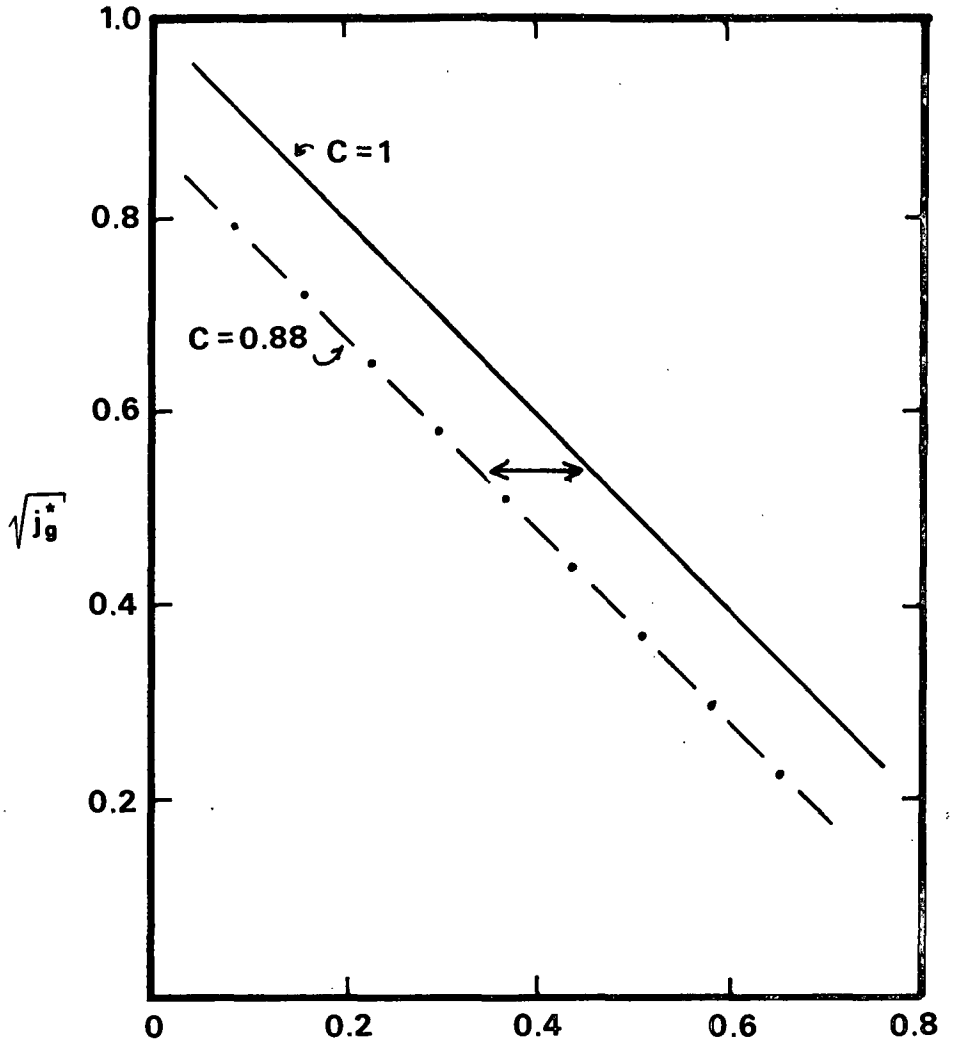

$$j_f^* = j_f \rho_f^{1/2} [g_c D (\rho_f - \rho_g)]^{-1/2} , \quad j_g^* = j_g \rho_g^{1/2} [g_c D (\rho_f - \rho_g)]^{-1/2}$$

Figure 14. Wallis (91) plot of flooding data.

In a system with solids content, the concentration in the newly deposited films must be calculated as well as the film thickness. In the model (Fig. 16), new films are deposited at the concentration of the slug at the start of the time increment, before it has been moved. After the slug has been moved, the contents of the

engulfed films are added to the contents remaining in the liquid lump, and the concentration of the slug is recalculated. Since the increments of length and time are very small, this procedure simulates near-perfect mixing. The actual mixing characteristics of the slug are unknown.

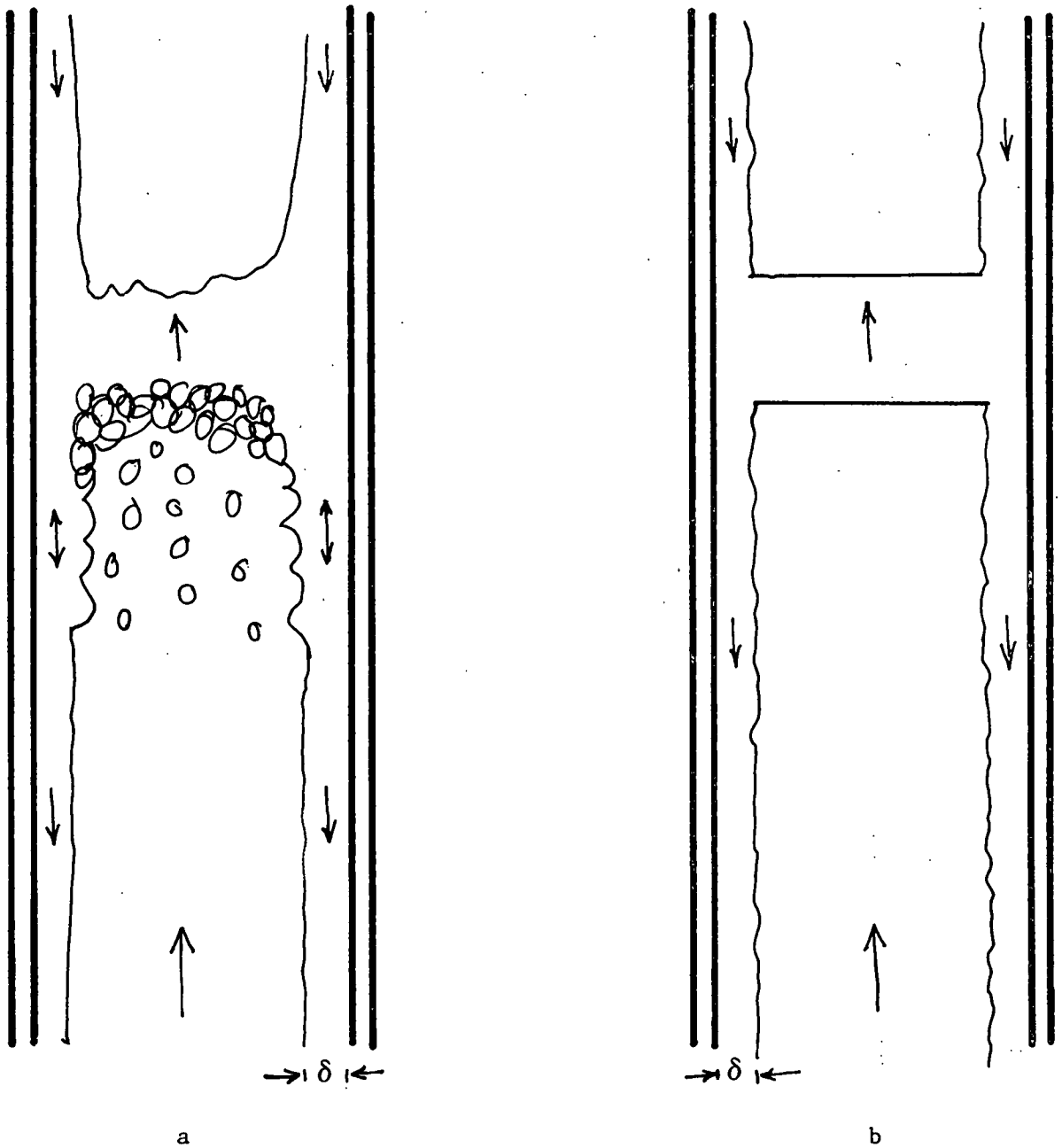

Figure 15. (a): Flooding in "real" system with jiggling gilms.
(b): Flooding in model. Flooding is instantaneous and the effects of jiggling films are ignored.

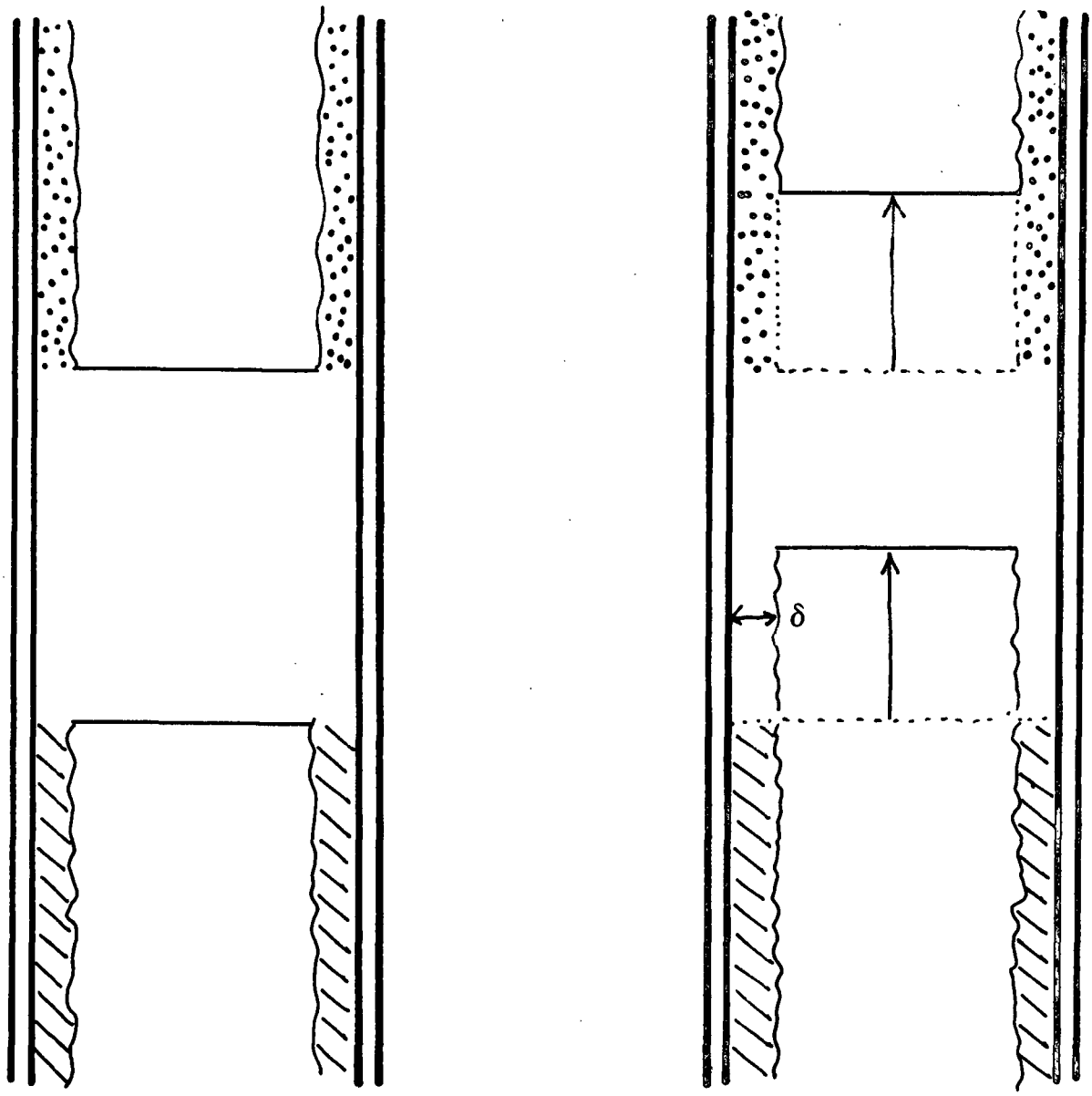

Figure 16. Slug movement in the model. Films are deposited at the concentration of the slug before it is moved. The engulfed film (dots) is added to the slug contents after the move.

Film Drainage

During the current increment of time, all the slugs in the tube have been located, their velocity and location at the end of the time increment have been calculated, and the thickness of film laid down by each slug over the length it has moved during the time increment has been estimated. Next, all the films in the tube, both newly deposited and "old," must be allowed to drain. Film drainage is

computed as follows (Fig. 17). The film thickness in each increment of length is known, either as a new deposition thickness or as a result of the drainage calculations of the previous increment of time. From the known film thickness in any increment of length, the corresponding film Reynolds number can be calculated using the Belkin (79) correlation.

$$\delta^* = \delta \, g_c^{1/3} \, (\rho_f - \rho_g)^{1/3} \, \rho_f^{1/3} \, \mu_f^{-2/3} \tag{150}$$

$$Re_\Gamma = (\delta^*/0.909)^3 \quad , \; Re_\Gamma < 1000 \tag{151}$$

or

$$Re_\Gamma = (\delta^*/0.063)^{1.5} \quad , \; Re_\Gamma > 1000 \tag{152}$$

where

$$Re_\Gamma = 4\Gamma/\mu_f \tag{153}$$

This film Reynolds number will be used in calculating the heat transfer coefficient, as well as providing the film flow rate for the length increment. A mass balance is then performed over the increment of length in question. The amount of liquid which flows out of this section of film during the current increment of time is calculated from the film Reynolds number and set aside.

$$W_{out} = Re_\Gamma \, (\mu_f/4) \, \pi \, D \tag{154}$$

The amount of evaporation from the increment of film over the increment of time is then calculated. Finally, the flow into the given length increment from the next higher length increment is added to the remaining contents of the given length increment.

$$W_{film,new} = W_{film,old} + W_{in} - W_{out} - W_{evaporated} \tag{155}$$

The contents of the length increment are then well mixed, and the new concentration in the increment is calculated and stored. The new thickness of the increment of film is calculated from the change in volume of liquid in the increment computed from the mass balance.

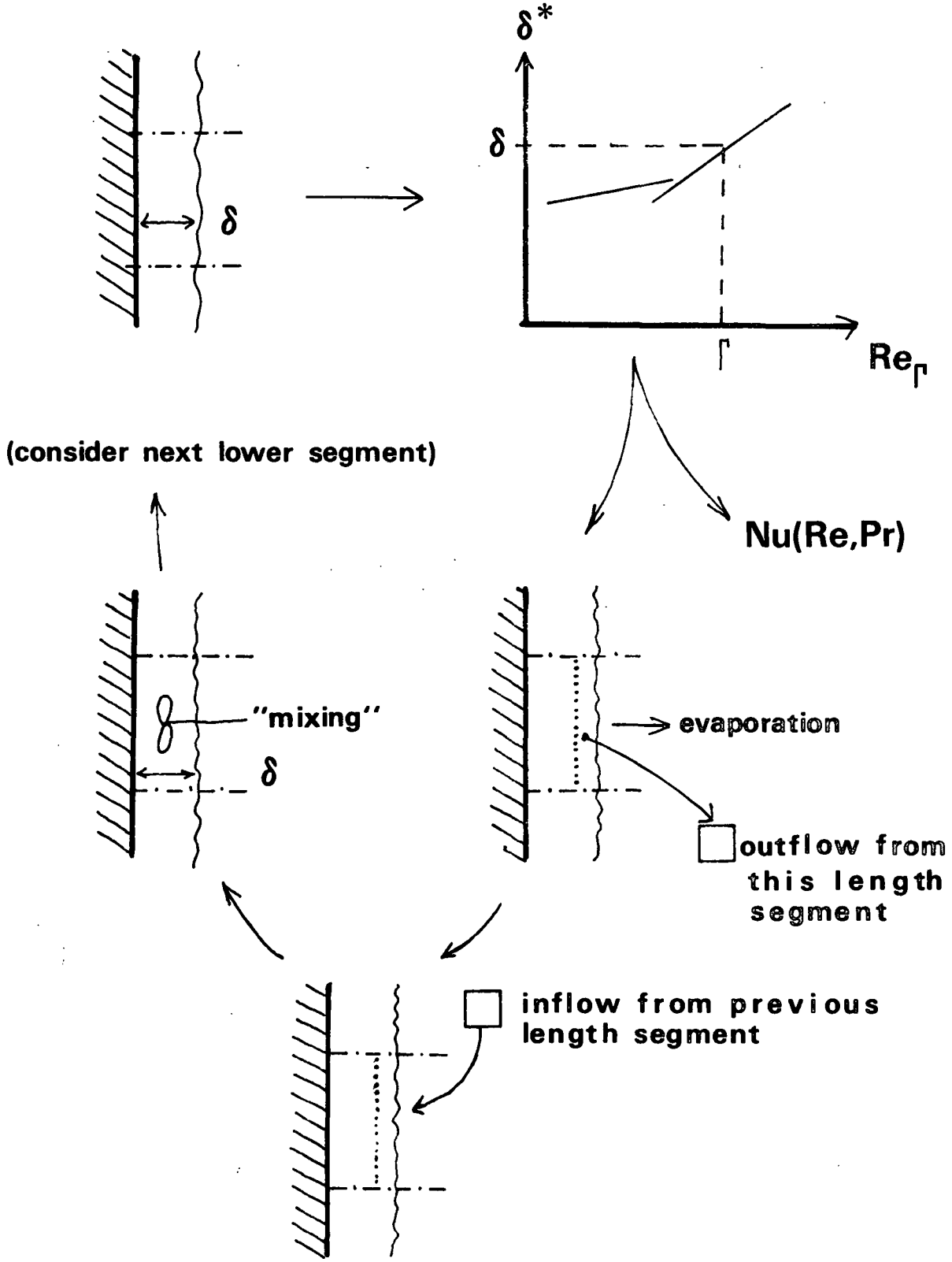

Figure 17. Film drainage from an increment of length calculated from the film thickness in the increment by a mass balance over the increment length, using the Belkin (79) correlation to estimate the flow out of the increment.

Then, the next lower increment of length is considered. The cycle sketched in Fig. 17 is repeated for this increment of length, and the flow rate out of the increment just considered becomes the flow rate into the current increment of length. After repeating this process for every increment of length, the film Reynolds number and updated thicknesses and concentrations are known for each increment of length.

Estimation of the Heat Transfer Coefficient

The empirical correlation for heat transfer to evaporating falling films developed by Chun and Seban (81) was used to relate the film Reynolds number of a length increment to the heat transfer coefficient of the increment. This correlation is graphed in Fig. 18. For laminar flow, this correlation predicts

$$h = 0.606\ (k_f^3\ g_c/\nu_f^2)^{1/3}\ (Re_\Gamma/4)^{-0.22} \tag{156}$$

and for turbulent flow

$$h = 0.0038\ (k_f^3\ g_c/\nu_f^2)^{1/3}\ Re_\Gamma^{0.4}\ Pr_f^{0.65} \tag{157}$$

The laminar-turbulent transition is given by

$$Re_{\Gamma,\ transition} = 5800\ Pr_f^{-1.06} \tag{158}$$

If a given length increment contains a slug rather than a section of falling film, the heat transfer coefficient is estimated using the Dittus-Boelter equation

$$Nu = 0.023\ Re^{0.8}\ Pr^{0.4} \tag{159}$$

with the slug rise velocity (j_b) taken as the characteristic velocity in the Reynolds number.

At this point in the model calculations, the heat transfer coefficient has been estimated for each increment of length at the current increment of time. To obtain average heat transfer coefficient values, a series of time increments must be

observed. For each increment of time, the entire process of moving slugs, calculating film deposition thicknesses, allowing the films to drain, and estimating the heat transfer coefficients is repeated. The most relevant average heat transfer coefficient is that defined over a single slug cycle, defined as the time between two successive slugs leaving the tube. In a system with solids content, the model must continue through many slug cycles until the average concentrations in the films approach their steady state value.

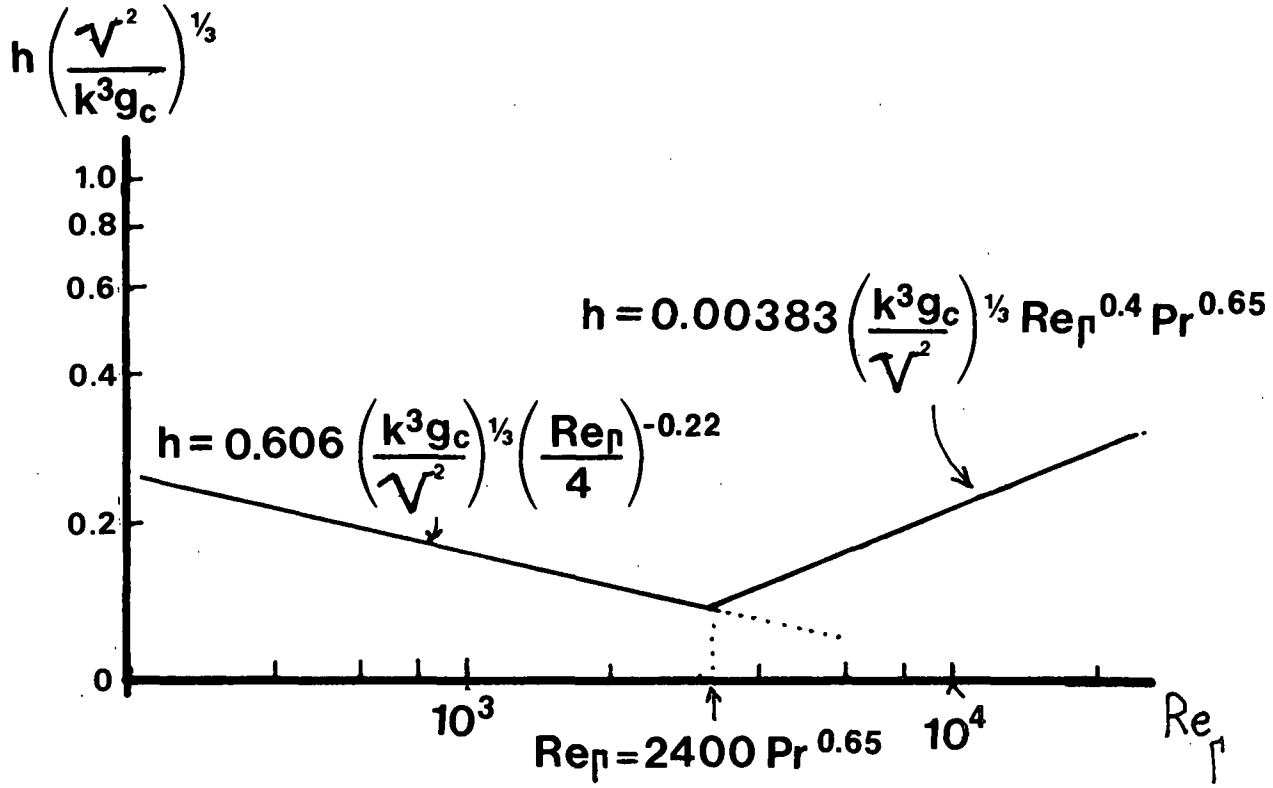

Figure 18. The Chun and Seban correlation for heat transfer to evaporating falling films.

CONCLUSION

A simple numerical model for slug and churn flow heat transfer has been developed by combining published semiempirical correlations for the motion of vapor bubbles and the deposition of films behind such bubbles. These correlations have been extrapolated beyond the limits of their data base by applying them to a boiling

system; however, they represent the best available information for this type of flow and will help us understand the influence of various variables on slug and churn flow heat transfer. The most serious conceptual defect in the model is the method used to account for flooding, which assumes that the flooding process is completed instantaneously, leaving an undisturbed film immediately behind the slug nose. It is known that the flooding process is not completed instantaneously, and that the films spend much of their lifetimes jiggling up and down in flooding hysteresis loops. The model thus overpredicts the amount of downflow. There is too little known about the flooding process to be able to correct for the effect of jiggling films.

EXPERIMENTAL

INTRODUCTION

Accurate measurements of local inside film heat transfer coefficients were needed to evaluate the heat transfer mechanisms discussed in the previous chapters. To meet this demand for accurate measurements of heat transfer, a new, electrically heated pilot evaporator was designed and built. This chapter is a description of the design and operation of this pilot evaporator.

PRINCIPLES OF THE DESIGN OF THE PILOT EVAPORATOR

Accurate measurements of heat fluxes and inside wall temperatures are the first requirement of any careful heat transfer study. Making either of these measurements in a steam-heated evaporator is a difficult experimental problem. The present pilot evaporator was therefore electrically heated, using the wall of the evaporator tube as a resistance heater. There are problems with electrically heated systems, since the heat flux is not necessarily constant over time due to line voltage fluctuations, or along the tube, due to variations in the thickness and electrical resistance of the tube walls. Nevertheless, the heat fluxes in an electrically heated system are more easily measured and much more reproducible than those in a steam-heated system. Inside tube wall temperatures are calculated from the measured outside wall temperatures using a conduction equation. The thermocouples which measure the outside wall temperature are easily soldered onto the evaporator tube. The most serious problem with electrical heating is electrical interference to thermocouple readers, pressure transducers, and other instruments. This problem may be overcome by choosing instruments with exceptionally good noise rejection and, when possible, by isolating the instruments from the experimental apparatus.

Other features of the pilot evaporator built for this study included forced convection flow to insure good control of the feed rate, and fiber optical phase detection probes and dye tracer equipment for studying flow patterns.

The materials and dimensions of the apparatus were chosen to duplicate the typical black liquor evaporator, which is constructed of two-inch (5.08 cm) nominal outer diameter stainless steel tubing. The electrical heating system provided heat fluxes up to 22,000 Btu/hr ft^2 (69.4 kW/m^2). This maximum heat flux is slightly higher than the heat fluxes found in industrial black liquor evaporators. All pipework was of stainless steel to resist the corrosive effects of black liquors.

DESCRIPTION OF THE APPARATUS

PIPING AND ELECTRICAL SYSTEMS

In the following section, the pilot evaporator will be described component-by-component. First, the flow loop will be discussed, and then the design of the electrical heating system will be reviewed. Finally, the installation of the temperature and pressure sensors will be described.

The Flow Loop

A flowsheet of the apparatus is presented in Fig. 19. The letters in parentheses refer to locations on this flowsheet.

Test liquors are made up in the delivery tank (a), a 100-gallon (379 liter) stainless steel tank equipped with a steam coil for heating and a "Lightnin" mixer. The liquids are pumped from the delivery tank by an Eastern Industries type U-34-D centrifugal pump (b). For most runs, the flow rate was measured by either of the two rotameters (c), one with a zero to one gallon per minute (3.70 L/min) range, and the other zero to 4.7 gallons per minute (17.8 L/min). A Foxboro magnetic flow meter was used to measure and control the flow rates for the black liquor runs. The

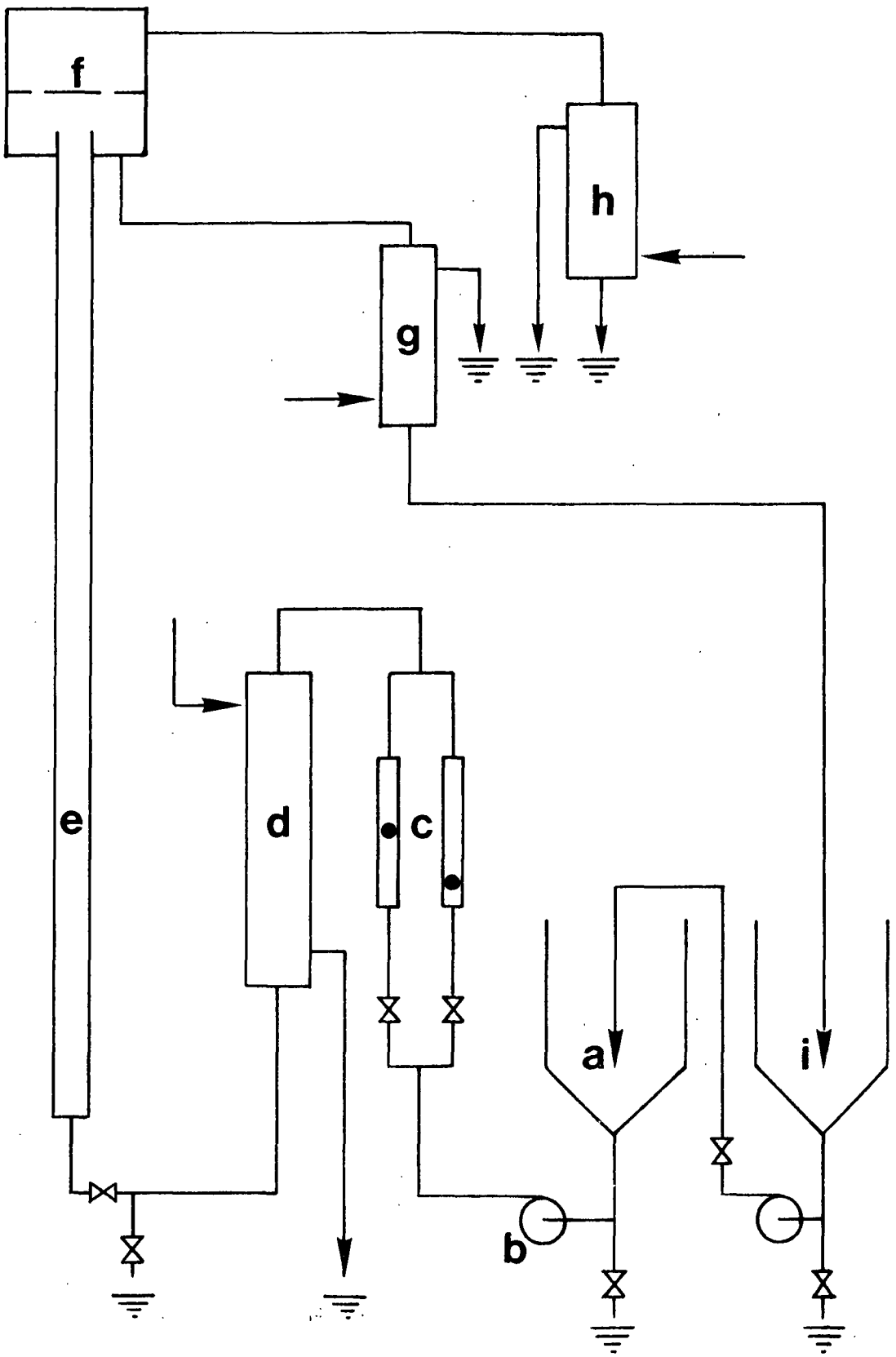

Figure 19. The flow loop.

control valve for the flow rate is located downstream from the rotameters and the steam-heated preheater (d) to keep a back pressure on the preheater to discourage boiling in the preheater. The test section (e) is a ten-foot (3.05 meter) piece of typical black liquor evaporator tubing. It is a type 304 stainless steel tube of two-inch (0.051 m) nominal outside diameter and 0.065-inch (1.65×10^{-3} m) wall thickness. The test liquid is evaporated in the test section, and the liquid-vapor mixture which results is separated in the vapor head (f). The vapor is condensed in a water-cooled heat exchanger (h), and the condensate is collected and measured. The liquid is cooled in another water-cooled heat exchanger (g), and is collected in a 100-gallon (379 liters) receiving tank (i). At the end of a run, the receiving tank contents are pumped back into the supply tank (a). The apparatus is a once-through system. Test liquids were made up to the desired concentration before each run.

The Electrical Heating System

A sketch of the electrical system is presented in Fig. 20.

The heat to effect evaporation in this pilot evaporator is provided by alternating current resistance heating. The tube walls (a) serve as resistance heaters. Electricity is delivered to the tubes by brass clamps (b) bolted around the tube. The clamps are located eight feet (2.4 meters) apart. Two parallel, one-inch (2.54 centimeter) square copper bus bars connect the clamps to the transformer (d). Flexible sections of copper braid allow for thermal expansion in the apparatus. Teflon spools (c) at either end of the test section insulate the rest of the piping system from the electrical heating loop, as well as providing some leeway for thermal expansion of the test section.

The transformer (d) is a low voltage, high amperage secondary type built on special order by Tech Tran Corporation. It is an open-type Class 220 transformer

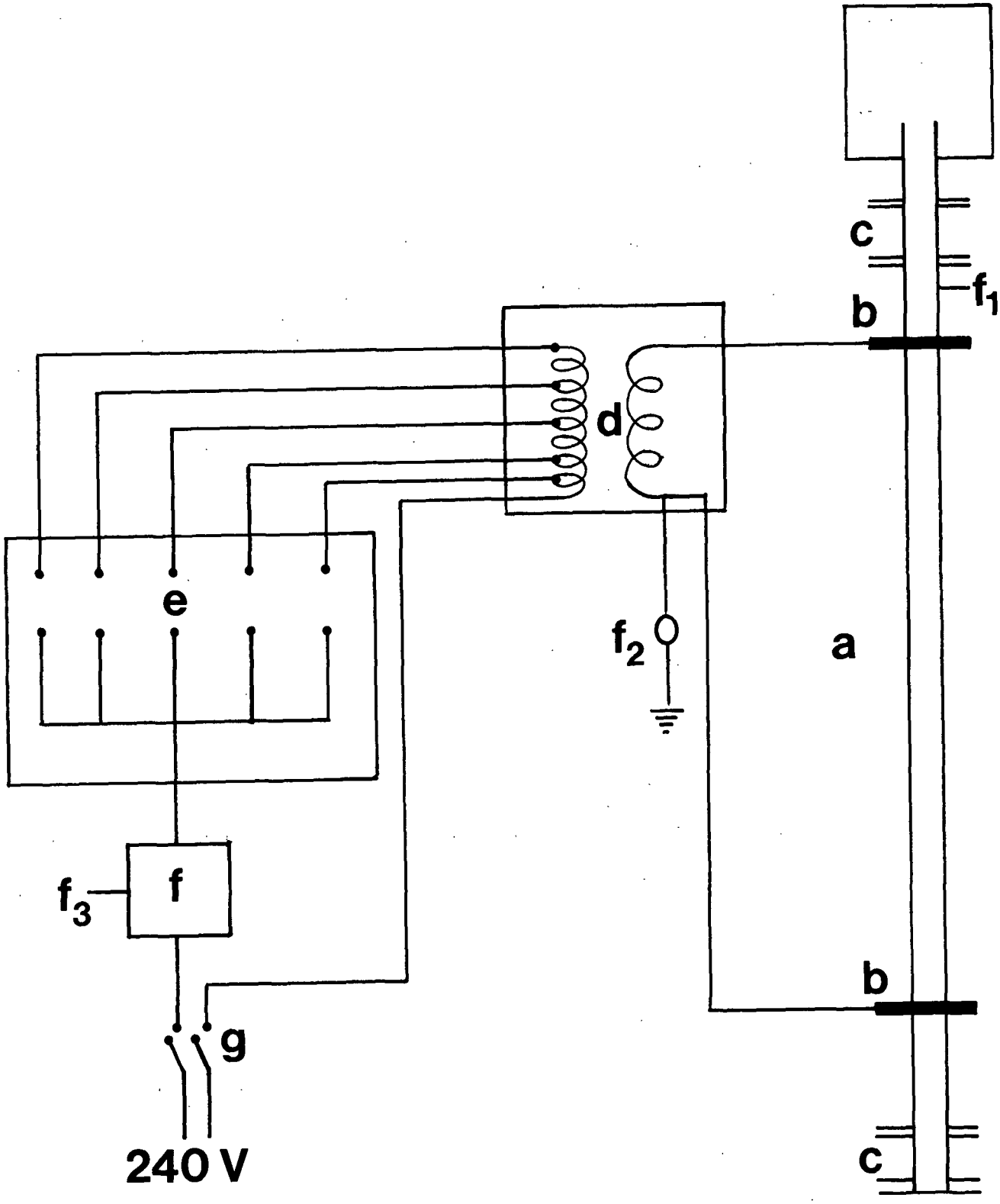

Schematic of Electrical Heating System

Figure 20. The electrical heating system.

which operates with its primary fed by 240-V, 1-phase, 60-Hz current. Taps on the primary side give voltages to the test section of 6, 8, 10, 12, and 14 V at loads of up to 2000 amp. The voltage is selected by putting a fuse into the appropriate socket in the fuse box (e).

The electrical system includes several safety devices connected to a circuit breaker (f). A bimetallic thermostat (f_1) is clamped onto the tube by hose clamps. It throws the breaker if the tube wall temperature exceeds 300°F (149° C). A coil to ground (f_2) defends against the possibility of a short between the primary and secondary sides of the transformer. The coil trips the breaker to prevent 240-V current from entering the apparatus. The circuit breaker also serves two remote shut off buttons (f_3). Power to the system is fed through a main switch and protective fuses (g).

Mounting of the Temperature and Pressure Sensors

Figure 21 illustrates how the important sensors were mounted in the apparatus. The detailed specifications of the instrumentation are discussed in a later section.

The outside wall temperatures are measured by iron-constantan thermocouples (a) soldered to the outside of the tube wall. There are ten such thermocouples along the middle six feet (1.83 meters) of the eight-foot (2.4 meters) heated section - one every eight inches (0.203 meters). The thermocouples are selected by a switch and read by an Omega digital thermocouple reader. The inside wall temperature (T_w) is calculated from the measured outside wall temperature (T_o) by a conduction equation derived in Appendix II.

The fluid temperature (T_f) is measured by a traveling thermocouple (b) which, with the attached air-purged pressure probe (c), may be pulled up the tube by the Teflon tubing which protects the thermocouple lead wires and pressure probe air supply. The traveling thermocouple was originally built for the experimental work

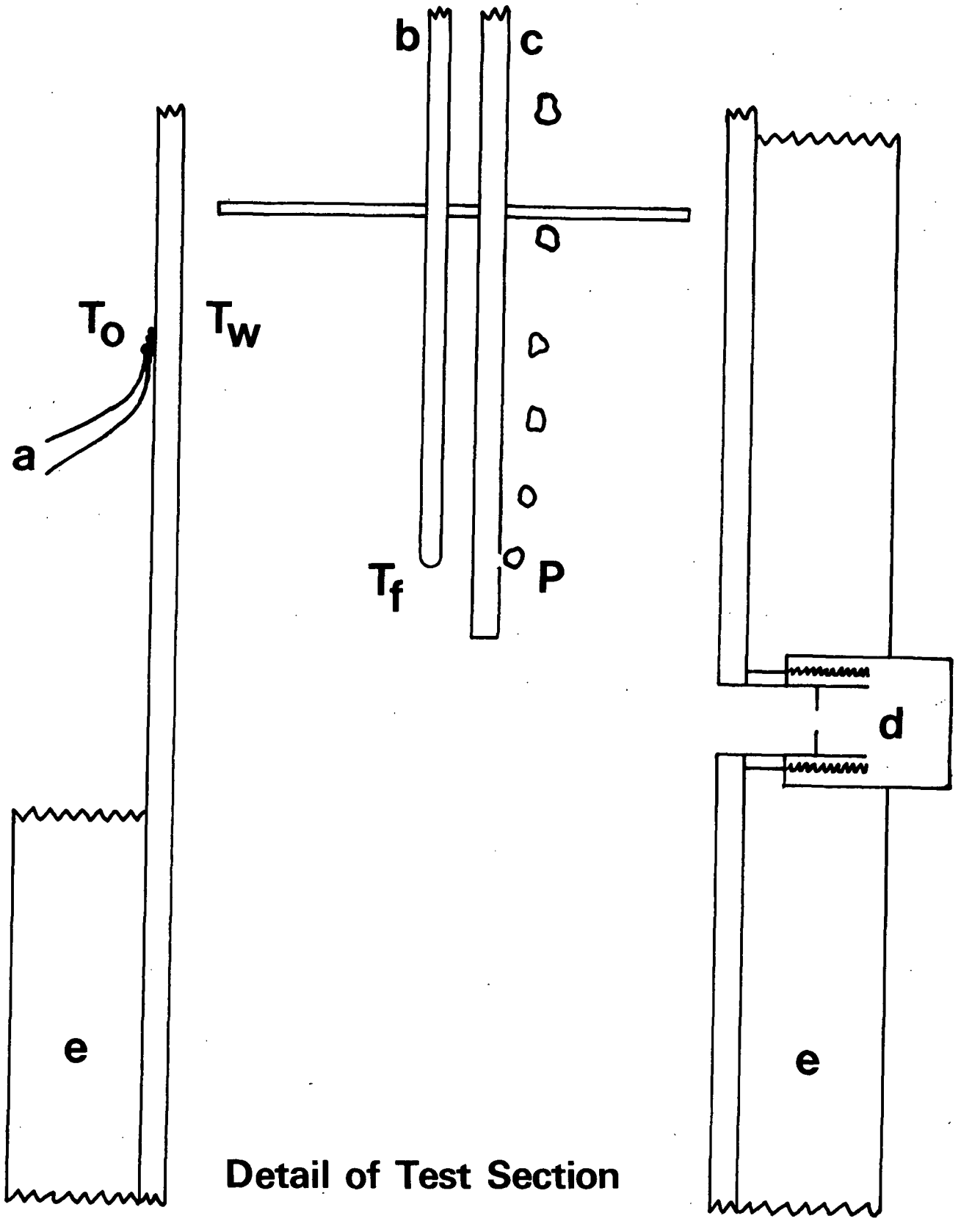

Figure 21. Detail of the test section.

of ± 0.7°F (0.4°C). The manufacturer's estimate of maximum instrument error over a three-month period is ± 1.2°F (0.67°C). The 2170 A includes internal reference junction compensation and automatic zero correction. It does not provide any way for the user to adjust the calibration or zero point. It measures average temperature values at the rate of 2.5 readings per second.

The calibration of the thermocouple reader was checked for all ten wall thermocouples and the traveling thermocouple probes in an ice bath and a boiling distilled water bath against an NBS-certified, mercury-in-glass thermometer. The readings were all within 0.2°F (0.11°C) of the bath temperatures. Hence, the accuracy of the outside wall temperature and fluid temperature measurement is ± 0.2°F.

The inside wall temperature is calculated from the outside wall temperature by a conduction equation

$$T_w = T_o - \frac{a\ q}{k_{ss}\ (b^2 - a^2)} \left(\frac{a^2 - b^2}{2} + b^2 \ln \frac{b}{a}\right) \tag{160}$$

where b is the radius of the outside of the pipe wall and a is the radius of the inside of the pipe wall. This equation is derived in Appendix IV. Substituting the nominal tube radius and wall thickness values and taking the thermal conductivity of type 304 stainless as k_{ss} = 9.4 Btu/hr ft °F from Peckner and Bernstein (92), this equation becomes

$$T_w = T_o - 2.847 \times 10^{-4}\ q \tag{161}$$

Assuming that the major error is in the heat flux measurement rather than in the nominal tube dimensions and thermal conductivity, or in thermocouple errors such as contact resistance or the uncertainty in the exact location of the thermocouple junction on the tube wall, the 22,000 ± 500 Btu/hr ft^2 (69.4 ± 2 kW/m^2) heat flux case would yield a temperature drop through the wall of between 6.4 and 6.1°F (3.6

to 3.4°C), and 0.3°F (0.16°C) uncertainty. Adding this to the measurement error of 0.2°F, the total error in the worst case is about 0.5°F. Since the slugging flow in the tube produces heat transfer oscillations which lead to measured wall temperature fluctuations of 1.0°F (0.6°C) or more, the worst error in the temperature measurement comes from the visual averaging of fluctuating readings rather than instrument error. This error will be approximately the magnitude of the temperature fluctuations, usually ± 1.0°F (0.6°C).

Flow Measurement

Although the flow was monitored by either rotameters or by the Foxboro magnetic flow meter, the primary standard is a 5-gallon (18.9 liter) bucket-and-stopwatch method. The contents of the bucket were weighed to the nearest quarter pound (± 0.11 kg), and the stopwatch could be read to the nearest 0.2 second. The interval of time was at least one minute. This leads to a flow measurement error of about 15 lb/hr (6.8 kg/hr) in the worst case. The flow in the system was reasonably stable. The rotameters indicated fluctuations of ± 25 lb/hr (11.34 kg/hr) over a typical hour run.

Pressure Measurement

The traveling pressure probe is of the same type described by Fong, King, and Sephton (93,94). The probe itself is a 1/8-inch (3.2×10^{-3} m) diameter stainless steel tube. The end of the tube was soldered shut and then a 1/16-inch (1.6×10^{-3} m) hole was drilled in the side of the tube just above the closed end. A very slow flow of air, measured by counting bubbles, keeps the probe clear of steam and liquid. The probe air system is sketched in Fig. 22. The air flow rate, corresponding to one 1/4-inch (6.4×10^{-3} m) diameter bubble per second, is provided from the Institute air lines via an air regulator. The pressure in the line is measured by a Pace Validyne DP 15 TL differential pressure transducer with a 5-psi stainless steel diaphragm, read by a Validyne model CD 12 transducer indicator. The indicator reads

to ± 1% of full scale, which corresponds to ± 5 x 10^{-2} psi (2.58 mm Hg). The pressure transducer/indicator was calibrated against a mercury manometer before each run.

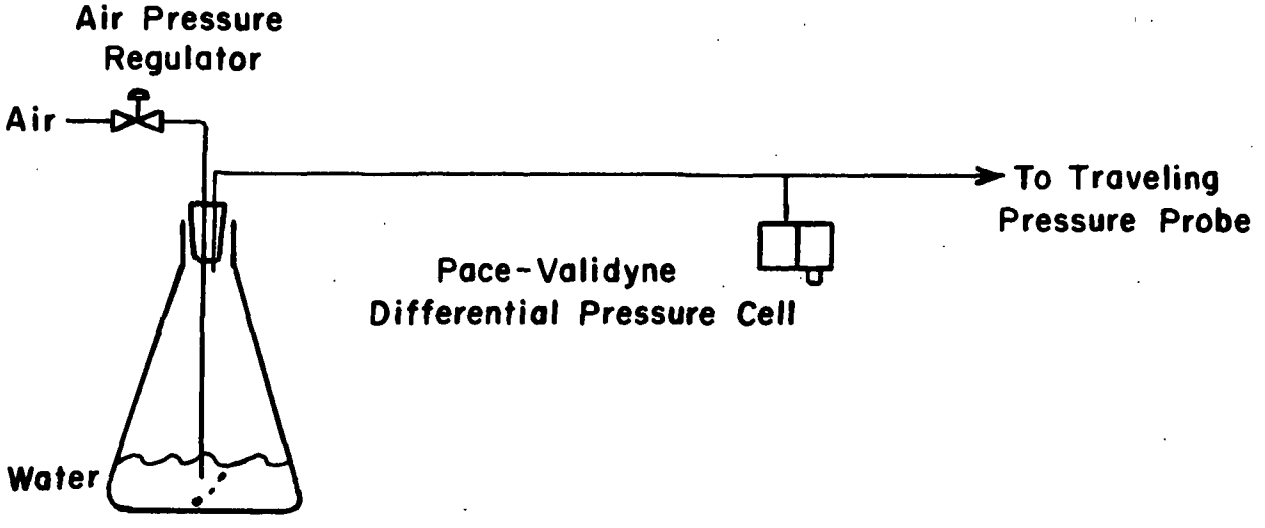

Figure 22. Air purge system for the traveling pressure probe.

Calculation of Heat Flux

The heat flux in an electrically heated evaporator can be calculated from the wattage consumed by the evaporator. A wattmeter and digital voltmeter were included in the original instrumentation of this apparatus. Unfortunately, the voltmeter was strongly influenced by the path to ground provided by the test liquids and could not be used. The wattmeter was mounted on the primary of the transformer and required calibration to correct for electrical losses in the transformer and bus bars. The heat flux had to be measured by the second-best method of measuring the temperature rise of test liquids pumped through the heated test section. The traveling thermocouple was used to measure the inlet and exit temperatures. Room-temperature test liquids were pumped through the electrified section at high rates, 1000 lb/hr (454 kg/hr) or more. Since the feed temperature was steady, the major temperature measurement error came from the oscillations in the exit temperature, which were generally about ± 0.6°F (0.33°C). The flow rate measurement error is about ± 25 lb/hr (11.3

kg/hr), as discussed in "Flow Measurement." As a result, the error in heat flux measurement on a 22,000 Btu/hr ft^2 heat flux is about $\pm$ 500 Btu/hr ft^2 (1.6 kW/m^2).

The Overall Error of the Heat Transfer Coefficient

From the errors in heat flux ($\pm$ 500 Btu/hr ft^2, 1.6 kW/m^2) and temperature drop [0.2°F (0.11°C) for the liquid temperature, 1.0°F (0.6°C) for the wall temperature], we can estimate that the heat transfer coefficient error for the 22,000 Btu/hr ft^2 case is about $\pm$ 100 Btu/hr ft^2 °F (0.14 kW/m^2 °K) for a heat transfer coefficient of about 1500 Btu/hr ft^2 °F (2.2 kW/m^2 °K).

Fiber Optics

Since most of the argument in this thesis is based on considerations of flow patterns, a limited flow pattern identification study was carried out. The fiber-optical phase detection probe was chosen for this work because the equipment was already available at the Institute. A review of other phase detection techniques is available in Hewitt (95). The fiber-optical phase detection technique uses a bifurcated fiber-optic probe having a tip ground and polished to the form of a right-angled cone (Fig. 23). In media of low refractive index, such as air or steam, total internal reflection occurs at the probe tip, and the light is returned from the surface of the probe to the detector. If the probe is submerged in a material of high refractive index, such as water, the light leaves the tip, and very little of it is reflected back to the detector. In a two-phase flow, the probe yields a train of square waves whose peaks indicate vapor and whose valleys indicate liquid covering the tip. These wave trains can be analyzed to provide void fraction data and histograms of phase duration for each phase. Miller and Mitchie (96) found that their void fraction readings agreed with quick-closing valve measurements to within $\pm$ ten percent. The orientation of the probe in the flow did not affect the results.

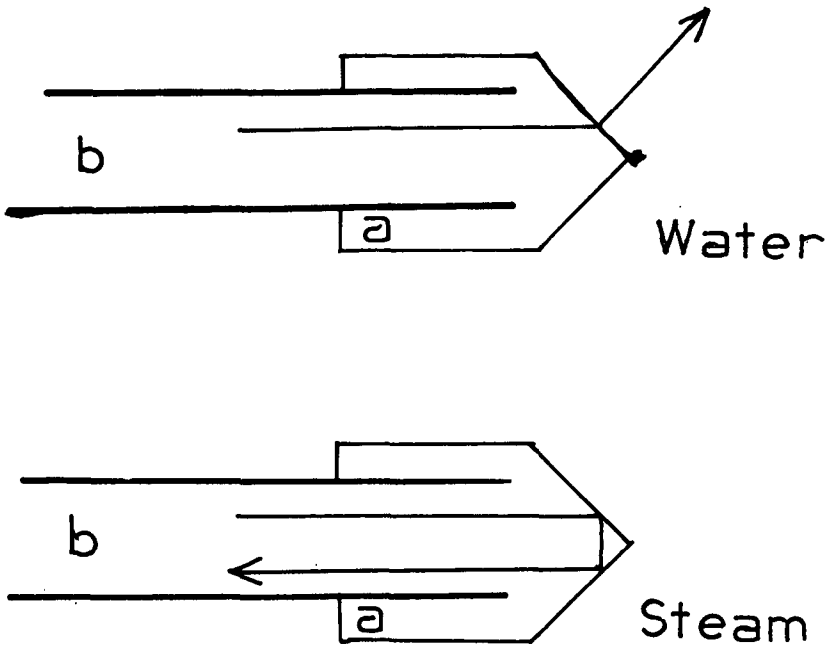

a: conical tip

b: fiber-optic probe

Figure 23. Design of the fiber-optical phase detection probe tip.

The probe available at the Institute was an 1/8-inch (3.18×10^{-3} m) random fiber pattern probe. A conical tip machined from clear Lexan polycarbonate was glued to the end of the probe with clear epoxy. The probe is introduced into the tube through the five access holes on the tube and is perpendicular to the flow direction. This probe cannot detect droplets smaller than 1/8-inch (3.18×10^{-3} m), which is probably a good feature in flow pattern studies, since entrained droplets of liquid will not complicate the signal; however, this compromises the accuracy of the void fraction measurement. The probe is insensitive to the proximity of reflective surfaces while in the gas phase and shows only a weak response when submerged in liquid. Thus, the passage of reflective interfaces does not interfere with the probe signal.

Figure 24 is a sketch of the fiber-optical phase detection and signal processing system. The light which returns from the probe tip is detected by a photocell, and

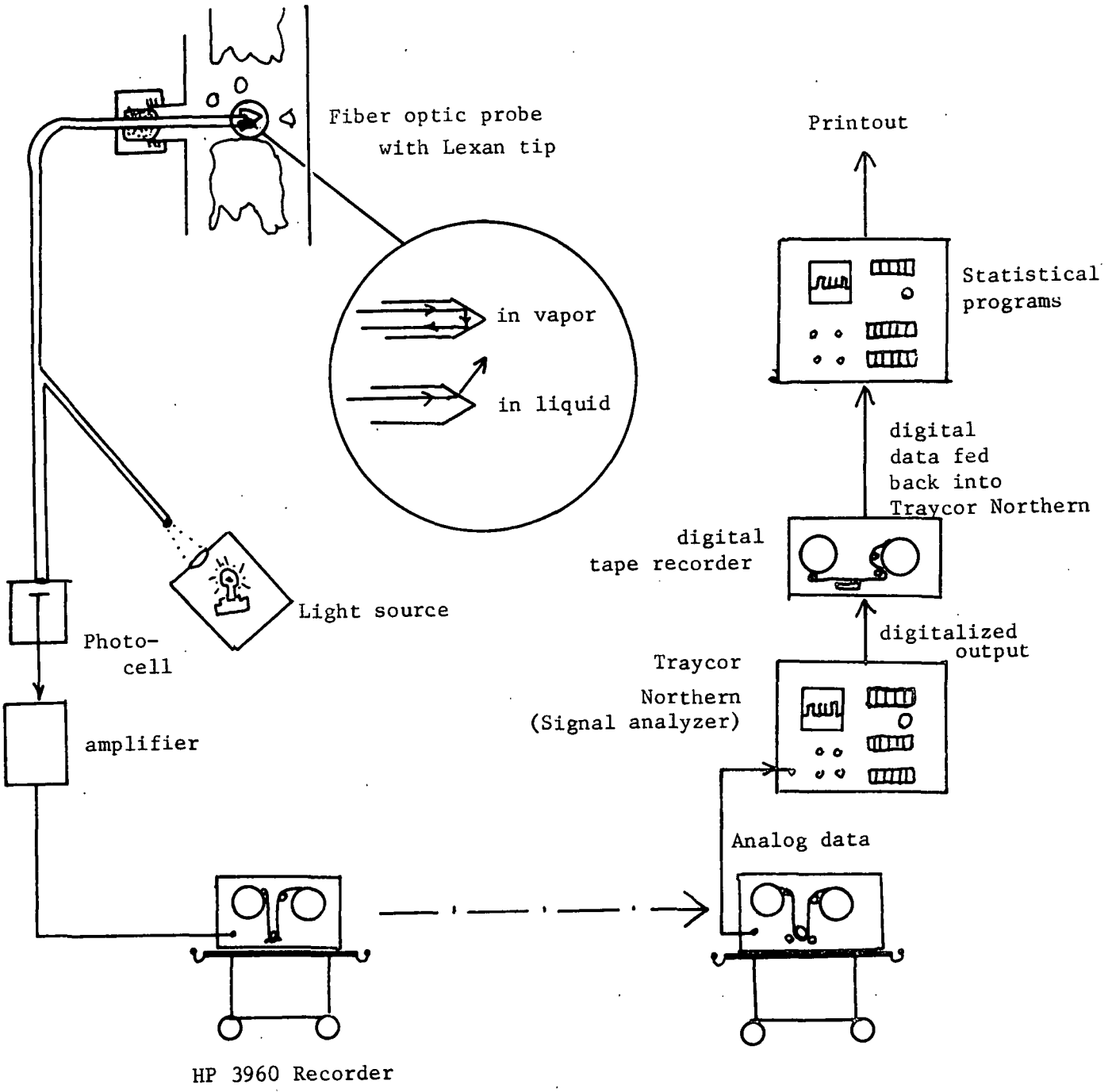

Figure 24. Schematic of the fiber-optical phase detection probe signal processing system.

the signal from the photocell is recorded by a Hewlett-Packard model 3069 instrumentation recorder. The analog signal from this tape is digitalized using a Traycor Northern model 1500 signal analyzer. The BASIC language program for operating the

Traycor Northern 1500 is presented in Appendix III. The program functions by reading the taped signal at two-millisecond intervals and storing these discrete values in a series of memory channels which are then copied onto digital tape. To process the data, the digital tape is read back into the Traycor Northern 1500. A liquid-vapor threshold value is set by inspection of the signal display on the signal analyzer CRT. The BASIC language program steps through the complete set of memory channels, one channel at a time, comparing the channel contents with the threshold value. The program sorts each "above" or "below" reading into a system of accumulators, which is described in the printout (Appendix IV). The program returns an average void fraction and histograms of vapor and liquid phase duration. Sixty-One and four tenths seconds of real time were analyzed for each run.

The correctness of the program was checked by generating and processing artificial signals. These signals were produced by rotating a toothed cardboard disc between the light source and the supply branch of the fiber-optical probe. A sketch of one such disc together with the program printout and known characteristics of the signal is presented in Appendix V. The agreement is very good, the discrepancies probably being the result of irregularities in the rotation rate of the disc, which was driven by a variable speed drill.

At each access port along the tube, five readings were taken at radii 0 (center line), 0.38, 0.66, 0.78, and 0.89 inch (0, 9.6, 16.8, 19.8, and 22.6 x 10^{-3} m), representing the centers of annuli of approximately equal area. Profiles of void fraction and phase duration across the tube could be obtained from these runs.

The fiber-optical probe was destroyed by the potassium carbonate test solutions early in the experimental program, so only data from boiling distilled water and potassium carbonate solutions were obtained.

Dye Tracer

Two simple dye tracer experiments were run using the injection and sampling scheme illustrated in Fig. 25. Dye was pumped into the top access port at a rate of 10 mL/minute by a peristaltic pump. Samples were drawn from the bottom access port after ten minutes of continuous evaporation and dye feed. The concentration of the dye at the bottom access hole was measured using a spectrophotometer and a calibration curve constructed from quantitative dilutions of the dye feed by invoking the Lambert-Beer Law

$$C = -k \log T$$

where T is the measured percent transmittance and k is the optical density of the dye. This was not intended to be a highly accurate experiment, since the pilot evaporator was not designed to permit a sophisticated dye tracer study. The sole purpose of this work was to demonstrate backflow in the tube during slug flow boiling of water and foam flow boiling of 12% by weight potassium carbonate solution.

Viscosity

The only physical property measured in this work was the viscosity of guar gum and sodium carboxymethylcellulose solutions near the boiling point of the solutions. These viscosities were determined in an Ostwald (Cannon-Fenske) number 50 viscometer. The viscometer constant was determined using triple-distilled water near its boiling point. All runs were done with the viscometer immersed in a bath of boiling deionized water. The viscometer was carefully cleaned before each test using hot sulfuric-dichromate cleaning solution followed by distilled water and acetone rinses. The flow time was measured using a stopwatch with 0.2-second resolution.

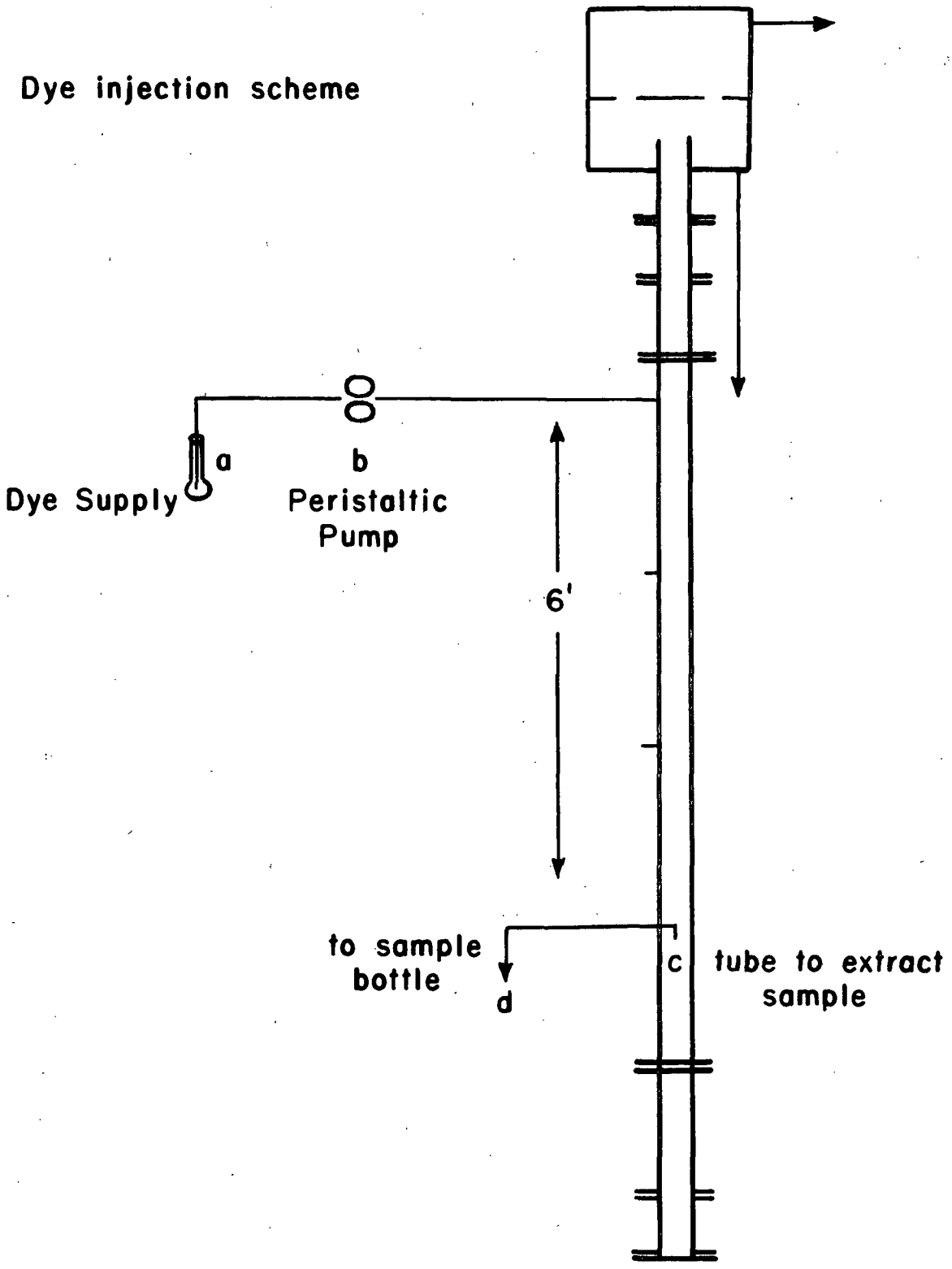

Figure 25. Dye injection and sampling system.

OPERATION OF THE APPARATUS

Degassing

Dissolved gases in evaporating liquids have a drastic effect on nucleate boiling. It is, therefore, good practice to degas test liquids before an experimental evaporator run. In the pilot evaporator, degassing is accomplished by boiling the test liquors before each run. The liquors are heated above their normal boiling point in the preheater and then allowed to flash across the control valve. The test section is electrified during the degassing phase to force further boiling.

Running an Experiment

After a test liquid has been degassed, the actual heat transfer experiment may be run. The feed rate is set to the desired value, and the preheater steam pressure is adjusted until the inlet temperature measured by the traveling thermocouple is just below the local saturation temperature. The power to the tube is then turned on, and adjustments to the flow rate and preheater temperature are made until the conditions at the entrance stabilize. This usually requires between a half and three-quarters of an hour. Then, the traveling thermocouple and pressure probe are pulled up the tube to locations corresponding to the outside wall thermocouples. The temperature and pressure at each measurement site are recorded. After the traveling thermocouple is pulled into the vapor head, the wall temperatures are read by switching to each thermocouple and visually averaging the fluctuating digital readout over about one minute. The average wall temperature and temperature range are recorded. The heat flux is known for the test liquid at the given voltage tap setting from a previous heat flux measurement run, as described in "Calculation of Heat Flux." The temperature drop through the wall is then computed from Eq. (161) and subtracted from the outside wall temperature measurement to give the inside wall temperature. The heat transfer coefficient may be computed from this data.

At the end of a test run, the power to the test section is switched off using the remote stop buttons. Then the steam to the preheater is shut off. After allowing some time for the preheater to cool down, the feed pump is shut off. The receiving tank contents are pumped back into the supply tank. This concludes the run.

BLACK LIQUOR MODEL SOLUTIONS

INTRODUCTION

The ideal black liquor evaporator study would use real black liquor. Unfortunately, black liquors are extremely variable in composition, making a definitive study impossible. Furthermore, it would be very difficult to evaluate the physical properties used in any boiling heat transfer model for even one sample of black liquor. As a result of these problems, this study was based on black liquor model solutions of known composition and physical properties.

THE CHOICE OF BLACK LIQUOR MODEL SOLUTION COMPONENTS

The Major Characteristics of Black Liquors

As may be seen in Table II, black liquor contains a large number of components. This picture may be simplified by lumping together the heat transfer effects of certain groups of materials in black liquor. First, there are the inorganic salts and volatile materials, including alcohols and certain extractives. The most drastic effect of these materials in the presence of nucleate boiling would be mass diffusion control of bubble growth and so of nucleate boiling heat transfer, as an excess of a salt or a deficiency of some volatile material at the bubble surface would make further bubble growth dependent on the rate at which the excess salt could diffuse away from the bubble surface or volatile material could diffuse to the surface.

TABLE II

TYPICAL BLACK LIQUOR COMPOSITION

Component	Percent of Total Solids
Alkali lignin	41
Extractives	3
Hydroxy acids and lactones	28
Acetic acid	5
Formic acid	3
Methanol	1
Sulfur	3
Sodium	16

[Data from Rydholm (97), page 774]

Second, black liquor contains surface-active substances, including extractives and alkali lignin. Surfactants can change boiling heat transfer in two ways. First, surfactants can promote foaming flow. Foam in the evaporator tube reduces the slip between the vapor and liquid phases, increasing the average two-phase velocity and so increasing the heat transfer coefficient. Second, reducing surface tension augments nucleate boiling by reducing the amount of work necessary to form a new bubble surface. This effect is reflected in the $(\sigma^{-0.5})$ term in the Chen correlation, Eq. (7).

Finally, the large quantity of relatively high molecular weight alkali lignin causes black liquors to have high viscosities. For example, the viscosity of boiling 45% solids black liquor is 11 lb/hr ft (26.6 cp) according to Jagannath (98).

Materials Chosen as Black Liquor Model Solution Components

The possibility of mass diffusion control of heat transfer was tested using solutions of potassium carbonate. Potassium carbonate was chosen instead of sodium carbonate because of the poor room temperature solubility of sodium carbonate, which could have resulted in deposits in the apparatus. Concentrations of 12.5 and 35 weight percent potassium carbonate were tested. Volatile compounds were not included in this study because the pilot evaporator design did not provide any protection against the experimental hazards of boiling volatile organic liquids.

Surfactant effects were observed by making dilute solutions (100 ppm) of commercial surfactants, including low-foaming Igepal CO-610 [nonylphenoxypoly (ethyleneoxy) ethanol], and high foaming Deriphat 160-C (sodium N-lauryl-beta-iminodipropionate).

High viscosities were obtained with solutions of extra-high viscosity sodium carboxymethylcellulose (Dow Chemical Co.) and Stein-Hall Co. Lycold-DR guar gum. Viscosities of up to 9.5 lb/hr ft (22.9 cp) could be obtained with 0.46 weight percent guar gum.

In addition to these model solutions, the boiling behavior of water was studied extensively. Water runs were repeated at intervals throughout the experimental program to check on the reproducibility of the data from the pilot evaporator.

Finally, a sample of mill-mix black liquor from a Georgia pulp mill was tested at concentrations of 25, 35, and 45 percent by weight solids. This liquor was shipped to the Institute at 25 percent solids and concentrated to higher solids in the steam-heated pilot evaporator. It was not an entirely typical black liquor, since the extractives were not skimmed off as the liquor was concentrated. It foamed more readily than most black liquors.

CONCLUSION

The black liquor model solutions described in the previous section were evaporated in the pilot evaporator and their heat transfer behavior was recorded. Three feed rates (1/2, 1, and 2 gpm) and three heat fluxes (11,500, 16,500, and 22,000 Btu/hr ft^2) were run for most samples following the procedures outlined in "Operation of the Apparatus." The results from these runs could then be compared with the predictions of mechanistic models to verify or refute the models. The results of this study will be presented in the next chapter.

RESULTS AND DISCUSSION

INTRODUCTION

This chapter is a discussion of the saturated boiling two-phase flow experiments performed for this project. An overview of the experimental program is presented in Table III. The various solutions in Table III were chosen to represent some of the major features of black liquor. The potassium carbonate solutions provided a test of the effects of dissolved salts in black liquor on heat transfer. In particular, these salt solutions were tested to observe whether mass transfer controlled heat transfer might be important in black liquor evaporators. The carbohydrate gums simulated the high viscosities and non-Newtonian behavior of black liquor. Finally, high-foaming and low-foaming surfactants were evaporated to observe the effects of foam flows with differing foam stabilities. Most of the liquids tested during the program were evaporated at the nine different flow rate and heat flux conditions listed in Table IV. All experiments were run with the vapor head at atmospheric pressure.

WATER RESULTS

HEAT TRANSFER

Comparison with the Chen Correlation Model

The complete results of the water heat transfer experiments are tabulated in Appendix VI, Series B and B replicates. The heat transfer coefficient is dependent on the heat flux but nearly independent of the flow rate. The heat transfer coefficients decrease with increasing heat flux, in contradiction to the predictions of the Chen correlation (Fig. 26). In addition to showing that the Chen correlation should not be extrapolated to the conditions used in these experiments, this reversed heat flux effect makes it very unlikely that nucleate boiling is a major

heat transfer mechanism under these conditions. The concept of a significant nucleate boiling mechanism is further undermined by the observation that there is no significant difference between the heat transfer coefficients for degassed, deionized water at 1/2 gpm and 16,500 and 22,000 Btu/hr ft^2 heat fluxes and the replicates of these runs using fresh, thoroughly aerated Appleton city water. The presence of dissolved gases should facilitate nucleate boiling and increase the heat transfer coefficient, as discussed by Collier (3), p. 160.

TABLE III

INDEX OF EXPERIMENTS; SMALL LETTERS REPRESENT EXPERIMENTAL CONDITIONS DESCRIBED IN TABLE IV

Experimental Series	Material	Concentration	Test Conditions[a]
B	Distilled water	--	a-i
B-replicates	Water	--	a-i
C	Potassium carbonate solution	12.5%	a,b,d,e,g,a,d,g
D	Potassium carbonate solution	35.0%	a,c,g,i
E	Surfactant (Igepal 610)	100 ppm	a-i
F	Surfactant (Deriphat 160C)	100 ppm	a-i
G	Cornstarch	1.25%	a-i
H	Sodium carboxymethylcellulose	0.15%	a-i
I	Sodium carboxymethylcellulose	0.19%	a-i
J	Sodium carboxymethylcellulose	0.10%	a,c,g,i
K	Sodium carboxymethylcellulose	0.06%	a,g
L	Black liquor	25%	a-i
M	Black liquor	35%	a-i
N	Black liquor	45%	a-f,h,i
O	Potassium carbonate solution	12%	a-i
P	Potassium carbonate plus Deriphat 160C surfactant	12% 100 ppm	a-i
R	Guar gum	0.25%	a-i
S	Guar gum	0.46%	a-i
T	Guar gum plus Deriphat 160C surfactant	0.46% 100 ppm	a,c,g,i
U	Guar gum plus Deriphat 160C surfactant	0.30%	a,c,g,i
V	Guar gum plus Deriphat 160C surfactant	0.15% 100 ppm	a,c,g,i

[a]Test conditions are explained in Table IV.

TABLE IV

EXPERIMENTAL FLOW RATE AND HEAT FLUX CONDITIONS

Flow rate:	1/2 gpm	1 gpm	2 gpm
Heat flux			
11,500:	a	b	c
16,500:	d	e	f
22,500:	g	h	i

(Btu/hr ft^2)

Comparison with the Slug-churn Flow Model

A comparison between the experimental results and the predictions of the slug/churn model may be made by consulting Fig. 27-29. The slugging rate used in the model program was determined by listening to and timing the slugging noises in the vapor head, supported by measurements of the frequency of the pressure fluctuations. For all these experiments, the pressure fluctuations were of a very regular 90 cycles per minute frequency, either read from the pressure transducer record or measured by counting the deflections of the top of the vapor head. The slugging noises were less regular, with the time between "bangs" corresponding to 60 to 120 slugs per minute, with an average of 90 slugs per minute.

There is good agreement in magnitude and trends between the experimental heat transfer coefficients and those calculated using the numerical model of slug flow. The model predicts no flow rate effect, and no such effect is observed in the data. At the lowest heat flux (11,500 Btu/hr ft^2), the model predictions are generally within about $\pm$ 15 percent of the data (Fig. 27). For the next higher heat flux, (16,500 Btu/hr ft^2) the model successfully predicts the decrease in the heat transfer coefficient (Fig. 28), again giving agreement within $\pm$ 15 percent of the data. The model curves all predict a stronger influence of position along the tube

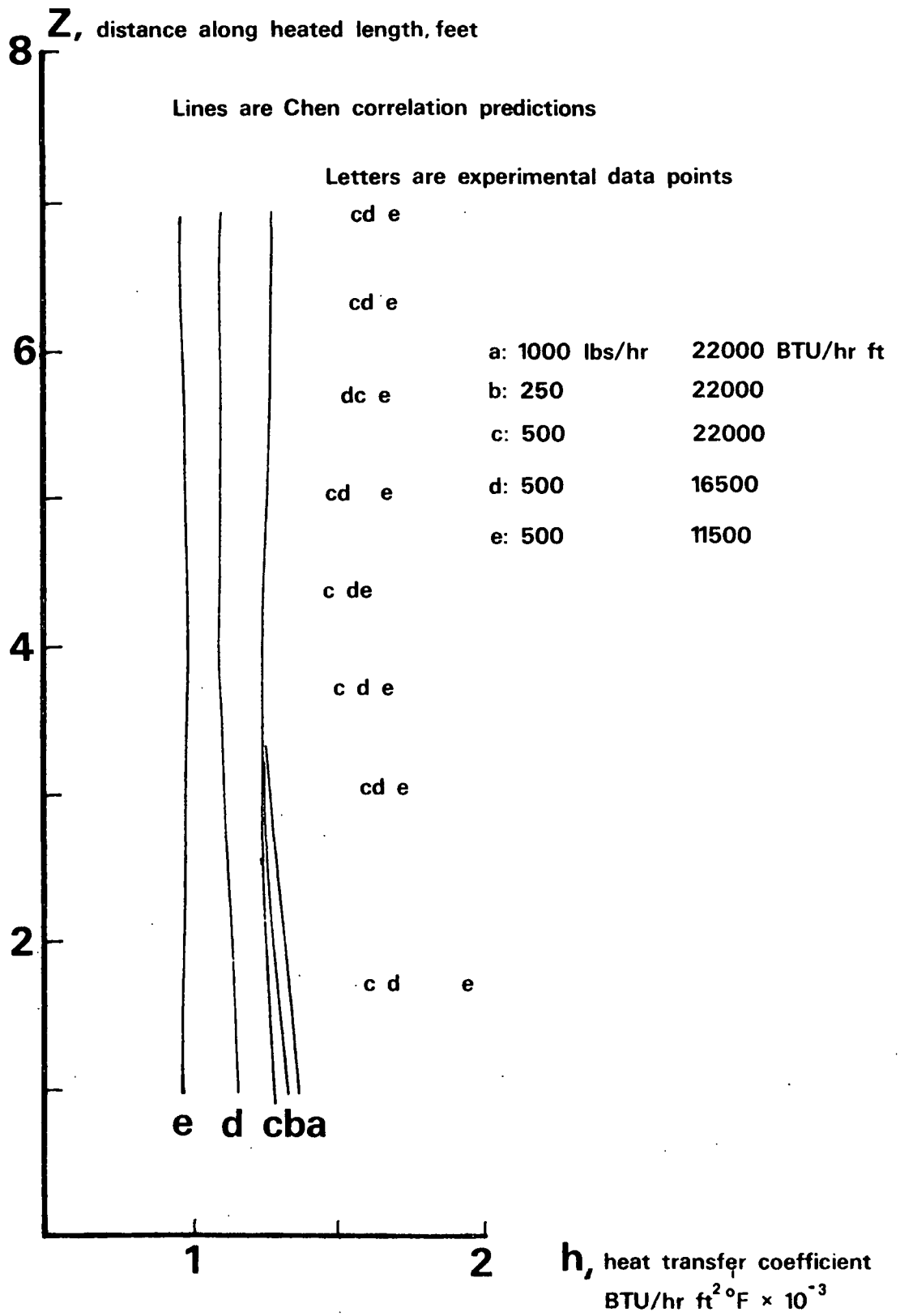

Figure 26. Chen correlation predictions compared with selected data, for boiling water in 2-inch tube.

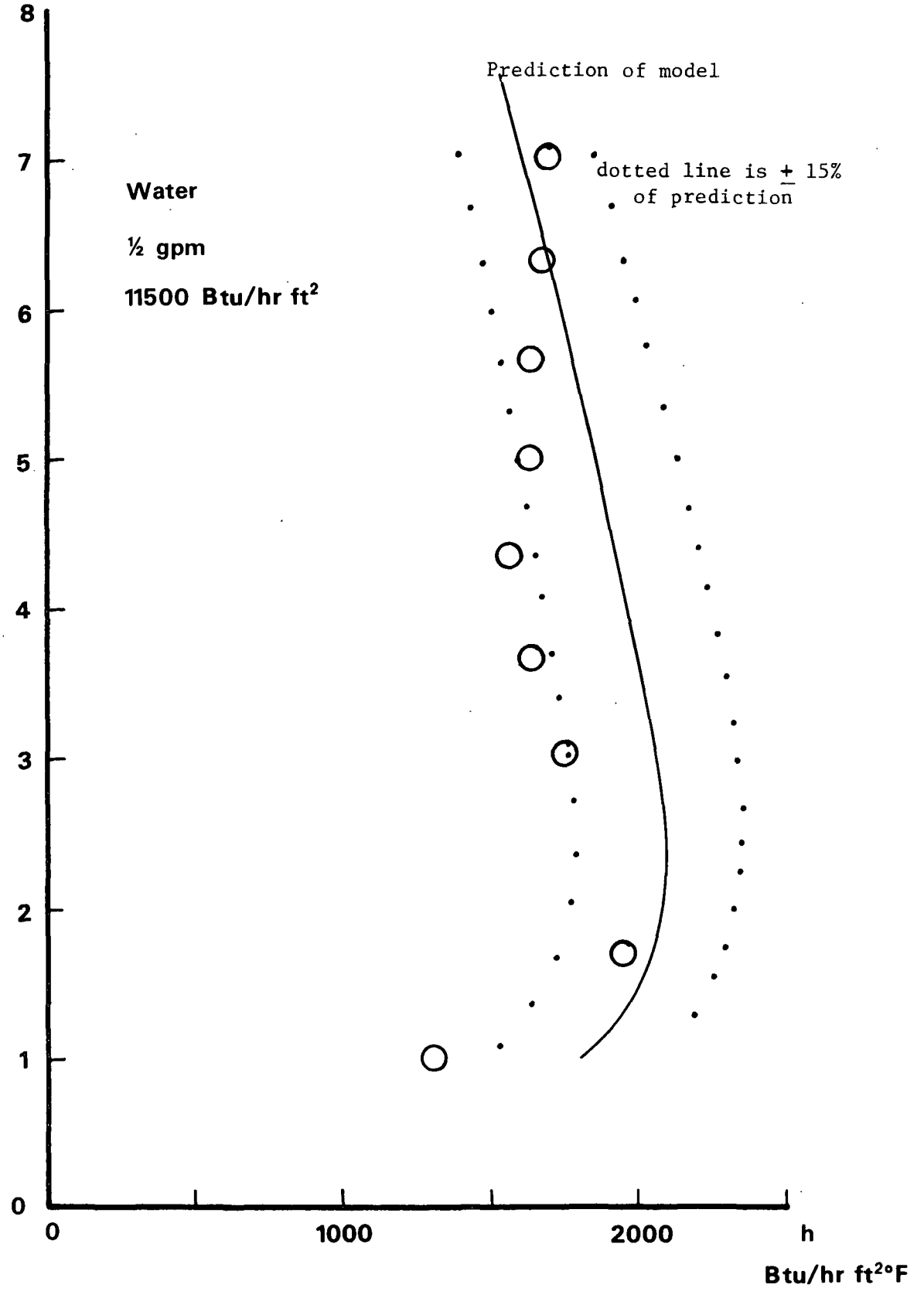

Figure 27. Comparison of the predictions of the slug/churn model with data. Water, 1/2 gpm; 11,500 Btu/hr ft^2 heat flux.

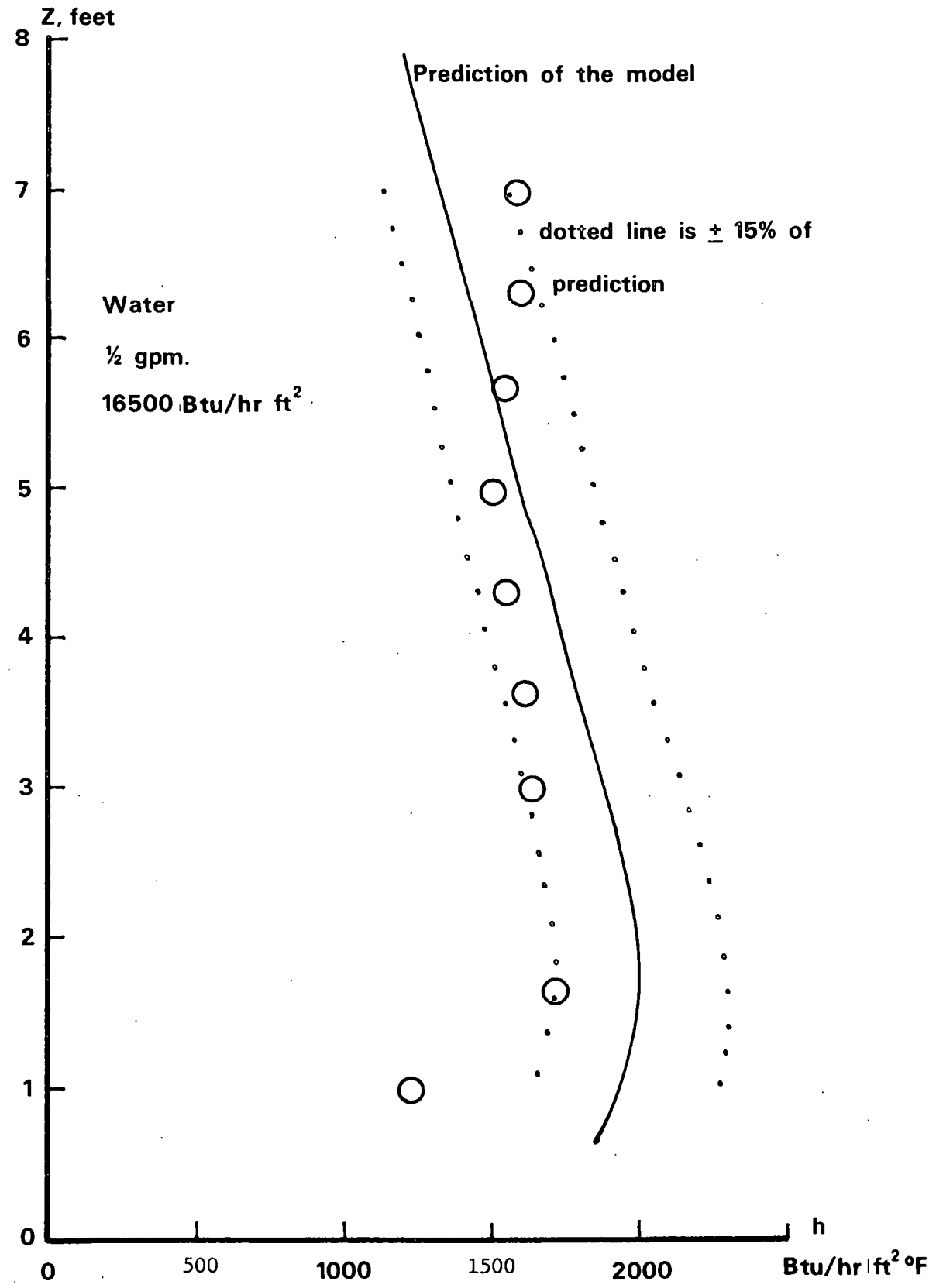

Figure 28. Comparison of the predictions of the slug/churn model with experimental data. Water, 1/2 gpm; 16,500 Btu/hr ft^2.

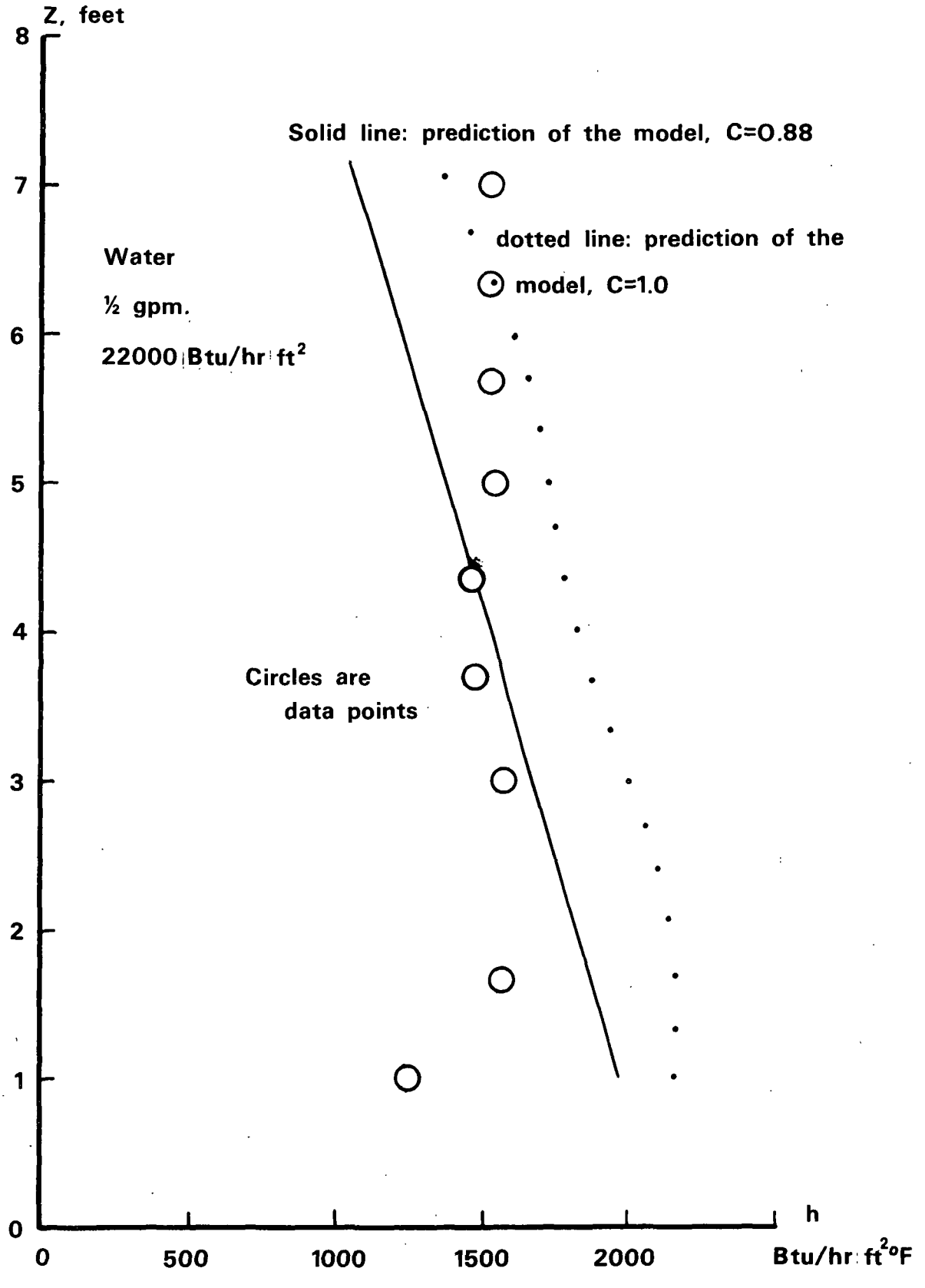

Figure 29. Comparison of the predictions of the slug/churn model with experimental data. Water, 1/2 gpm; 22,000 Btu/hr ft^2.

than is seen in the data. The error from this trend becomes serious in the highest case (22,000 Btu/hr ft^2, Fig. 29). The average agreement is still good for this case, but the drop-off in heat transfer predicted toward the exit of the tube is excessive. This exaggerated effect of position along the tube is probably due to the assumption of instantaneously completed flooding in the model. The real situation near the end of the tube in experiments with higher exit vapor mass qualities almost certainly includes flooding hysteresis loops ("jiggling films") which would produce both downflow and net upflow contributions to heat transfer in the films. The present model only accounts for downflow heat transfer effects. In addition, the jiggling films would result in less backflow than is predicted by the model. This would influence heat transfer toward the bottom of the tube, because the average film flow rates there would be lower, reducing heat transfer. Thus, accounting for the effects of noninstantaneous flooding would improve the performance of the model, increasing the heat transfer coefficients toward the top of the tube and decreasing those toward the bottom. Unfortunately, there is no good way to account for these effects.

Figure 29 also illustrates the sensitivity of the model to changing the flooding parameter C in the Wallis (91) flooding correlation. The prediction line based on C = 0.88 represents the lower limit of flooding. Films thinner than this line would not be subject to flooding under any conditions at the local vapor flow rate. The C = 1.0 line represents the other extreme, the thickest film which would not flood under ideal conditions. Increasing the value of C causes the model to predict somewhat higher heat transfer coefficients. The agreement between the model and the data is improved toward the top of the tube but is worsened toward the bottom. The average agreement is best with the C = 0.88 line.

The other variable in the model which might be adjusted as a free variable is the slug rate. Figure 30 shows the effects of changing the slug rate over the range

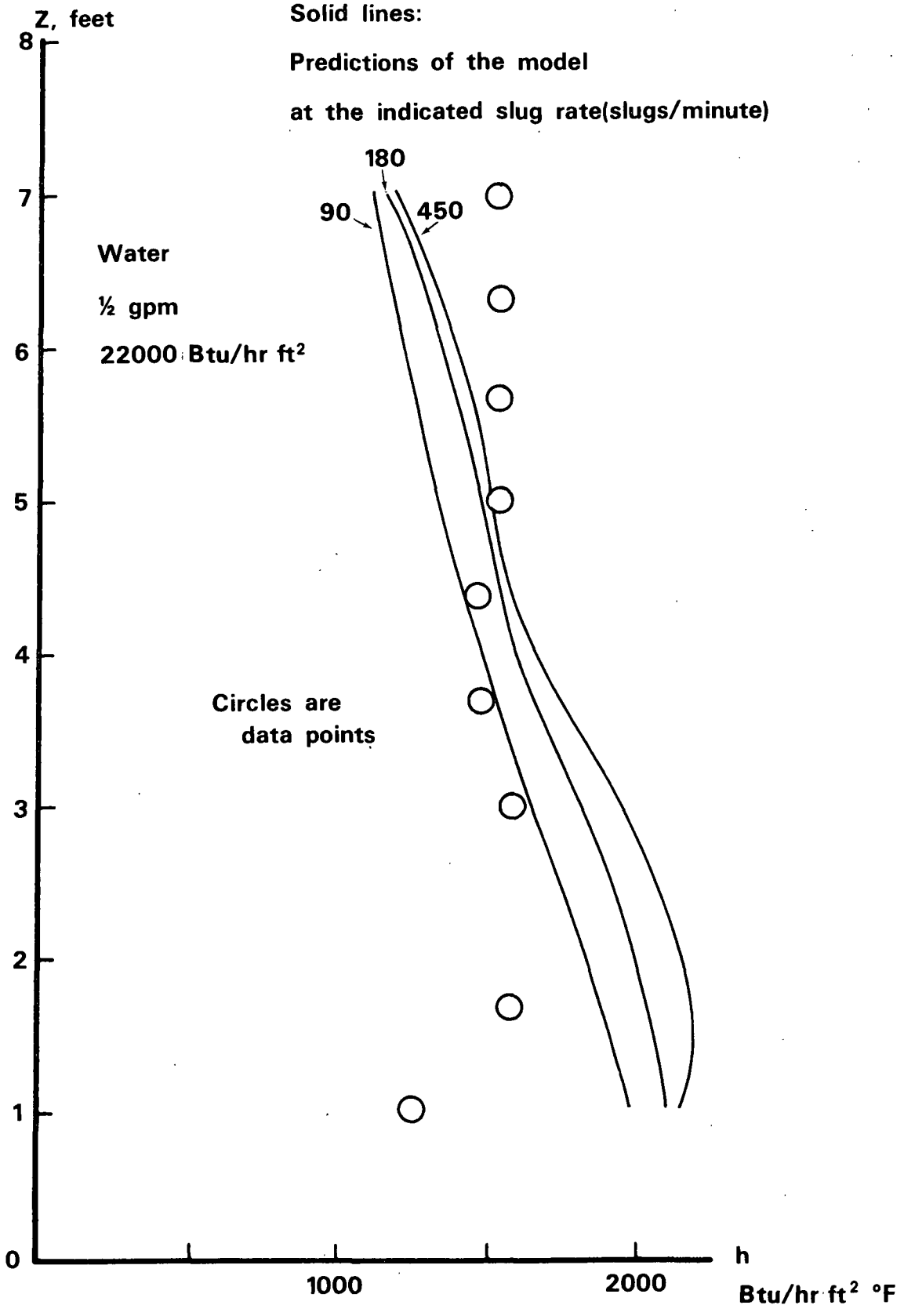

Figure 30. Effect of changing the slug rate parameter in the computer model, compared with the experimental data.

of 90 to 450 slugs per minute. The effect on the heat transfer coefficient predictions is not large. The best average agreement is obtained with the 90 slugs per minute experimental slug rate. Thus, there would be no merit in considering an "effective slugging rate" as a way around the flooding prediction problem.

The data in Appendix VI are all time-averaged heat transfer coefficients. Figure 31 illustrates the instantaneous heat transfer behavior which has been averaged to give these data. At points toward the tube exit, the film thickness after the passage of a slug is reduced because of flooding. Flooded films are thinner than nonflooded films. As the vapor velocity increases, flooding becomes more important and the initial thickness of the film is reduced. This effect causes the "reverse" dependence of the heat transfer coefficient on the heat flux. At higher heat fluxes, there is more cumulative evaporation at any point, which results in a higher vapor velocity and so more flooding and thinner films. The films drain over time, becoming thinner and less turbulent, and then are renewed as the next slug passes the point. The heat transfer history of a point near the top of the tube (1.0 foot location) shows a turbulent-laminar transition effect. The film has thinned to the point where conduction through the laminar film is the important heat transfer mechanism, and the heat transfer coefficient rises as the film becomes thinner.

Reproducibility of the Results

The water data were also used as a control on the reproducibility of the results and as a check on the condition of the test equipment. Water experiments were rerun at intervals throughout the experimental program. The data were very reproducible, as may be seen by comparing the B-series replicates done before Series Q with the B-series runs which began the experimental program (Appendix VI). These replicates were done after completion of the corrosive salt and black liquor runs which would have had the most serious effect on the condition of the apparatus. There is no

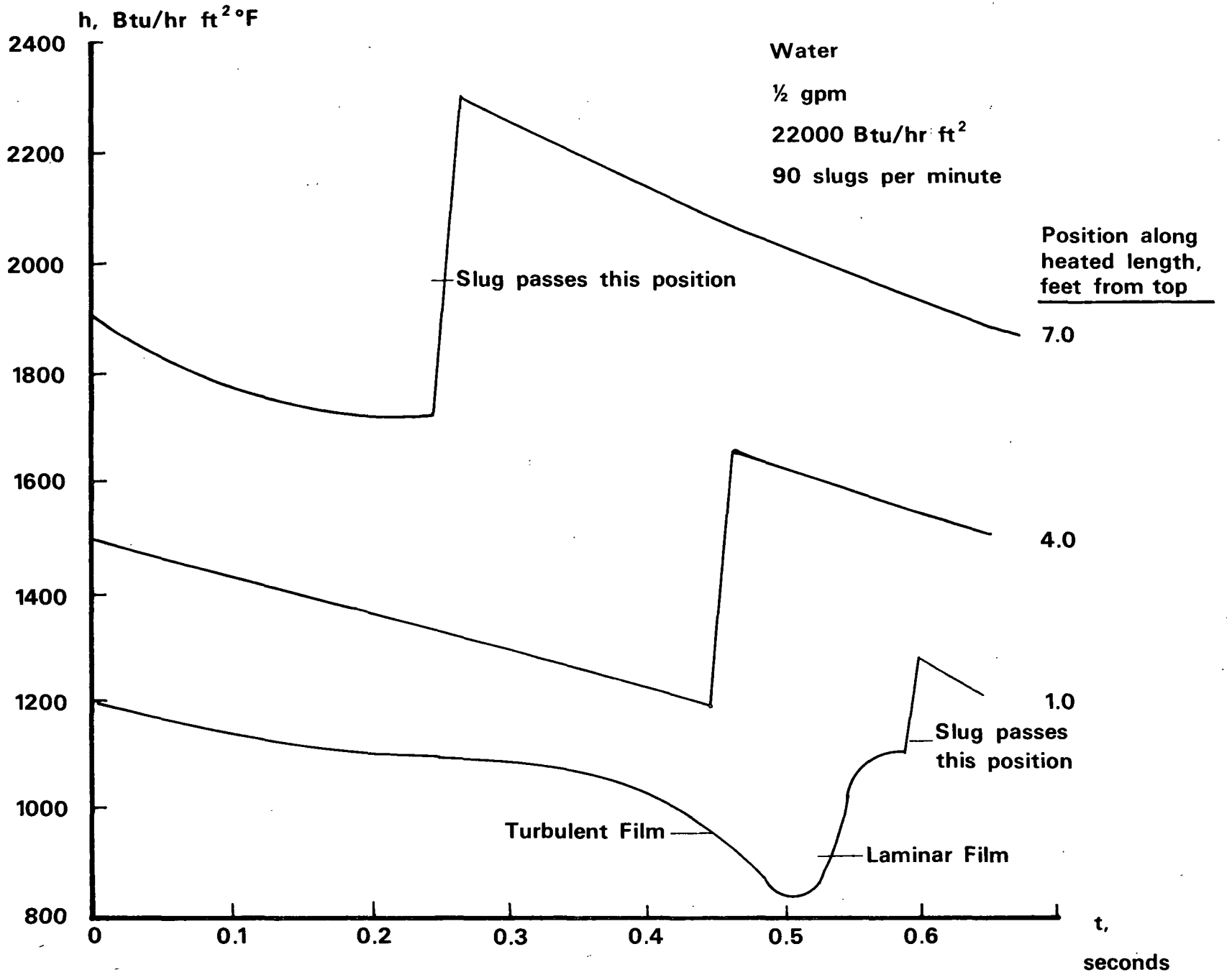

Figure 31. Time dependence of the heat transfer coefficient calculated by slug/churn model.

significant difference between the results of the original runs and these replicates. The two sets of data were taken four months apart. Thus, neither corrosion nor the passage of time changed the performance of the pilot evaporator.

DYE TRACER EXPERIMENT

One dye tracer experiment was performed to demonstrate the reality of downflow in the evaporator tube. The conditions chosen were those least likely to have a significant backflow, so a backflow in this case implies that backflow exists under the other, less severe experimental conditions. During a 1/2 gpm, 22,000 Btu/hr ft^2 experiment, dye was pumped into the top access tap (23 inches from the exit) at a rate of 1.32 lb/hr of concentrated dye. [One packet of Rit brand marine blue dye dissolved in one liter (0.26 gallon) of boiling water was used.] A sample drawn from the bottom access tap (96 inches from the exit) had a dye concentration of 0.00014 lb dye/lb water measured by spectrophotometric methods. This represents a significant backflow. The mass balance for the experiment closed reasonably with 1.32 lb/hr dye fed and 1.18 lb/hr dye calculated from the measured exit concentration.

The computer model simulation of this experiment using the experimental 90 slugs/minute slug rate predicts a concentration at the bottom port of 0.0027 lb/lb, which is too high by a factor of twenty. This overprediction could be expected because of the neglect of jiggling film behavior in the model, as mentioned in a previous section. This behavior would reduce the total amount of downflow. In the model, predicted backflow can be reduced by increasing the slug rate. The effect of a higher nominal slug rate on the model backflow predictions may be seen in Fig. 32, which shows that it is possible to simulate the measured backflow using the slug/churn model. The effect of higher slug rates on the heat transfer coefficient predictions was shown in Fig. 30. Unfortunately, the improved agreement between measured and predicted backflow is at the expense of decreased agreement on heat transfer.

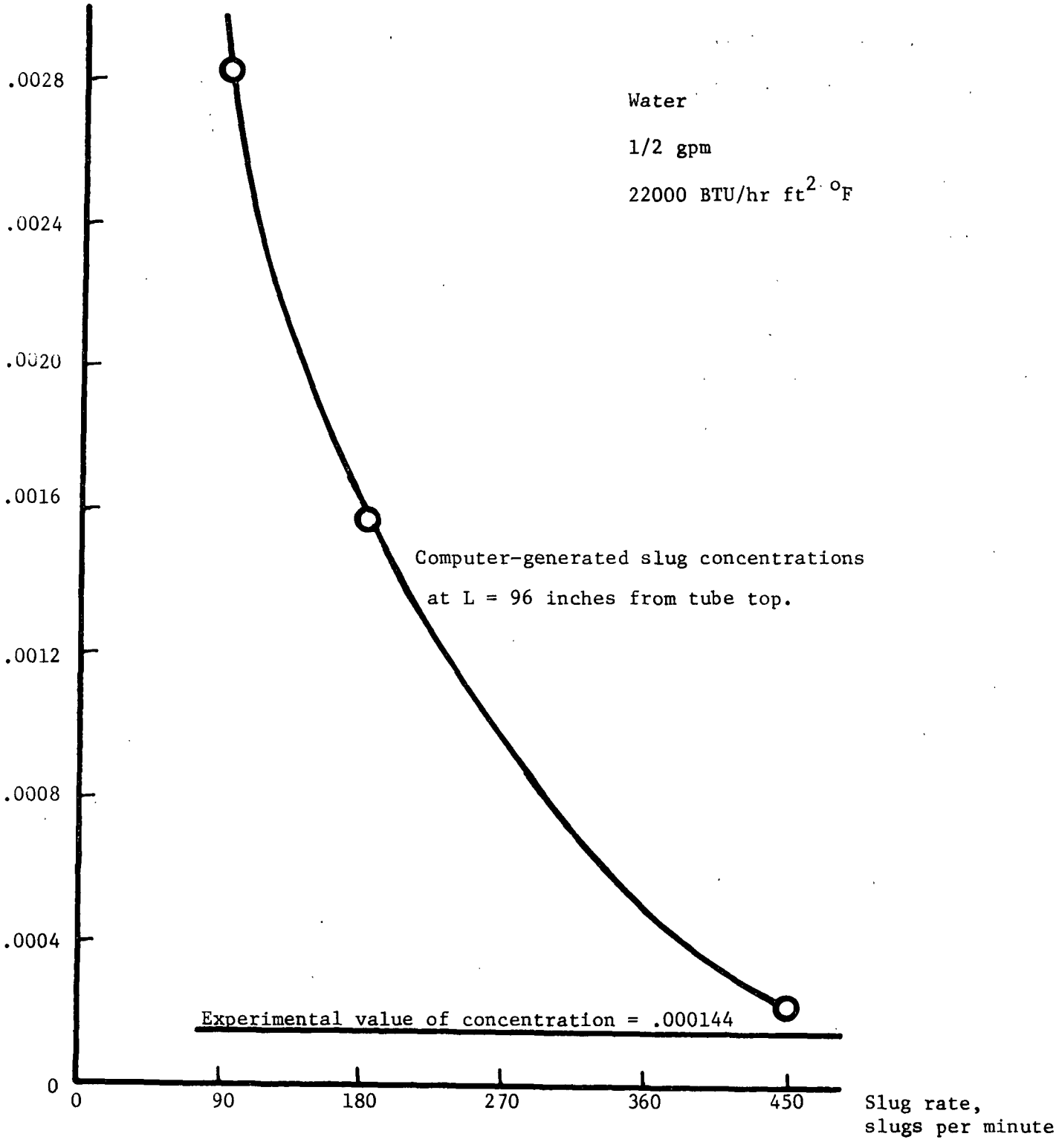

Figure 32. Simulation of dye tracer experiment, varying the slug rate.

FIBER-OPTICAL STUDIES

The results of the fiber-optical phase detection studies are presented in Appendix VII in the form of tube cross-sectional profiles of void fraction and phase duration. The bubble, slug, and annular flow regimes can be diagnosed from these graphs. The changes between the regimes are sharply defined. Bubble flow exhibits low, uniform void fractions at all points across the tube ($\alpha < 0.4$) and substantial liquid phase durations of about 40 ms at the tube centerline. Slug flow shows a smooth void fraction curve rising to centerline void fraction values of 0.6 to 0.8. Vapor and liquid phase durations are uniform over most of the tube in the range of 10 to 30 milliseconds. "Annular" flow produces very high centerline void fractions ($\alpha > 0.85$) and vapor phase durations (> 50 milliseconds).

The flow pattern diagnoses are summarized in Fig. 33. The bulk of the data is in the slug and churn flow regimes. A few points taken at the lowest access port at the lowest heat flux, highest flow rate conditions were still in bubble flow. These heat fluxes were lower than those studied in the heat transfer experiments (4,800 and 8,400 Btu/hr ft^2). An annular type flow was detected for the top access port at all flow rates for the highest heat flux (22,000 Btu/hr ft^2). The "annular" flow is not true climbing film annular flow, as was shown by the dye tracer experiments. It may represent churn flow where the liquid lump has become filled with entrained vapor bubbles. As the probe will not detect liquid phase structures with dimensions less than 1/8-inch (3.18×10^{-3} m), a churn flow lump approaching a foamlike structure would not be detected as a liquid lump.

POTASSIUM CARBONATE SOLUTION RESULTS

The potassium carbonate used in these runs was a technical grade calcined material supplied by IMC Electrochemicals Co. Table V gives the results of an analysis on this material run by the IPC analytical section. Although the sample of

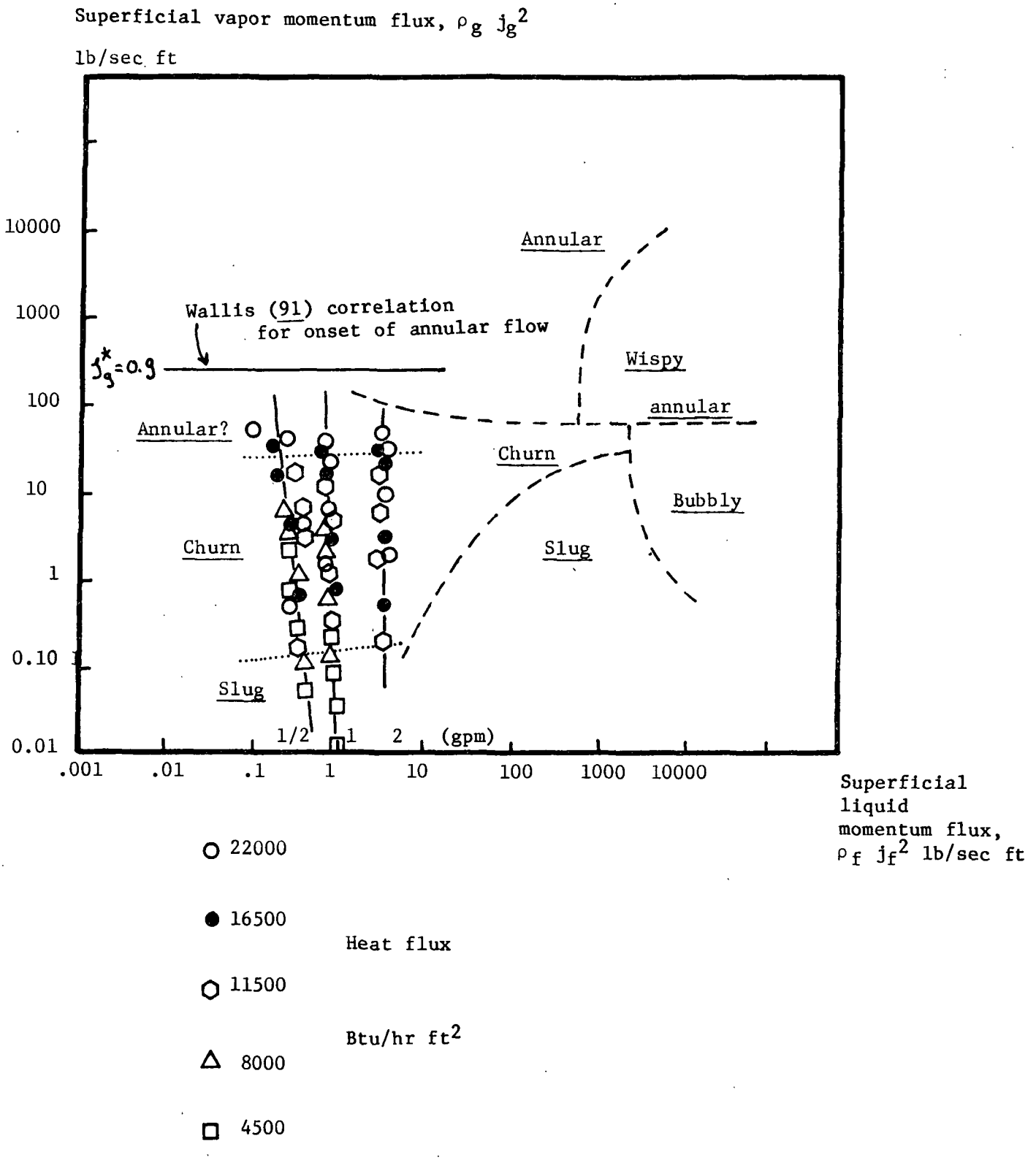

Figure 33. Flow pattern diagnoses plotted on a Hewitt and Roberts flow pattern map. [Collier (3), page 15].

TABLE V

POTASSIUM CARBONATE ANALYSIS

(a). Carbonate content of the potassium carbonate used in the heat transfer experiments

Sample Identification	Percent Carbonate
IMC Electrochemicals potassium carbonate-calcined-technical grade	39.6

Reported on oven-dried basis; method is TAPPI T 624 os-68

(b). Emission spectrographic analysis of the potassium carbonate used in the heat transfer experiments, including an alternate measurement of potassium content by flame emission.

Element	Percent by Weight (oven-dried)
Aluminum	0.010
Copper	0.00098
Iron	0.016
Potassium	35[a]
Silicon	0.024
Sodium	0.44

[a]Potassium is major metal; the emission spectrographic analysis may be in error due to the high concentration. Flame emission gives a more reliable 52.0% potassium measurement.

All tests were performed by the IPC analytical group and documented in A-400 File 211389.

potassium carbonate is reasonably pure, it did contain a trace of surface-active contaminants. The room-temperature (68°F, 20°C) surface tension of the 12% potassium carbonate measured by the deNouy ring method was 70.5 dynes/cm, while the surface tension of the makeup water was 72.7 dynes/cm, which is close to normal. The surface

tension of the salt solution should have been higher than the pure water (76 dynes/cm, estimated from sodium carbonate data). This contaminant produced foaming in the 12% solution but not in the 35% solution where the increased viscosity and density probably discouraged foaming. This section will present the heat transfer results for the 35% potassium carbonate solution first, followed by the heat transfer, flow pattern diagnoses, and dye tracer results for the foaming 12% potassium carbonate runs.

35% POTASSIUM CARBONATE SOLUTION RUNS

Heat Transfer Results

The heat transfer results for 35% potassium carbonate solutions are tabulated in Appendix VI, Series D. The results of these runs and the predictions of the computer model of slug and churn flow are in excellent agreement (Fig. 34 and 35). The model has successfully accounted for a liquid feed viscosity increase to three times the viscosity of water and a density increase to about 1.4 times that of water. The flow rate effect which is present because the average concentrations in the tube change when the flow rates are varied at a given heat flux is both predicted and observed in the data. The physical properties of boiling potassium carbonate which are used in the computer model are interpolated from the tables in Piret and Isbin (32).

Evidence for Backflow in the 35% Potassium Carbonate Runs

Information on the backflow of films in the boiling 35% carbonate solution can be recovered from the traveling thermocouple and pressure probe data. Figure 36 is a graph of the concentration profile along the tube calculated by finding the boiling temperature of water corresponding to each pressure reading and then taking the difference between this local water saturation temperature and the measured potassium

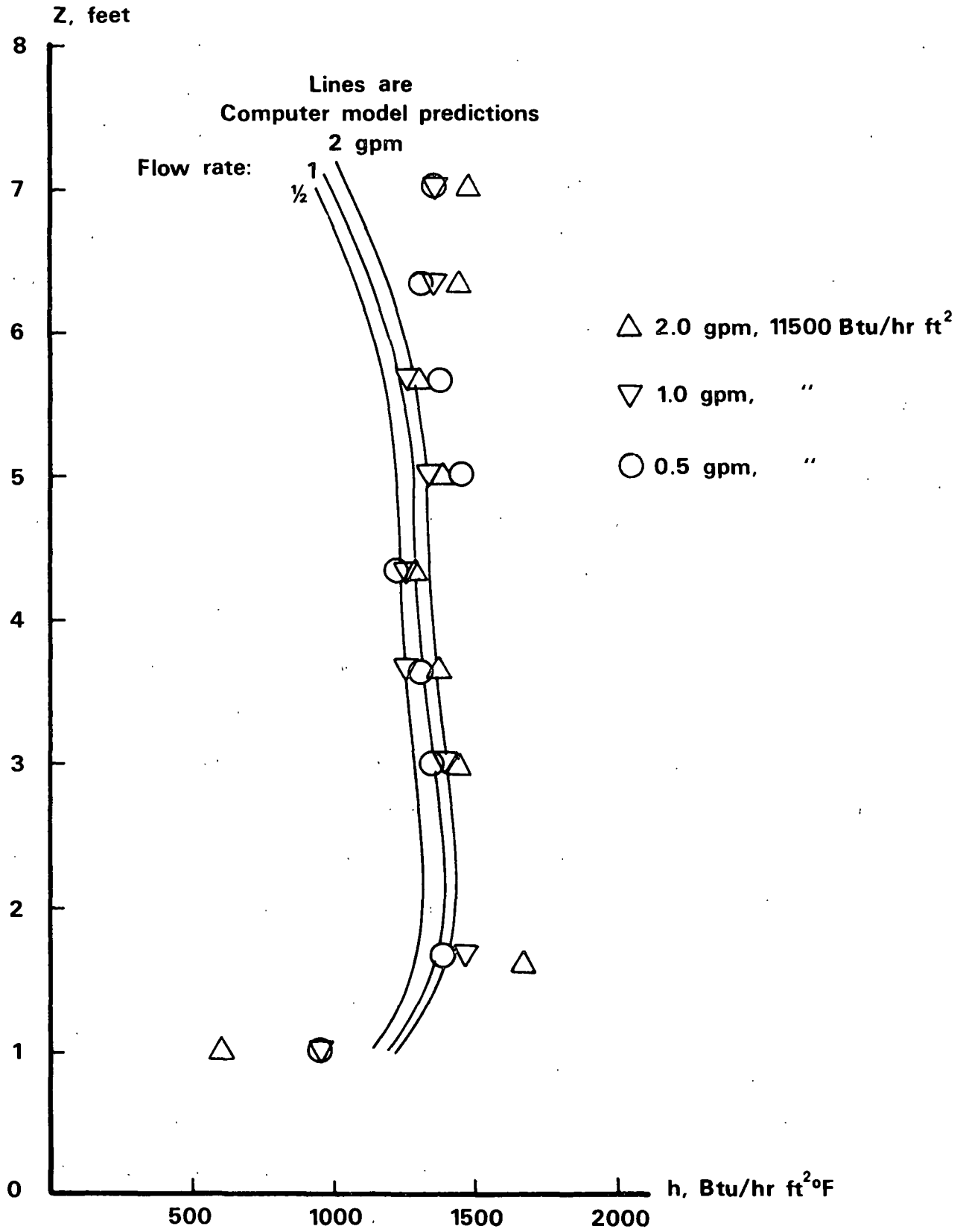

Figure 34. Effect of flow rate on the heat transfer coefficient of 35% solids potassium carbonate at 11,500 Btu/hr ft^2. Lines are the predictions of the computer model.

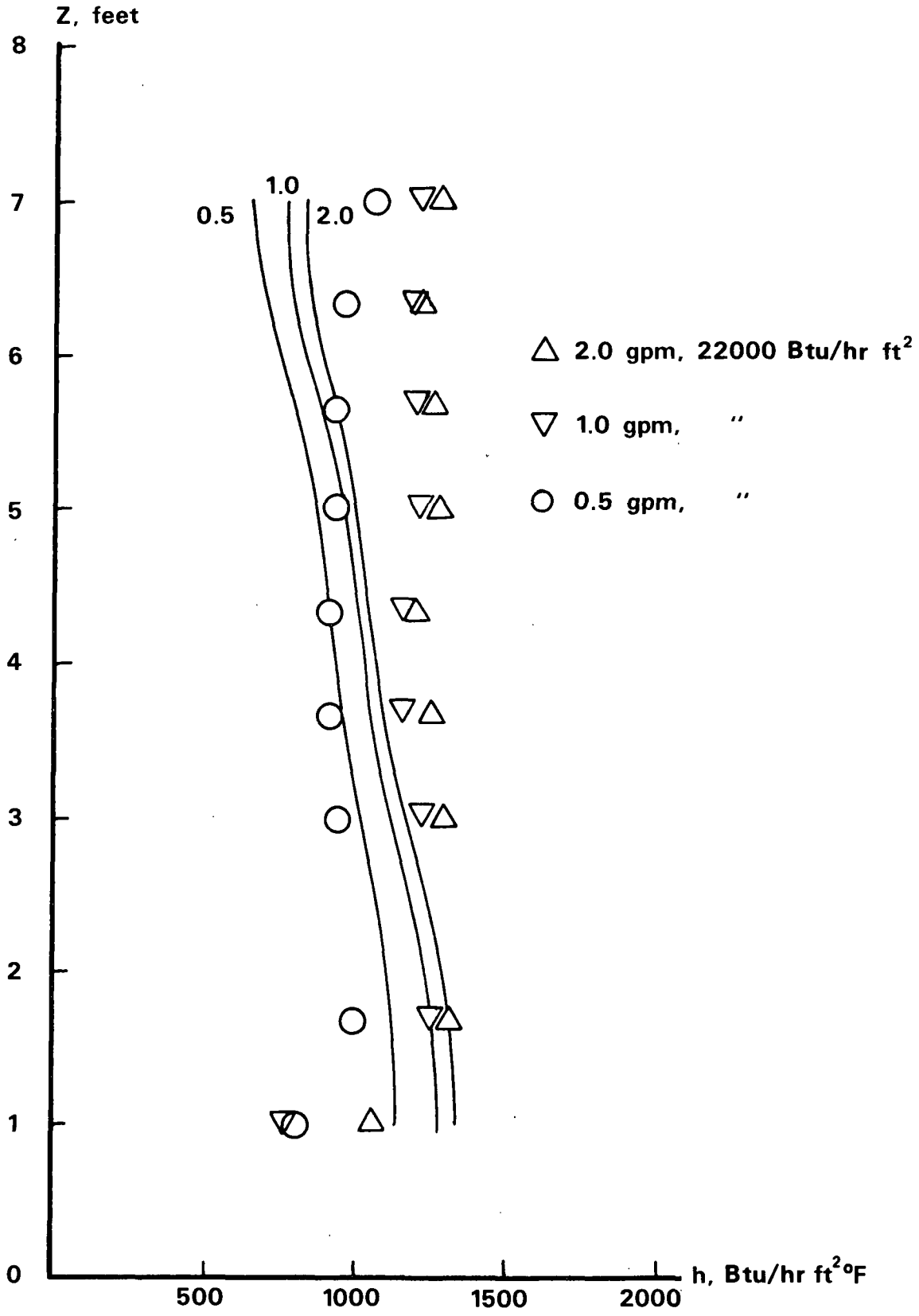

Figure 35. Effect of flow rate on the heat transfer coefficients of 35% potassium carbonate at 22,000 Btu/hr ft^2. Lines are the predictions of the computer model.

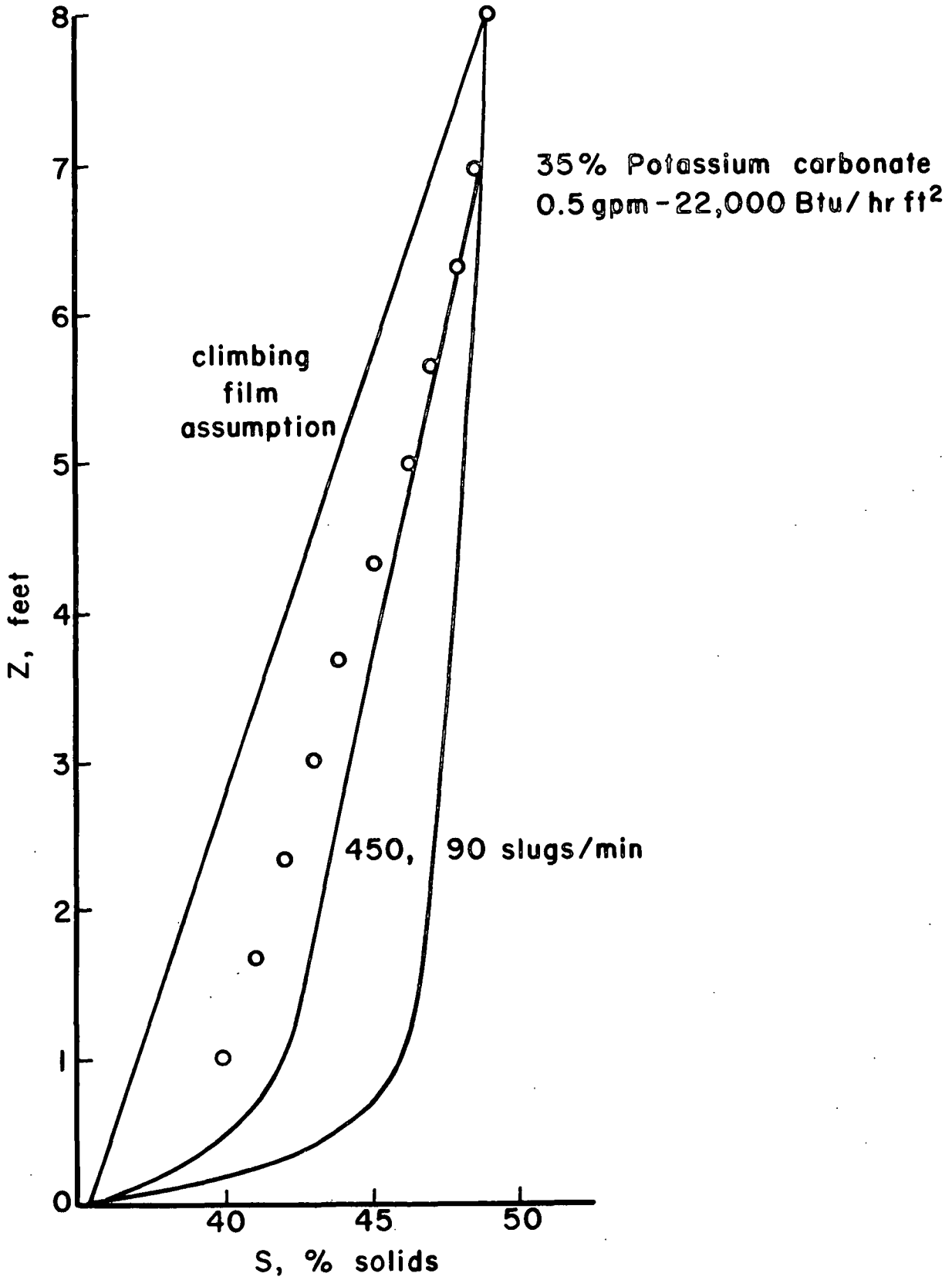

Figure 36. Concentration profiles of 35% potassium carbonate solution resulting from evaporation at 0.5 gpm and 22,000 Btu/hr ft^2. Lines are calculated from the computer model using various flow assumptions.

carbonate solution temperature as the boiling point rise due to the local concentration of potassium carbonate. The boiling point elevation may be related to the concentration using the data of Piret and Isbin (32). The concentration at any point is higher than the concentration which would be predicted from a uniform upward flow model. The concentration profile can be closely approximated by the slug-churn flow model if a slug rate of 450 slugs per minute is used in the calculations. The experimental 90 slugs per minute rate leads to overprediction of the amount of backflow, as has been discussed above.

12% POTASSIUM CARBONATE SOLUTION RUNS

Heat Transfer Results

Two sets of experiments were performed on 12% potassium carbonate solutions. The first batch of test solution (Series C) was seriously contaminated with surfactants, probably due to insufficient rinsing in a boil-out preceding the runs. The replicate solution (Series O) was carefully prepared to avoid contamination but still contained surface-active materials which may have been in the chemical as received. The surface tension of the first solution was 64.6 dynes/cm, and for the replicate solution, 70.5 dynes/cm. Both series of runs gave foaming behavior. The agreement between the model predictions and the data is poor, as may be seen in Fig. 37. However, the agreement between the results for the two test solutions is also poor. This nonreproducible behavior points to the strong effects trace constituents can have on foaming heat transfer.

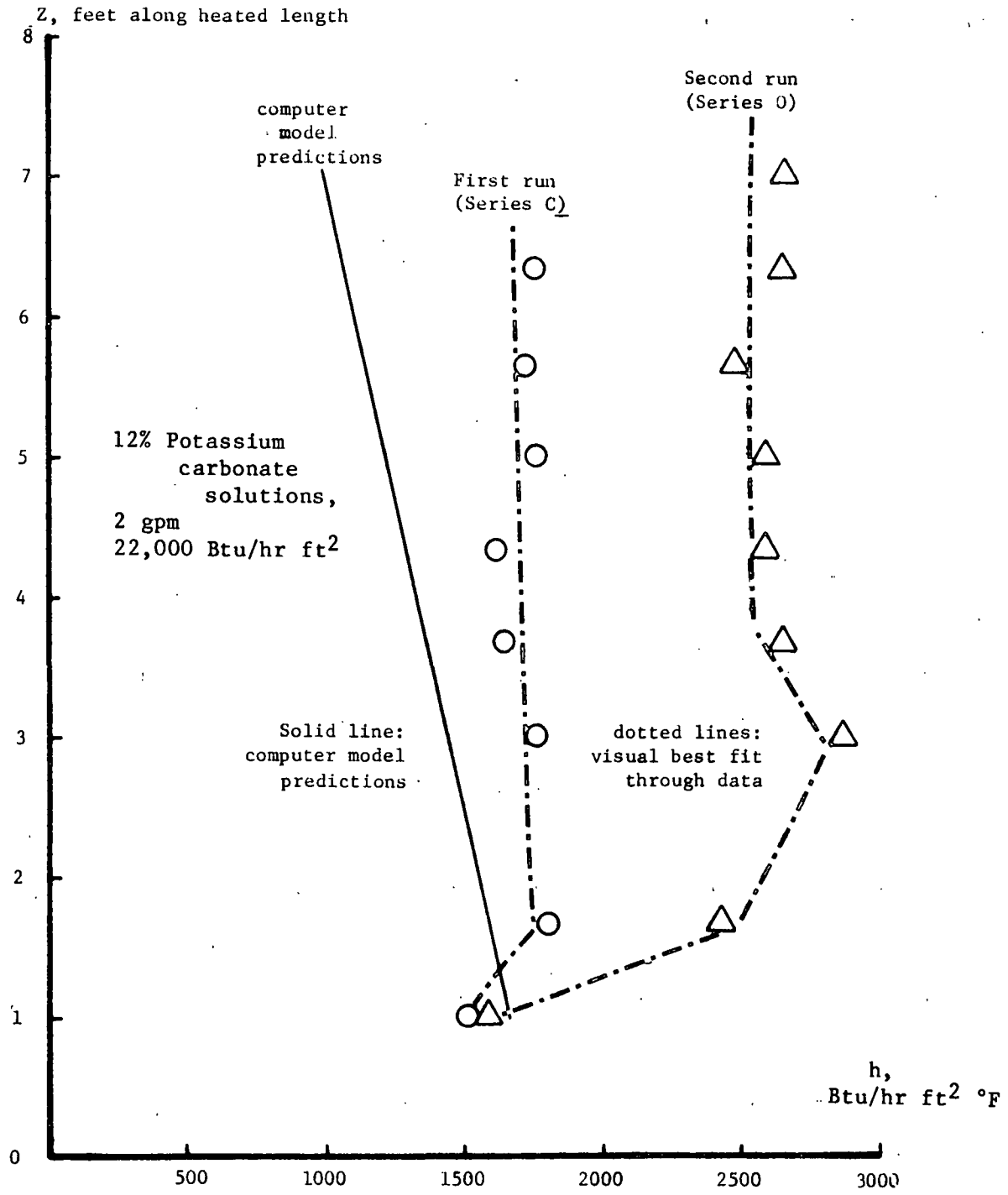

Figure 37. Foaming effects on the heat transfer to 12% potassium carbonate solutions; 2 gpm, 22,000 Btu hr ft^2, Series C and O.

Fiber-Optical Studies of 12% Potassium Carbonate Solution

The results of the fiber-optical phase detection studies on the first (Series C) 12% potassium carbonate solution are presented in Appendix VIII. If the profiles of

void fraction and phase duration are compared with the corresponding water experiment (Appendix VII), it is apparent that the void fraction and average vapor phase duration profiles are much higher for the salt solution than for water at the same feed rate and heat flux. This is probably the result of foam flow in the tube. The probe is not able to detect the liquid held up in the bubble walls in a foam, since the dimensions of the bubble walls would be generally less than the 1/8-inch (3.18×10^{-3} m) resolution of the probe. The diagnosis of foam flow is supported by the appearance of the flow to the receiving tank, as well as the absence of slugging noises in the vapor head, and the small amplitude of the pressure fluctuations (typically $\pm$ 0.015 psi for the carbonate solution of Series C, $\pm$ 0.075 psi for the water runs of Series B).

Dye Tracer Study

One dye tracer experiment was performed on the Series C batch of 12% potassium carbonate solution at 1/2 gpm and 22,000 Btu/hr ft^2. Dye was fed at the top access port at the rate of 1.32 lb/hr. No dye was detected at the bottom port in this case. The mass balance for the experiment closed reasonably, with an exit dye rate calculated from the measured exit concentration of 1.30 lb/hr. There was thus no backflow detected in this foaming flow system.

GUAR GUM AND SODIUM CARBOXYMETHYLCELLULOSE RUNS

HEAT TRANSFER

Comparison of the Data with the Slug-Churn Flow Model

The results of the experiments with sodium carboxymethylcellulose and guar gum solutions are presented in Fig. 38-42, plotted on heat transfer coefficient *vs.* liquid feed viscosity coordinates. These data are tabulated in Appendix VI, Series H, I, J, K, R, and S. The predictions of the computer model are also plotted on these graphs. The vertical bars represent the range of the data (highest reading to

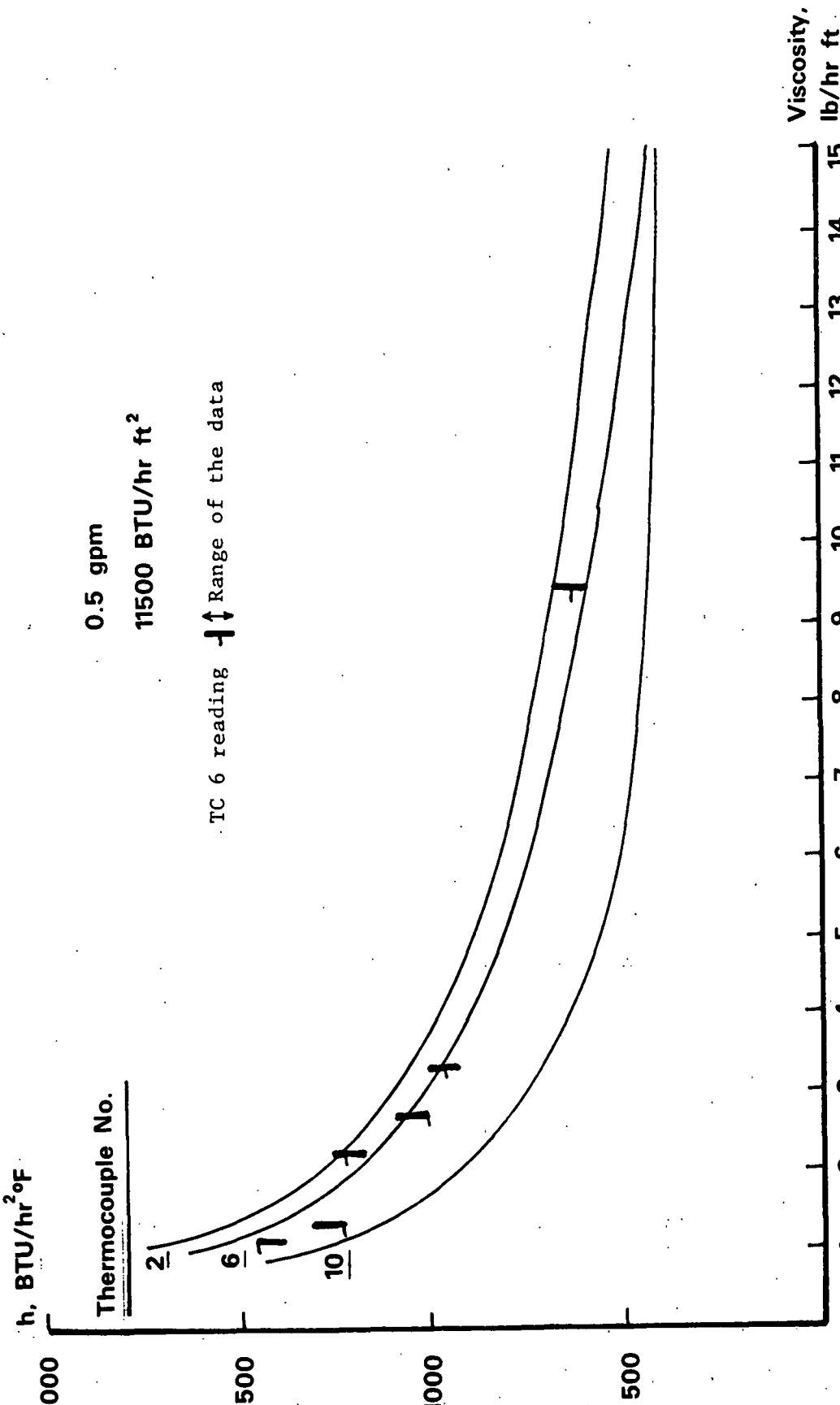

Figure 38. Effects of viscosity on heat transfer coefficients at three positions along the tube. Lines are the predictions of the computer model, vertical bars are data points from NaCMC and guar gum runs. 0.5 gpm, 11,500 Btu/hr ft^2.

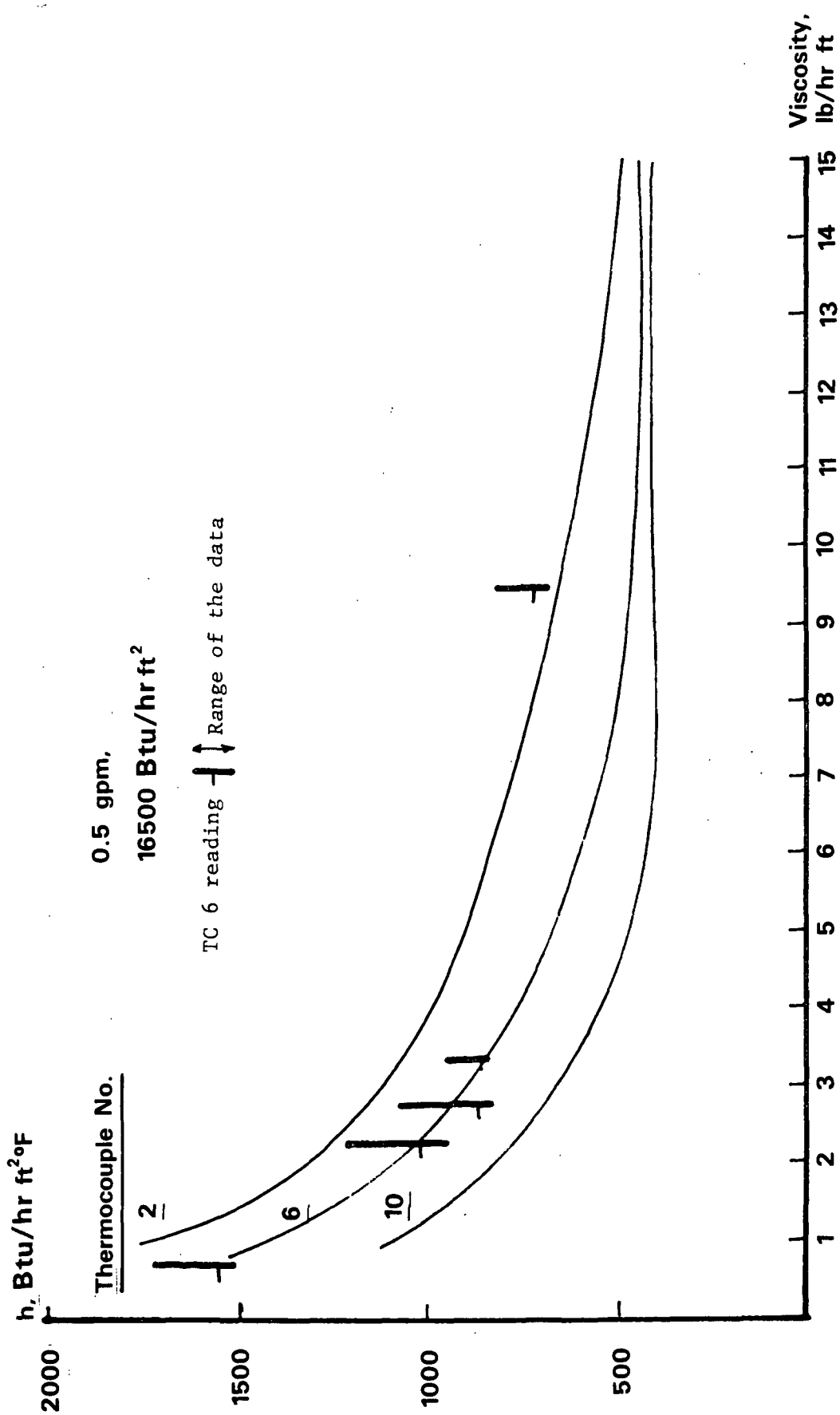

Figure 39. Effects of viscosity on heat transfer coefficients at three positions along the tube. Lines are the predictions of the computer model, vertical bars are data points from NaCMC and guar gum runs. 0.5 gpm, 16,500 Btu/hr ft^2.

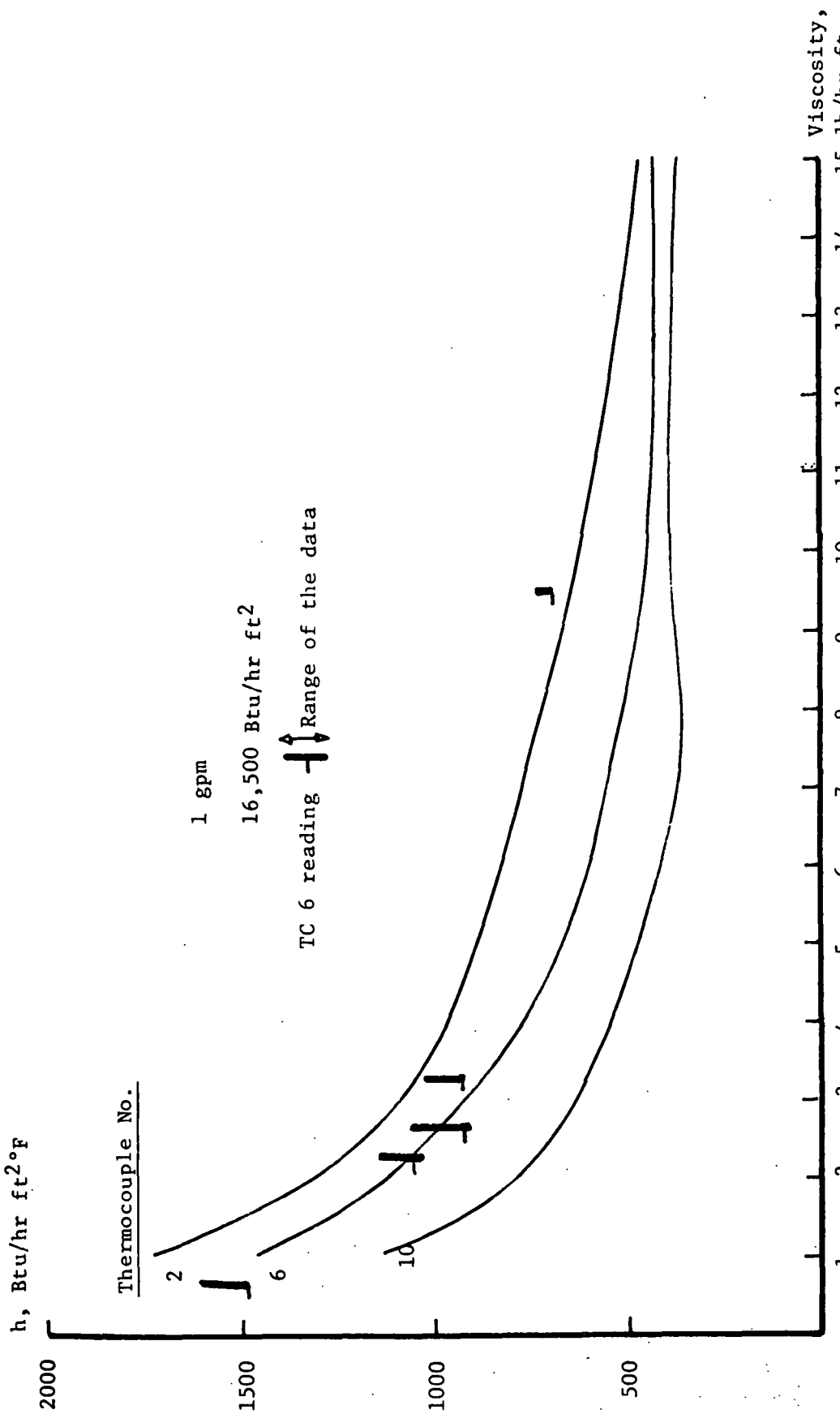

Figure 40. Effects of viscosity on heat transfer coefficients at three positions along the tube. Lines are the predictions of the computer model, vertical bars are data points from NaCMC and guar gum runs. 1 gpm, 16,500 Btu/hr ft^2.

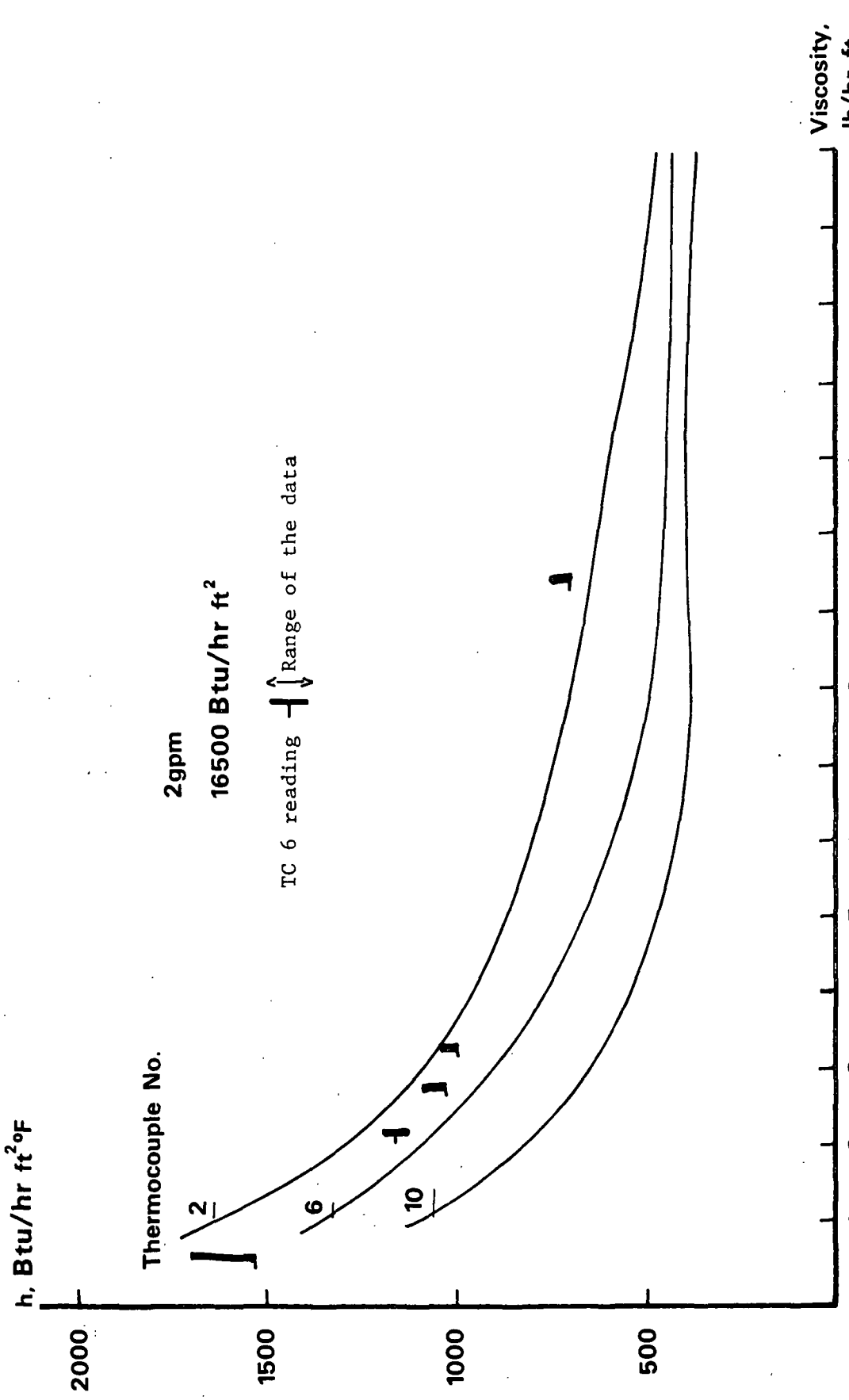

Figure 41. Effects of viscosity on heat transfer coefficients at three positions along the tube. Lines are the predictions of the computer model, vertical bars are data points from NaCMC and guar gum runs. 2 gpm, 16,500 Btu/hr ft^2.

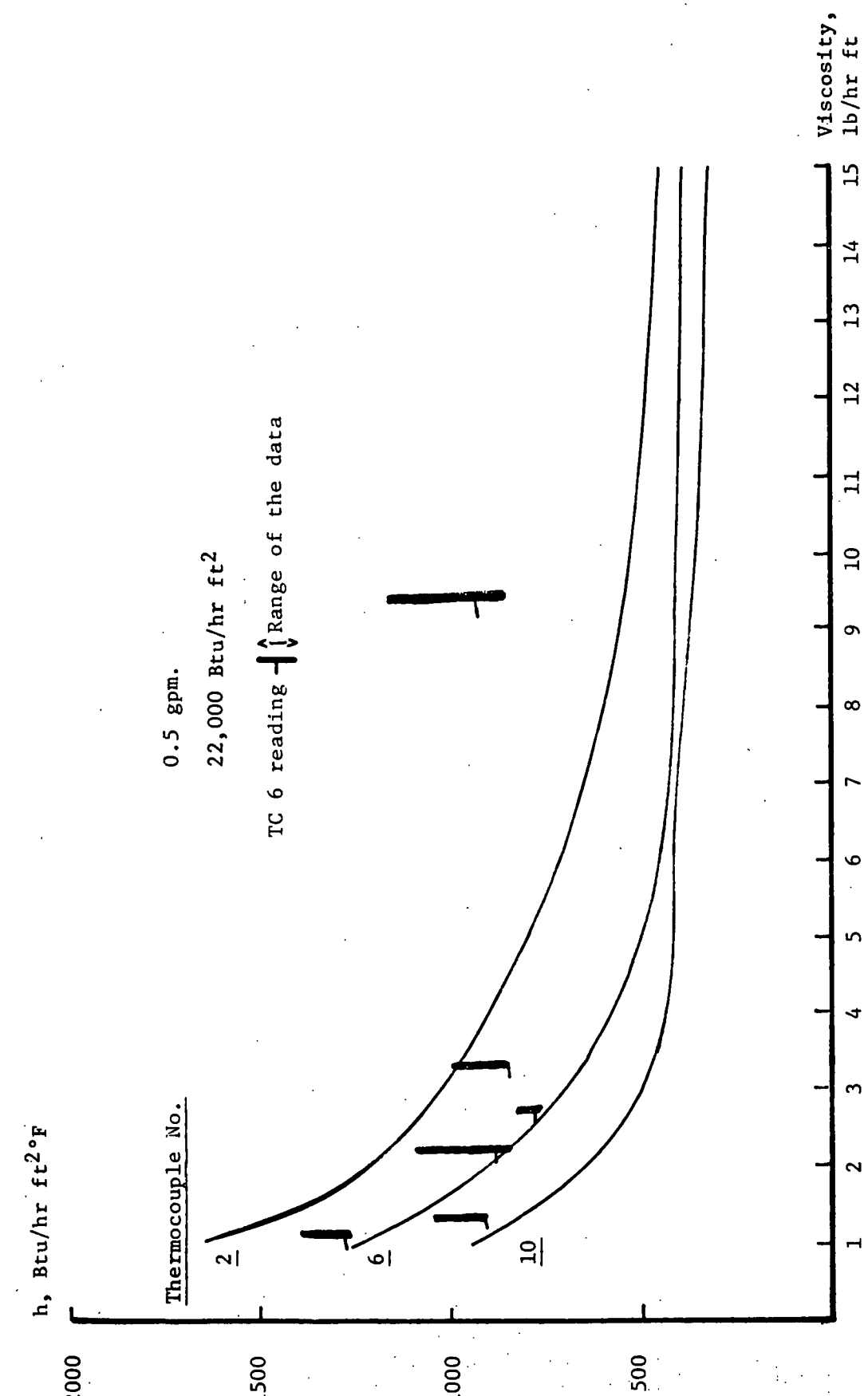

Figure 42. Effects of viscosity on heat transfer coefficients at three positions along the tube. Lines are the predictions of the computer model, vertical bars are data points from NaCMC and guar gum runs. 0.5 gpm, 22,000 Btu/hr ft^2.

lowest reading) along the tube length. The horizontal line near the center of each bar is the local heat transfer coefficient at the tube midpoint (Thermocouple 6). The three curves are the local heat transfer coefficients predicted by the computer model for thermocouple locations 2, 6, and 10. The agreement between the data and the model predictions is excellent for the 0.5 gpm, 11,500 Btu/hr ft^2 case (Fig. 38), although the model again overpredicts the drop in heat transfer along the tube. The model successfully predicts the decline of the heat transfer coefficients with increasing viscosity, which is caused by thicker film deposition and slower drainage in the higher viscosity films hindering the convective transport of heat across the film. The agreement between the data and the model is still reasonable at the next higher heat flux (0.5 gpm and 16,500 Btu/hr ft^2, Fig. 39), but the highest viscosity data point (9.5 lb/hr ft) is significantly higher than predicted. This behavior is also found in the higher feed rates at the same 16,500 Btu/hr ft^2 heat flux (1 gpm, Fig. 40 and 2 gpm, Fig. 41) and is especially serious in the 0.5 gpm, 22,000 Btu/hr ft^2 case (Fig. 42). In all these plots, the low feed viscosity (less than 5 lb/hr ft) data agree well with the model predictions, but the high feed viscosity point (9.5 lb/hr ft) is higher than the predictions. This is not necessarily the result of a defect in the model, since these carbohydrate gum solutions are thioxotropic, and the actual viscosity at the high shear conditions of the higher heat flux runs is probably lower than that measured in the low-shear Ostwald (Cannon-Fenske) viscometer. The thixotropy of the gum solutions would become more pronounced at higher gum concentrations, explaining why the lower viscosity data agree reasonably well with the model, whereas the high viscosity results do not.

SURFACTANT SOLUTION RESULTS

INTRODUCTION

The foam flow experiments which are described in this section had more modest objectives than the slug and churn flow experiments discussed in the first half of

this chapter. There is no possibility of predicting foam flow heat transfer because of the significant effect of foam stability on the heat transfer behavior of foaming flows. Foam stability under high shear conditions cannot be predicted from present knowledge and will probably be different for each surfactant. The problem of foam stability may be further complicated by synergistic effects between the components of a solution. The goal of the present experiments was, therefore, to check on some of the characteristics of foaming flow and especially to confirm the strong effect of viscosity on foam flow heat transfer reported by Gudmundson (20). The discussion of foam flow heat transfer in this section will therefore have to be qualitative and restricted to pointing out the features of the data which reflect the influence of foam stability.

HEAT TRANSFER TO VARIOUS SURFACTANT SOLUTIONS

Heat Transfer to Water Plus Deriphat 160C and Igepal 610 Surfactants

The heat transfer of boiling foaming water was tested using 100-ppm solutions of Deriphat 160C or Igepal 610. Igepal 610 is a low-foaming surfactant. A 100-ppm solution of this material had a surface tension at 68°F of 32.0 dynes/cm^2. The results of the Igepal 610 runs are tabulated in Appendix VI, Series E. Deriphat 160C is a high-foaming surfactant which has a surface tension of 51.7 dynes/cm^2 at a 100-ppm concentration at 68°F. The results for this material are tabulated in Series F of Appendix VI.

Figure 43 illustrates the effect of heat flux on the heat transfer coefficients for the Deriphat 160C solution. The heat transfer coefficients at all three heat fluxes are much higher than for pure water. There is a clear maximum in the heat transfer curves in the bottom third of the heated length. The heat transfer coefficients then decline toward the exit. This is probably a foam stability effect. As the vapor velocity increases along the tube, the heat transfer first rises, as

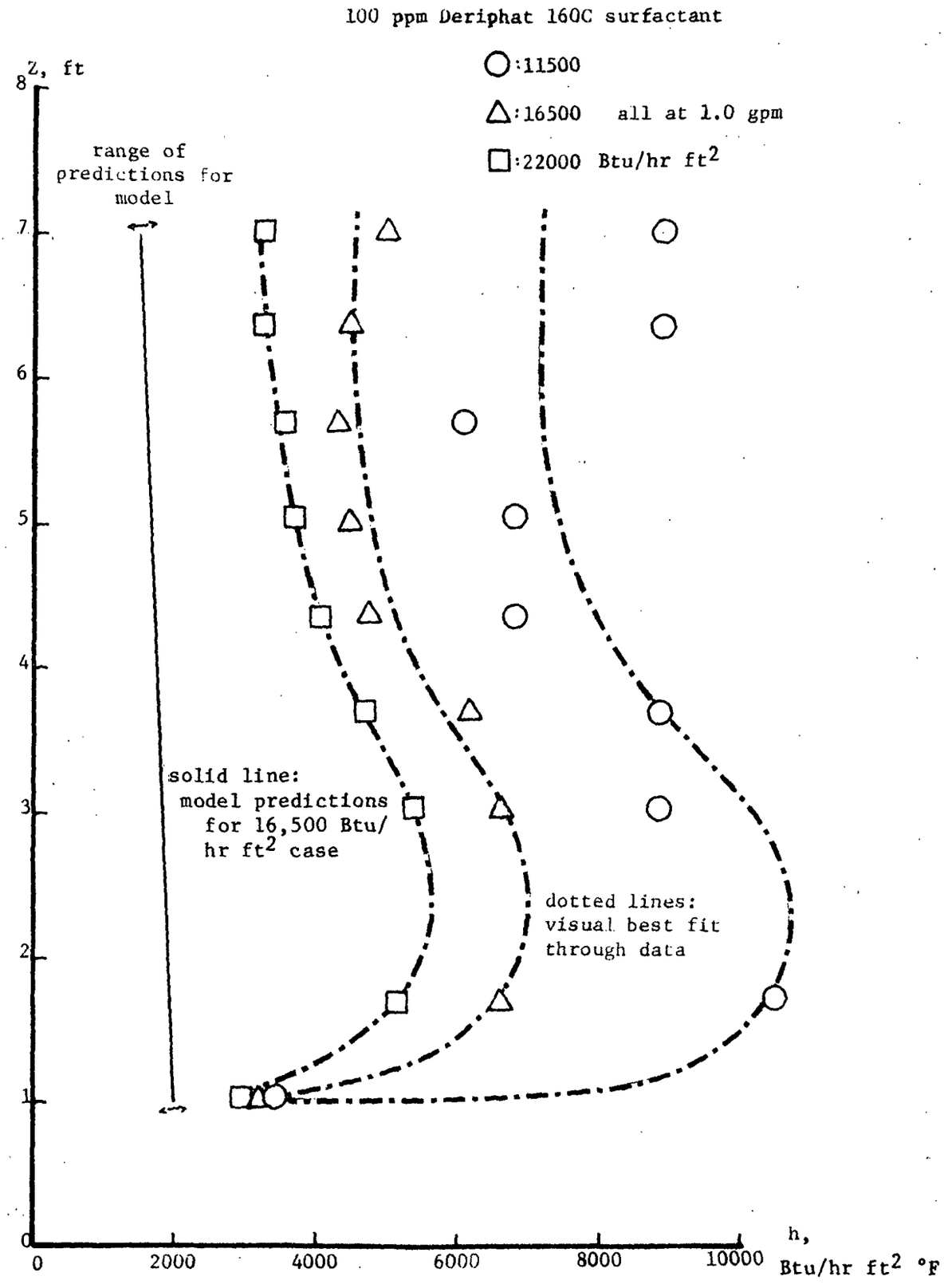

Figure 43. Effect of heat flux on the heat transfer coefficients of a foaming solution (*Deriphat 160C*).

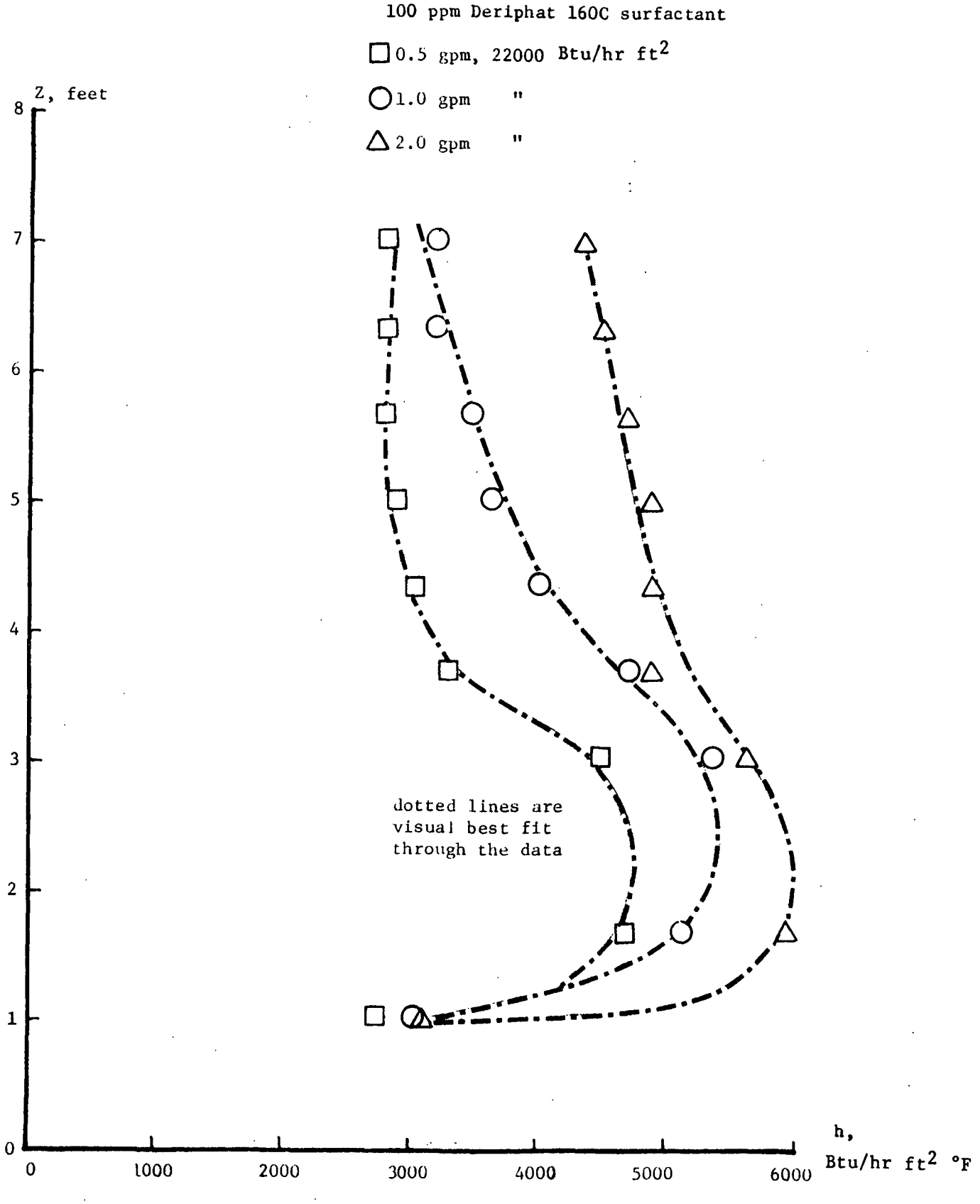

Figure 44. Effect of flow rate on the heat transfer coefficients of a foaming solution (Deriphat 160C).

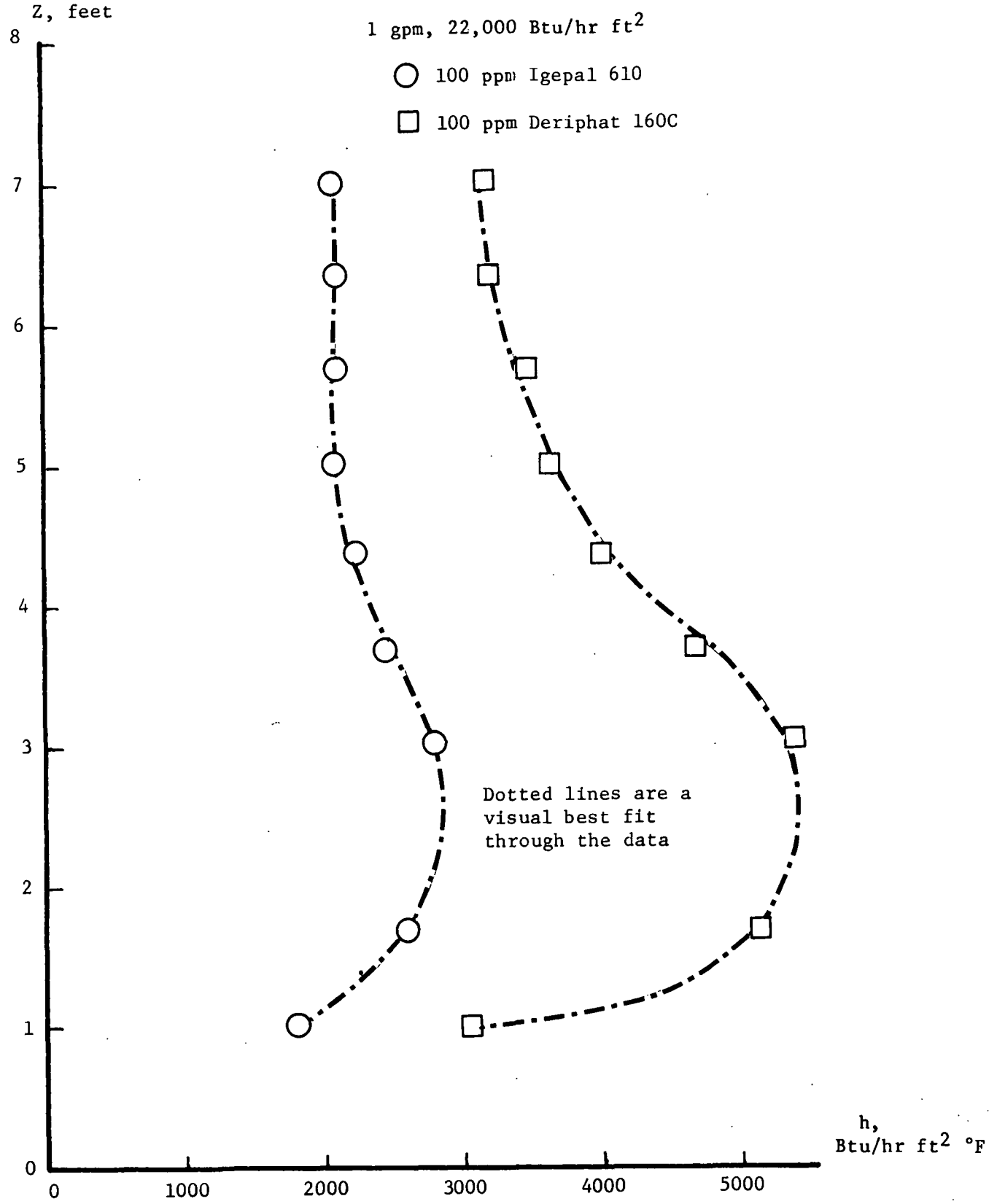

Figure 45. Effect of changing surfactants on the heat transfer coefficients of foaming solutions.

Heat Transfer to 12% Potassium Carbonate Plus Deriphat 160C

Deriphat 160C produces extremely vigorous foaming in salt solutions, since its manufacturer developed it as a dispersant for oil-well drilling brines. This property (Appendix VI, Series P and Fig. 46) leads to an extremely high heat transfer coefficient in 12% potassium carbonate with an added 100 ppm of Deriphat 160C. There is no maximum in heat transfer near the bottom of the tube in this case (Fig. 46). The heat transfer coefficient continues to rise toward the tube exit, since the foam is strong enough to resist disruption. As was discussed in "Fiber Optical Studies of 12% Potassium Carbonate Solution," the 12% potassium carbonate solution was foaming even without added surfactant. Therefore, Fig. 46 also shows the drastic effect increasing foam stability may have on heat transfer in a foaming flow.

Heat Transfer to Guar Gum Solutions with Deriphat 160C Surfactant

A series of experiments on guar gum solutions of different concentrations with 100 ppm of Deriphat 160C added were run (Appendix VI, Series T, U, and V) to confirm a viscosity effect on foam flow reported by Gudmundson (20). When boiling sugar solutions with detergents were added, Gudmundson noted that heat transfer in foaming flow decreased with increasing viscosity. No foam effects were observed at viscosities above 9.6 lb/hr ft (4.0 cp). Gudmundson (20) interpreted this behavior as a foam stability effect.

Figure 47 shows this effect in the present experiments. The heat transfer coefficient is halved when the viscosity is increased from 0.685 lb/hr ft to 1.8 lb/hr ft and decreases more gradually thereafter. The four points toward the top of the tube in the 7.7 lb/hr ft viscosity experiment are not significantly different from the corresponding points in a nonfoaming run with a viscosity of 9.6 lb/hr ft.

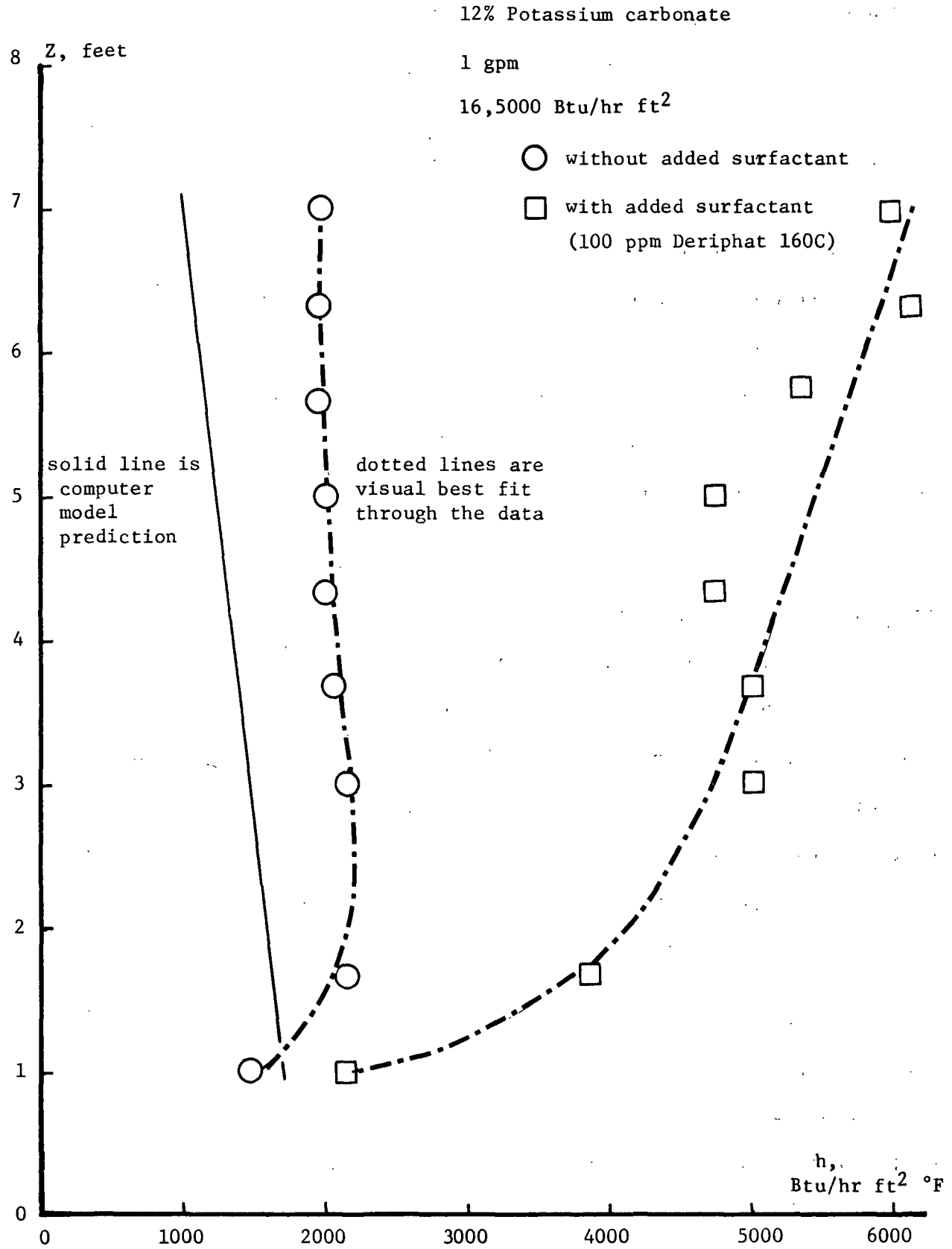

Figure 46. Effect of adding surfactant to 12% potassium carbonate solution. 1 gpm feed, 16,500 Btu/hr ft^2 heat flux.

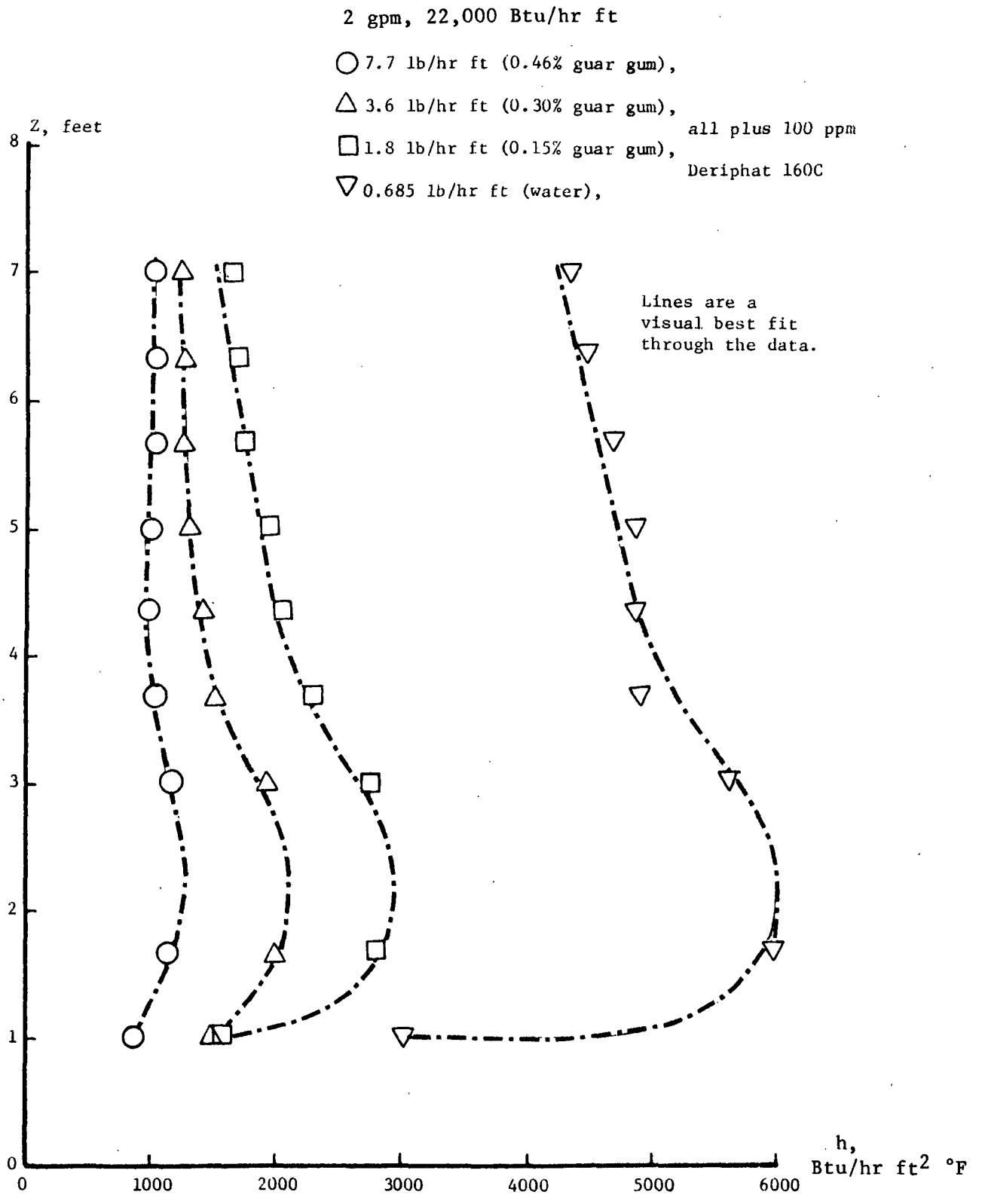

Figure 47. Effect of viscosity on heat transfer in foaming solutions at 2 gpm and 22,000 Btu/hr ft^2.

The comparison between foaming and nonfoaming flow of viscous solutions may be more readily made by consulting Fig. 48. The foaming and nonfoaming heat transfer coefficients converge as the viscosity increases. Near the tube exit, these two curves are converging rapidly below 4 lb/hr ft but approach one another much more slowly as the viscosity is further increased. Above 8 lb/hr ft, the foaming and nonfoaming curves are nearly identical.

Thus, the effect of viscosity on foaming flow heat transfer observed by Gudmundson is confirmed by this study.

BLACK LIQUOR RESULTS

HEAT TRANSFER TO BLACK LIQUOR AT VARIOUS SOLIDS LEVELS

Results for 25% Solids Black Liquor

The results of the heat transfer experiments on 25% solids black liquor are tabulated in Appendix VI, Series L. This solids level of the Georgia mill-mix black liquor foamed vigorously, and the foam flow heat transfer characteristics discussed in the previous section are found in these data as well. The stability of the foam is indicated by the continuing rise in heat transfer along the tube for most flow rates (Fig. 49). At the lowest (0.5 gpm) feed rate, there appears to be insufficient liquid available for a stable foam, and the heat transfer coefficients are lower than those for the higher feed rates. The heat flux effects (Fig. 50) include the decrease in heat transfer with increasing heat flux discussed above.

Results for 35% Solids Black Liquor

The next higher solids level data (Series M in Appendix VI) are still dominated by foaming flow. The average heat transfer coefficients have dropped off substantially, probably due to the effects of increasing viscosity on foam stability. The

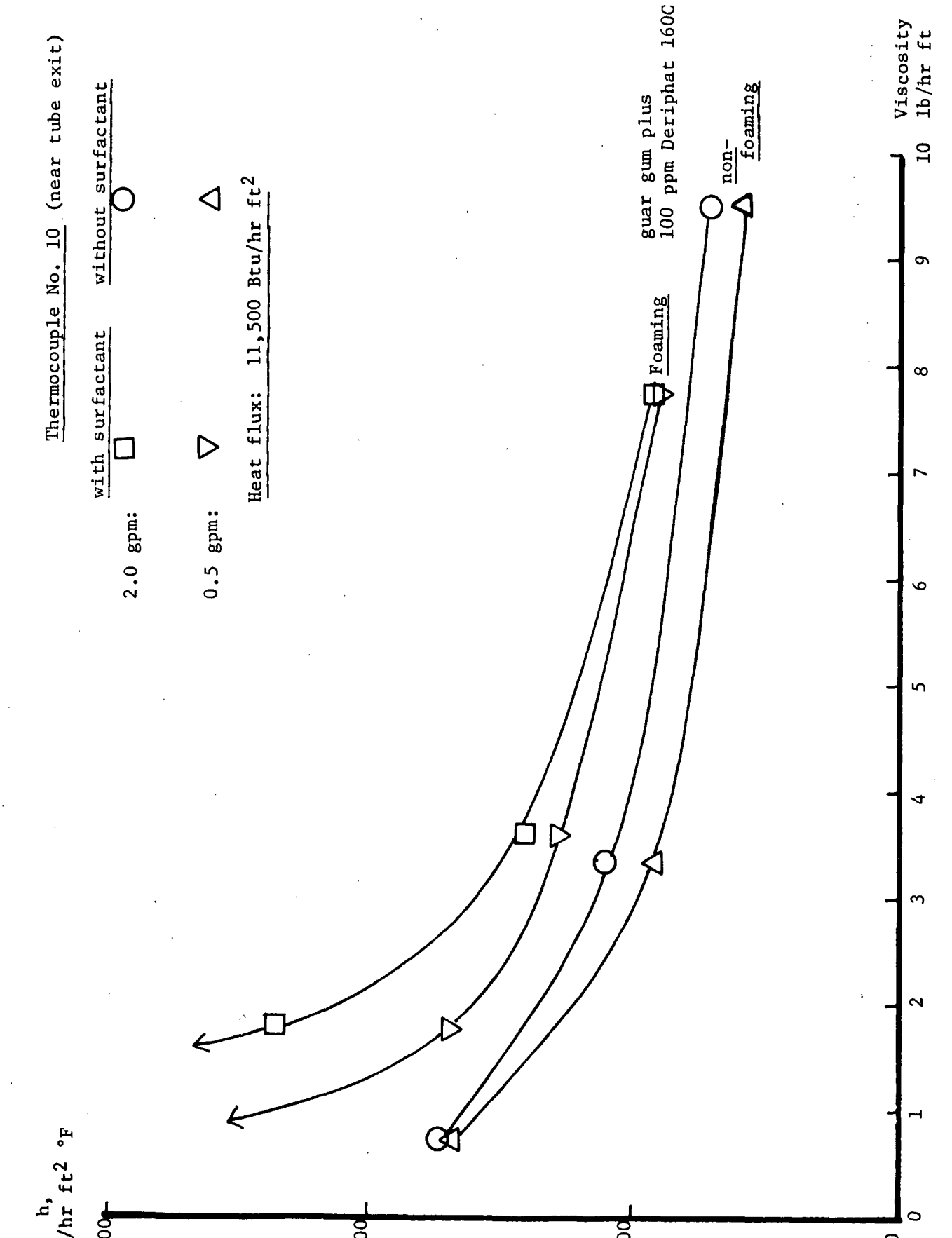

Figure 48. Heat transfer coefficients for guar gum solutions with and without added surfactant.

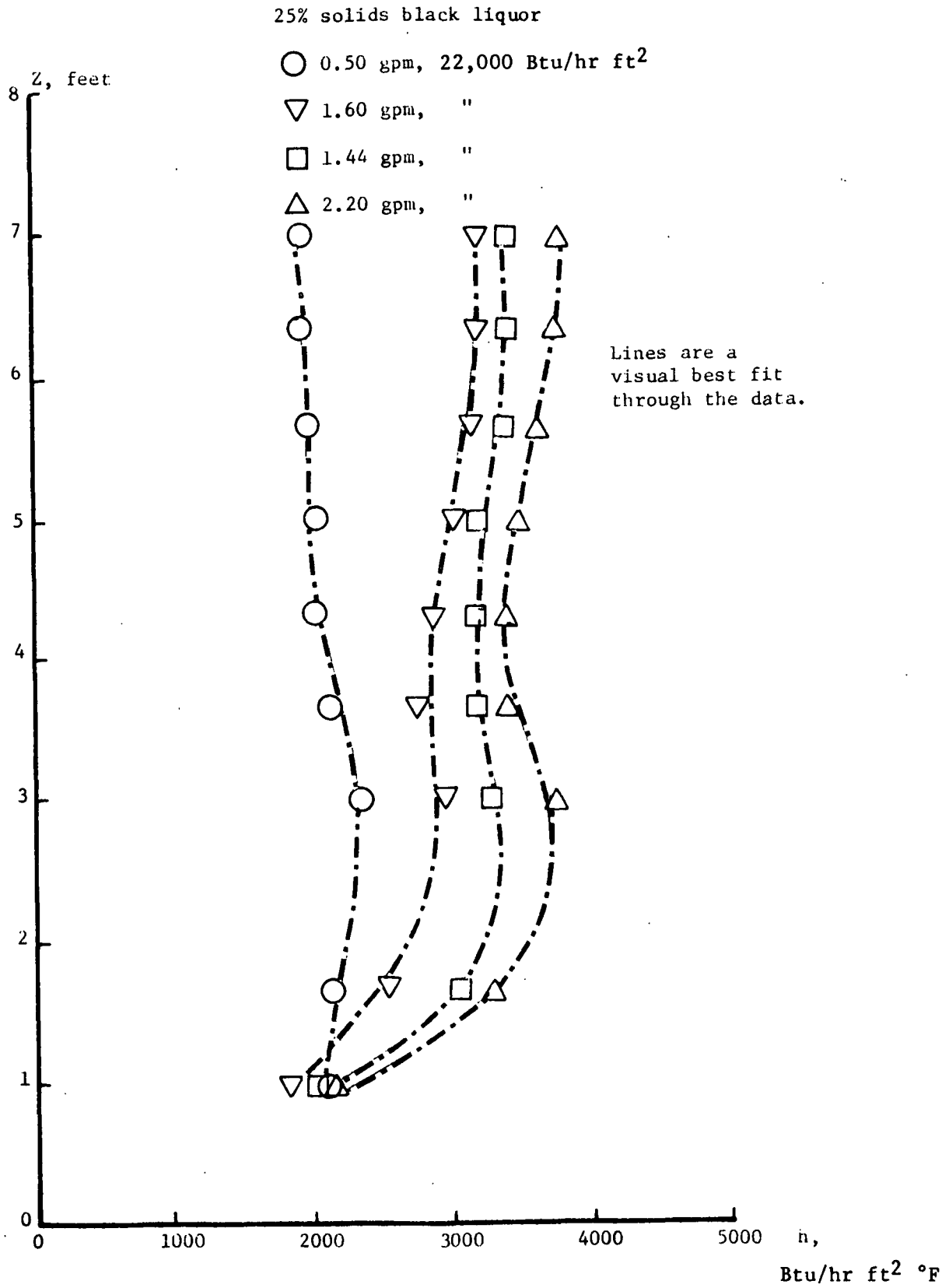

Figure 49. Effects of flow rate on the heat transfer coefficients for 25% solids black liquor at 22,000 Btu/hr ft^2.

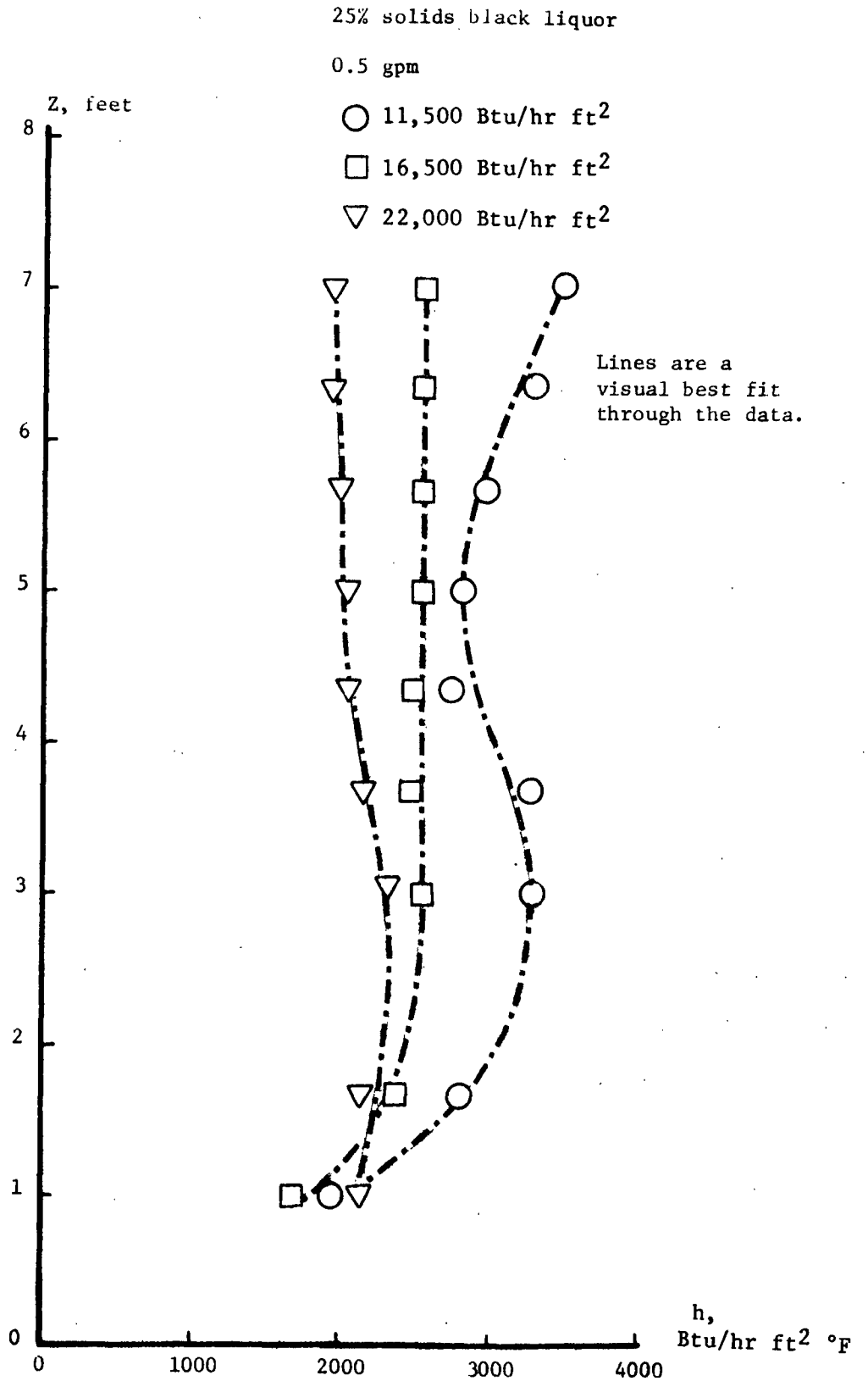

Figure 50. Effects of heat flux on the heat transfer coefficients for 25% solids black liquor at 0.5 gpm feed rate.

effects of feed rate (Fig. 51) and heat flux (Fig. 52) are less extreme than in the 25% solids case but follow similar trends. There is a more pronounced decline in heat transfer along the tube than in the 25% solids experiments, which may also be the result of reduced foam stability in the 35% solids liquor. Agreement between the slug and churn flow computer model predictions and the data is poor, as would be expected given the foaming behavior of this liquor.

Results for 45% Solids Black Liquor

The 45% solids black liquor data (Series N in Appendix VI) continues the expected trend of declining foam flow heat transfer with increasing viscosity. The heat transfer coefficients are closer to the predictions of the slug and churn flow model in this case (Fig. 53) but are still about twice the magnitude of the model predictions. The trends in heat flux (Fig. 53) and feed rate (Fig. 54) are those discussed previously for foaming flows. The decline in heat transfer along the tube is greater in this case than in the 35% and 25% solids experiments, probably as a result of viscosity destabilization of the foam.

CONCLUSION

The experimental program which was discussed in this chapter dealt with two classes of test liquids: those which foam readily and those which do not foam. Nonfoaming liquids, including water and potassium carbonate and carbohydrate gum solutions, give slug and churn flow behavior under the experimental conditions of this study. The heat transfer data for the nonfoaming liquids show an inverse dependence of the heat transfer coefficient on the heat flux. No effect of flow rate on heat transfer is observed for water under these conditions. The flow rate effects observed for the nonfoaming solutions appear to be due to changes in concentration. These observations contradict the predictions of the Chen correlation, which assumes that the upward-flow convective and nucleate boiling mechanisms are

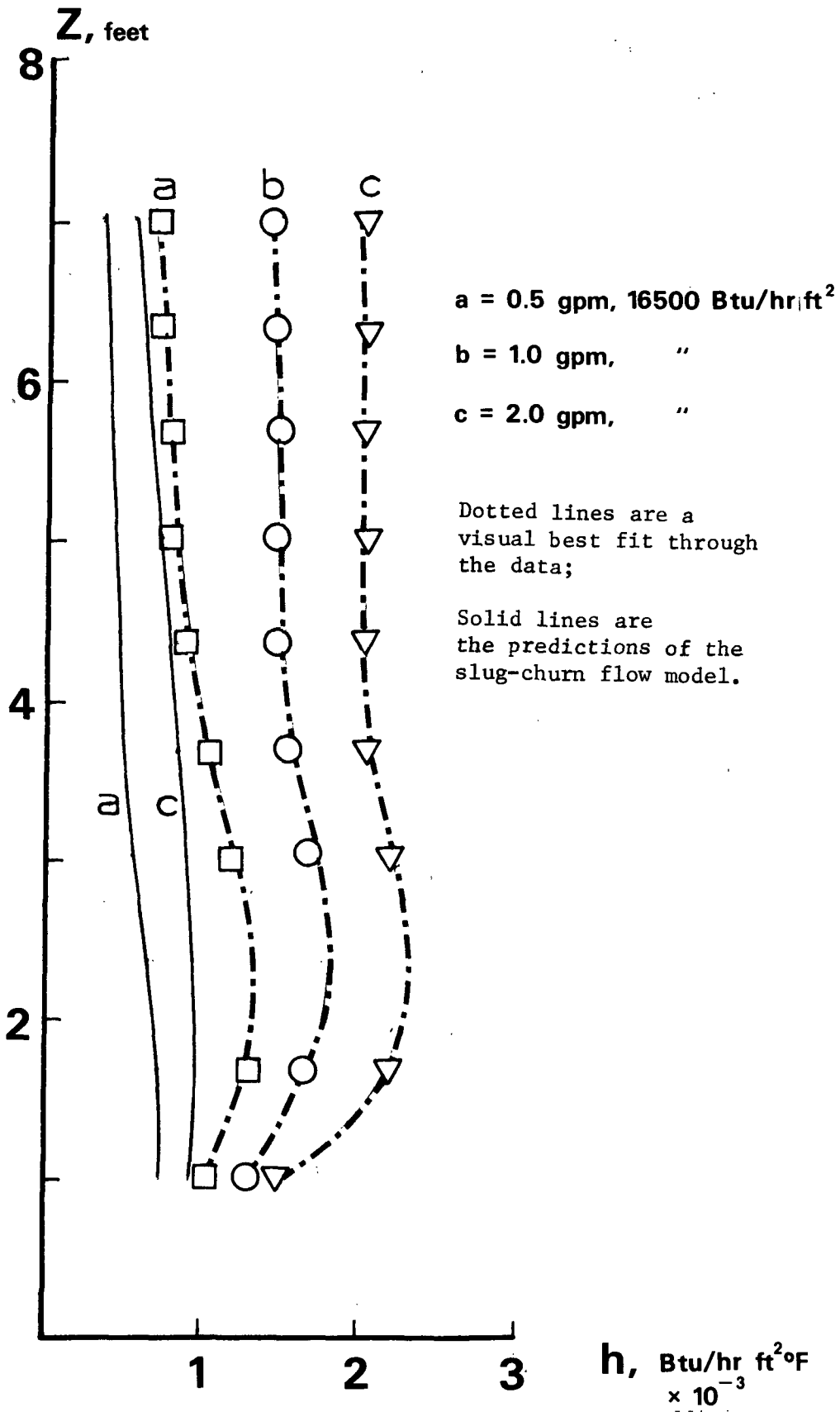

Figure 51. Effect of flow rate on the heat transfer coefficients of 35% solids black liquor at 16,500 Btu/hr ft^2.

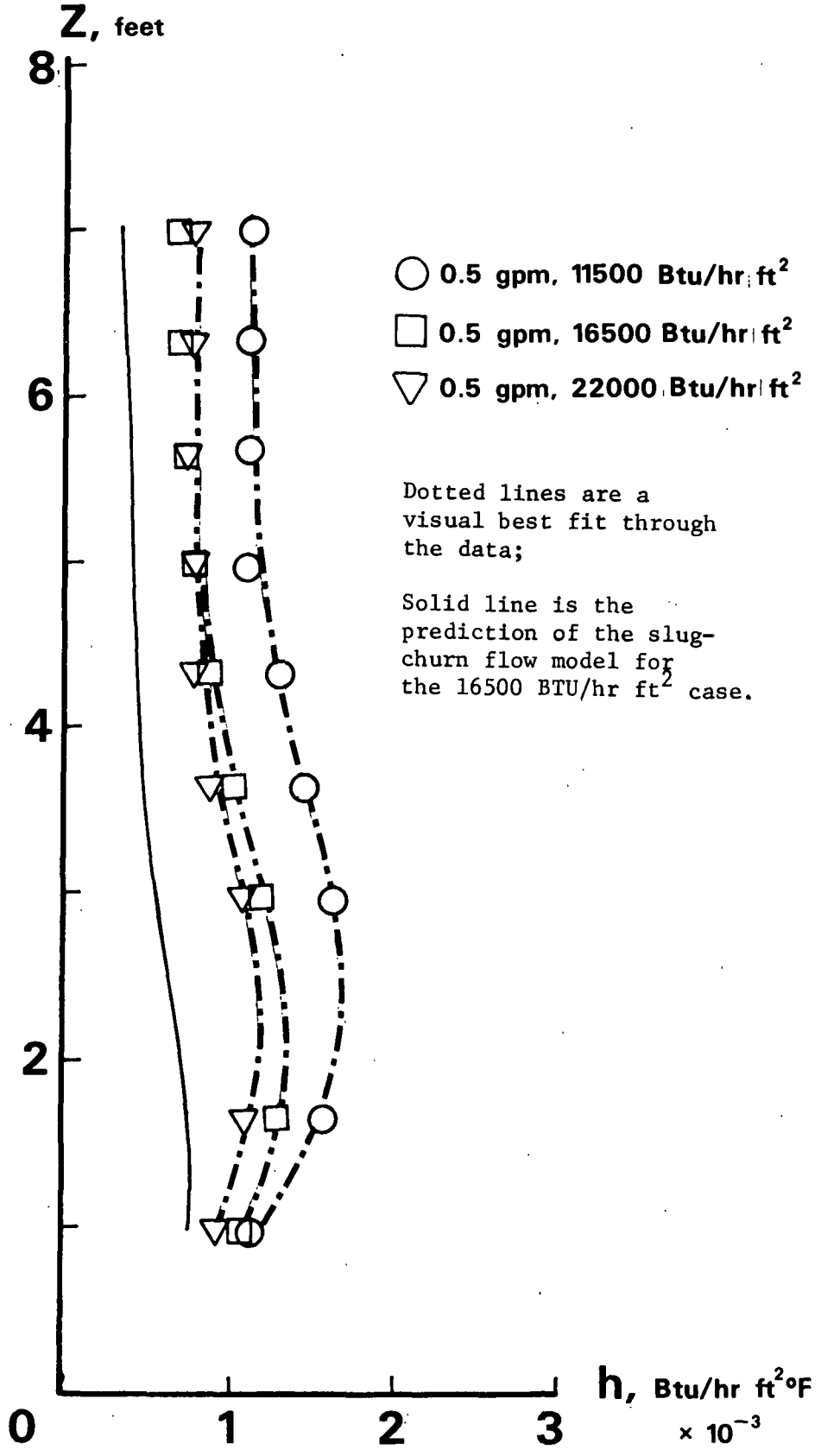

Figure 52. Effect of heat flux on the heat transfer coefficients of 35% solids black liquor at 0.5 gpm.

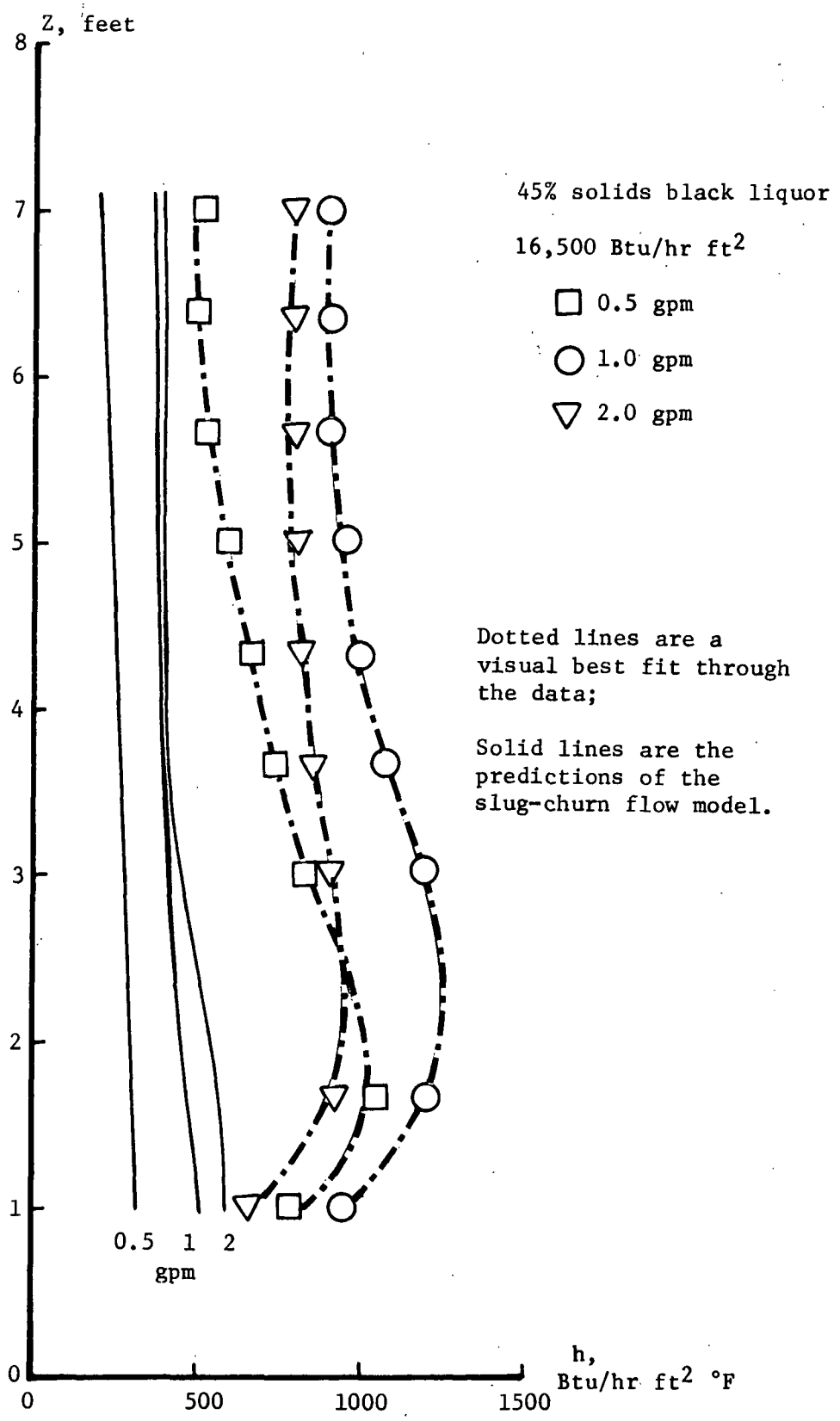

Figure 53. Effect of flow rate on the heat transfer coefficients of 45% solids black liquor at 16,500 Btu/hr ft^2.

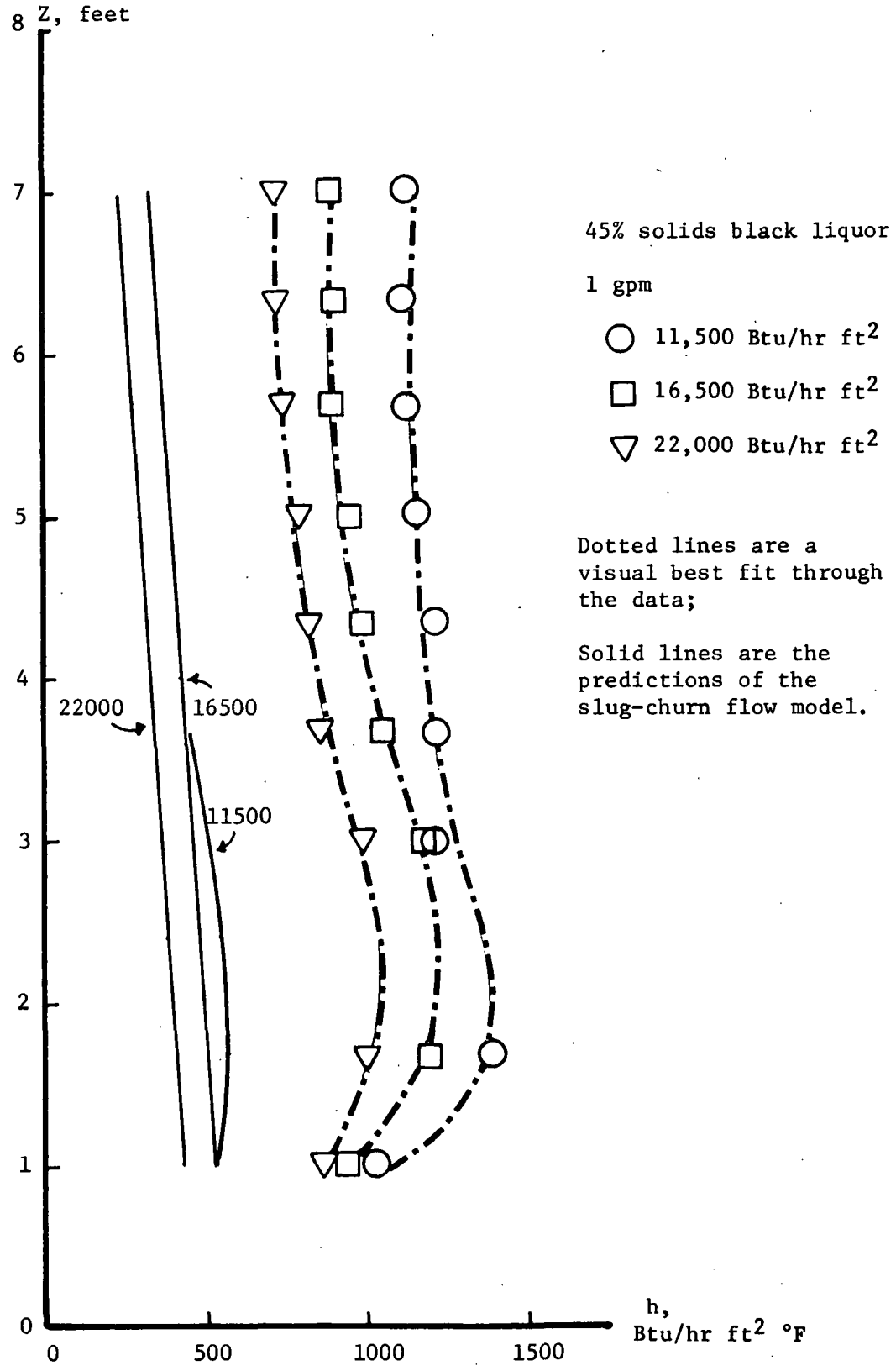

Figure 54. Effect of heat flux on the heat transfer coefficients of 45% solids black liquor at 1 gpm feed rate.

the dominant heat transfer mechanisms. However, the simple numerical model of heat transfer to intermittently renewed falling films, described in "A Numerical Model for Slug and Churn Flow," adequately predicts both the heat flux and the flow rate effects.

The experimental evidence thus supports the hypothesis that the major heat transfer mechanism for nonfoaming flow under conditions typical of black liquor evaporation is the convective transport of heat across intermittently renewed falling films.

The model is not completely successful, however, since it overpredicts the amount of backflow in the films, probably because of the inadequate methods which are used in the model to deal with the phenomena of flooding.

Heat transfer to foaming liquids is not as easily explained, but most of the effects observed in the data may be qualitatively explained by considering an upward convective mechanism in which the holdup of most of the liquid in the foam walls leads to low interphase slip and thus to a high mixture velocity with thin and highly agitated films on the tube walls. This mechanism is counterbalanced by the tendency of the foam to break down under increasing shear as evaporation proceeds or as the heat flux is increased. When the foam breaks down, interphase slip increases and the films will become thicker and slower moving, and may ultimately revert to the falling film situation described for slug and churn flow. Foam stability is also decreased by increasing viscosity and may be altered by the presence of trace materials in a solution.

CONCLUSIONS

SYNOPSIS OF THE RESULTS OF THIS STUDY

The slug and churn flow regimes have been identified in the literature as the principal flow regimes in black liquor evaporators in the absence of foaming. This information about the flow regimes does not tell us enough about the mechanisms of heat transfer in the evaporators, since these complex flow patterns potentially include several mechanisms which could be important in heat transfer. The first possible mechanism is the convective transport of heat effected by the net-upward flow, either by turbulence in the liquid lumps or by agitation of the films on the tube walls by the flow of vapor. The second mechanism involves the transport of heat by the growth and departure of bubbles on the tube walls known as nucleate boiling. A third mechanism operates by the convective transport of heat across the intermittently renewed falling films deposited on the tube walls. The initial hypothesis of this study was that the combination of the upward convection and nucleate boiling mechanisms expressed in the widely successful Chen correlation for annular flow boiling would account for the major effects of the experimental variables on the process of evaporation.

This hypothesis was shown to be false by using careful measurements of the inside film heat transfer coefficients of solutions evaporating in an electrically heated pilot black liquor evaporator. In particular, the Chen correlation predicts an increasing heat transfer coefficient with increasing heat flux due to a combination of intensified nucleate boiling and higher mixture velocities at any given point as the heat flux is increased. The experimental data, taken on water and solutions of potassium carbonate and carbohydrate gums, show the opposite effect - the heat transfer coefficients decrease as the heat flux is increased.

A simple numerical model of the deposition, drainage, and heat transfer of falling films in slug and churn flow was successful in explaining these effects. The explanation for the observed heat flux effect offered by this model is that the higher cumulative evaporation, and so vapor velocity, at a given point as the heat flux is increased causes more complete flooding of the films deposited at that point. Higher heat fluxes thus result in thinner falling films. As the film flow rate is tied to film thickness, a thinner film will drain more slowly, and therefore have a lower Reynolds number and, so long as the film remains turbulent, a lower heat transfer coefficient.

The success of this slug and churn flow model in predicting the effects of heat flux, flow rate, density, and viscosity on heat transfer to nonfoaming solutions supports the conclusion that the major heat transfer mechanism in black liquor evaporators in the absence of foaming is the convective transport of heat across intermittently renewed downward-flowing films.

Data were also collected under foaming flow conditions. Foam flow heat transfer appears to be dominated by an upflow convective mechanism which is strongly influenced by the stability of the foam under high shear conditions. Too little is known about foam stability under such conditions to elaborate this hypothesis into a formal heat transfer model.

SUGGESTIONS FOR FURTHER WORK

The long-tube vertical black liquor evaporator was adopted by the paper industry as a developed technology which could be easily applied to fill a pressing need. It is not necessarily the best piece of equipment to serve the required purpose. This study indicates a fundamental problem with the LTV evaporator: a heat transfer maximum in the middle of the tube caused by unfavorable developments in the flow regimes which occur naturally and inevitably along the tube. The good heat transfer

in slug and churn flow is a result of falling films; therefore, it seems logical to investigate the true falling film evaporator as an alternative to the LTV evaporator.

In existing evaporator installations, it may be worthwhile to check:

1. Whether the slug rate can be changed by pressure oscillations imposed on the evaporator system, and whether the heat transfer performance can be improved by increasing the slug rate as suggested by the model predictions.

2. Whether the drop-off in heat transfer toward the top of the tube can be controlled by permitting some flooding in the vapor head, leading to flow back into the tubes which would prevent thinning of the films on the tube walls.

3. Whether increasing recycle may be a better way to increase evaporation rather than just turning up the steam pressure, since increasing vapor mass quality by itself will tend to cause an unfavorable flow regime development.

Further experiments which could be done on the pilot evaporator constructed for this work include:

4. Studying the effects of pressure on slug and churn flow, and whether the model can account for such effects.

5. More sophisticated tracer studies (probably using radioactive tracers and complex detection equipment) to check on backflow, film lifetimes and mixing between the films on the walls and passing slugs. Such a study could be valuable in understanding the scale formation process.

When a more powerful computer becomes available, the slug and churn flow model could be modified by:

6. Incorporating the Dukler (80) theoretical treatment of falling film flow and heat transfer into the model in place of the Belkin (79) empirical correlation. The Dukler model can account for interfacial friction between the rising vapor and the falling liquid and might offer a way around the instantaneous flooding assumption that is the worst flaw in the model developed for this study. This would be a difficult and extremely long-running computer program.

ACKNOWLEDGMENTS

I would like to acknowledge Dr. W. J. Frederick for suggesting this research topic, and to thank Drs. Frederick, T. Grace, and M. Doshi for serving on the thesis advisory committee.

The details of the electrical system design were worked out by M. Godschalx, and the electrical components were installed by R. Mirabello, L. Vandenberg, and J. Chew. P. Van Rossum and M. Filz machined many parts for the equipment. O. Kuehl and B. Andrews gave invaluable assistance in getting the experimental equipment to work.

Finally, I wish to thank The Institute of Paper Chemistry and its member companies for the financial support which made this project possible.

NOMENCLATURE

a	Constant, Eq. (14)	dimensionless
a	inside radius of pipe wall	ft
A	constant, Eq. (4)	dimensionless
A	constant, Eq. (6)	dimensionless
A	heat production per volume of wall	Btu/ft^3 hr
A	Stephan-Korner parameter, Eq. (73)	dimensionless
A_o	Stephan-Korner parameter, Eq. (74)	dimensionless
A	area	ft^2
b	outside radius of pipe wall	ft
b	constant, Eq. (6) (14)	dimensionless
B	constant, Eq. (14)	dimensionless
B_o	"Boiling number" (q/h_{fg} G)	dimensionless
c_p	heat capacity	Btu/lb °F
c	constant, Eq. (6)	dimensionless
C	flooding constant, Eq. (113)	dimensionless
C_d	drag coefficient	dimensionless
C_f	friction coefficient	dimensionless
d	droplet diameter, tube diameter in Eq. (87) only	feet
D	tube diameter	feet
D	diffusion coefficient	ft^2/hr
E	a nucleate boiling factor, Eq. (41)	dimensionless
F	a nucleate boiling factor, Eq. (38)	dimensionless
F	Chen two-phase Reynolds number correction factor	dimensionless
F	mass fraction of a component	dimensionless
g_c	gravitational constant	ft/hr^2
G	mass flux	lb/hr ft^2
h	inside film heat transfer coefficient	Btu/hr ft^2 °F
$\overline{h}_b$	h based on averaged wall and liquid temperatures	Btu/hr ft^2 °F
$\overline{h}_{local}$	h based on average values over a section of tube	Btu/hr ft^2 °F
h_{lo}	h defined by Eq. (5)	Btu/hr ft^2 °F
h_l	h from definition $h_l = (1 - x)^{0.8} h_{lo}$	Btu/hr ft^2 °F
h_{mic}	microconvective h, Eq. (70)	Btu/hr ft^2 °F
h_{mac}	macroconvective h, Eq. (54)	Btu/hr ft^2 °F
h_{mic}°	pool boiling microconvective h, Eq. (67)	Btu/hr ft^2 °F
h_{fg}	specific latent heat of vaporization	Btu/lb

h_m	mass transfer coefficient	ft/hr
h_z	axial coordinate relative to bubble nose	ft
j	superficial velocity	ft/hr
j	mass flux	lb/hr ft^2
j*	dimensionless velocity, Eq. (111)	dimensionless
k	thermal conductivity	Btu/hr ft^2 °F
M	molecular weight	lb/mole
n	constant, Eq. (4)	dimensionless
Nu	Nusselt number, (hD/k)	dimensionless
N_f	dimensionless reciprocal viscosity	dimensionless
p	pressure	psia
Δp	pressure drop	psi
Pr	Prandtl number (c_p μ/k)	dimensionless
q	heat flux	Btu/hr ft^2
Q	heating rate	Btu/hr
Q	volumetric flux	ft^3/hr
r	radial coordinate with respect to tube axis	ft
r*	critical bubble radius	ft
r_c	radius of cavity mouth	ft
R	gas constant	ft lb_f/lb_m °F
R	bubble radius	ft
$\dot{R}$	bubble radial growth rate	ft/hr
$\ddot{R}$	bubble radial acceleration	ft/hr^2
Re	Reynolds number (ρ vD/μ) or $Re_\Gamma = (4\Gamma/\mu)$	dimensionless
S	Chen nucleate boiling suppression factor	dimensionless
S_{binary}	Chen nucleate boiling suppression factor for binary mixture	dimensionless
Sc	Schmidt number (μ/ρD)	dimensionless
t	time	hr
T	temperature	°F
ΔT	temperature drop	°F
$\widetilde{\Delta T}$	temperature drop defined by ($T_w - T_i$)	°F
u	velocity	ft/hr
$\overline{u}$	average superficial vapor velocity, Eq. (7)	ft/hr
u_m	log-mean velocity, Eq. (17)	ft/hr
u_{ave}	average velocity defined by Eq. (40)	ft/hr
U	overall heat transfer coefficient	Btu/hr ft^2 °F
U_B	U evaluated over boiling length only	Btu/hr ft^2 °F
U_{local}	sectional overall heat transfer coefficient	Btu/hr ft^2 °F

v	specific volume	ft^3/lb
v_∞	rise velocity of slug, Eq. (94)	ft/hr
v_{gj}	drift velocity of slug, Eq. (96)	ft/hr
v_b	corrected drift velocity of slug, Eq. (97)	ft/hr
v_g^s	superficial vapor velocity	ft/hr
v_g^t	true vapor velocity ($v_g^t = v_g^s (1 - \alpha)$)	ft/hr
W	mass flow rate	lb/hr
We	Weber number ($Du^2/\rho\sigma g_c$)	dimensionless
x	vapor mass quality	dimensionless
x	liquid mole fraction of a component	dimensionless
x_∞	liquid mole fraction of a component far from the wall	dimensionless
y	radial coordinate taken with the wall as zero	ft
y	vapor mole fraction of a component	dimensionless
y_∞^*	vapor mole fraction corresponding to x_∞	dimensionless
z	axial coordinate with zero at tube entrance	ft

GREEK

α_{fg}	slip ratio	dimensionless
α	void fraction	dimensionless
α_t	thermal diffusivity	ft^2/hr
Γ	film flow rate	lb/hr ft of wall
δ	boundary layer thickness	ft
δ	falling film thickness	ft
δ^*	dimensionless film thickness, Eq. (116)	dimensionless
ε	eddy momentum diffusivity	ft^2/hr
θ	contact angle	degrees
κ	von Kármán constant, Eq. (119)	dimensionless
μ	viscosity	lb/hr ft
υ	kinematic viscosity	ft^2/hr
ρ	density	lb/ft^3
τ	shear stress	$lb/ft\ hr^2$

SUBSCRIPTS

a	"inside wall of tube"
ave	"average"
A	"component A"

b	"on outside wall of tube"
b	"of a bubble"
b	"boiling"
B	"component B"
B	"boiling"
c	"critical"
e	"effective"
f	"liquid phase"
fg	"of vaporization"
g	"vapor phase"
gj	"drift (velocity)"
i	"interfacial"
in	"at tube inlet"
local	"of one section of the tube"
m	"log mean"
mac	"macroconvective"
mic	"microconvective"
sat	"saturated"
ss	"stainless steel"
t	"total flow"
TP	"two-phase"
tt	"turbulent liquid - turbulent vapor"
v	"vapor phase"
w	"wall"
∞	"far from the wall"

SUPERSCRIPTS

°	"nucleate pool boiling conditions"
*	"dimensionless"
*	"critical (as in r*)"
-	"averaged over tube length"
t	"true (not superficial)"
s	"superficial (not true)"
	"based on interface conditions"
·	"first derivative with respect to time"
"	"second derivative with respect to time"

LITERATURE CITED

1. Chen, J. C. A correlation for boiling heat transfer to saturated liquids in convective flow. ASME Paper 63-HT-34, 1963.

2. Butterworth, D. and Hewitt, G. F., editors. Two phase flow and heat transfer. Oxford University Press, 1977.

3. Collier, J. G. Convective boiling and condensation. McGraw Hill Co., N.Y., N.Y., 1972.

4. Hewitt, G. F. and Hall-Taylor, N. Annular two-phase flow. Pergamon Press, N.Y., N.Y., 1970.

5. Hsu, Y.-Y. and Graham, R. W. Transport processes in boiling and two-phase systems. Hemisphere Publishing Co., Washington, 1976.

6. Wallis, G. B. One dimensional two-phase flow. McGraw Hill Co., N.Y., N.Y., 1969.

7. Soo, S. L. Fluid dynamics of multiphase systems. Blaisdell Publishing, Waltham, MA, 1967.

8. Tong, L. S. Boiling heat transfer and two-phase flow. John Wiley and Sons, Inc., N.Y., N.Y., 1965.

9. Wills, W. R. and Hedström, B. Experimental and theoretical studies of long-tube vertical evaporators - Part 1: Statement of the problem, presentation, and qualitative discussion of observed phenomena. Svensk Papperstid. 66(17): 667-76(1963).

10. Wills, W. R. and Hedström, B. Experimental and theoretical studies of long-tube vertical evaporators - Part 2: Presentation and discussion of quantitative data. Svensk Papperstid. 67(11):457-66(1964).

11. McKee, H. R. Thermosiphon reboilers - a review. Ind. Eng. Chem. 62(12):76 (1970).

12. Brooks, C. H. and Badger, W. L. Heat transfer coefficients in the boiling section of a long-tube, natural circulation evaporator. Trans. AIChE 1937:392-415.

13. Taitel, Y., Bornea, D., and Dukler, A. E. Modelling flow pattern transitions for steady upward gas-liquid flow in vertical tubes. AIChE 26(3):345-54(May, 1980).

14. Gudmundson, C., Alsholm, H., and Hedström, B. Heat transfer in industrial black liquor plants. Svensk Papperstid. 19:773-83(Oct., 1972).

15. Badger, W. L. How the long-tube evaporator works. Chem. and Metall. Eng. 46(10):640-1(Oct., 1939).

16. Stroebe, G. W., Baker, E. M., and Badger, W. L. Boiling film heat transfer coefficients in a long-tube vertical evaporator. Trans. AIChE 35:17-43(1939).

17. Cessna, O. C., Lientz, J. R., and Badger, W. L. Heat transfer in a long tube vertical evaporator. Trans. AIChE 36:759-79(1940).

18. Kirschbaum, E. Neues zum Wärmeübergang mit und ohne Änderung des Aggregatzustandes. Chem. Ing. Tech. 24:393-400(1952).

19. Coulson, J. M. and Mehta, R. R. Heat transfer coefficients in a climbing film evaporator. Trans. Instn. Chem. Engrs. 31:208-28(1953).

20. Gudmundson, C. Heat transfer in industrial black liquor plants. Svensk Papperstid. 22:901-8(Dec., 1972).

21. Grace, T. and Andrews, B. D. Study of evaporator scaling - soluble carbonate-sulfate scales. IPC Report, Project 3234, Report Two, Jan. 25, 1977.

22. Olson, G. M. Heat transfer coefficients in a LTV black liquor evaporator. IPC Master's Degree Research (A-291) Report, March 25, 1979.

23. McAdams, W. H. Heat transmission. McGraw Hill Co., N.Y., N.Y., 1954.

24. Pozzuto, S. Heat transfer in long-tube vertical evaporators. IPC Master's Degree Research (A-291) Report, Feb. 14, 1978.

25. Sephton, H. H. Interface enhancement for vertical tube evaporators: a novel way of substantially augmenting heat and mass transfer. ASME Paper 71-HT-38. 1971.

26. Anderson, G. H., Haselden, G. G., and Mantzouranis, B. G. Two-phase (gas-liquid) flow phenomena-IV. Experimental study of water evaporation in a vertical tube. Chem. Eng. Sci. 17:751-69(1962).

27. Bennett, J. A. R., Collier, J. G., Pratt, H. R. C., and Thornton, J. D. Heat transfer to two-phase gas-liquid systems - Part I: Stream water mixtures in the liquid dispersed region in an annulus. U.K.A.E.R.E. Report AERE-R3159, 1959; Trans. Instn. Chem. Engrs. 39:113ff(1961).

28. Collier, J. G., Lacey, P. M. C., and Pulling, D. J. Heat transfer to two-phase gas-liquid systems - Part II: Further data on steam-water mixtures in the liquid dispersed region in an annulus. Trans. Instn. Chem. Engrs. 42:T127-39 (1964).

29. Dengler, C. E. and Addoms, J. N. Heat transfer mechanisms for vaporization of water in a vertical tube. Chem. E. Prog. Symp. Ser. 52(18):95-103(1956).

30. Guerrieri, S. A. and Talty, R. D. A study of heat transfer to organic liquids in single-tube, natural convection, vertical tube boilers. Chem. Eng. Prog. Symp. Ser. Heat Transfer, Louisville 52(18):69-77(1956).

31. Penman, T. O. and Tait, R. W. F. Heat transfer in liquid film flow. Ind. Eng. Chem. Fund. 4(4):407(1965).

32. Piret, E. L. and Isbin, H. S. Natural circulation evaporation - two-phase heat transfer. Chem. Eng. Prog. 50(6):305-11(June, 1954).

33. Schrock, V. E. and Grossman, L. M. Forced convection boiling studies - forced convection vaporization project. U.S.A.E.C. Report TID-14632. 1959.

34. Shock, R. A. W. The evaporation of binary mixtures in forced convection. Oxford (U.K.) University Ph.D. thesis, 1973.

35. Shock, R. A. W. Nucleate boiling in binary mixtures. Int. J. Heat Mass Transfer 20:701-9(1977).

36. Toral, H., Kenning, D. B. R., and Shock, R. A. W. Flow boiling of binary mixtures. AERE Harwell Report HTFS-RS248, 1978.

37. von Kármán T. The analogy between fluid friction and heat transfer. Trans. Amer. Soc. Mech. Engrs. 61:705-10(1939).

38. Hewitt, G. F. Analysis of annular two-phase flow: application of the Dukler analysis to vertical upward flow in a tube. U.K.A.E.R.E Report R3680 (1961).

39. Deissler, R. G. Analytical and experimental investigation of adiabatic turbulent flow in a smooth tube. NACA Tech. Note 2138. 1952.

40. von Kármán, T. Mechanical theory of turbulence. Third Int'l. Congress Appl. Mech., Stockholm, 1:85(1930).

41. Collier, J. G. and Pulling. D. J. Heat transfer to two-phase gas-liquid systems. - Part II: Further data on steam-water mixtures in the liquid dispersed region in an annulus. U.K.A.E.A. Report No. AERE-R3809 (1962). Also published as: Trans. Instn. Chem. Engrs. 42:127-39(1964).

42. Lockhart, R. W. and Martinelli, R. C. Proposed correlation of data for isothermal, two-component flow in pipes. Chem. Eng. Prog. 45(1):39-48 (Jan., 1949).

43. Shock, R. A. W. Estimation methods for forced convective boiling. Chapter 10 of Butterworth and Hewitt, 1977.

44. Davis, E. J. and David, M. M. Two-phase gas-liquid convection heat transfer. I&EC Fundam. 3(2):111-18(May, 1964).

45. Davis, E. J. and David, M. M. Heat transfer to high quality steam-water mixtures flowing in a horizontal rectangular duct. Can. J. Chem. Eng. June, 1961. pp. 99-112.

46. Anderson, G. H. and Mantzouranis, B. G. Two-phase (gas-liquid) flow phenomena-I. Pressure drop and hold-up for two-phase flow in tubes. Chem. Eng. Sci. 12:109-26(1960).

47. Anderson, G. H. and Mantzouranis, B. G. Two-phase (gas-liquid) flow phenomena-II. Liquid entrainment. Chem. Eng. Sci. 12:233-42(1960).

48. Anderson, G. H., Haselden, G. G., and Mantzouranis, B. G. Two-phase (gas-liquid) flow phenomena-III. The calculation of heat transfer in a vertical long-tube evaporator. Chem. Eng. Sci. 16:222-30(1961).

49. Kenning, D. B. R. Pool boiling. Chapter 7 in Butterworth and Hewitt, 1977.

50. Schrock, V. E. and Grossman, L. M. Forced convection in tubes. Nuc. Sci. Eng. 12:474-81(1962).

51. Rohsenow, W. M. A method of correlating heat transfer data for surface boiling of liquids. Trans. ASME Aug., 1952:969-76.

52. Chen, J. C. A correlation for boiling heat transfer to saturated fluids in convective flow. I&EC Process Design Devt. 5(3):322-9(1966).

53. Forster, H. K. and Zuber, N. Dynamics of vapor bubbles and boiling heat transfer. AIChE J. 1(4):531-5(1955).

54. Plesset, M. S. and Zwick, S. A. Growth of vapor bubbles in superheated liquids. J. Appl. Phys. 25(4):493-500(April, 1954).

55. Stephan, K. and Körner, M. Calculation of heat transfer in evaporating binary liquid mixtures. Chemie-Ingenieur-Technik 41(7):409-17(1969).

56. Bennett, D. L. and Chen, J. C. Forced convective boiling in vertical tubes for saturated pure components and binary mixtures. AIChE J. 26(3):454-61(May, 1980).

57. Florschuetz, L. W. and Khan, A. R. Growth rates of free vapor bubbles in binary liquid mixtures at uniform superheats. Fourth Int'l. Heat Transfer Conference, Paris, France, 1970.

58. Moles, F. D. and Shaw, J. F. G. Boiling heat transfer to subcooled liquids. Trans. Instn. Chem. Eng. 50:76-84(1972).

59. Mesler, R. An alternative to the Dengler and Addoms convection concept of forced convection boiling heat transfer. AIChE J. 23(4):448-53(July, 1977).

60. Nishikawa, K., Kusada, H., Yamasaki, K., and Tanaka, K. Nucleate boiling at low liquid levels. Bull. Japanese Soc. Mech. Eng. 10:328(1967).

61. Mesler, R. A mechanism supported by extensive experimental evidence to explain high heat fluxes observed during nucleate boiling. AIChE J. 22(2):246-52(March, 1976).

62. Griffith, P. and Wallis, G. B. Two-phase slug flow. J. Heat Transfer. Aug., 1961. pp. 307-20.

63. Davies, R. M. and Taylor, G. I. The mechanics of large bubbles rising through liquids in tubes. Proc. Royal Soc. (London), Vol. 200, Ser. A, pp. 375-90 (Feb. 7, 1950).

64. White, E. T. and Beardmore, R. H., The velocity of rise of single cylindrical air bubbles through liquids contained in vertical tubes. Chem. Eng. Sci. 17:351-61(1962).

65. Nicklin, D. J., Wilkes, J. O., and Davidson, J. F. Two-phase flow in vertical tubes. Trans. Instn. Chem. Eng. 40:61(1962).

66. Griffith, P. The prediction of low-quality boiling voids. ASME Paper 63-HT-20, National Heat Transfer Conf., Boston, MA (1963).

67. Hewitt, G. F. and Wallis, G. B. Flooding and associated phenomena in falling film flow in a vertical tube. U.K.A.E.R.E. Report AERE-R4022, 1963.

68. Dukler, A. E. The role of waves in two-phase flow: some new understandings. Chem. Eng. Education, Summer 1977. pp. 108-138.

69. Dukler, A. E., Chopra, A. Moalim, D., and Semiat, R. Two-phase interactions in countercurrent flow. U.S. Nuclear Regulatory Commission Report NUREG/CR-0669 (Dec., 1978).

70. Dukler, A. E. and Smith, L. Two-phase interactions in countercurrent flow: studies of the flooding mechanism. U.S. Nuclear Regulatory Commission Report NUREG/CR-0617, Dec., 1977.

71. Hinze, J. E. Fundamentals of the hydrodynamic mechanism of splitting in dispersion processes. AIChE J. 1:289(1955).

72. Nusselt, W. Surface condensation of water vapor. Z. Ver. dt. Ing. 60(27): 541-6(1916).

73. Tailby, S. R. and Portalski, S. The hydrodynamics of liquid films flowing on a vertical surface. Trans. Instn. Chem. Engrs. 38:324-30(1960).

74. Dukler, A. E. Characterization, effects, and modeling of the wavy gas-liquid interface. Progress in Heat and Mass Transfer 6:207-34(1972).

75. Chu, K. J. and Dukler, A. E. Statistical characteristics of thin, wavy films. - Part II: Studies of the substrate and its structure. AIChE J. 20(4):695-706 (July, 1974).

76. Chu, K. J. and Dukler, A. E. Statistical characteristics of thin, wavy films. - Part III: Structure of large waves and their resistance to gas flow. AIChE J. 21(3):583-93(May, 1975).

77. Chu, K. J. Statistical characterization and modeling of wavy liquid films in vertical two-phase flow. University of Houston Ph.D. Thesis, University Microfilms, 1973.

78. Portalski, S. Eddy formation in film flow down a vertical plate. I&EC Fundam. Feb., 1964:49-53.

79. Belkin, H. H., Macleod, A. A., Monrad, C. C., and Rothfos, R. R. Turbulent liquid flow down vertical walls. AIChE J. 5(2):245-8(1959).

80. Dukler, A. E. Fluid mechanics and heat transfer in vertical falling film systems. Chem. Eng. Prog. Symp. Ser. 56(30):1-10(1960).

81. Chun, K. R. and Seban, R. A. Heat transfer to evaporating films. J. Heat Transfer 93(4):391-6(1971).

82. Abou, P. and Huyghe, J. Experimental study of evaporation heat transfer in a falling film. Instn. Chem. Engrs. Symp. Ser. No. 38, Vol. 1, Paper D5, 1974.

83. Kunz, H. R. and Yerazunis, S. An analysis of film condensation, film evaporation, and single-phase heat transfer. J. Heat Transfer. Aug., 1969. pp. 413-20.

84. Narayana-Murthy, V. and Sarma, P. K. Falling film evaporators - a design equation for heat transfer rates. Can. J. Chem. E. 55(6):732-5(Dec., 1977).

85. Narayana-Murthy, V. and Sarma, P. K. A note on thin film evaporation - prediction of heat transfer rates. J. Chem. Eng. Japan 6(5):457-9(1977).

86. Butterworth, D. An analysis of film flow and its applications to condensation in a horizontal tube. Int. J. Multiphase Flow 1:671-82(1974).

87. Perry, J. H. Chemical engineer's handbook. McGraw Hill Co., N.Y., N.Y., Fourth edition, 1963.

88. Walker, J. E., Whan, G. A., and Rothfuss R. R. Fluid friction in noncircular ducts. AIChE J. 3:484-9(1957).

89. Fujita, T. and Ueda, T. Heat transfer to falling liquid films and film breakdown - Part I: Subcooled liquid films. Int. J. Heat Mass Transfer 21:97-108 (1978).

90. Fujita, T. and Ueda, T. Heat transfer to falling liquid films and film breakdown - Part II: Saturated liquid films with nucleate boiling. Int. J. Heat Mass Transfer 21:109-18(1978).

91. Wallis, G. B. The transition from flooding to upwards cocurrent annular flow in a vertical pipe. U.K.A.E.R.E. Document AEEW-R142, 1963.

92. Peckner, D. and Bernstein, I. M. Handbook of stainless steels. McGraw Hill Co., N.Y., N.Y., 1977.

93. Fong, H. L., King, C. J., and Sephton, H. H. Upflow vertical tube evaporation with interface enhancement; pressure drop reduction and heat transfer enhancement by the addition of a surfactant. Desalination 16:15-38(1975).

94. Fong, H. L., King, C. J., and Sephton, H. H. An experimental study of heat transfer in upflow vertical tube evaporation. ASME Paper 75-HT-46 (1975), San Francisco, Aug. 11-13, 1975.

95. Hewitt, G. F. Measurement of two phase flow parameters. Academic Press, London, 1978.

96. Miller, N. and Mitchie, R. E. Measurement of local voidage in liquid-gas two-phase flow systems using a universal probe. J. Brit. Nucl. Energy Soc. 9:94-100(1970).

97. Rydholm, S. Pulping processes. Interscience Publishers, N.Y., N.Y., 1965.

98. Jagannath, S. Black liquor properties. Tappi 62(12):113-14(Dec., 1979); 63(3):117-18(March, 1980).

99. Carslaw, H. S. and Jaeger, J. C. The conduction of heat in solids. Second edition. Clarendon Press, Oxford, 1959.

100. Jeglic, F. A. An analytical determination of temperature oscillations in a wall heated by alternating current. NASA Tech. Note TN-D-1286, 1962.

APPENDIX I

DESCRIPTION OF THE COMPUTER PROGRAM FOR SLUG-CHURN FLOW

INTRODUCTION

The computer program works by dividing the tube into arbitrary increments of length and by then keeping accounts of the thickness, weight, and concentration of the liquid film within each increment of length over a succession of time increments. Slugs are started at the bottom of the tube at a given rate, and the location and contents of the slugs are computed at each time increment. This procedure - making slugs, moving slugs, and calculating the drainage of films behind the slugs - continues until the concentrations in the tube approach their asymptotic values.

ROUTINE MAIN AND SUBROUTINES START AND SMAKE

The routine named MAIN controls the input and output of data and performs the iterations over length and time, which are the backbone of the program. It first calls subroutine START, which simply provides initial values for all the arrays used in the program. In particular, provision has been made to start with estimated final concentrations to reduce computation time.

The calculations begin as MAIN enters its time loop. For each increment of time, subroutines SMAKE and SMOVE are called. SMAKE determines whether or not a slug should be introduced into the bottom of the tube at the given time increment. SMOVE updates the location of all the slugs in the tube and then calls subroutines SCONC, FILM, and FLOOD to perform mass balances and film deposition thickness calculations over the length each slug has been moved.

MAIN then begins a length loop which, starting from the top of the tube and proceeding to the bottom, performs mass balances on the falling film with the aid of subroutine BALAN. This step updates the film thickness and Reynolds number of the

film located in each increment of length. The length loop also adjusts the slug contents for inflows from and outflows to the films on either side of the slug.

At the end of the length loop, subroutine HEAT is called to estimate the heat transfer coefficients from the Reynolds numbers calculated in the length loop. The program then returns to the top of the time loop and considers what happens over the next increment of time.

Once the concentrations in the film have stabilized, a listing of both instantaneous and time-averaged heat transfer coefficients and film contents is printed out.

SUBROUTINE PROPS

The subroutine PROPS is called at a number of points in the program to provide the physical properties of the test liquid at its local concentration. The properties included are viscosity, heat capacity, heat of vaporization, thermal conductivity, and liquid and vapor densities. The values used for each material tested are listed in the printouts. All properties are evaluated at the normal boiling point of the liquid, since no effort has been made to predict or correct for the pressure drop in the tube.

SUBROUTINE SMOVE

Subroutine SMOVE executes all the steps necessary to move slugs in the tube, keep account of slug contents, and determine the appropriate deposited film thickness and Reynolds number. SMOVE examines each length increment from the top of the tube to the bottom, looking for slugs; when it finds one, it calculates the vapor mass quality at that location and, from this, the local superficial vapor velocity. The rise velocity of the slug is then calculated by the methods of Wallis (6), that is,

$$V_\infty = 0.345 \left(g\ D\ [\rho_f - \rho_g]\right)^{1/2} [\rho_f]^{-1/2} \qquad (162)$$

This is the rise velocity in a stagnant liquid, the corrected velocity for a system with net upward liquid flow being

$$j_b = 1.2\ j + V_\infty \qquad (163)$$

as was discussed in "Drift Velocity of a Slug." This equation is used to find the distance traveled by the slug over the increment of time. Should the slug leave the tube, its exit weight and solids are printed out. Subroutine SCONC is called to update slug concentrations from a mass balance on the films engulfed and deposited by the moving slug. SCONC in turn calls FILM and FLOOD to estimate the deposited film thickness. From the current slug weight returned by SCONC, SMOVE calculates the slug length and thus locates the upper end of the slug. When all the slugs in the tube have been moved, SCONC ends and MAIN resumes control.

SUBROUTINE SCONC

The purpose of subroutine SCONC is to keep track of the weight and solids content of the slug. As a slug moves along the tube, it engulfs increments of old film and deposits increments of new film. SCONC first adds up the total weight and solids engulfed during the current slug movement, then calls FILM and FLOOD to find the deposited film thickness. The concentration in the deposited film is taken to be the slug concentration before it engulfs the old film. Next, SCONC sums up the deposited weight and solids and adjusts the slug weight and solids for the difference between the engulfed and deposited materials. SCONC then checks whether or not the slug still exists after this move and, if it does, calculates the new concentrations and returns to SMOVE.

SUBROUTINE FILM

FILM uses the methods of Wallis (6) to estimate the thickness of a film deposited by a slug moving at the rate calculated in SMOVE. This method requires the simultaneous solution of

$$\frac{j_f'}{V_\infty} = \left(1.2\,\frac{j}{V_\infty} + 1\right)\left(1-2\,\frac{\delta}{D}\right)^2 - \frac{j}{V_\infty} \qquad (164)$$

and

$$\frac{j_f'}{V_\infty} = 190\,\left(\frac{\delta}{D}\right)^{1.5}\ ,\ \mathrm{Re} \geq 3500 \qquad (165)$$

or, for very low Reynolds numbers,

$$\frac{j_f'}{V_\infty} = 3.85\,N_f\,\left(\frac{\delta}{D}\right)^3\ ,\ \mathrm{Re} < 3500 \qquad (166)$$

FILM performs this simultaneous solution using a guess-and-step routine, varying δ/D at the given j/V_∞ until a reasonable guess of δ/D is returned. This value of δ/D is assigned to that length of film which was newly deposited by the slug. Finally, the film Reynolds number is calculated.

$$\mathrm{Re} = 0.345\,\frac{j_f'}{V_\infty}\,N_f \qquad (167)$$

FILM then returns its results to SCONC.

SUBROUTINE FLOOD

Subroutine FLOOD is called immediately after FILM in subroutine SCONC. FLOOD first evaluates the film thickness estimated by FILM to determine whether it

is thick enough to be subject to flooding at the local vapor flow rate. The Wallis (91) criterion is used for this evaluation.

$$j_f^{*1/2} + j_g^{*1/2} \geq C \tag{168}$$

The constant C is between 0.88 and 1.0; 0.88 has been used in most of the calculations, since it represents the lower flooding boundary. In effect, FLOOD assumes that a film which is thick enough to flood will do so instantaneously and directly behind the slug which deposited the film and that the film will no longer be subject to flooding. This assumption is not strictly true, and deviations from this idealization can account for most of the discrepancies between the predictions of the model and the experimental data.

If the film deposited in FILM is too thin to flood, the results of FILM are returned unaltered to SCONC. If, however, the film is flooding, the stable film thickness is calculated from the following series of equations:

$$j_f^* = (C - j_g^{*1/2})^2 \tag{169}$$

$$j_f = j_f^* \, V_\infty / 0.345 \tag{170}$$

$$\Gamma = j_f \, \rho_f \, (\pi D^2/4)/\pi D = j_f \, \rho_f \, D \tag{171}$$

$$Re = 4 \, \Gamma/\mu_f \tag{172}$$

and

$$\delta/D = 0.909 \, Re^{1/3}/N_f^{2/3} \quad Re < 1000 \tag{173}$$

or

$$\delta/D = 0.063 \, Re^{2/3}/N_f^{2/3} \quad Re \geq 1000 \tag{174}$$

where

$$N_f = [D^3 \, g \, (\rho_f - \rho_g) \, \rho_f]^{1/2}/\mu_f^{1/2} \tag{175}$$

These values of δ/D and Re are assigned to the deposited film and returned to SCONC.

SUBROUTINE BALAN

Subroutine BALAN is called in MAIN and serves to update the thickness and Reynolds number of each increment of length by performing simple mass balances on the falling film. The flow rate into the current length increment is known to be the flow rate out of the next higher increment, calculated in the previous iteration of BALAN. The flow rate out of the current length increment is calculated from the film thickness, which was estimated either by FILM or FLOOD, or by BALAN in the previous time loop. The method used in this subroutine was suggested by Wallis (6).

$$\delta^* = \delta\, g^{1/3}\, (\rho_f - \rho_g)^{1/3}\, \rho_f^{1/3} / \mu_f^{2/3} \tag{176}$$

$$Re = (\delta^*/0.909)^3 \quad , \; Re < 1000 \tag{177}$$

or

$$Re = (\delta^*/0.063)^{1.5} \quad , \; Re > 1000 \tag{178}$$

where

$$Re = 4\, \Gamma/\mu_f \tag{179}$$

$$W_{out} = Re\, (\mu_f/4)\, \pi\, D \tag{180}$$

The balance,

$$W_{film,new} = W_{film,old} + W_{in} - W_{out} - W_{evaporated} \tag{181}$$

is then performed, and the thickness of film required to contain this new weight is calculated. The old Reynolds number is retained for use in the heat transfer coefficient calculations in subroutine HEAT. BALAN then stores the value of W_{out} to use as W_{in} in the next increment of length and returns to MAIN.

SUBROUTINE HEAT

HEAT is used to estimate the heat transfer coefficient from the film Reynolds numbers calculated elsewhere in the program. The empirical correlation of Chun and Seban (81) for boiling falling films is used by HEAT.

For laminar flow, this correlation predicts

$$h = 0.606\ (k^3\ g/\nu^2)^{1/3}\ (Re/4)^{-0.22} \tag{182}$$

and for turbulent flow,

$$h = 0.0038\ (k^3\ g/\nu^2)^{1/3}\ (Re)^{0.4}\ (Pr)^{0.65} \tag{183}$$

The laminar-turbulent transition Reynolds number is predicted by

$$Re_{TRANS} = 5800\ (Pr)^{-1.6} \tag{184}$$

If a given length increment contains a slug rather than a falling film, the heat transfer coefficient is estimated using the Dittus-Boelter equation

$$Nu = 0.023\ Re^{0.8}\ Pr^{0.4} \tag{185}$$

with the slug drift velocity as the characteristic velocity in the Reynolds number.

DEFINITION OF PARAMETERS USED IN THE COMPUTER PROGRAM

AREA	Cross-sectional area of liquid film in a length increment
BALN	Slug weight at exit plus weight of steam generated over slug cycle
BPR	Boiling point rise
C	Constant in Wallis (90) flooding criterion [Eq. (113)]
CAV	Average concentration (lb/lb) over a slug cycle in selected increments of length
CDIFF	Criterion for approach to steady state: program ends when two successive slug cycles differ in concentration by less than CDIFF at length increment INCL = 29.
CFEED	Concentration of dye in the dye injection stream
CINIT	Concentration of solids in liquor feed (lb/lb)
CONCEN	Concentration in the films in each length increment
CRIT	Convergence criterion in subroutine FILM

CZERO	Concentration of solids in liquor feed (lb/lb)
C29	Storage variable for CAV at INCL = 29 from previous slug cycle (see CDIFF)
D	Tube diameter
DEL	Step size in convergence routine of Subroutine FILM
DENSG	Vapor density
DENSL	Liquid density
DLENG	Length of an increment of length
DRATIO	Film thickness divided by the tube diameter, δ/D
DTEST	Storage variable for TEST1 in the Subroutine FILM convergence scheme
DTIME	Duration of an increment of time
DTURB	Storage variable for DRATIO in the Subroutine FILM convergence scheme
EFFVSC	Dimensionless reciprocal viscosity [Eq. (95)], N_f
EVAP	Weight of steam evaporated over a slug cycle
EXITS	Solids weight in slug at exit
EXITW	Total weight of slug at exit
FLOW	Film flow rate, Γ, [Eq. (145)]
FLUXF	Superficial liquid flow rate, j_f, [Eq. (144)]
FSTAR	Dimensionless liquid flux, j_f^*, [Eq. (143)]
G	Gravitational constant
GRATIO	Component of GSTAR in Subroutine FLOOD
GSTAR	Dimensionless vapor flow rate, j_g^*, [Eq. (142)]
H	Heat transfer coefficient
HAV	Average heat transfer coefficient over a slug cycle
HTCAP	Heat capacity
HTEVAP	Latent heat of vaporization
HTFLUX	Heat flux
IFEED	Increment of length where dye stream is injected
IFLAG	Dummy variable to count time increments between slug starts

INCL	Length increment identification number
INCLHT	Storage variable for INCL
INCT	Time increment identification number
IPRIN	Dummy variable to control printout (1 = print, 0 = suppress)
IPRINT	Alternate name for IPRIN
ISLUG	Number of time increments per slug start
ITIME	Variable to count increments of time in a slug cycle
J	Dummy variable in DO loops
JSL	Indicates the contents of each increment of length (1 = film, 2 = slug, 3 = bottom of slug)
J460	Dummy variable to control averaging over the slug cycle [1 = suppress averaging, 2 = begin and continue averaging, 3 = end of cycle, print out averages and reset accumulators (CAV, HAV) to zero]
KOUNT	Dummy variable in DO loops
LASTHT	Increment number of last increment of length which is heated
LASTL	Increment number of the tube bottom
LASTT	Largest allowed time increment number
LOC	Increment of length containing the bottom of a slug after the slug has been moved
LSLUG	Length of slug in increments of length
M	Dummy variable to select printout device (6 = line printer)
OLD	Storage variable in Subroutine FILM
PI	3.141 etc.
POSIT	Location of the bottom of each slug in feet from the tube exit
POSN	Alternative name for POSIT
PR	Prandtl number
RE	Reynolds number, Re_Γ
REY	Alternative name for RE
RISE	Distance moved by a slug over an increment of time
S	Alternative name for CONCEN

SF	Solids content in an increment of length
SFILM	Solids content in each increment of length containing films
SLDIN	Solids flow into a length increment over a time increment
SLDOUT	Solids flow out of a length increment over a time increment
SOLIDS	Solids content in a film increment
SOLIN	Alternative name for SLDIN
SOLOUT	Alternative name for SLDOUT
SRATE	Slug rate (slugs per minute)
SSLUG	Solids content of a slug
T	Temperature (°R)
TCOND	Thermal conductivity
TEST1	Equation of flow for falling films, [Eq. (104) or (105)]
TEST2	Continuity equation for asymptotic film conditions, [Eq. (103)]
TEST3	Dummy variable in FILM
TEST4	Dummy variable in Subroutine FLOOD
THICK	Film thickness in a length increment, δ
TIME	Time into a slug cycle, (seconds)
TRANS	Transition Reynolds number in the Chun and Seban (79) correlation, [Eq. (129)]
TSTAR	Dimensionless film thickness, δ^*, [Eq. (113)]
VDRIFT	Correct slug rise velocity, [Eq. (98)], V_b
VISCL	Viscosity of liquid, μ_f
VOLUME	Volume of liquid in an increment of film
VRATIO	Ratio of average volumetric flux to the stagnant liquid rise velocity of a slug, j_f/V_∞
VRISE	Slug rise velocity in a stagnant liquid, [Eq. (94)], V_∞
W	Liquid feed rate, lb/hr
WEIGHT	Total weight of liquid in a length increment

WGTIN	Total weight flowing into a length increment over a time increment
WGTOUT	Total weight flowing out of a length increment over a time increment
WT	Alternative name for WEIGHT
WTEVAP	Weight evaporated from each length increment over one increment of time
WTFEED	Dye injection stream feed rate (lb/hr)
WTFILM	Total weight of film in each length increment
WTIN	Total weight flow into a length increment over a time increment
WTOUT	Total weight flow out of a length increment over a time increment
WTSLUG	Total weight of a slug
WTS	Total weight of a slug, alternative name for WTSLUG
WTTEST	Criterion for slug breakage: slug must contain at least as much weight as the film it would deposit during its movement
X	Vapor mass quality

Flow chart for the MAIN program

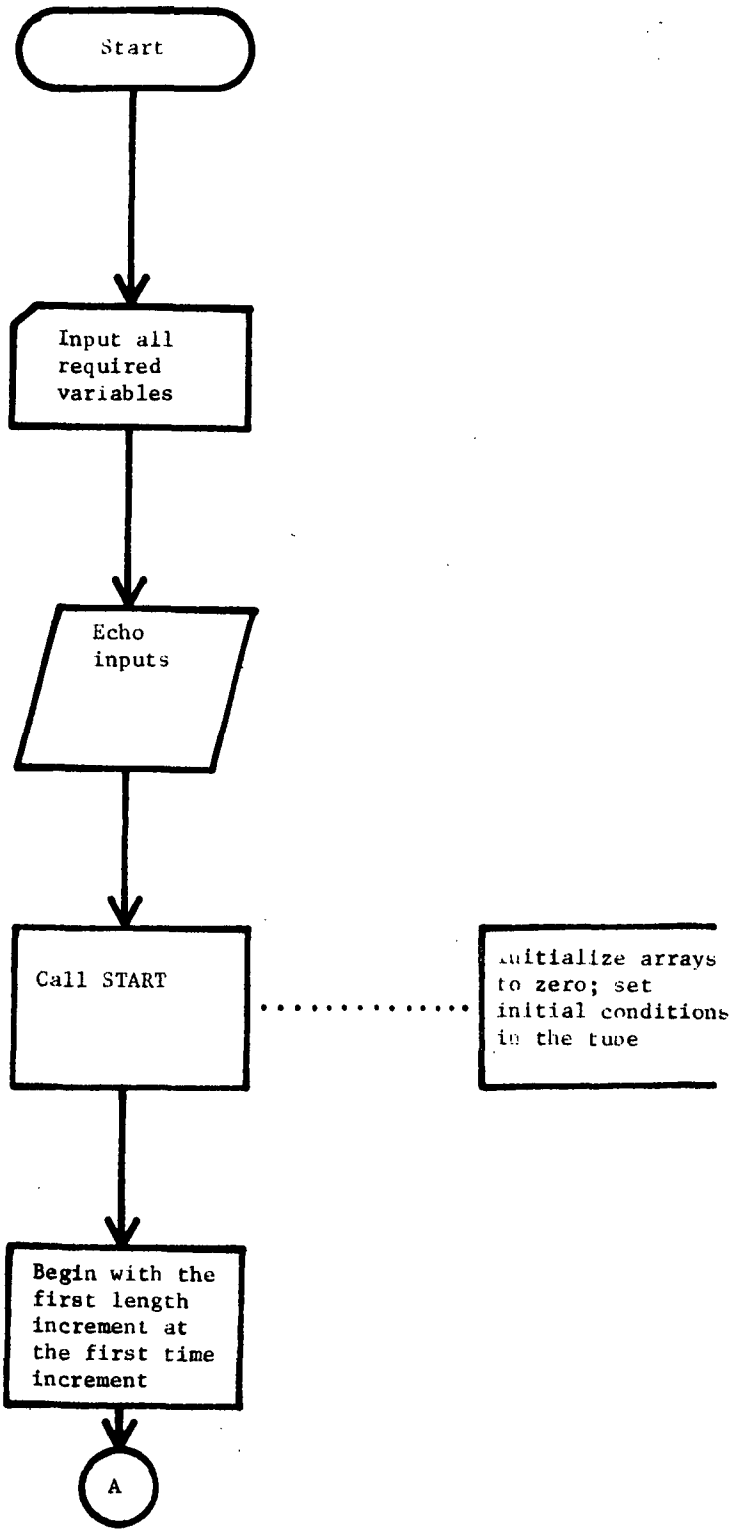

MAIN program

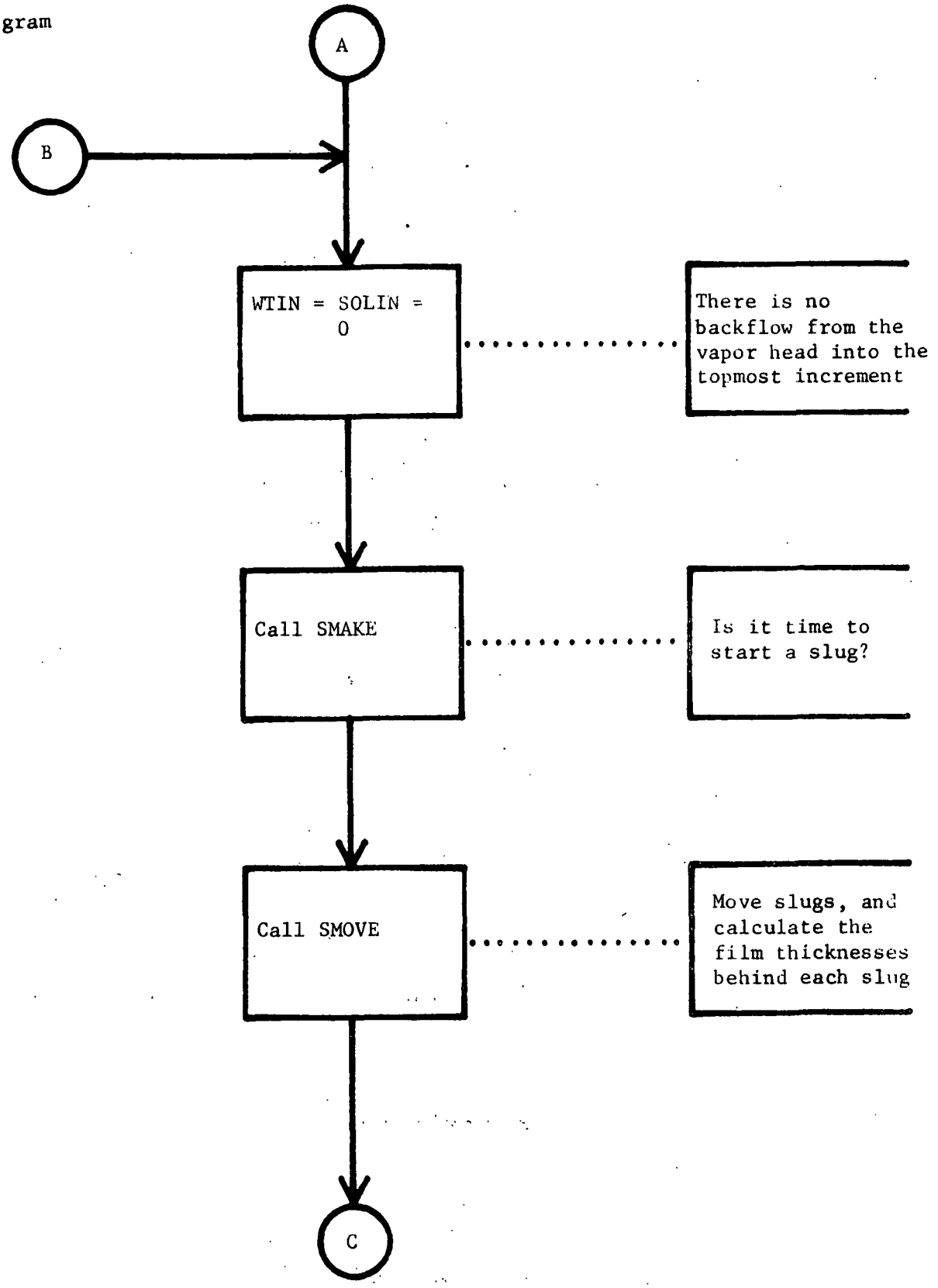

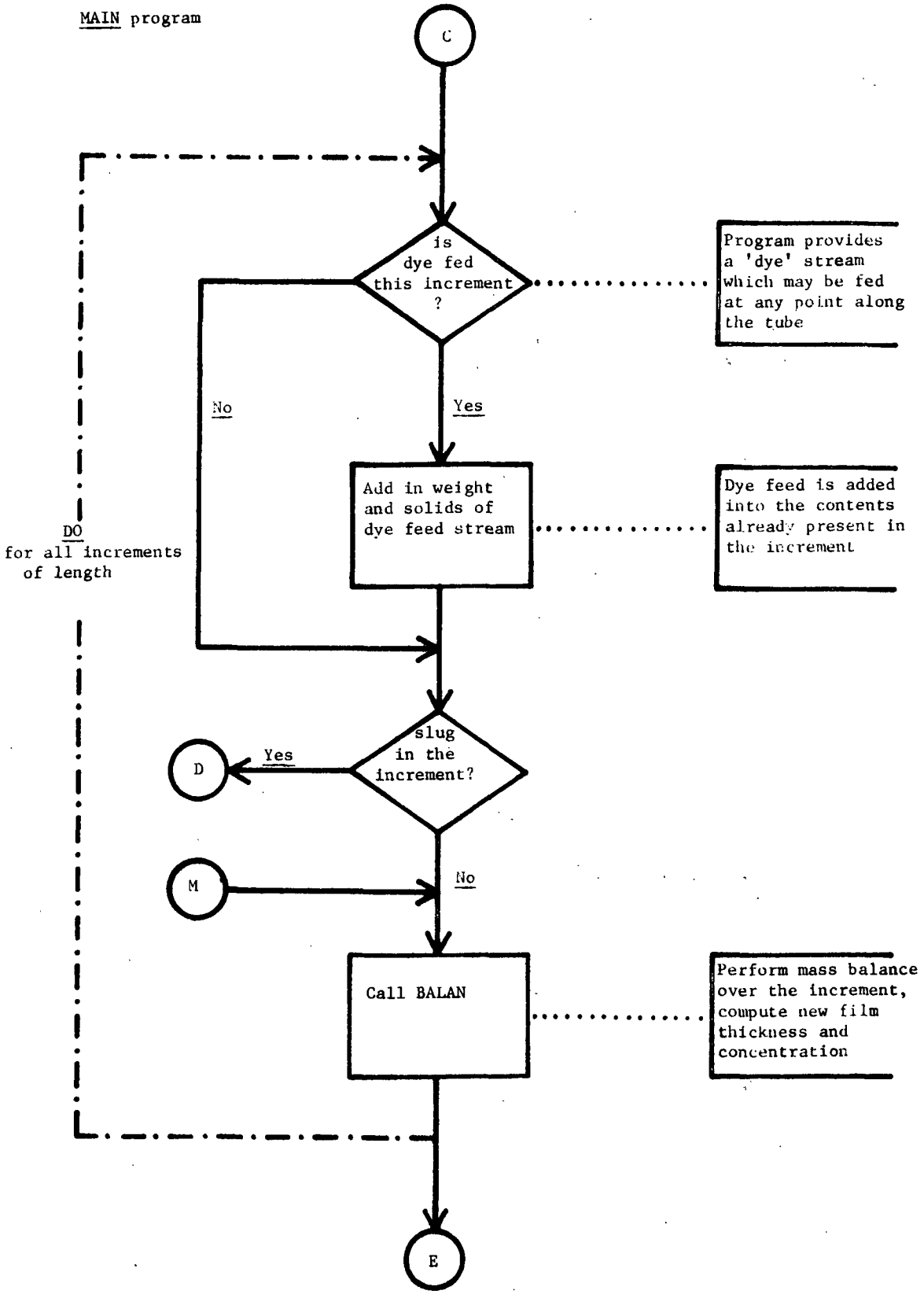
MAIN program
C
is dye fed this increment ?
Program provides a 'dye' stream which may be fed at any point along the tube
No
Yes
Add in weight and solids of dye feed stream
Dye feed is added into the contents already present in the increment
DO for all increments of length
slug in the increment?
Yes
D
M
No
Call BALAN
Perform mass balance over the increment, compute new film thickness and concentration
E

MAIN program

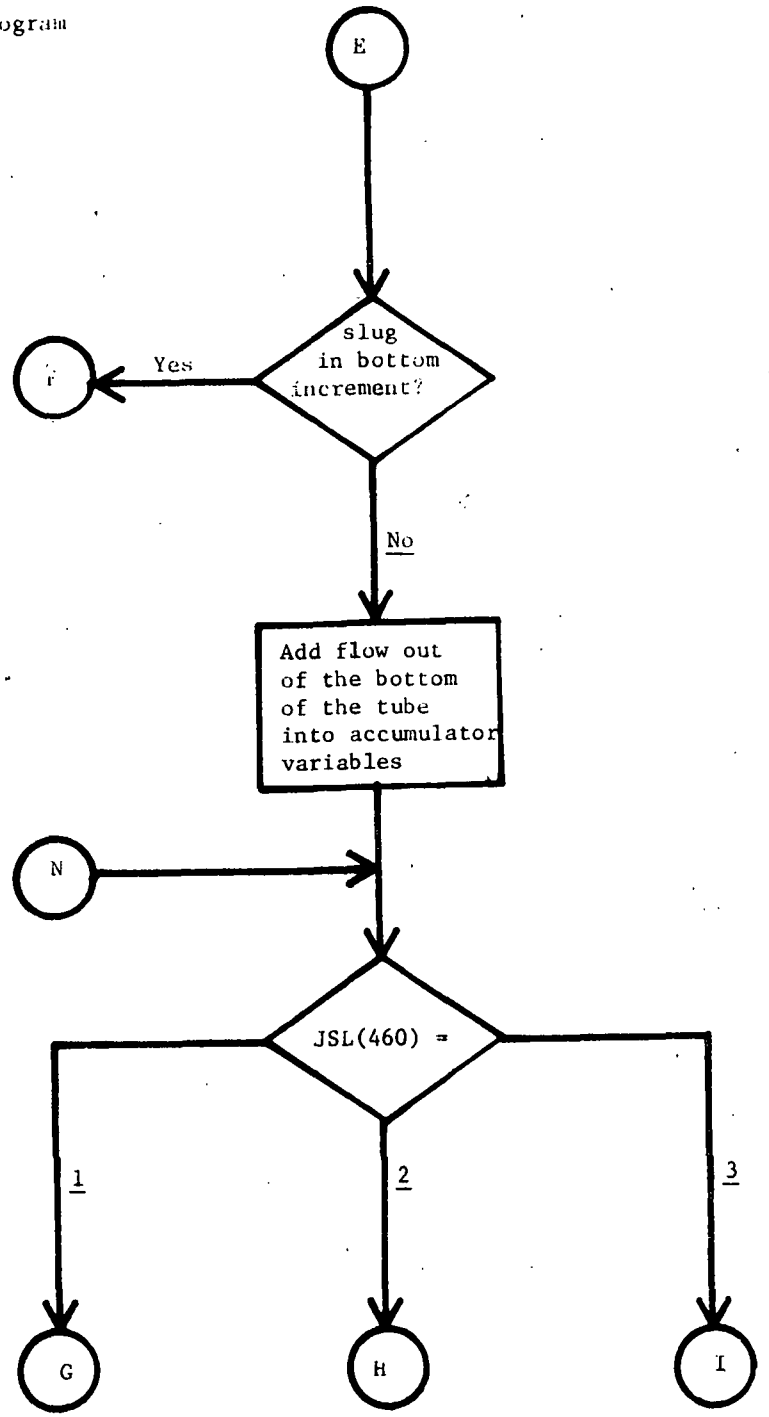

JSL(460) is a dummy variable,
= 1 during first slug cycle; all results are discarded
= 2 during subsequent slug cycles; h is calculated and accumulators are used to sum up variables over time
= 3 at the end of each slug cycle; averages are parformed and the results are printed out.

MAIN program

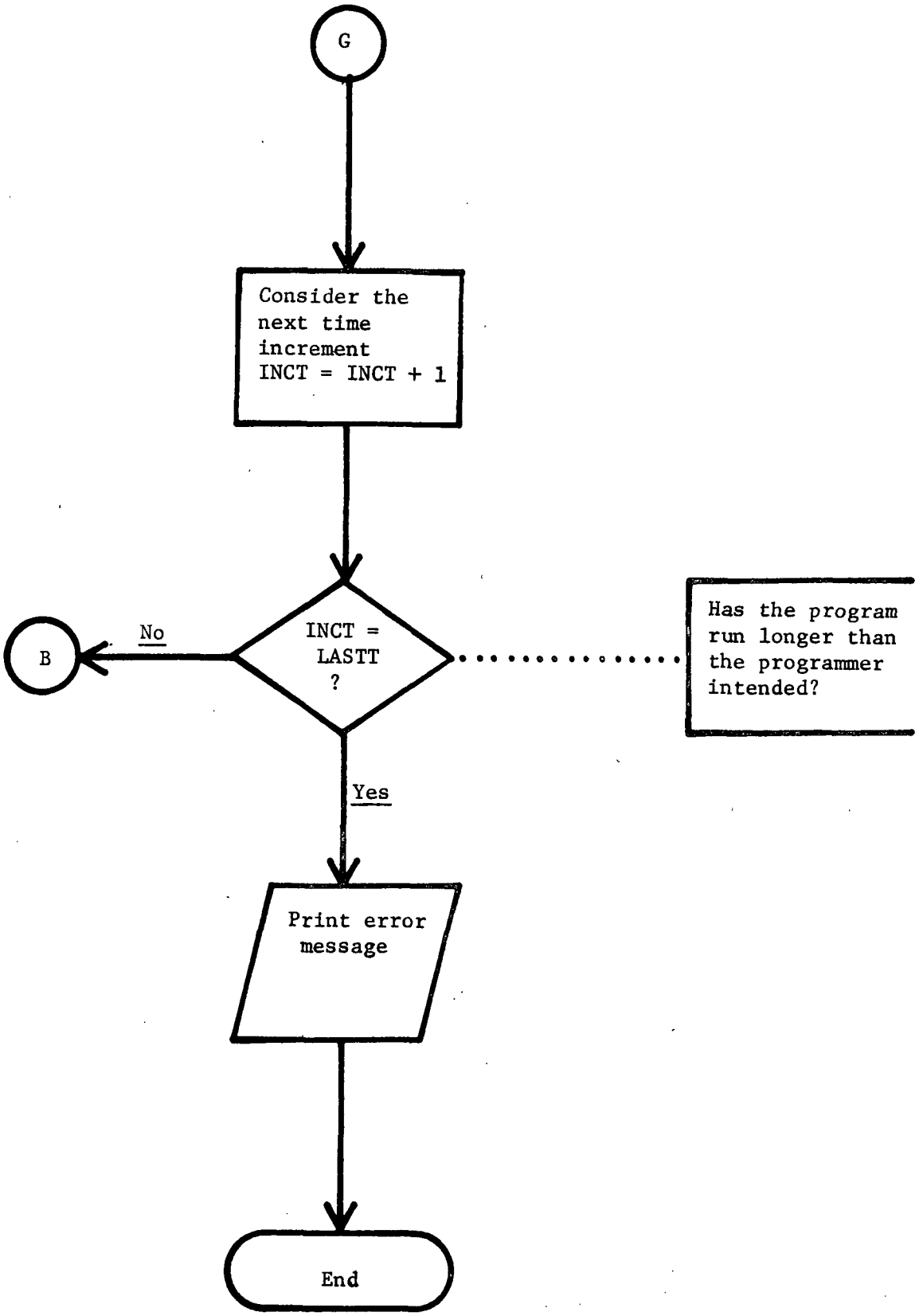

MAIN program

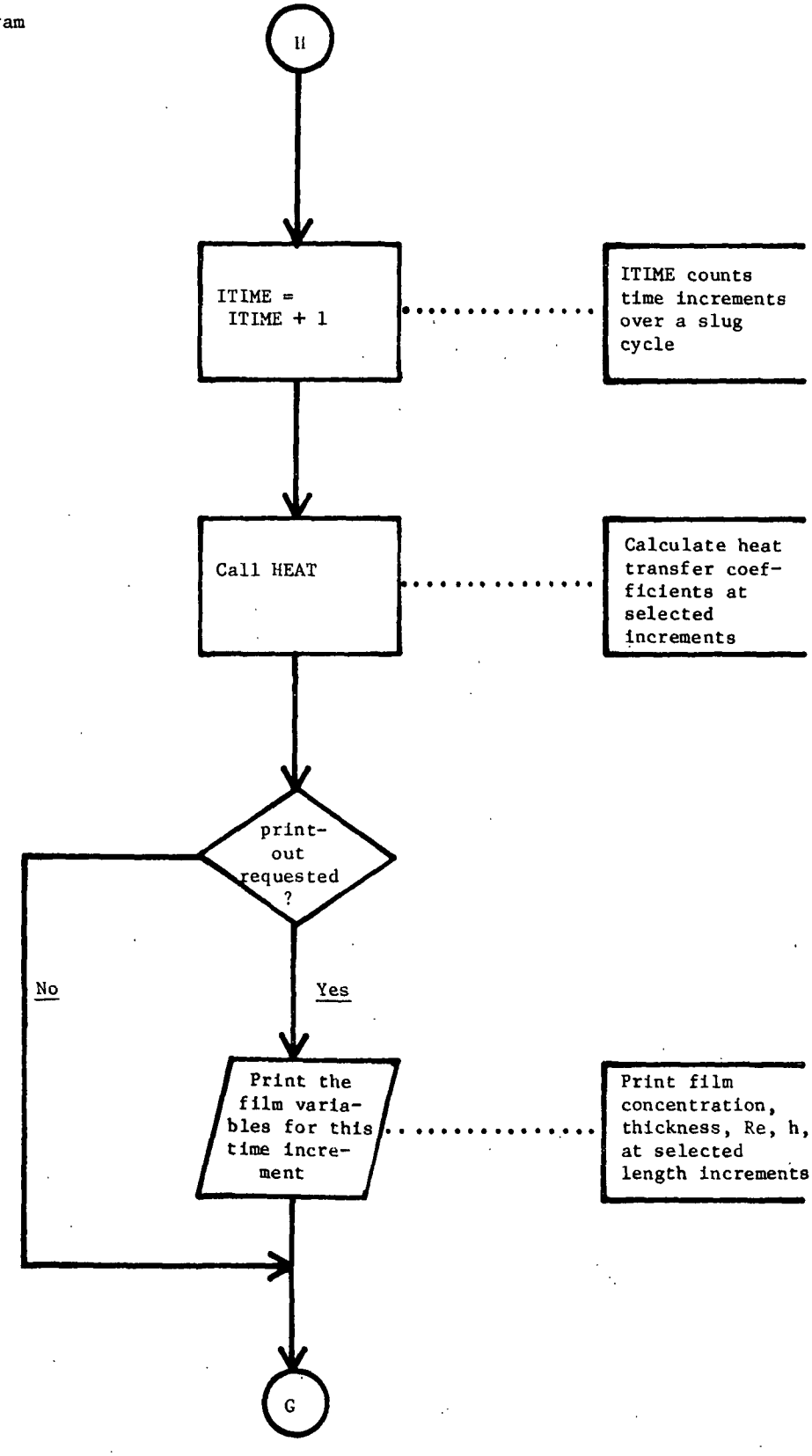

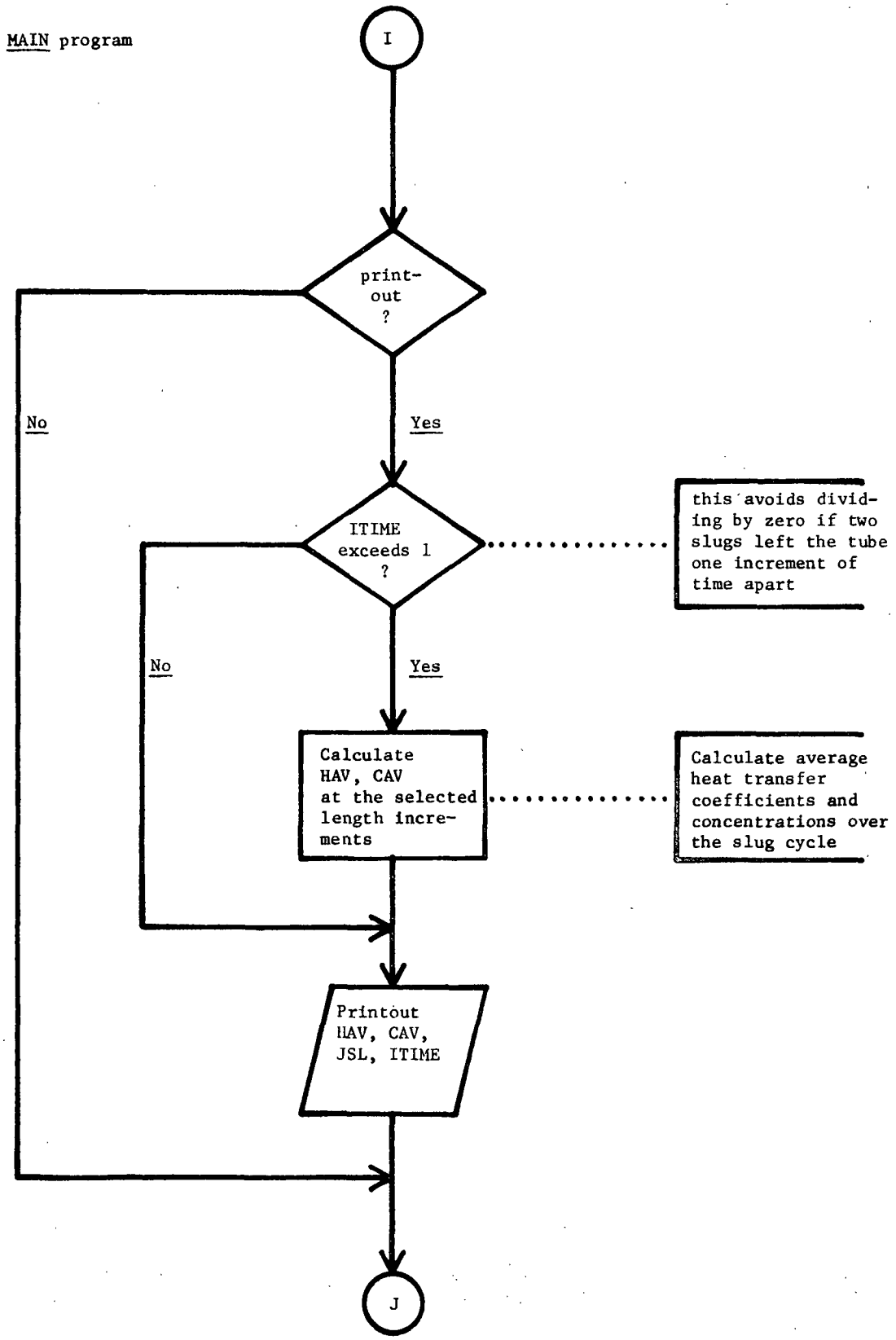
MAIN program
I
print-out ?
No
Yes
ITIME exceeds 1 ?
this avoids dividing by zero if two slugs left the tube one increment of time apart
No
Yes
Calculate HAV, CAV at the selected length increments
Calculate average heat transfer coefficients and concentrations over the slug cycle
Printout HAV, CAV, JSL, ITIME
J

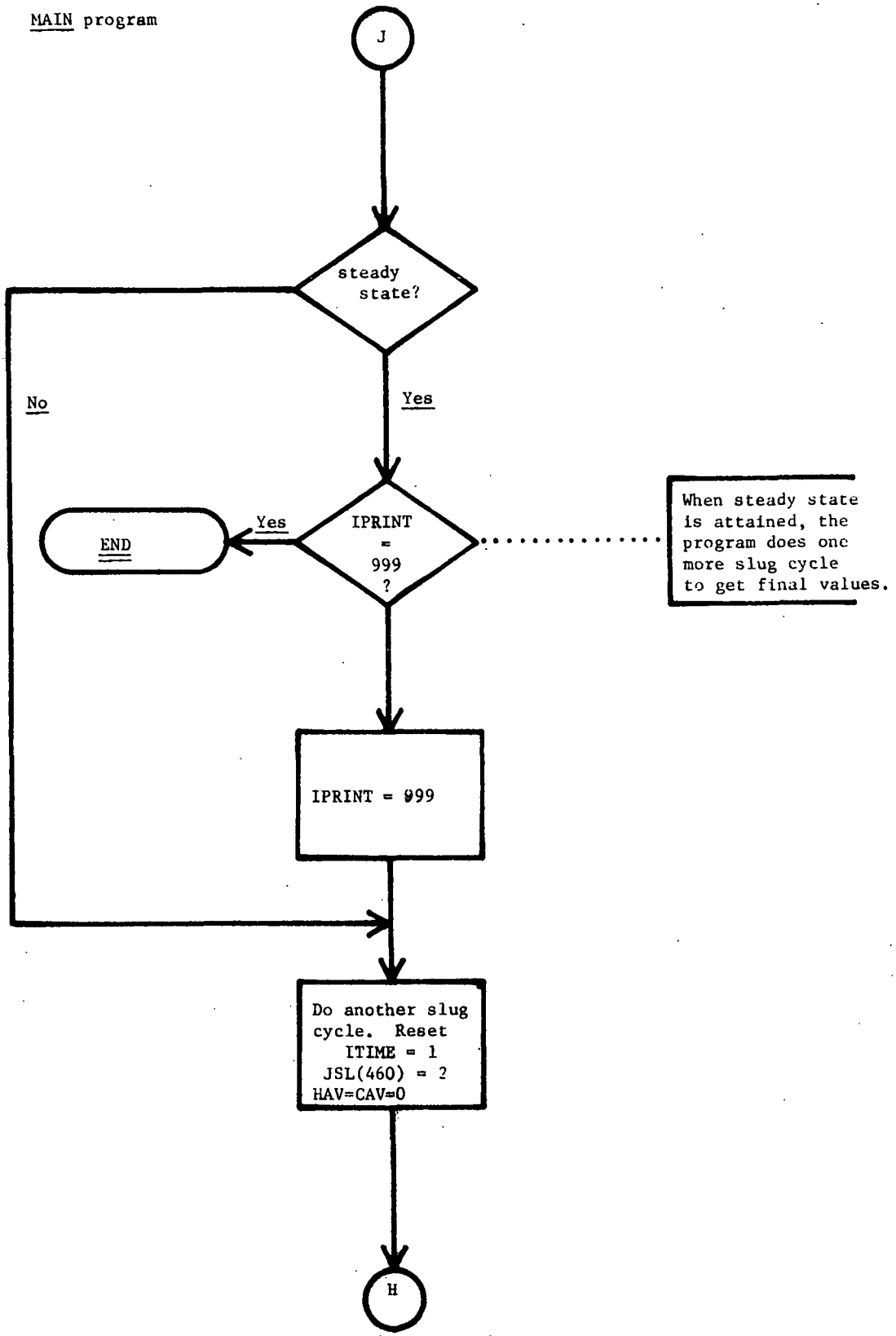
MAIN program
J
steady state?
No
Yes
IPRINT = 999 ?
Yes
END
When steady state is attained, the program does one more slug cycle to get final values.
IPRINT = 999
Do another slug cycle. Reset
ITIME = 1
JSL(460) = 2
HAV=CAV=0
H

Flow chart for the MAIN program

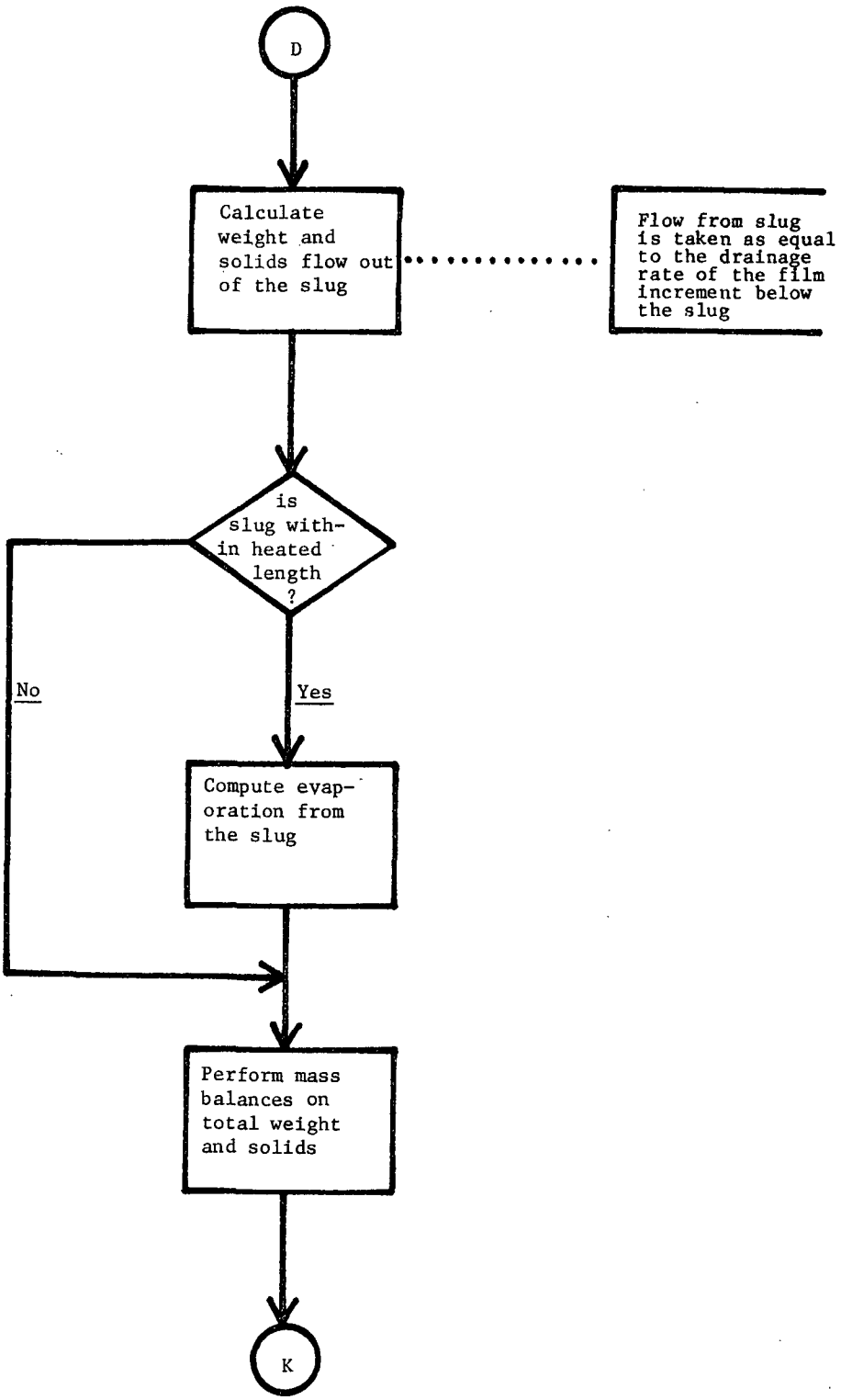

MAIN program

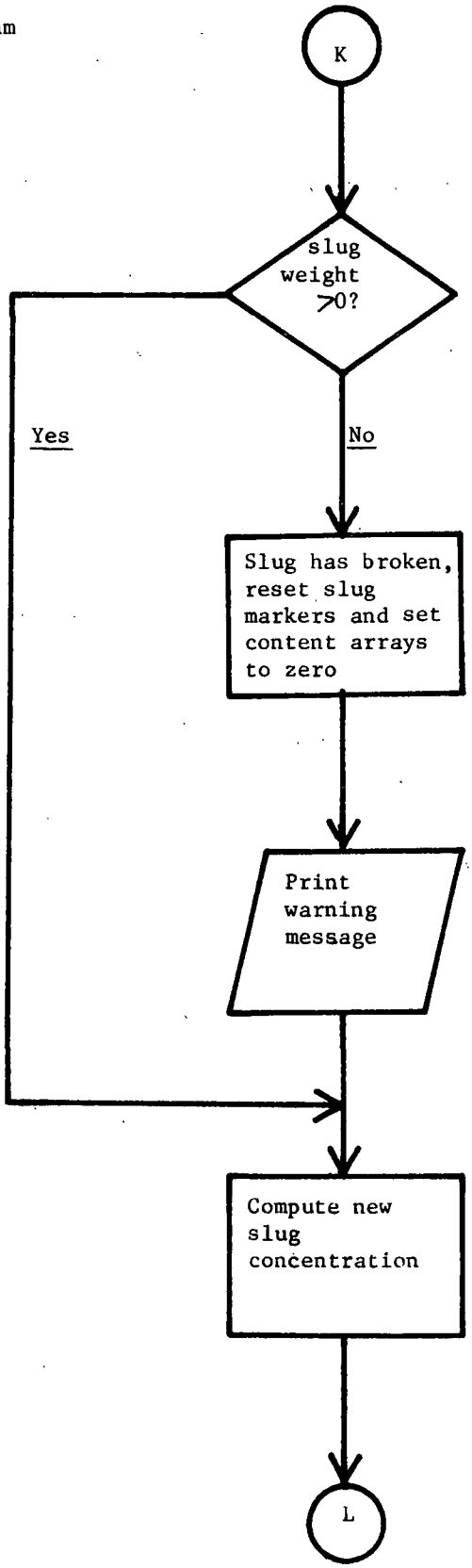

MAIN program

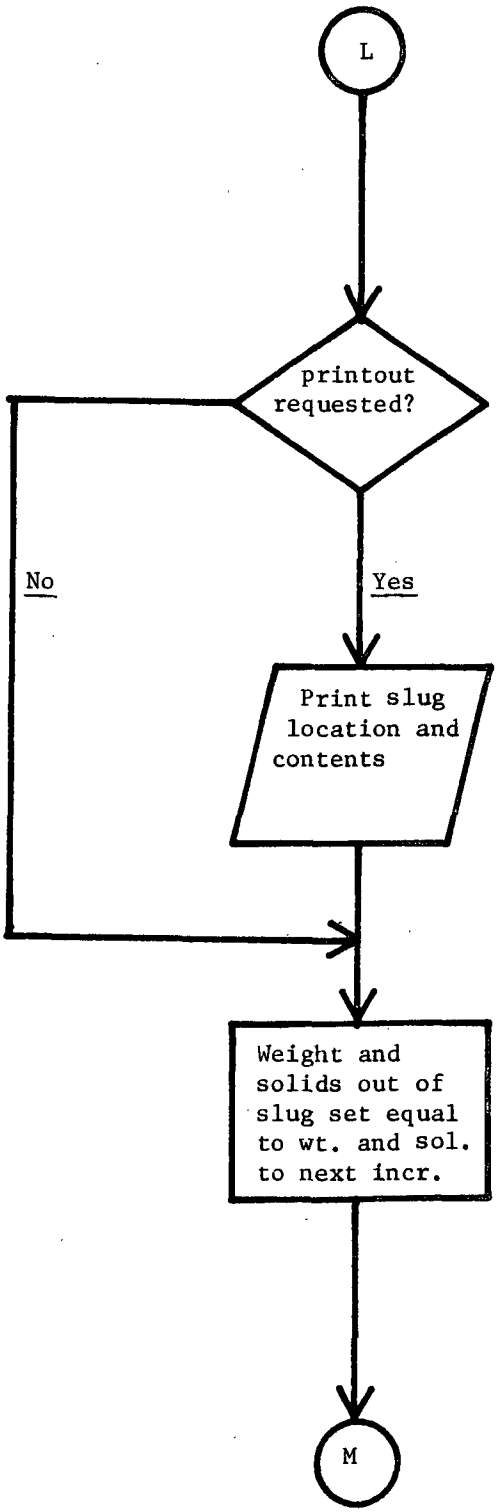

MAIN program

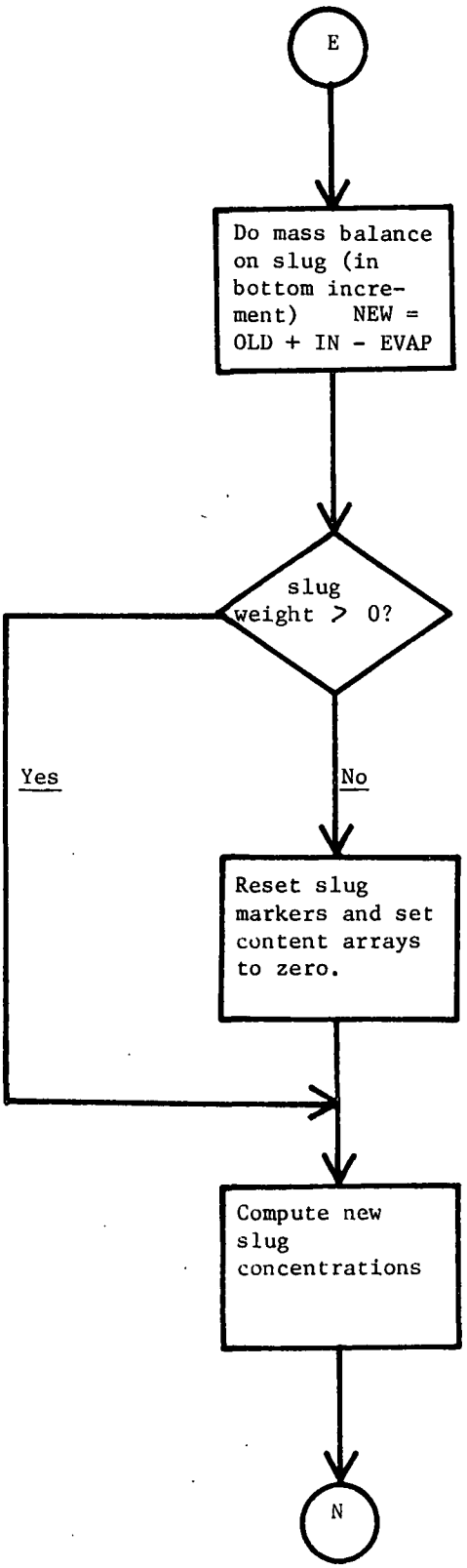

Flow chart for Subroutine BALAN

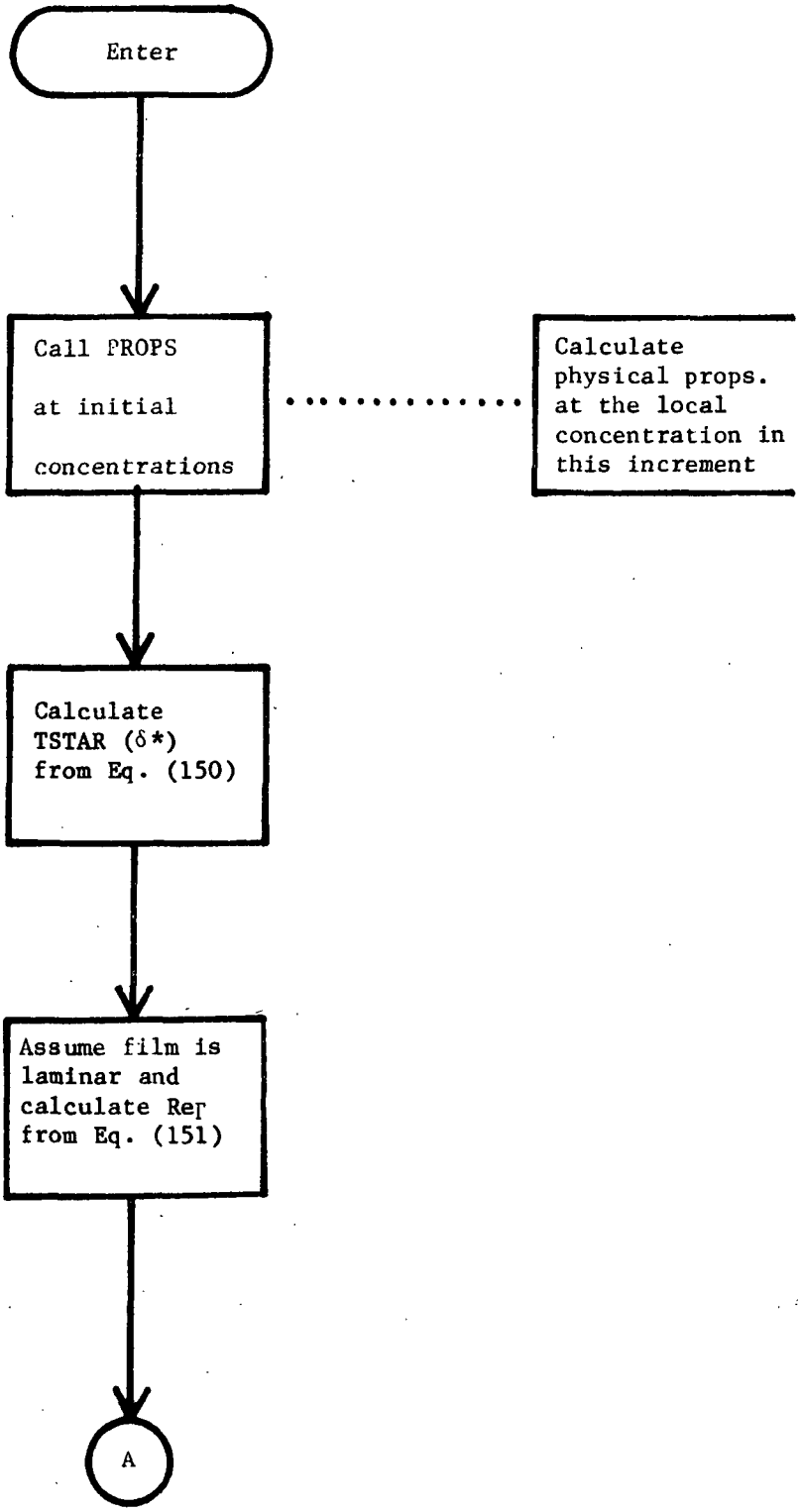

Flow chart for Subroutine BALAN
(page 2 of 5)

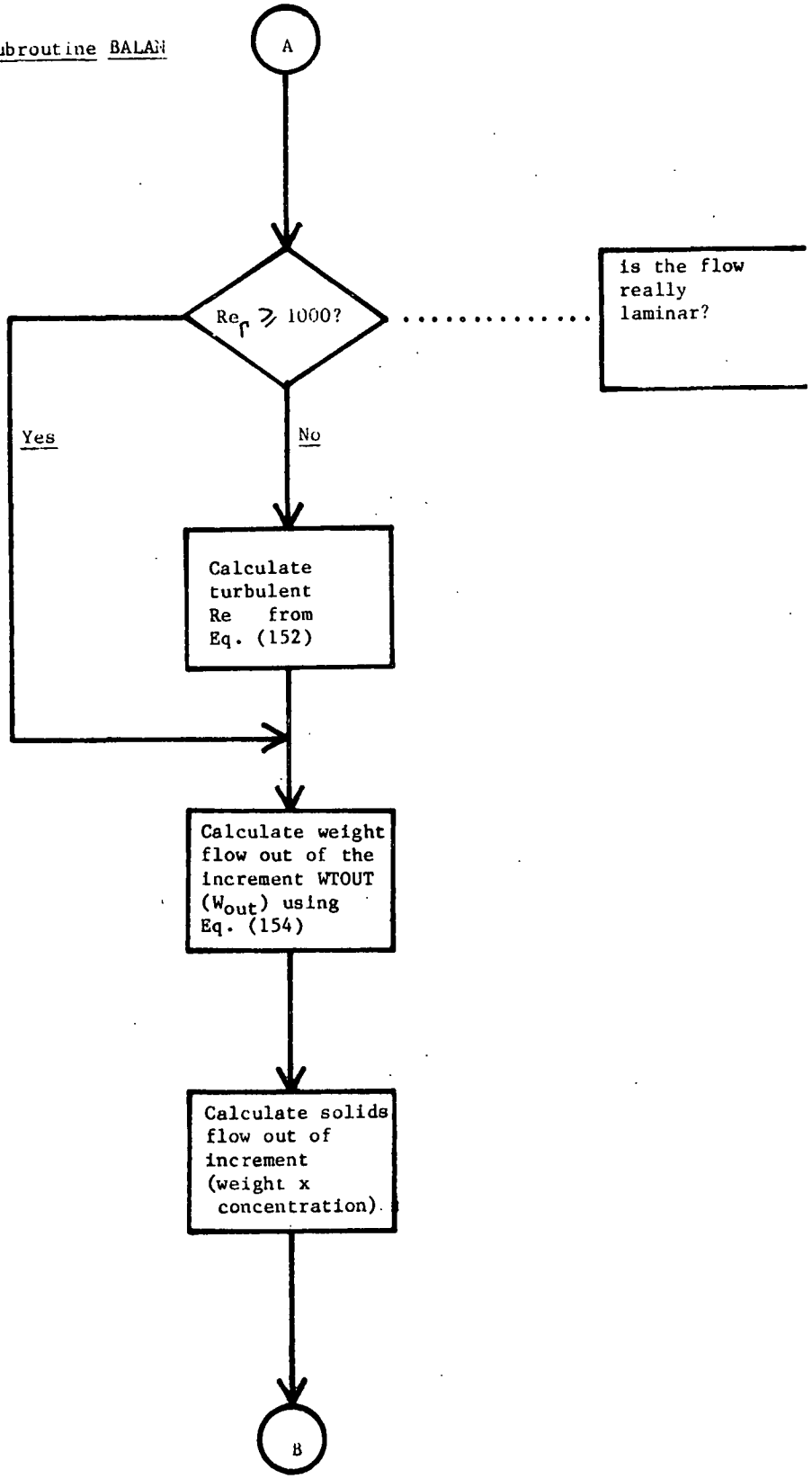

Flow chart for Subroutine BALAN
(page 3 of 5)

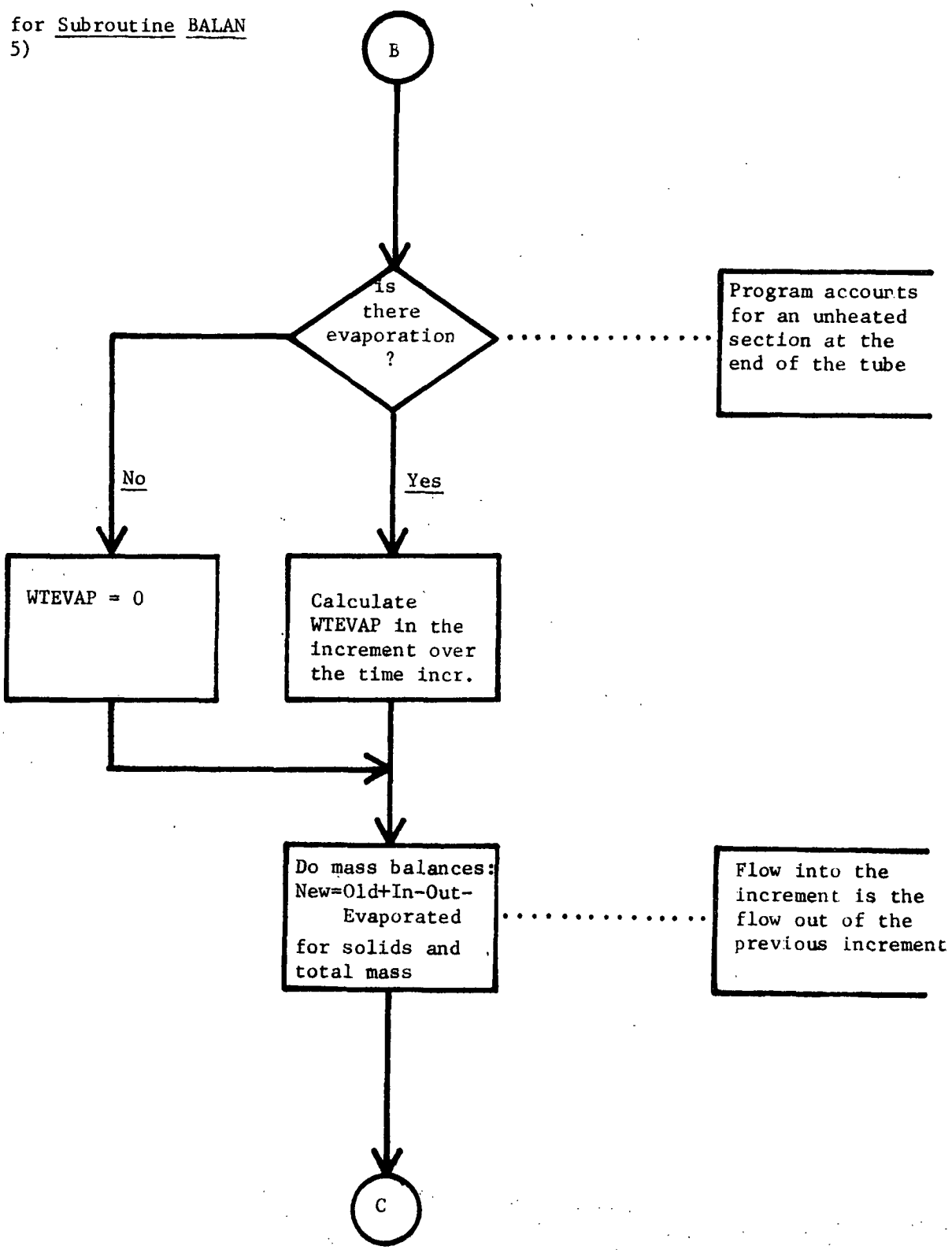

Flow chart for Subroutine BALAN
(page 4 of 5)

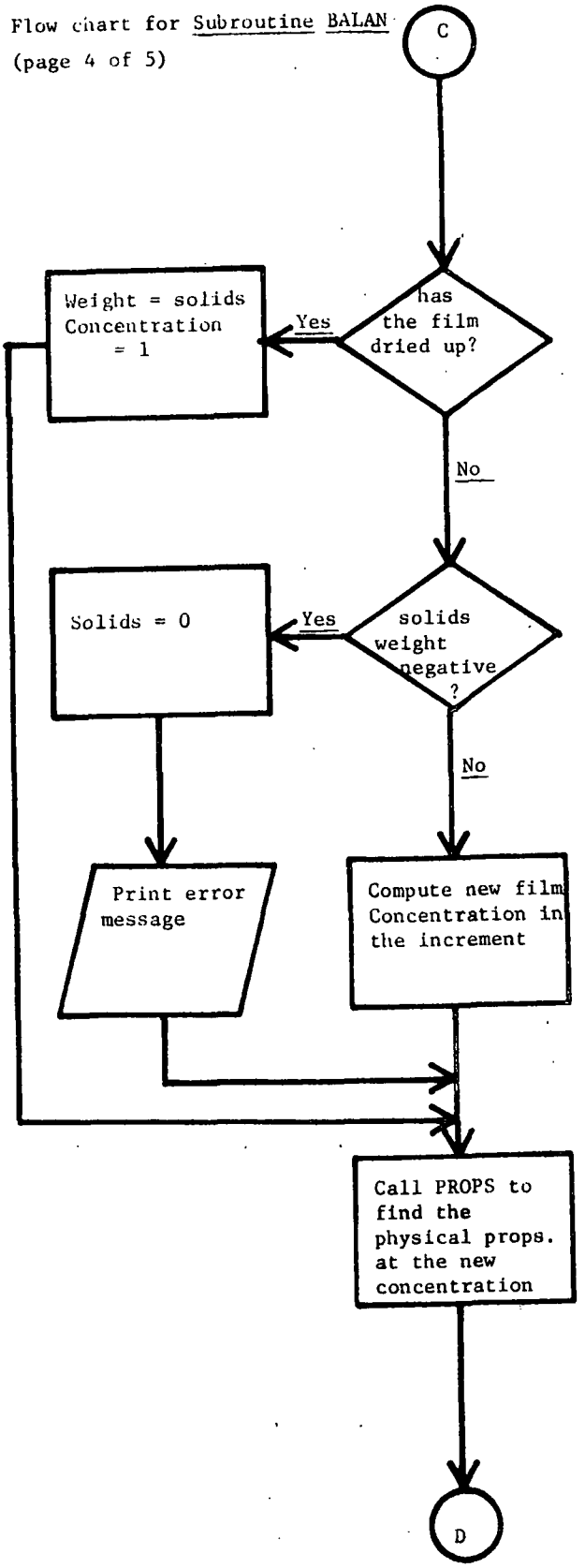

Flow chart for Subroutine BALAN

(page 5 of 5)

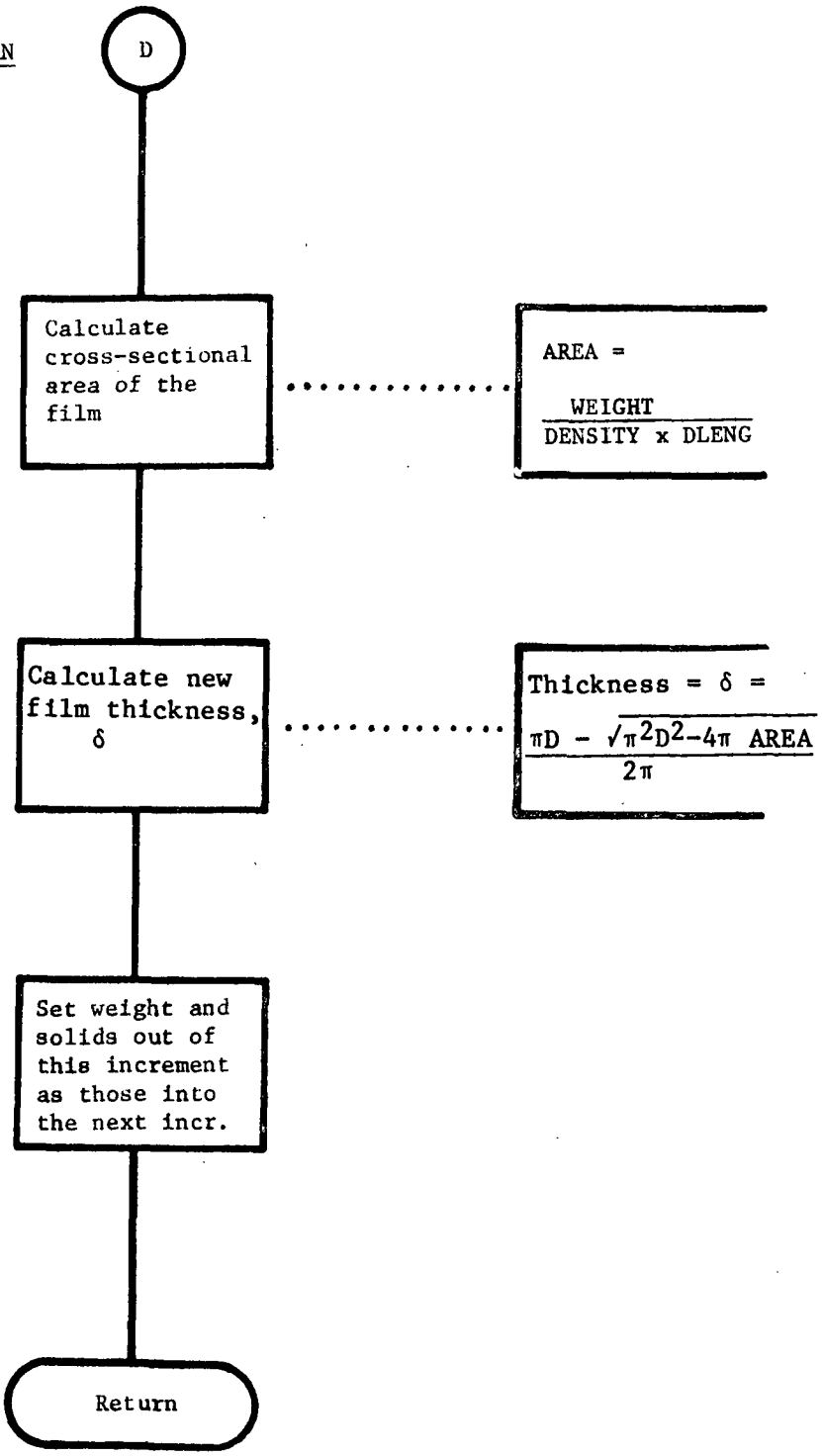

Flow chart for the Subroutine FILM

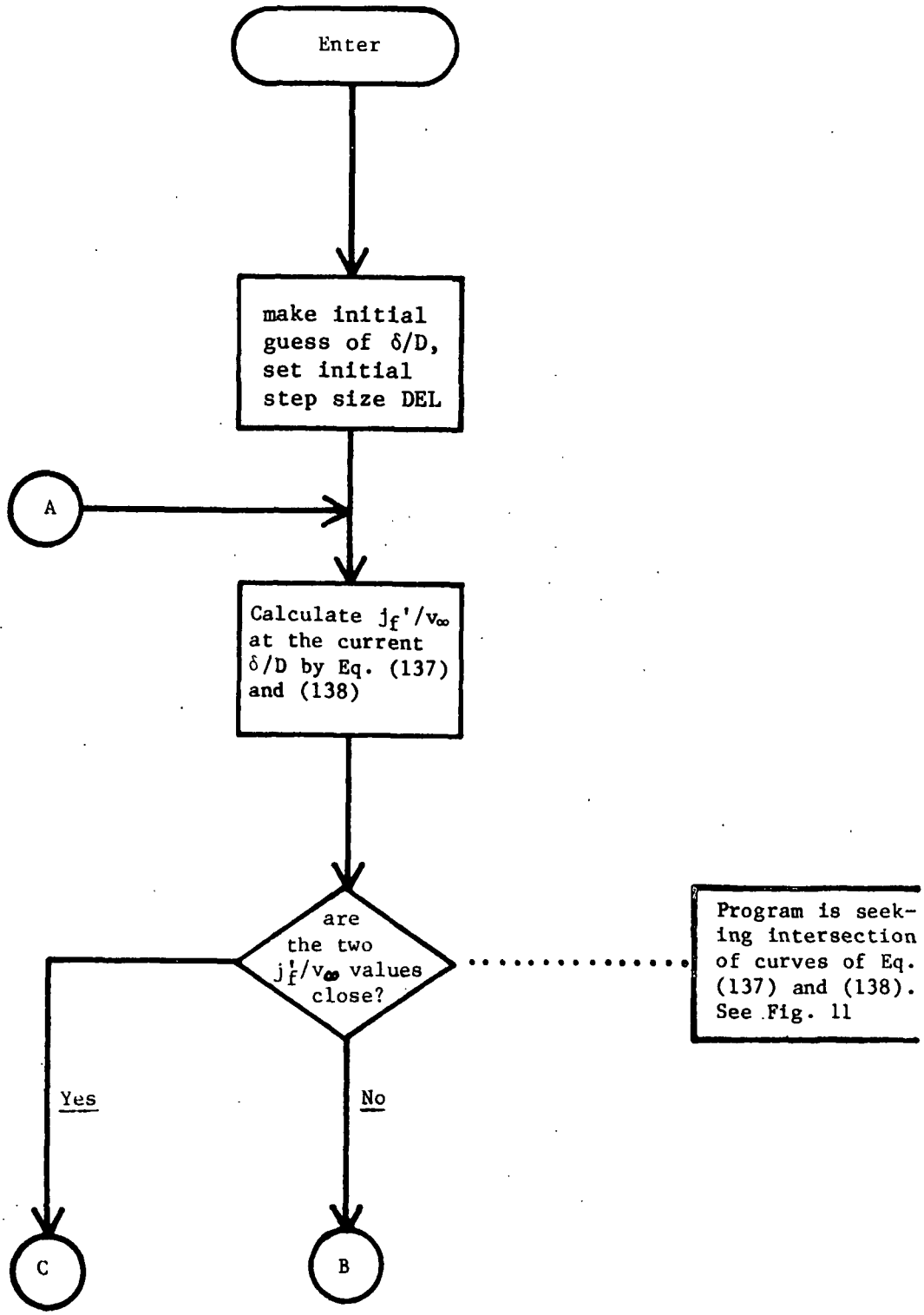

Flow chart for the Subroutine FILM (page 2 of 3)

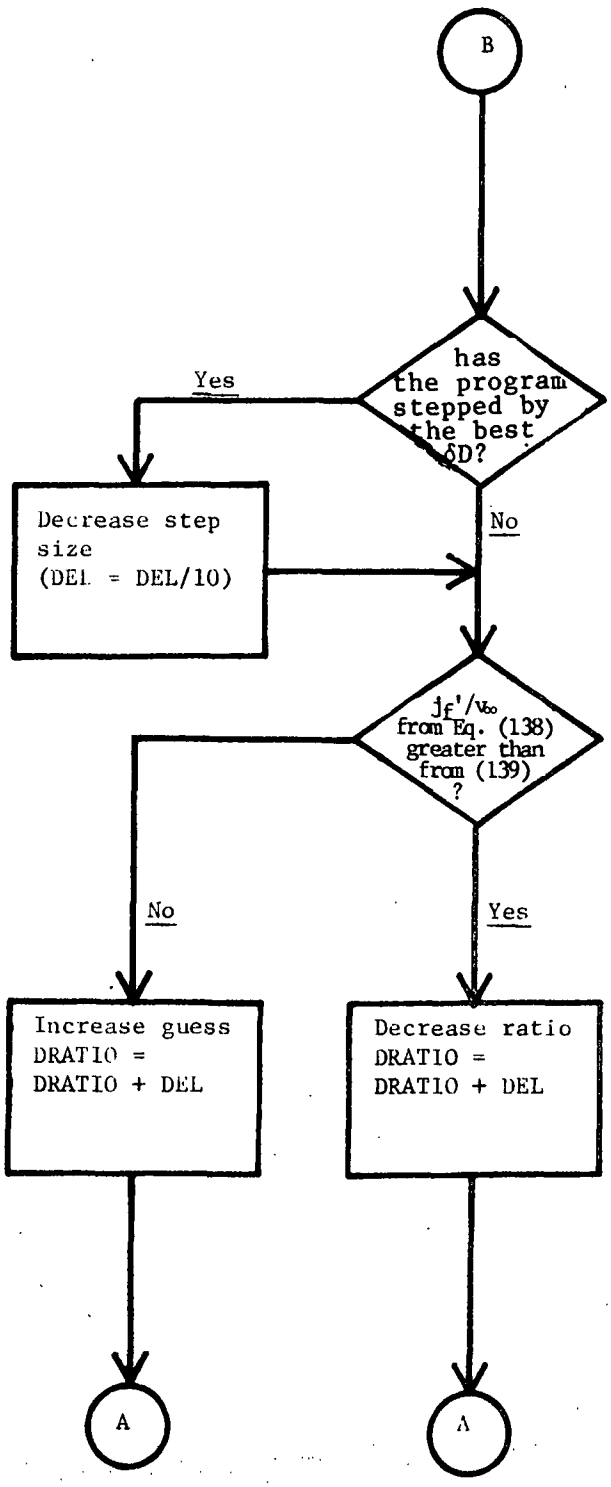

Flow chart for the Subroutine FILM (concluded)

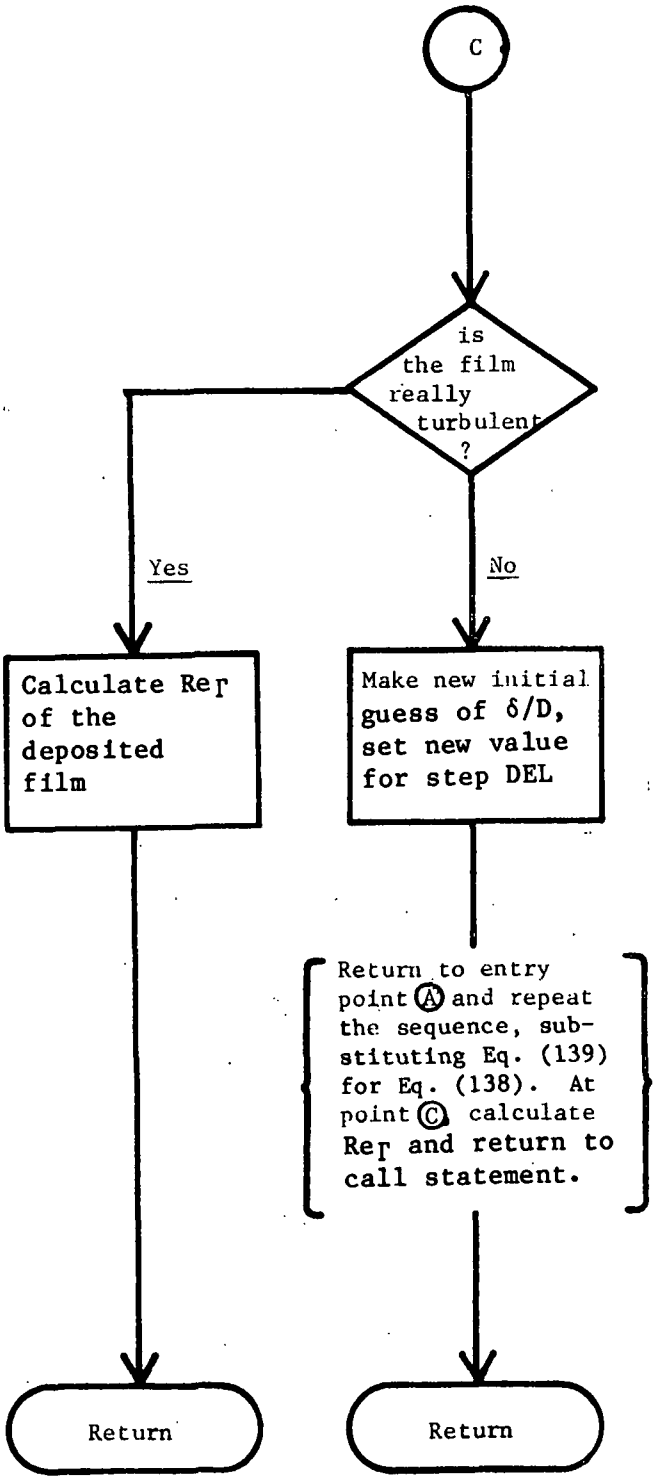

Flow chart for Subroutine FLOOD

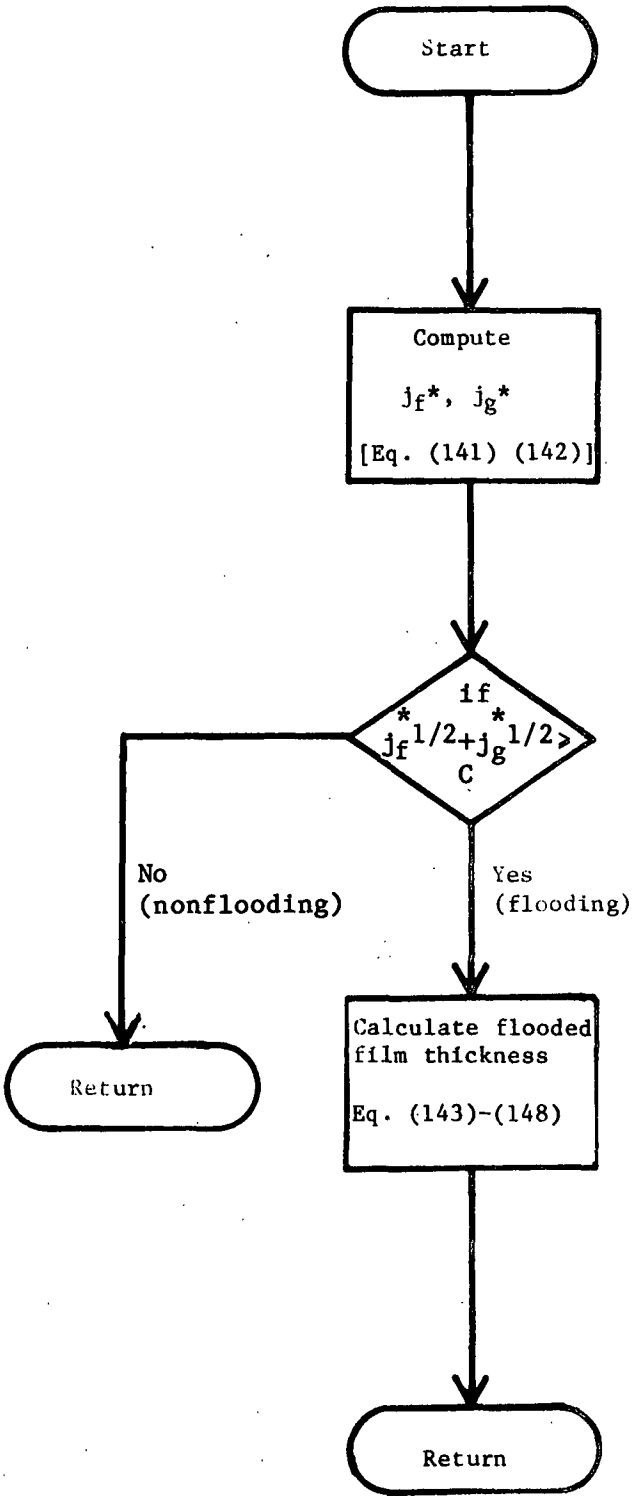

Flow chart for Subroutine HEAT

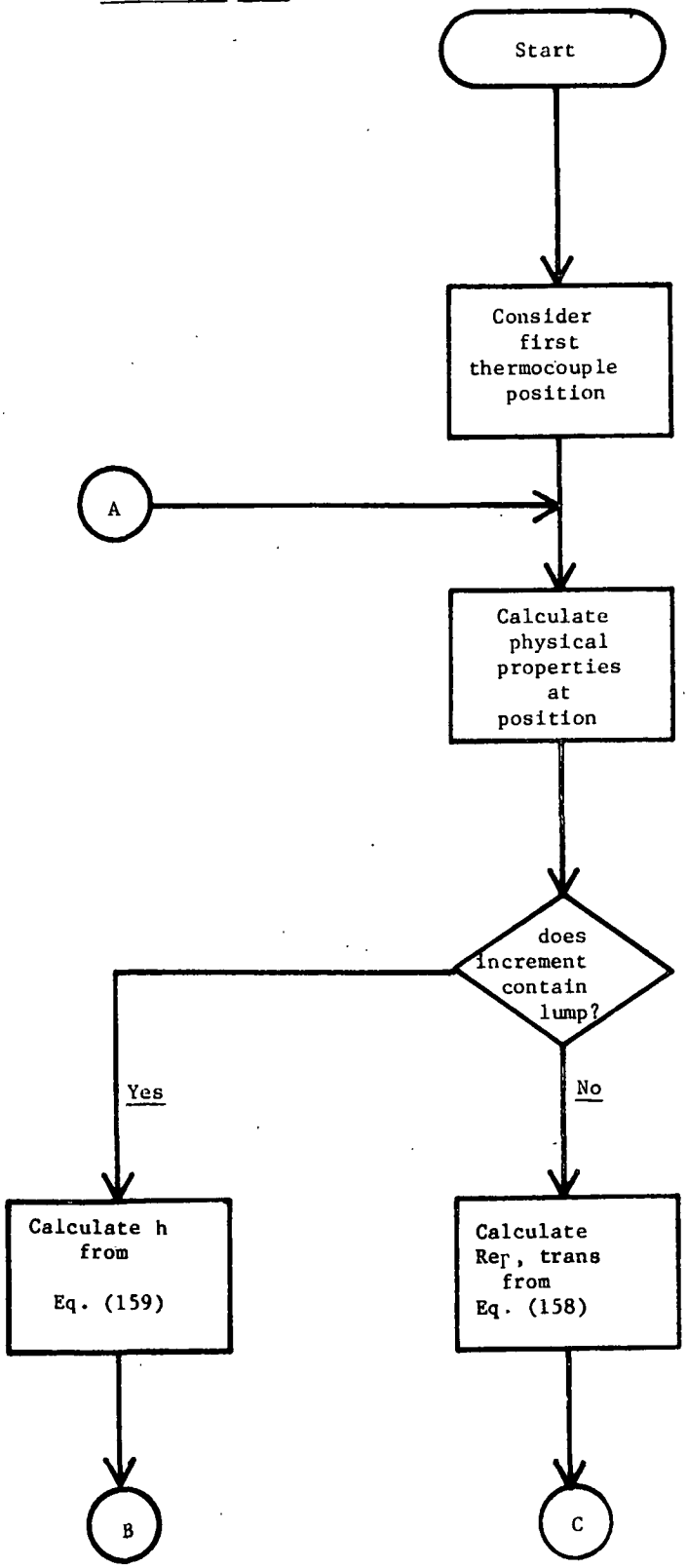

Flow chart for the Subroutine HEAT (concluded)

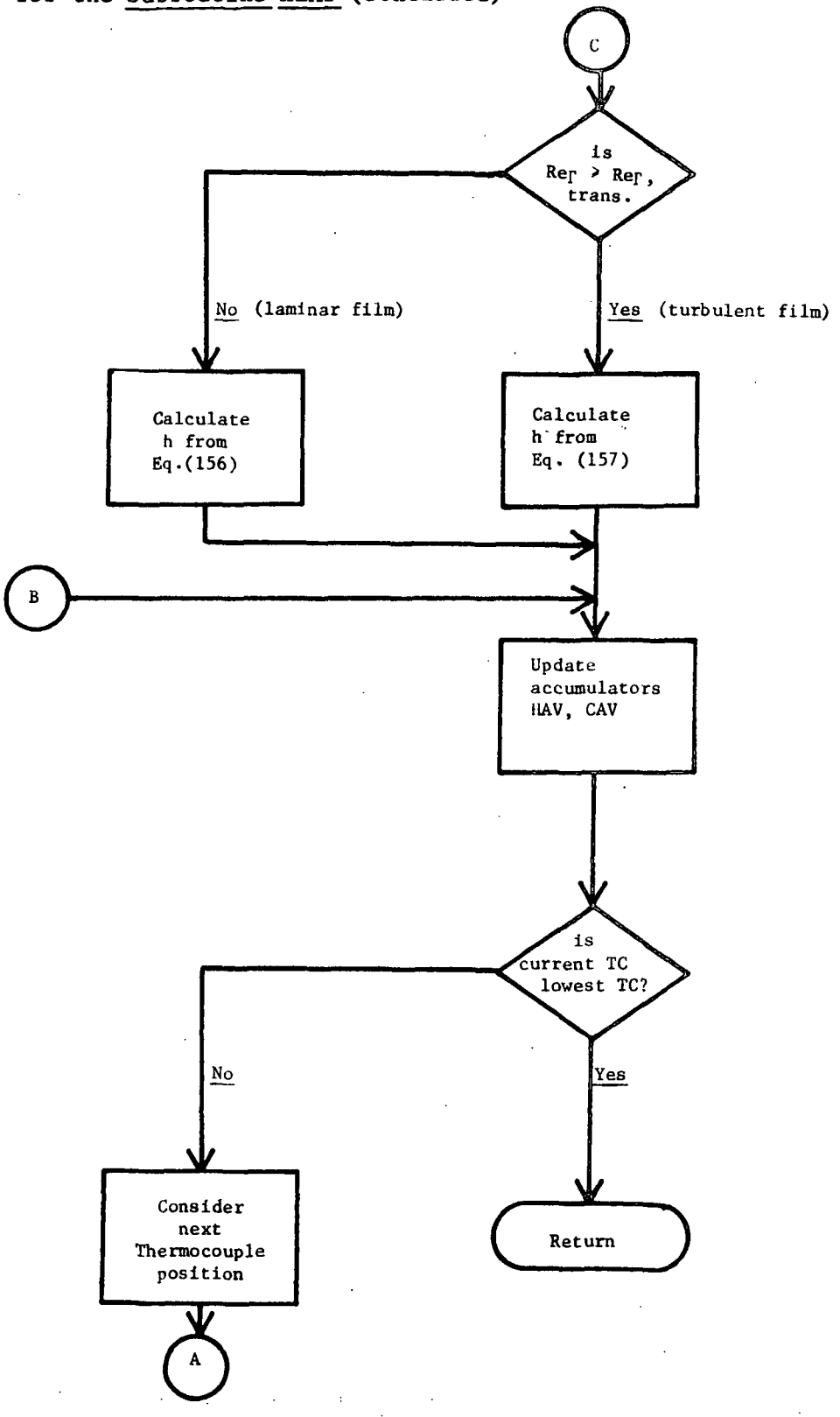

Flow chart for Subroutine PROPS

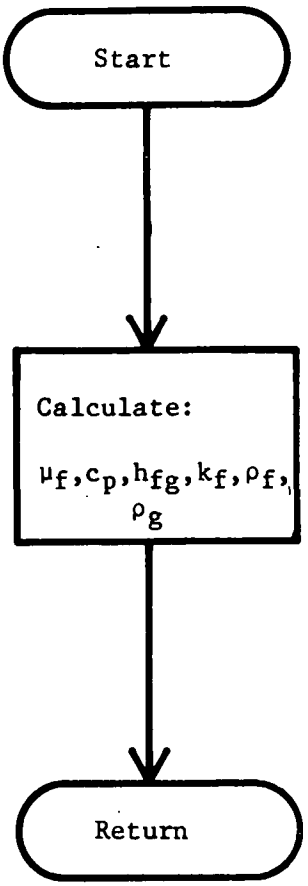

Flow chart for the Subroutine SCONC

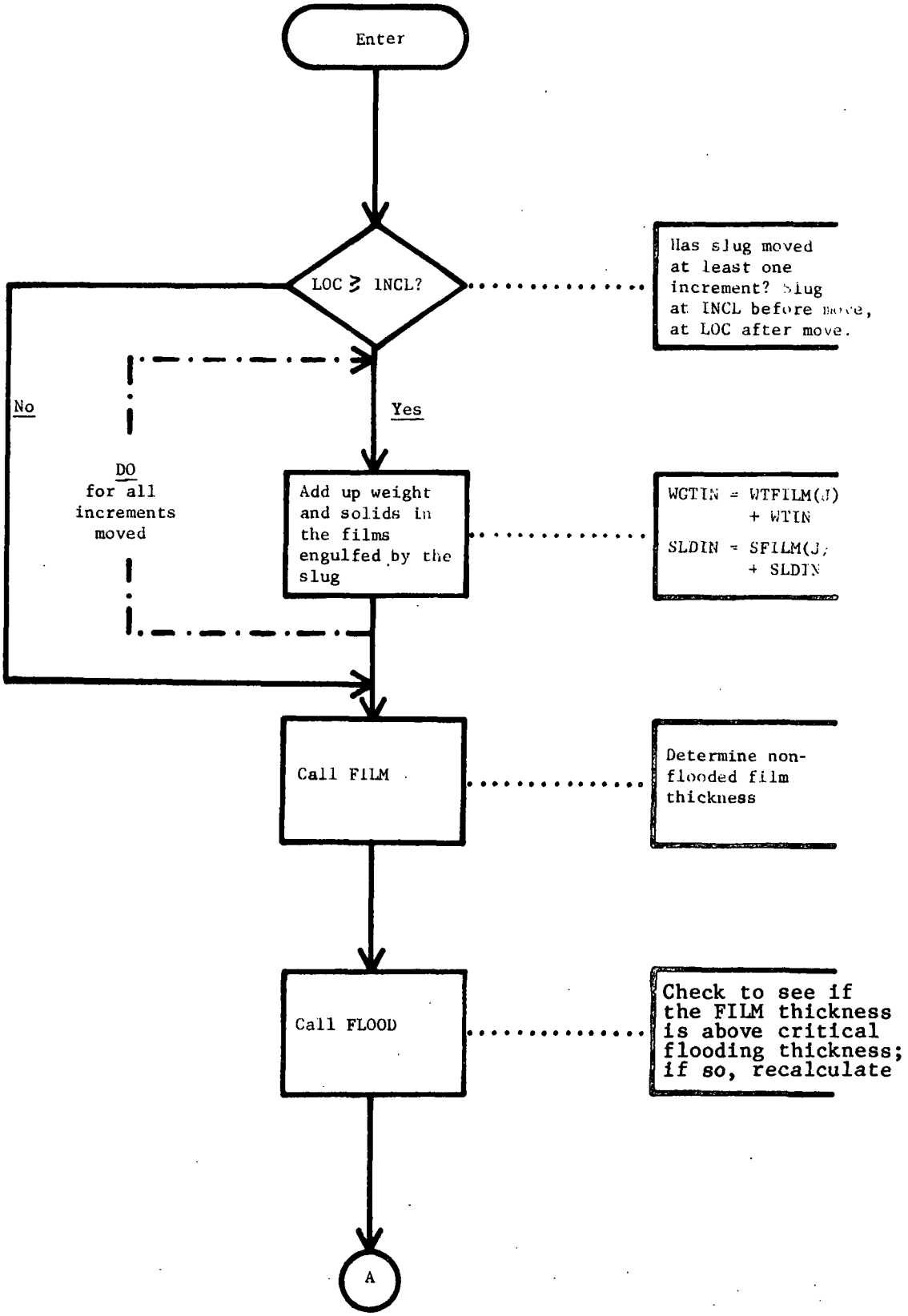

Flow chart for the Subroutine SCONC
(page 2 of 5)

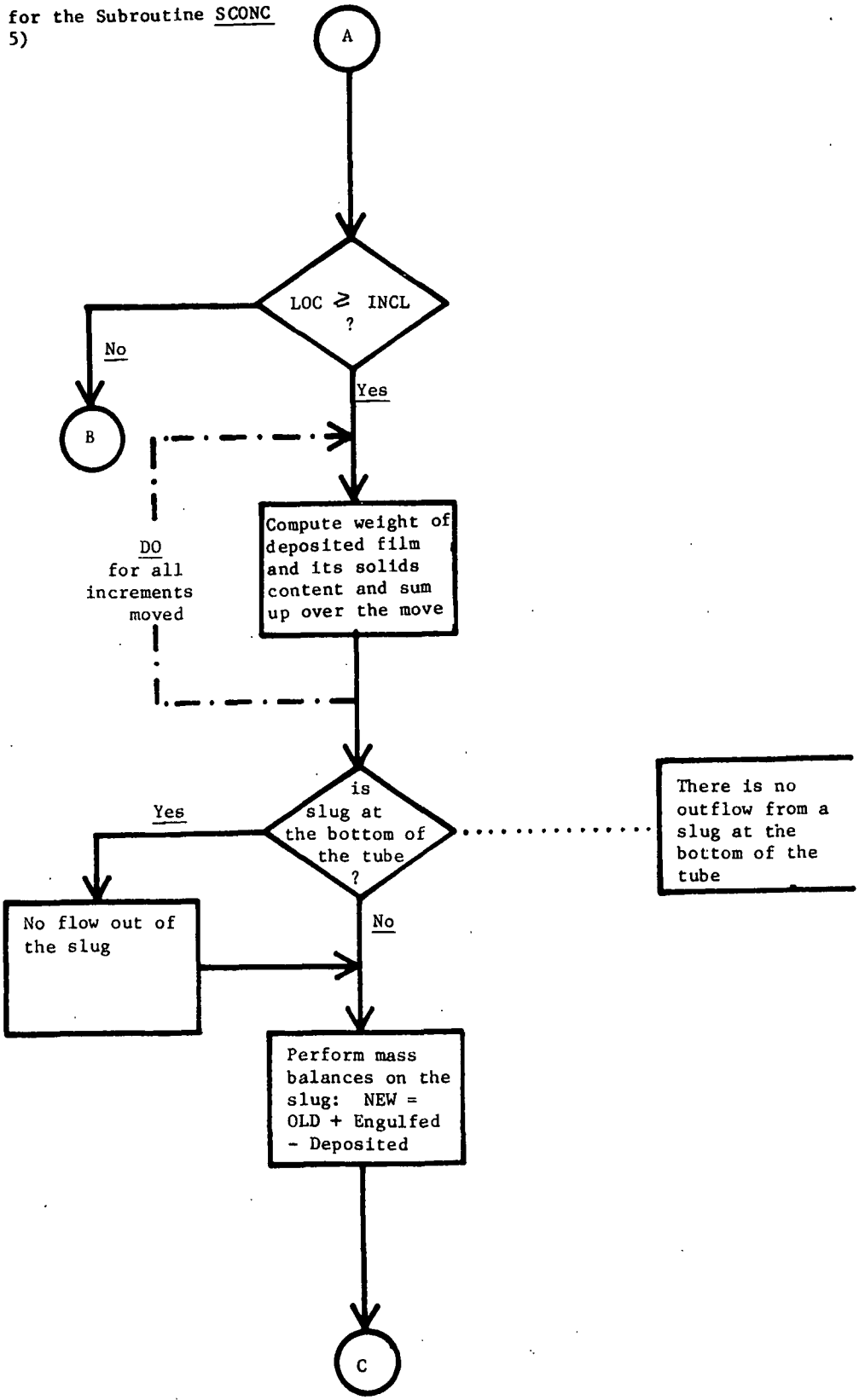

Flow chart for the Subroutine SCONC
(page 3 of 5)

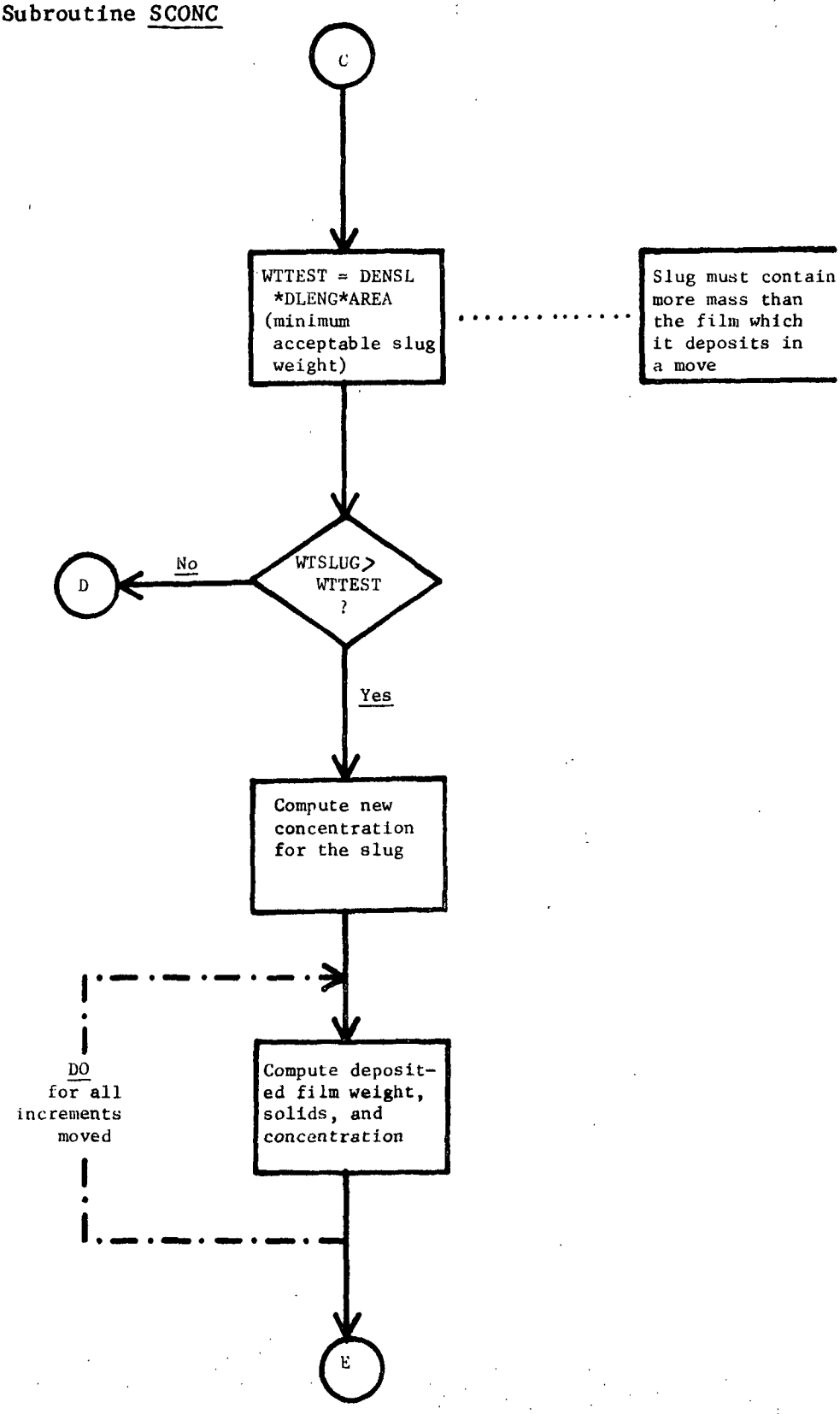

Flow chart for the Subroutine SCONC
(page 4 of 5)

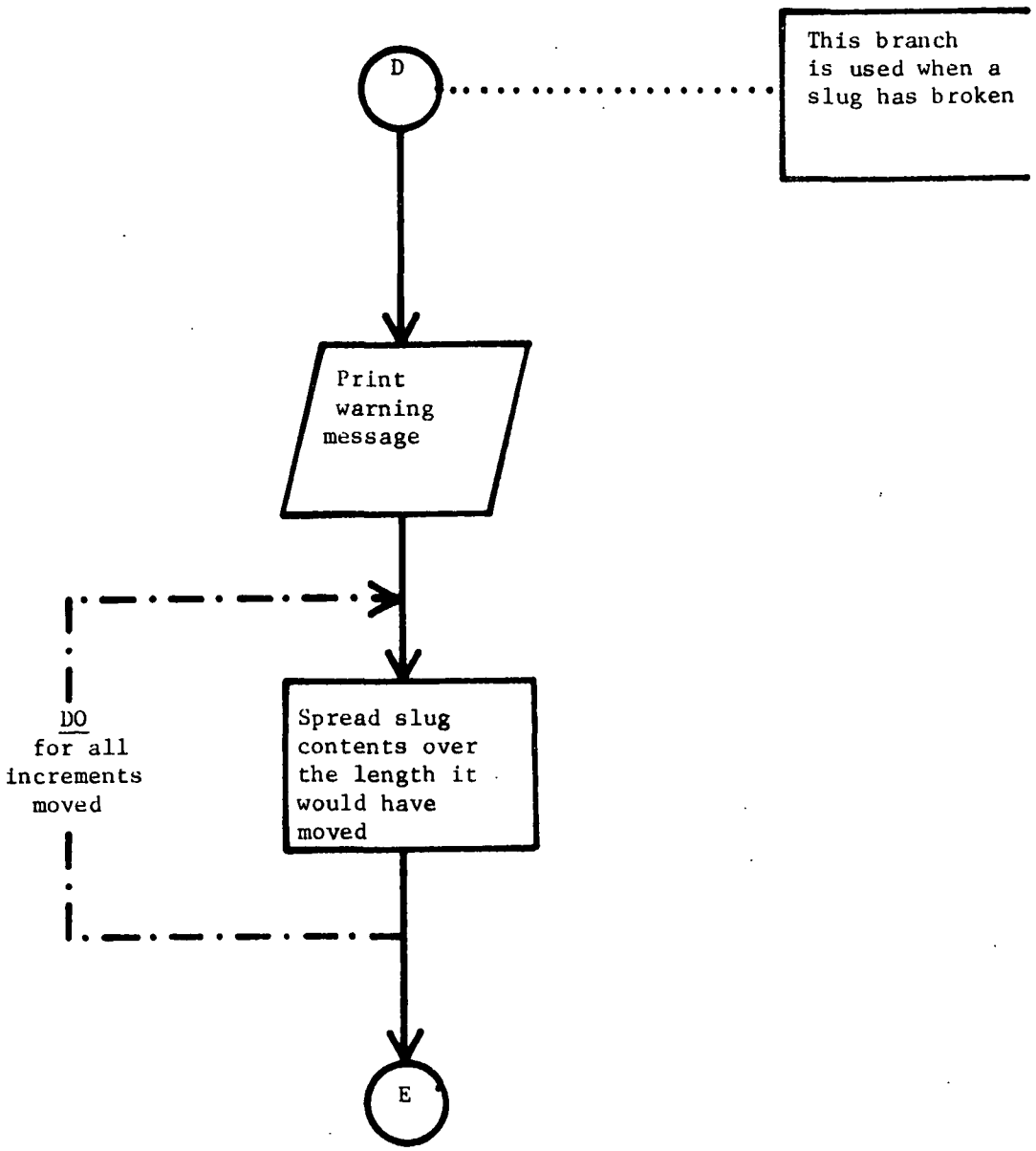

Flow chart for the Subroutine SCONC
(page 5 of 5)

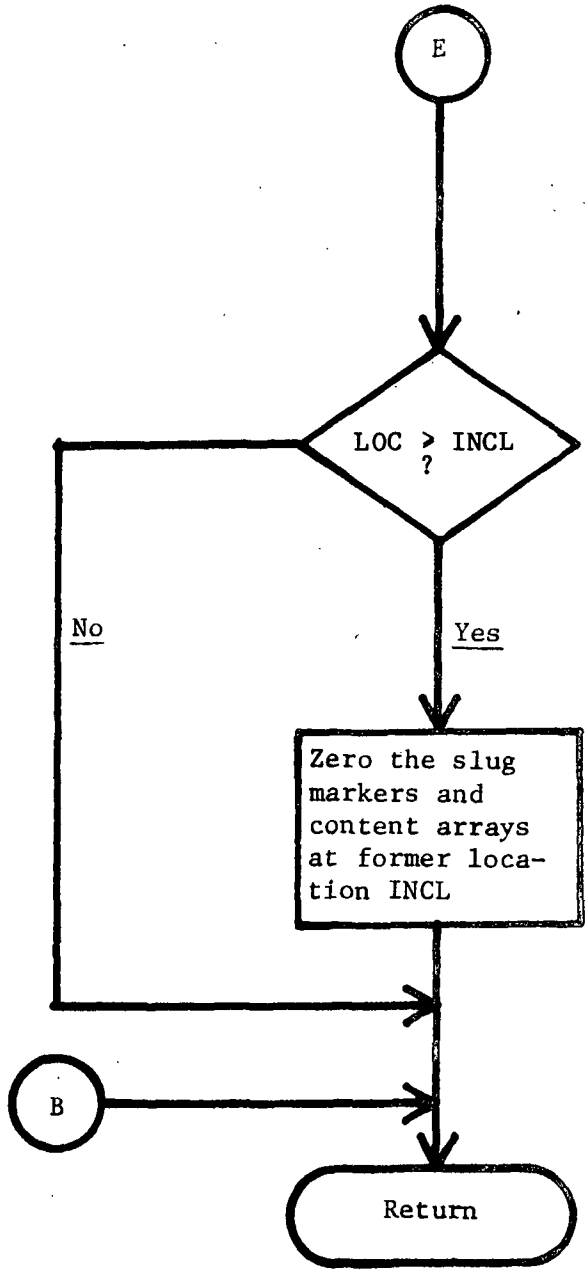

Flow chart for Subroutine SMAKE

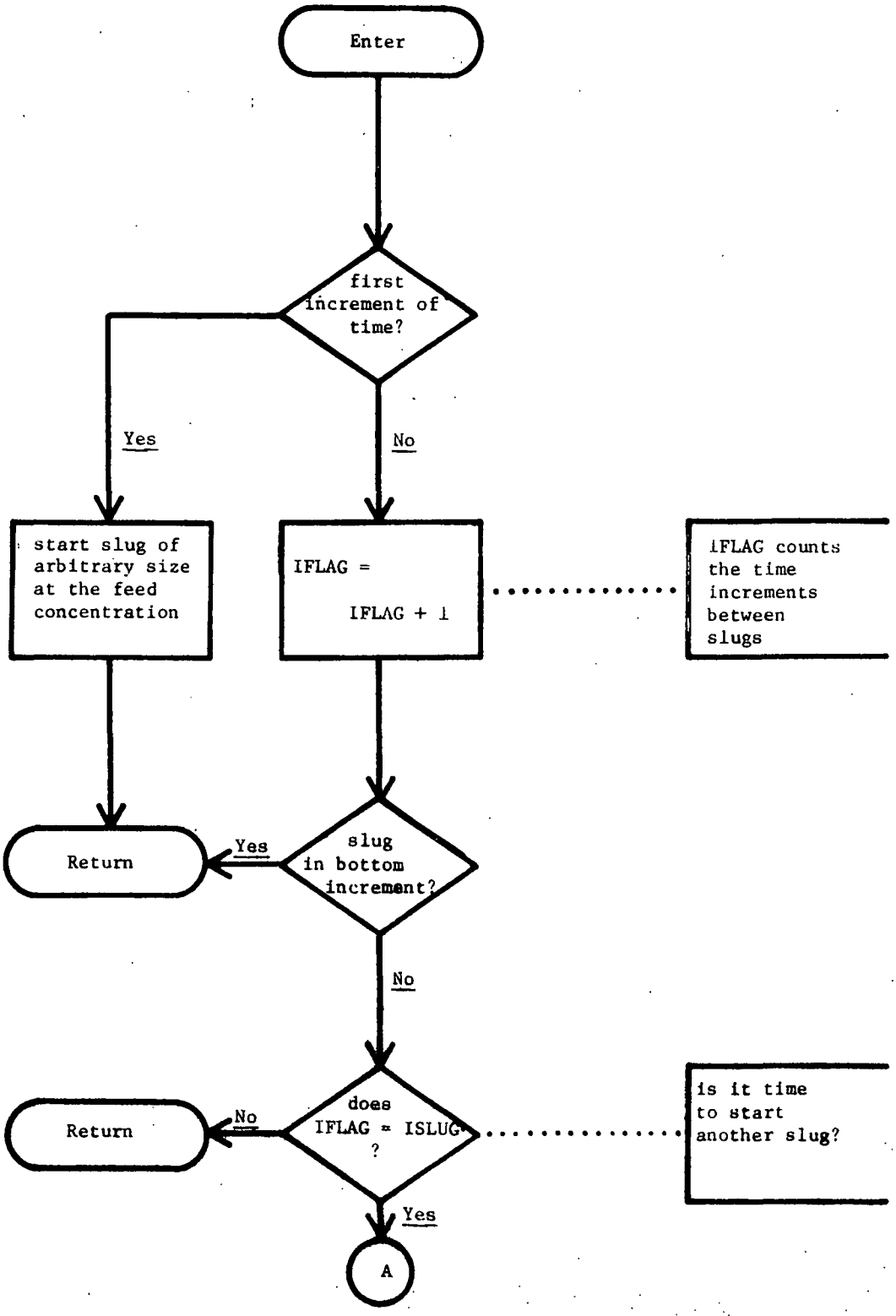

Flow chart for Subroutine SMAKE (concluded)

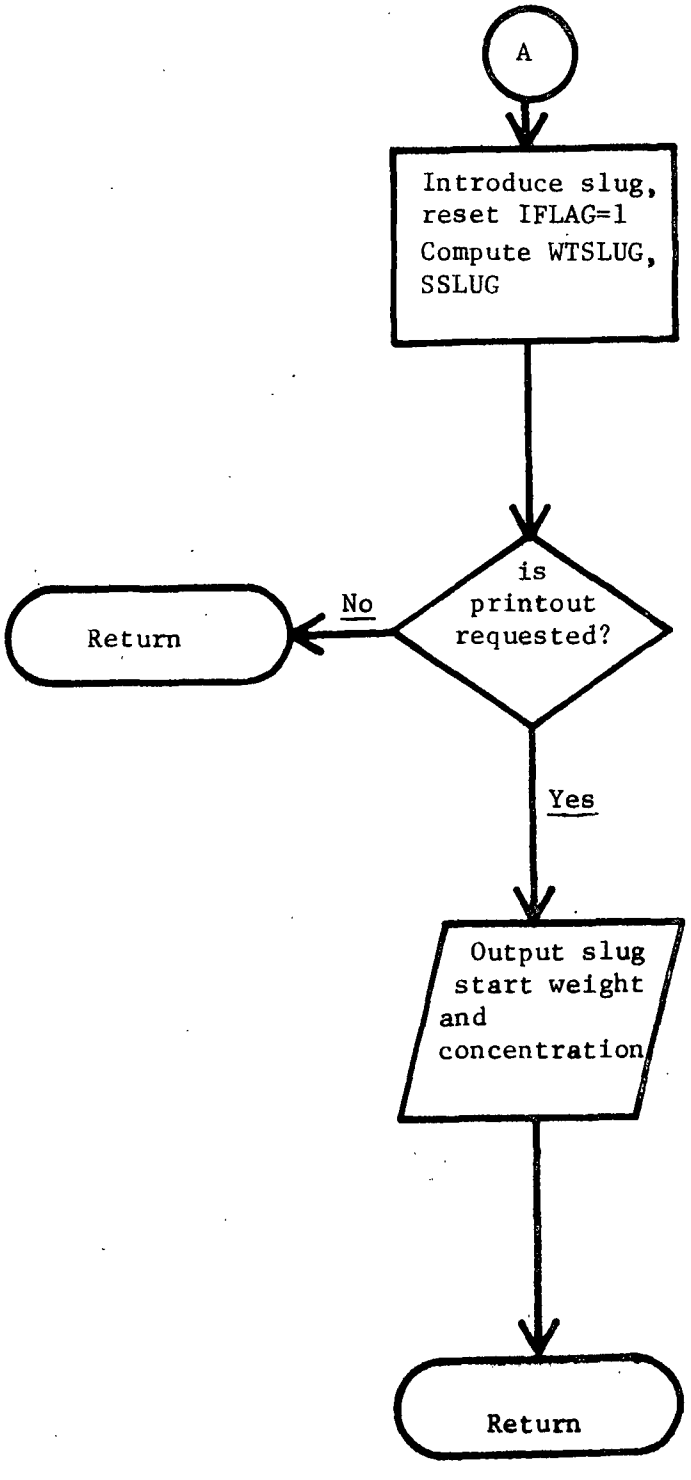

Flow chart for Subroutine SMOVE

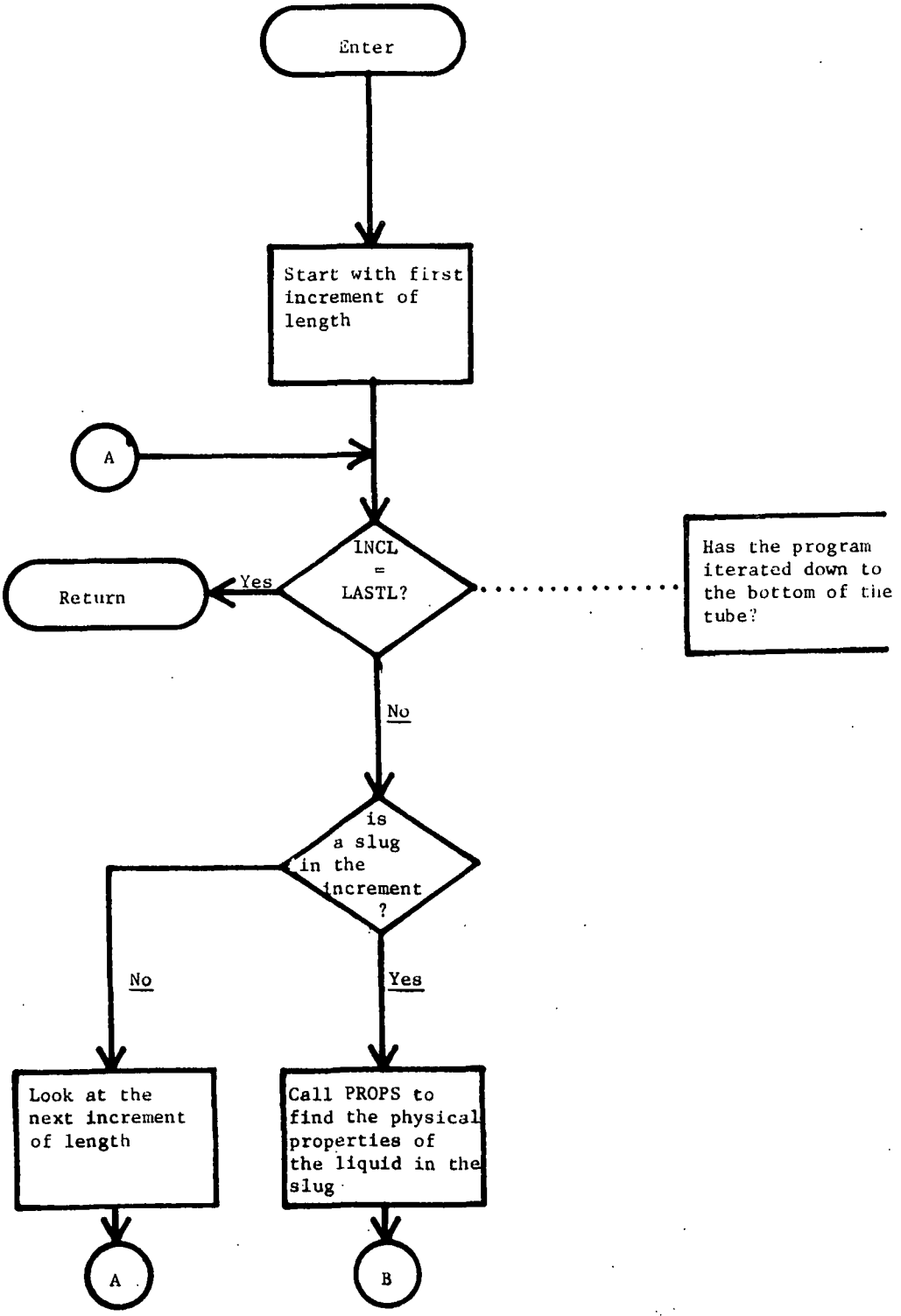

Flowchart for Subroutine SMOVE
(page 2 of 4)

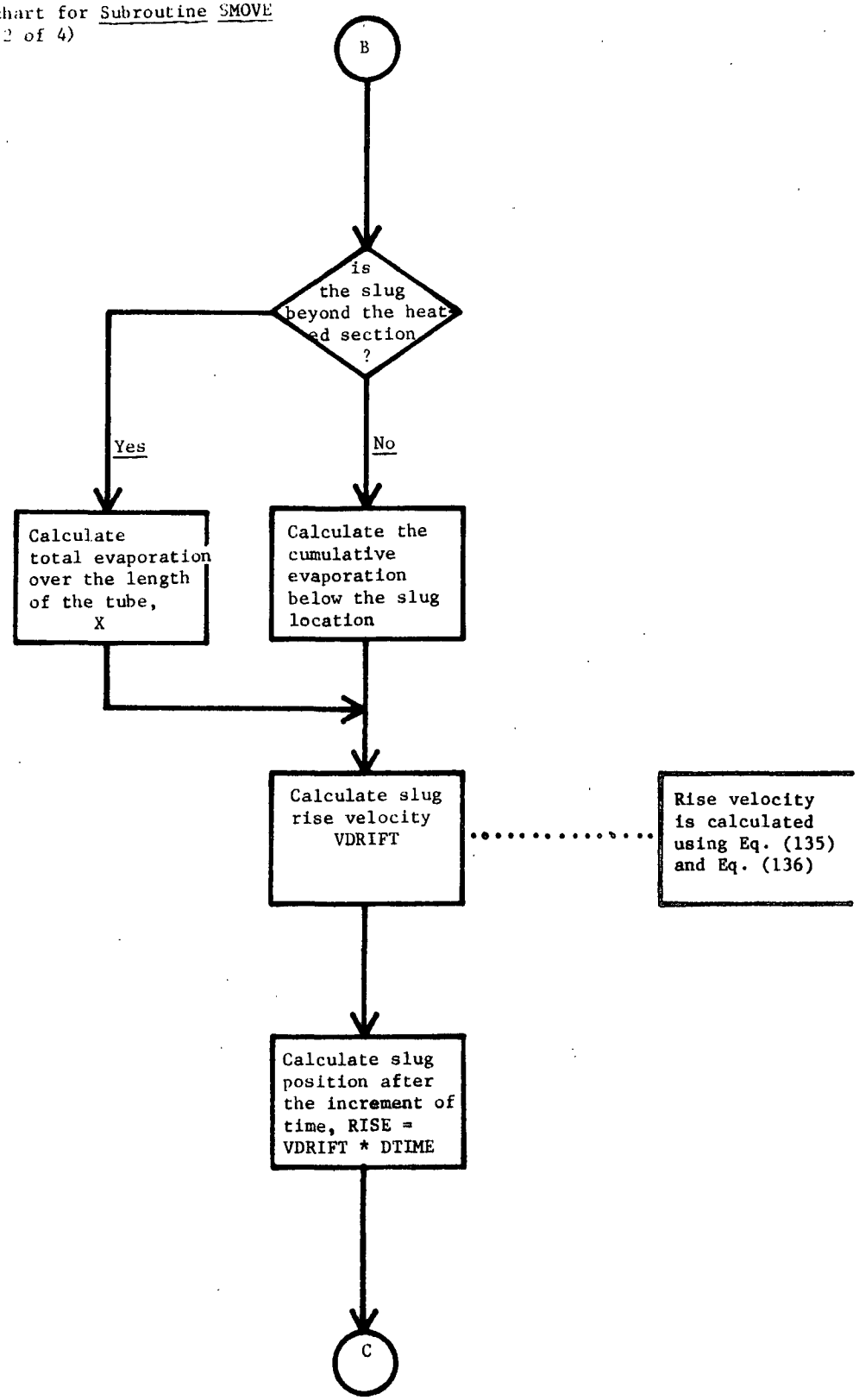

Flow chart for Subroutine SMOVE
(Page 3 of 4)

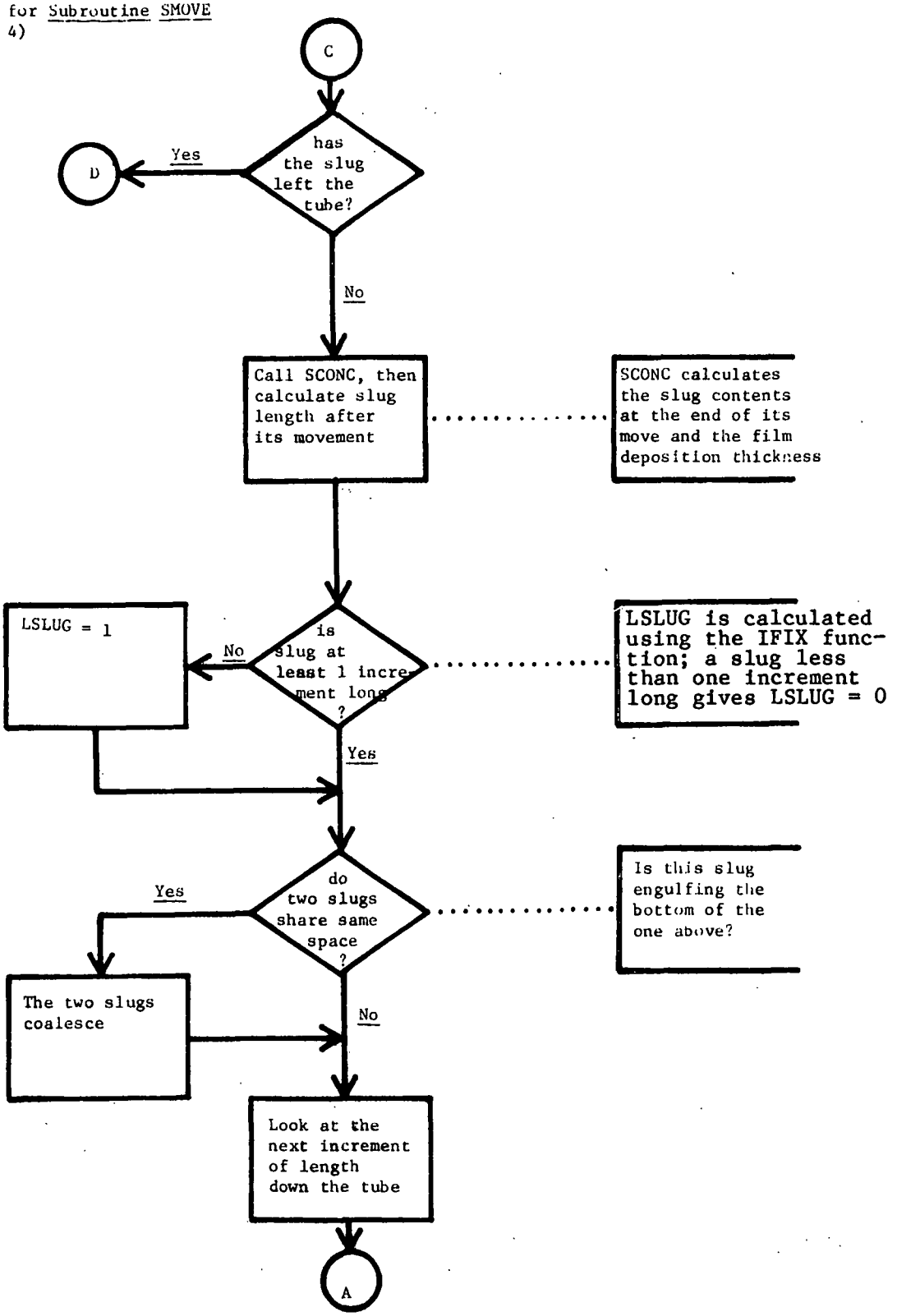

Flow chart for Subroutine SMOVE
(Page 4 of 4)

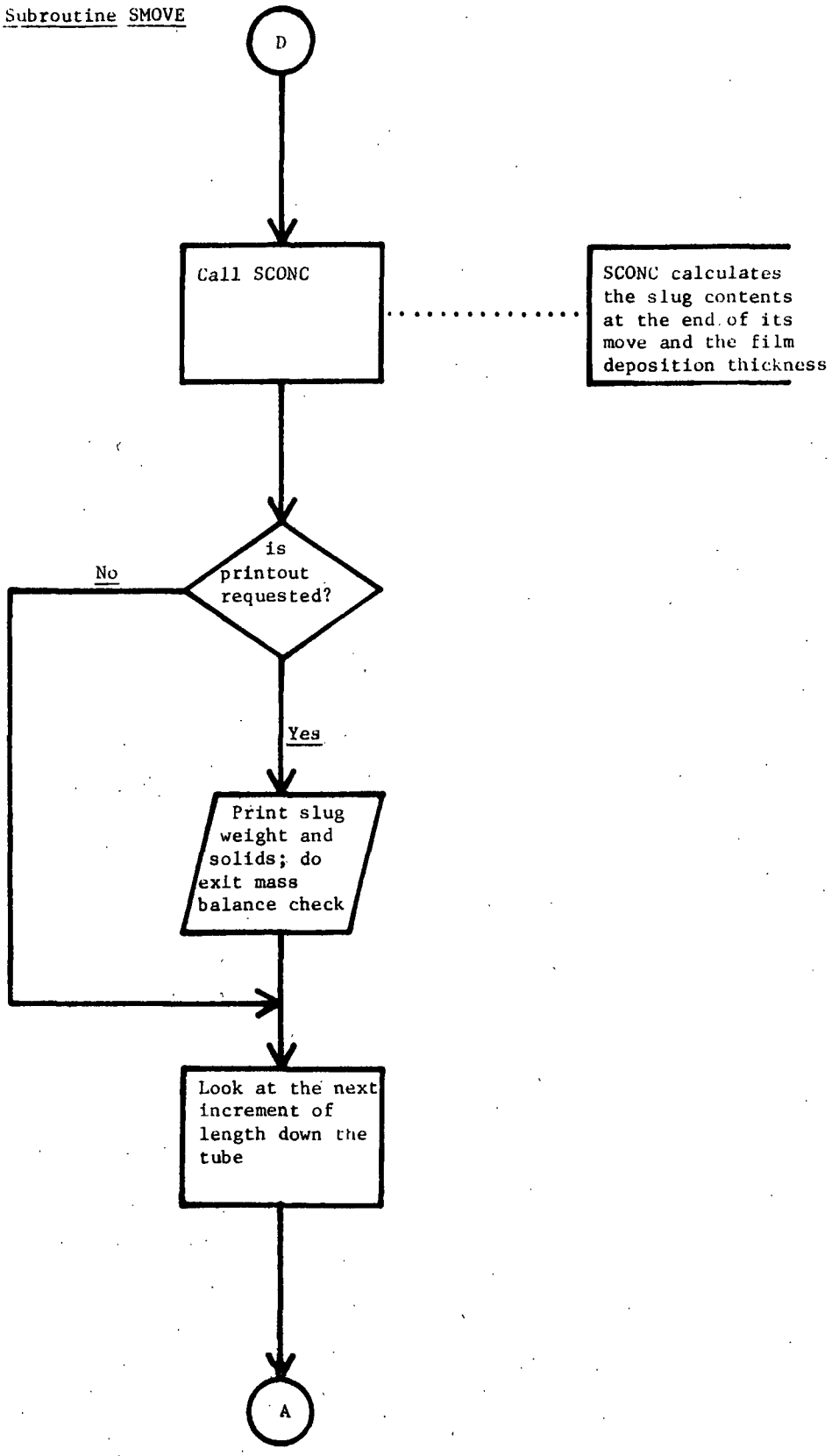

Flow chart for Subroutine START

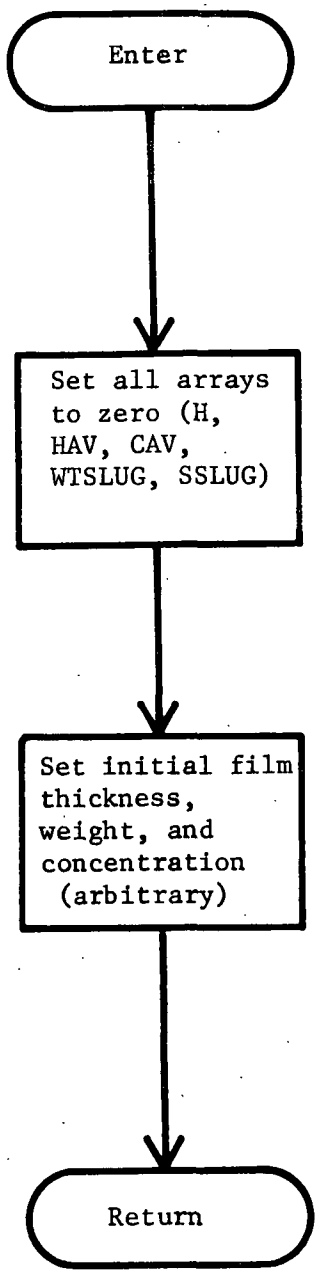

MAIN Program

```
      DIMENSION JSL(460),THICK(460),RE(460),H(10),HAV(10)
      DIMENSION POSIT(460),CONCEN(460),WTFILM(460),SFILM(460)
      DIMENSION WTSLUG(460),SSLUG(460),CAV(10)
      M=6
 1000 FORMAT(F10.5)
 1001 FORMAT(I5)
      DO 190 KOUNT=1,100
      READ(5,1000) W
      IF(W) 11,11,12
   11 KOUNT=100
      GO TO 190
   12 READ(5,1000) HTFLUX
      READ(5,1000) SRATE
      READ(5,1000) CZERO
      READ(5,1000) WTFEED
      READ(5,1000) C
      READ(5,1000) DTIME
      DTIME=2.777E-07*DTIME
      READ(5,1000) DLENG
      DLENG=DLENG/12.
      READ(5,1001) LASTL
      READ(5,1001) LASTHT
      READ(5,1001) LASTT
      READ(5,1001) IFEED
      READ(5,1000) CFEED
      WTFEED=WTFEED*DTIME
      READ(5,1001) J460
      READ(5,1000) CDIFF
      READ(5,1000) D
      READ(5,1001) IPRIN
      PI=3.141592654
      G=4.173E+08
      JSL(460)=J460
      C29=0.
      IPRINT=IPRIN
      CONCEN(LASTL+2)=CZERO
      INCL=LASTL+2
      CALL PROPS(CONCEN,INCL,VISCL,HTCAP,HTEVAP,TCOND,DENSL,DENSG)
      X=HTFLUX*PI*D*DLENG*(LASTL-LASTHT)/(HTEVAP*W)
      CINIT=CZERO
      ISLUG=IFIX((1./(SRATE*60.*DTIME))+0.5)
      WRITE(6,15) LASTL,LASTHT,LASTT,IFEED,JSL(460),IPRINT
   15 FORMAT(' ',6(I5,5X))
      WRITE(6,16) DLENG,CDIFF,D,CFEED
   16 FORMAT(' ',4(E12.5,5X))
      WRITE(M,1) W
    1 FORMAT('1W= ',F12.4)
      WRITE(M,2) HTFLUX
    2 FORMAT(' HEAT FLUX = ',E12.4)
      WRITE(M, 3) SRATE
    3 FORMAT(' SLUGS PER MINUTE = ',E12.4)
      WRITE(6,4) CZERO
    4 FORMAT(' ENTRANCE CONCENTRATION = ',E12.4)
      WRITE(6,5) DTIME
    5 FORMAT(' HOURS/INCR. TIME = ',E12.4)
      WRITE(6,6) ISLUG
    6 FORMAT(' INCR. T/SLUG START = ',I6)
      WRITE(6,7)  VISCL
    7 FORMAT(' VISCOSITY= ',E12.4)
      WRITE(6,8)  DENSL
    8 FORMAT(' DENSITY= ',E12.4)
      WRITE(6,9) WTFEED
    9 FORMAT(' DYE FEED RATE, LBS/HR = ',E12.4)
      WRITE(6,10) C
   10 FORMAT(' FLOODING CRITERION C = ',E12.4)
      CALL START(JSL,THICK,RE,H,HAV,LASTL,WTSLUG,SSLUG,CAV,CONCEN,CINIT,
     1WTFILM,SFILM,PI,D,DENSL,DLENG)
```

```
      INCT=1
      ITIME=1
  170 CONTINUE
      WTIN=0.
      WTIN=WTIN*DTIME
      SOLIN=0.
      SOLIN=SOLIN*DTIME
      CALL SMAKE(INCT,JSL,LASTL,ISLUG,POSIT,DLENG,WTSLUG,SSLUG,W,SRATE,
     1CZERO,M,CINIT,WTFILM,SFILM,IPRINT)
      CALL SMOVE(JSL,HTFLUX,RE,THICK,CONCEN,POSIT,LASTL,LASTHT,DLENG,W,
     1CZERO,VISCL,HTCAP,HTEVAP,TCOND,DENSL,DENSG,PI,D,G,DTIME,WTSLUG,
     2SSLUG,INCT,M,WTFILM,SFILM,C,ISLUG,IPRINT)
      DO 150 INCL=1,LASTL
      IF(IFEED-INCL) 22,23,22
   23 WTIN=WTIN+WTFEED
      SOLIN=SOLIN+(CFEED*WTFEED)
   22 IF(JSL(INCL)-3) 111,121,121
  121 IF(INCL-LASTL) 122,150,150
  122 WTOUT=((PI*D*RE(INCL)*VISCL/4.)*DTIME)
      SOLOUT=(SSLUG(INCL)/WTSLUG(INCL))*WTOUT
      IF(INCL-LASTHT) 40,60,60
   60 WTEVAP=HTFLUX*PI*D*DLENG*DTIME/HTEVAP
      GO TO 80
   40 WTEVAP=0.
   80 WTS          =WTSLUG(INCL)+WTIN-WTOUT-WTEVAP
      IF(WTS) 30,30,32
   30 WTFILM(INCL)=WTSLUG(INCL)-WTEVAP
      SFILM(INCL)=SSLUG(INCL)
      WTSLUG(INCL)=0.
      SSLUG(INCL)=0.
      JSL(INCL)=0.
      WRITE(6,31) INCL,INCT
   31 FORMAT(' SLUG BROKE IN MAIN PROGRAM AT INCL= ',I4,' INCT= ',I4)
      GO TO 150
   32 SSLUG(INCL)=SSLUG(INCL)+SOLIN-SOLOUT
      WTSLUG(INCL)=WTS
      CONCEN(INCL)=SSLUG(INCL)/WTSLUG(INCL)
      IF(IPRINT-999) 104,105,104
  105 WRITE(6,106) INCL,WTSLUG(INCL),SSLUG(INCL),CONCEN(INCL)
  106 FORMAT(' SLUG AT INCL = ',I4,' HAS WEIGHT = ',E12.4,' ,SOLIDS = ',
     1E12.4,' ,CONCENTRATION = ',E12.4)
  104 CONTINUE
      WTFILM(INCL)=0.
      SFILM(INCL)=0.
      WTIN=WTOUT
      SOLIN=SOLOUT
      GO TO 150
  111 CALL BALAN(THICK,G,DENSL,DENSG,VISCL,RE,D,PI,WTIN,INCL,DTIME,
     1DLENG,LASTHT,CONCEN,SOLIN,HTCAP,HTEVAP,TCOND,HTFLUX,WTFILM,SFILM)
  150 CONTINUE
      IF(JSL(LASTL)-3) 172,176,176
  176 WTSLUG(LASTL)=WTSLUG(LASTL)+WTIN-(HTFLUX*PI*D*DLENG*DTIME/HTEVAP)
      IF(WTSLUG(LASTL)) 34,34,36
   34 WTSLUG(LASTL)=0.
      SSLUG(LASTL)=0.
      WTFILM(LASTL)=0.
      SFILM(LASTL)=0.
      JSL(LASTL)=1
      GO TO 174
   36 SSLUG(LASTL)=SSLUG(LASTL)+SOLIN
      CONCEN(LASTL)=SSLUG(LASTL)/WTSLUG(LASTL)
      WTFILM(LASTL)=0.
      SFILM(LASTL)=0.
      GO TO 174
  172 WTSLUG(LASTL+1)=WTIN+WTSLUG(LASTL+1)-(HTFLUX*PI*D*DLENG*DTIME/
     1HTEVAP)
      SSLUG(LASTL+1)=SOLIN+SSLUG(LASTL+1)
```

```
      174 IF(JSL(460)-2) 153,154,155
      154 ITIME=ITIME+1
          CALL HEAT(RE,TCOND,THICK,HTCAP,VISCL,DENSL,DENSG,G,HAV,H,
     1CAV,CONCEN,JSL,HTFLUX,PI,D,DLENG,LASTL,W)
          TIME=3600.*DTIME*(ITIME-2)
          IF(IPRINT-999) 153,100,100
      100 WRITE( 6,99)TIME
       99 FORMAT(/,' TIME INTO CYCLE, SECONDS = ',E12.4)
          WRITE( 6,52) (CONCEN(J),J=29,105,8)
          WRITE( 6,52) (THICK(J),J=29,105,8)
          WRITE(6,52) (RE(J),J=29,105,8)
          WRITE( 6,52) (H(J),J=1,10)
       52 FORMAT(' ',10(E10.3,2X))
      153 INCT=INCT+1
          IF(INCT-LASTT) 170,180,180
      155 IF(IPRINT-1) 156,157,157
      157 IF(ITIME-1) 188,188,189
      189 DO 182 J=1,10
          HAV(J)=HAV(J)/(ITIME-1)
      182 CAV(J)=CAV(J)/(ITIME-1)
      188 WRITE( 6,84) (HAV(J),J=1,10)
          WRITE( 6,84) (CAV(J),J=1,10)
       84 FORMAT(/,' ',10(E10.3,2X))
          WRITE(6,85) (JSL(J),J=1,5)
          WRITE(6,85) (JSL(J),J=6,65)
          WRITE(6,85) (JSL(J),J=66,113)
       85 FORMAT(' ',5(12I1,1X))
          WRITE(6,195) ITIME
      195 FORMAT(' ITIME AT EXIT = ',I3)
      156 IF(ABS(C29-CAV(1))-CDIFF) 101,101,102
      101 IF(IPRINT-999) 103,190,103
      103 IPRINT=999
      102 ITIME=1
          C29=CAV(1)
          JSL(460)=2
          DO 186 J=1,10
          HAV(J)=0.
      186 CAV(J)=0.
          GO TO 154
      180 CONTINUE
          WRITE(6,185)
      185 FORMAT(' INSUFFICIENT TIME ALLOWED FOR SLUGGING CYCLE')
      190 CONTINUE
          STOP
          END
```

Subroutine BALAN

```
      SUBROUTINE BALAN(THICK,G,DENSL,DENSG,VISCL,RE,D,PI,WTIN,INCL,
     1DTIME,DLENG,LASTHT,CONCEN,SOLIN,HTCAP,HTEVAP,TCOND,HTFLUX,
     1WTFILM,SFILM)
      DIMENSION THICK(1),RE(1),CONCEN(1),WTFILM(1),SFILM(1)
      CALL PROPS(CONCEN,INCL,VISCL,HTCAP,HTEVAP,TCOND,DENSL,DENSG)
      TSTAR=THICK(INCL)*(G**0.333)*((DENSL-DENSG)**0.333)*(DENSL**0.333)
     1/(VISCL**0.666)
      RE(INCL)=(TSTAR/0.909)**3
      IF(RE(INCL)-1000.) 410,420,420
  420 RE(INCL)=(TSTAR/0.063)**1.5
  410 WTOUT=((PI*D*RE(INCL)*VISCL)/4.)*DTIME
      SOLOUT=CONCEN(INCL)*WTOUT
      WEIGHT=WTFILM(INCL)
      SOLIDS=SFILM(INCL)
      IF(INCL-LASTHT)440,460,460
  460 WTEVAP=HTFLUX*PI*D*DLENG*DTIME/HTEVAP
      GO TO 480
  440 WTEVAP=0.
  480 WEIGHT=WEIGHT+WTIN-WTOUT-WTEVAP
      SOLIDS=SOLIDS+SOLIN-SOLOUT
      IF(WEIGHT-SOLIDS) 425,425,426
  425 VOLUME=0.
      WEIGHT=0.
      SOLOUT=0.
      WTFILM(INCL)=SFILM(INCL)
      SFILM(INCL)=SFILM(INCL)
      WTOUT=0.
      CONCEN(INCL)=1.
      GO TO 429
  426 IF(SOLIDS) 427,428,428
  427 SOLIDS=0.
      WRITE(6,430)INCL
  430 FORMAT(' ERROR IN BALAN, SOLIDS LESS THAN ZERO AT INCL = ',I3)
  428 CONCEN(INCL)=SOLIDS/WEIGHT
      WTFILM(INCL)=WEIGHT
      SFILM(INCL)=SOLIDS
  429 CALL PROPS(CONCEN,INCL,VISCL,HTCAP,HTEVAP,TCOND,DENSL,DENSG)
      VOLUME=WEIGHT/DENSL
      AREA=VOLUME/DLENG
      THICK(INCL)=(PI*D-SQRT(PI*PI*D*D-4.*PI*AREA))/(2.*PI)
      WTIN=WTOUT
      SOLIN=SOLOUT
      RETURN
      END
```

Subroutine FILM

```
      SUBROUTINE FILM(EFFVSC,VRATIO,RE,THICK,INCL,LASTL,LOC,TEST1)
      DIMENSION RE(1),THICK(1)
      D=0.1558
      OLD=1.0
      DEL=0.001
      CRIT=0.00001
      DRATIO=0.03
540   TEST1=190.*(DRATIO**1.5)
      TEST2=(((1.2*VRATIO)+1.)*((1.-2.*DRATIO)**2))-VRATIO
      IF(ABS(TEST1-TEST2)-CRIT) 560,560,500
500   TEST3=OLD*(TEST1-TEST2)
      IF(TEST3) 542,544,544
542   DEL=DEL/10.
      GO TO 544
544   OLD=TEST1-TEST2
      IF(TEST1-TEST2) 530,560,550
530   DRATIO=DRATIO+DEL
      GO TO 540
550   DRATIO=DRATIO-DEL
      GO TO 540
560   IF(EFFVSC-10000.) 598,575,575
598   DTURB=DRATIO
      DTEST=TEST1
      DEL=0.001
      OLD=1.0
      DRATIO=0.03
541   TEST1=3.85*EFFVSC*(DRATIO**3)
      TEST2=(((1.2*VRATIO)+1.)*((1.-2.*DRATIO)**2))-VRATIO
      IF(ABS(TEST1-TEST2)-CRIT) 561,561,501
501   TEST3=OLD*(TEST1-TEST2)
      IF(TEST3) 543,545,545
543   DEL=DEL/2.
      GO TO 545
545   OLD=TEST1-TEST2
      IF(TEST1-TEST2) 531,561,551
531   DRATIO=DRATIO+DEL
      GO TO 541
551   DRATIO=DRATIO-DEL
      GO TO 541
561   IF(DTURB-DRATIO) 575,570,570
570   DRATIO=DTURB
      TEST1=DTEST
      GO TO 575
575   REY=TEST1*0.345*EFFVSC
      DO 565 J=LOC,INCL
      RE(J)=REY
565   THICK(J)=DRATIO*D
      RETURN
      END
```

Subroutine FLOOD

```
1            SUBROUTINE FLOOD(VRATIO,TEST1,DENSL,DENSG,EFFVSC,LOC,INCL,RE,
1           1THICK,D,VDRIFT,PI,VRISE,VISCL,C)
2            DIMENSION RE(1),THICK(1)
3            GRATIO=VRATIO+TEST1
4            GSTAR=0.345*SQRT(DENSG/DENSL)*GRATIO
5            FSTAR=0.345*TEST1
6            TEST4=SQRT(GSTAR)+SQRT(FSTAR)
7            IF(TEST4-C ) 899,899,810
8         810 GSTAR=0.345*SQRT(DENSG/DENSL)*(1/VRISE)*VDRIFT
9            FSTAR=(C-SQRT(GSTAR))**2
10           FLUXF=FSTAR*VRISE/0.345
11           FLOW=FLUXF*DENSL*PI*D*D/4.
12           REY=4*(FLOW/(PI*D))/VISCL
13           IF(REY-1000.) 820,820,830
14        820 DRATIO=0.909*(REY**0.3333)/(EFFVSC**0.6667)
15           GO TO 840
16        830 DRATIO=0.063*(REY**0.6667)/(EFFVSC**0.6667)
17        840 DO 895 J=LOC,INCL
18           THICK(J)=DRATIO*D
19        895 RE(J)=REY
20        899 RETURN
21           END
```

Subroutine HEAT

```
1            SUBROUTINE HEAT(RE,TCOND,THICK,HTCAP,VISCL,DENSL,DENSG,G,HAV,H,
1           1CAV,CONCEN,JSL,HTFLUX,PI,D,DLENG,LASTL,W)
2            DIMENSION RE(1),THICK(1),HAV(1),H(1),CAV(1),CONCEN(1),JSL(1)
3            TRANS=1000.
4            INCL=29
5            J=1
6         600 CALL PROPS(CONCEN,INCL,VISCL,HTCAP,HTEVAP,TCOND,DENSL,DENSG)
7            PR=HTCAP*VISCL/TCOND
8            IF(JSL(INCL)-2) 680,690,690
9         690 X=HTFLUX*PI*D*DLENG*(LASTL-INCL)/(HTEVAP*W)
10           FLUXJ=((X*W/DENSG)+((1.-X)*W/DENSL))/(PI*D*D/4.)
11           VRISE=0.345*SQRT(G*D*(DENSL-DENSG))/SQRT(DENSL)
12           VDRIFT=1.2*FLUXJ+VRISE
13           B=DENSL*VDRIFT
14           REY=B*D/VISCL
15           H(J)=0.023*(REY**0.80 )*(PR**0.40)*TCOND/D
16           GO TO 630
17        680 A=((TCOND**3)*G*(DENSL**2)/(VISCL**2))**0.3333333333
18           TRANS=5800./(PR**1.06)
19           IF(RE(INCL)-TRANS) 610,620,620
20        610 H(J)=0.606*A/((RE(INCL)/4.)**0.22)
21           GO TO 630
22        620 H(J)=0.0038*(RE(INCL)**0.4)*(PR**0.65)*A
23        630 HAV(J)=HAV(J)+H(J)
24           CAV(J)=CAV(J)+CONCEN(INCL)
25           J=J+1
26           INCL=INCL+8
27           IF(INCL-105) 600,640,640
28        640 RETURN
29           END
```

Subroutine PROPS (for black liquor)

```
1             SUBROUTINE PROPS(CONCEN,INCL,VISCL,HTCAP,HTEVAP,TCOND,DENSL,DENSG)
2             DIMENSION CONCEN(1)
      C          THESE ARE THE PROPERTIES OF BLACK LIQUOR
      C          ACCORDING TO JAGANNATH (1979)(1980)
3             S=CONCEN(INCL)
4             BPR=41.4*((S+0.1)**2)
5             T=BPR+212.+460.0
6             IF(S-0.4) 1,2,2
7           1 VISCL=EXP(-(8.3E-03-(6.55E-03*S*S)+(5.62E-02*S*S*(T-660.)))+(5.7*S
7            1)-1.307)
8             GO TO 3
9           2 A    =-0.00049515*(T-460.)*100.*S
10            B    =0.0018003*S*S*100.*100.
11            C    =37.287E-06*(T-460.)*(T-460.)
12            D    =0.10178*S*100.
13            E    =-0.0032563*(T-460.)
14            F=EXP(A+B+C+D+E)
15            VISCL=0.06198889*F
16            GO TO 3
17          3 VISCL=2.4190883*VISCL
18            HTCAP=1.0-(323.4*S/T)
19            HTEVAP=970.
20            TCOND=0.394-( (0.210-(3.38E-04*(T-460.)) )*S)
21            DENSL=62.2*((1.96/(T**0.11))*EXP(3.558*S/(T**0.296)) )
22            DENSG=0.0463-(4.5E-05*(T-460.))
23            RETURN
24            END
```

Subroutine SCONC

```
      SUBROUTINE SCONC(THICK,RE,EFFVSC,VRATIO,INCL,LASTL,LOC,CONCEN,
     1CZERO,PI,D,DENSL,DLENG,WTSLUG,SSLUG,WTFILM,SFILM,JSL,DENSG,VDRIFT,
     1VRISE,VISCL,C)
      DIMENSION RE(1),THICK(1),CONCEN(1),WTSLUG(1),SSLUG(1),WTFILM(1),
     1SFILM(1),JSL(1)
      WGTIN=0.
      WGTOUT=0.
      SLDIN=0.
      SLDOUT=0.
      IF(LOC-INCL) 790,780,780
  790 IK=INCL-1
      DO 700 J=LOC,IK
      WGTIN=WTFILM(J)+WGTIN
      SLDIN=SFILM(J)+SLDIN
  700 CONTINUE
  780 CALL FILM(EFFVSC,VRATIO,RE,THICK,INCL,LASTL,LOC,TEST1)
      CALL FLOOD(VRATIO,TEST1,DENSL,DENSG,EFFVSC,LOC,INCL,RE,THICK,D,
     1VDRIFT,PI,VRISE,VISCL,C)
      IF(LOC-INCL) 785,730,730
  785 IK=LOC+1
      DO 710 J=IK,INCL
      WT          = DLENG*((PI*D*THICK(J))-(PI*(THICK(J)**2)))*DENSL
      WGTOUT=WGTOUT+WT
      SF       =(SSLUG(INCL)/WTSLUG(INCL))*WT
      SLDOUT=SLDOUT+SF
  710 CONTINUE
      IF(LOC-LASTL) 760,770,720
  770 WGTOUT=0.
      SLDOUT=0.
  760 WTSLUG(LOC)=WTSLUG(INCL)+WGTIN-WGTOUT
      WTTEST=DENSL*DLENG*((PI*D*THICK(LOC))-(PI*(THICK(LOC)**2)))
      IF(WTSLUG(LOC)-WTTEST) 750,750,755
  750 WRITE(6,758) INCL
  758 FORMAT(' SLUG BROKE AT INCL = ',I4)
      DO 751 J=LOC,INCL
      WTFILM(J)=(WGTIN+WTSLUG(INCL))/(INCL-LOC+1)
      SFILM(J)=(SLDIN+SSLUG(INCL))/(INCL-LOC+1)
      CONCEN(J)=SFILM(J)/WTFILM(J)
      CALL PROPS(CONCEN,INCL,VISCL,HTCAP,HTEVAP,TCOND,DENSL,DENSG)
  751 THICK(J)=(PI*D-SQRT((PI*PI*D*D)-(4.*PI*WTFILM(J)/(DLENG*DENSL))))/
     1(2*PI)
      WTSLUG(LOC)=0.
      SSLUG(LOC)=0.
      DO 757 J=LOC,INCL
  757 JSL(J)=1
      GO TO 756
  755 SSLUG(LOC)=SSLUG(INCL)+SLDIN-SLDOUT
      WTFILM(LOC)=0.
      SFILM(LOC)=0.
      CONCEN(LOC)=SSLUG(LOC)/WTSLUG(LOC)
      IK=LOC+1
      DO 711 J=IK,INCL
      WTFILM(J)=((PI*D*THICK(J))-(PI*(THICK(J)**2)))*DENSL*DLENG
      SFILM(J)=(SSLUG(INCL)/WTSLUG(INCL))*WTFILM(J)
      CONCEN(J)=SFILM(J)/WTFILM(J)
  711 CONTINUE
  756 IF(LOC-INCL) 740,730,720
  720 WRITE(6,721)
  721 FORMAT(' ERROR IN SUBROUTINE SCONC')
  740 WTSLUG(INCL)=0.
      SSLUG(INCL)=0.
  730 RETURN
      END
```

Subroutine SMAKE

```
1           SUBROUTINE SMAKE(INCT,JSL,LASTL,ISLUG,POSIT,DLENG,WTSLUG,SSLUG,W,
1          1SRATE,CZERO,M,CINIT,WTFILM,SFILM,IPRINT)
2           DIMENSION JSL(1),POSIT(1),WTSLUG(1),SSLUG(1),WTFILM(1),SFILM(1)
3           IF(1-INCT) 210,220,220
4         220 WTSLUG(LASTL+1)=1.
5           SSLUG(LASTL+1)=WTSLUG(LASTL+1)*CINIT
6           GO TO 250
7         210 IFLAG=IFLAG+1
8           IF(JSL(LASTL)-3) 270,230,230
9         270 IF(IFLAG-ISLUG) 230,250,250
10        250 JSL(LASTL)=3
11          POSIT(LASTL)=LASTL*DLENG
12          WTSLUG(LASTL)=W/(SRATE*60.)+WTFILM(LASTL)+WTSLUG(LASTL+1)
13          SSLUG(LASTL)=CZERO*(W/(SRATE*60.))+SFILM(LASTL) + SSLUG(LASTL+1)
14          WTFILM(LASTL)=0.
15          SFILM(LASTL)=0.
16          WTSLUG(LASTL+1)=0.
17          SSLUG(LASTL+1)=0.
18          IFLAG=1
19          IF(IPRINT-1) 230,280,280
20        280 IF(ISLUG-1) 230,230,260
21        260 WRITE( M,240)INCT
22        240 FORMAT(/,' SLUG STARTED AT TIME INCREMENT = ',I5)
23          WRITE( M,241)WTSLUG(LASTL),SSLUG(LASTL)
24        241 FORMAT(' SLUG WEIGHT AT START = ',E10.5,2X,'SLUG SOLIDS AT START =
          1',E10.5)
25        230 RETURN
26          END
```

Subroutine SMOVE

```
      SUBROUTINE SMOVE(JSL,HTFLUX,RE,THICK,CONCEN,POSIT,LASTL,LASTHT,
     1DLENG,W,CZERO,VISCL,HTCAP,HTEVAP,TCOND,DENSL,DENSG,PI,D,G,DTIME,
     1WTSLUG,SSLUG,INCT,M,WTFILM,SFILM,C,ISLUG,IPRINT)
      DIMENSION JSL(1),THICK(1),RE(1),POSIT(1),CONCEN(1)
      DIMENSION WTSLUG(1),SSLUG(1),WTFILM(1),SFILM(1)
      INCL=1
  300 IF(INCL-LASTL) 310,310,320
  310 IF(JSL(INCL)-3) 330,340,340
  330 JSL(INCL)=1
      INCL=INCL+1
      GO TO 300
  340 CALL PROPS(CONCEN,INCL,VISCL,HTCAP,HTEVAP,TCOND,DENSL,DENSG)
      IF(INCL-LASTHT) 342,344,344
  344 INCLHT=INCL
      GO TO 346
  342 INCLHT=LASTHT
  346 X=HTFLUX*PI*D*DLENG*(LASTL-INCLHT)/(HTEVAP*W)
      EFFVSC=SQRT((D**3)*G*(DENSL-DENSG)*DENSL)/VISCL
      FLUXJ=((X*W/DENSG)+((1.-X)*W/DENSL))/(PI*D*D/4.)
      VRISE=0.345*SQRT(G*D*(DENSL-DENSG))/SQRT(DENSL)
      VRATIO=FLUXJ/VRISE
      VDRIFT=1.2*FLUXJ+VRISE
      RISE=VDRIFT*DTIME
      POSN=POSIT(INCL)-RISE
      LOC=IFIX((POSN/DLENG)+0.99)
      IF(-LOC) 350,360,360
  350 DO 355 J=LOC,INCL
  355 JSL(J)=1
      JSL(LOC)=3
      CALL SCONC(THICK,RE,EFFVSC,VRATIO,INCL,LASTL,LOC,CONCEN,CZERO,
     1PI,D,DENSL,DLENG,WTSLUG,SSLUG,WTFILM,SFILM,JSL,DENSG,FLUXJ,VRISE,
     1VISCL,C)
      POSIT(LOC)=POSN
      LSLUG=IFIX((WTSLUG(LOC )/(DENSL*DLENG*PI*D*D/4.))+0.9999)
      LSLUG=LOC-LSLUG+1
      IF(LSLUG) 358,358,359
  358 LSLUG=1
  359 DO 356 J=LSLUG,LOC
      IF(JSL(J)-3) 356,357,357
  356 JSL(J)=2
  357 CONTINUE
      INCL=INCL+1
      GO TO 300
  360 LOC=1
      JSL(460)=JSL(460)+1
      CALL SCONC(THICK,RE,EFFVSC,VRATIO,INCL,LASTL,LOC,CONCEN,CZERO,
     1PI,D,DENSL,DLENG,WTSLUG,SSLUG,WTFILM,SFILM,JSL,DENSG,FLUXJ,VRISE,
     1VISCL,C)
      WTSLUG( 1 )=WTSLUG( 1 )-WTFILM( 2 )
      SSLUG(1)=SSLUG(1)-SFILM(2)
      CONCEN(1)=SSLUG(1)/WTSLUG(1)
      IF(IPRINT-1) 370,371,371
  371 WRITE(M,367) INCT
      WRITE( M,366)CONCEN(1)
  366 FORMAT(' CONCENTRATION OF SLUG AT EXIT = ',E12.4)
  367 FORMAT(/,' SLUG LEFT TUBE AT TIME INCREMENT = ',I5)
      WRITE( M,368)WTSLUG( 1 ),SSLUG( 1 )
  368 FORMAT(' SLUG WEIGHT AT EXIT = ',E12.4,2X,'SLUG SOLIDS AT EXIT = '
     1E12.4)
      EXITW=WTSLUG( 1 )/(DTIME*ISLUG)
      EXITS=SSLUG(1)/(DTIME*ISLUG)
      EVAP=HTFLUX*PI*D*DLENG*(LASTL-LASTHT)/HTEVAP
      BALN=EXITW+EVAP
      WRITE(6,369) EXITW,EXITS,EVAP,BALN
  369 FORMAT(' EXIT LIQUOR RATE = ',E12.4,' EXIT SOLIDS RATE = ',E12.4,
     1' STEAM RATE = ',E12.4,/,' TOTAL EXIT RATE = ',E12.4,' LBS/HR')
  370 DO 365 J=1,INCL
  365 JSL(J)=1
      INCL=INCL+1
      WTSLUG(1)=0.
      SSLUG(1)=0.
      WTFILM(1)=WTFILM(2)
      SFILM(1)=SFILM(2)
      GO TO 300
  320 RETURN
      END
```

Subroutine START

```
      SUBROUTINE START(JSL,THICK,RE,H,HAV,LASTL,WTSLUG,SSLUG,CAV,CONCEN,
     1CINIT,WTFILM,SFILM,PI,D,DENSL,DLENG)
      DIMENSION JSL(1),THICK(1),RE(1),H(1),HAV(1),WTSLUG(1),SSLUG(1),
     1CAV(1),CONCEN(1),WTFILM(1),SFILM(1)
      DO 50 J=1,10
      H(J)=0.
      HAV(J)=0.
      CAV(J)=0.
   50 CONTINUE
      L=LASTL+1
      DO 51 J=1,L
      THICK(J)=0.005
      WTSLUG(J)=0.
      SSLUG(J)=0.
      WTFILM(J)=DENSL*DLENG*((PI*D*THICK(J))-(PI*(THICK(J)**2)))
      SFILM(J)=WTFILM(J)*CINIT
      CONCEN(J)=CINIT
   51 JSL(J)=1
      RETURN
      END
```

APPENDIX II

CALCULATION OF THE TEMPERATURE DROP THROUGH THE WALL

From Carslaw and Jaeger (99), we know that the general relation for the conduction of heat in an isotropic, homogeneous medium is:

$$\nabla^2 T - \frac{1}{\alpha}\frac{\partial T}{\partial t} = -\frac{A\,(x,y,z,t)}{k} \tag{186}$$

where

T = temperature

t = time

$\alpha = k/\rho\, cp$

k = thermal conductivity

A (x,y,z,t) = heat production per volume of material.

In cylindrical coordinates, this equation becomes:

$$\frac{1}{r}\frac{\partial}{\partial r}\left(r\frac{\partial T}{\partial r}\right) + \frac{1}{r^2}\frac{\partial^2 T}{\partial \theta^2} + \frac{\partial^2 T}{\partial Z^2} - \frac{1}{\alpha}\frac{\partial T}{\partial t} = \frac{A\,(x,y,z,t)}{k} \tag{187}$$

Assume that

$$\left(\frac{\partial^2 T}{\partial \theta^2}\right) = 0$$

$$\left(\frac{\partial^2 T}{\partial Z^2}\right) = 0$$

$$\left(\frac{\partial T}{\partial t}\right) = 0$$

$$A\,(x,y,z,t) = \text{constant} = A_o$$

These last two assumptions are not strictly true for alternating current heating but will be justified below.

Having made these assumptions, the equation reduces to:

$$\frac{1}{r}\frac{\partial}{\partial r}\left(r\frac{\partial T}{\partial r}\right) + \frac{A_o}{k} = 0 \tag{188}$$

which has the general solution

$$T = A + B \ln r - (A_o r^2/4k) \tag{189}$$

Consider the case of a tube of inner radius a and outer radius b. The temperature difference between a and b becomes:

$$T_a - T_b = A - A + B \ln a - B \ln b - (A_o a^2/4k) + (A_o b^2/4k) \tag{190}$$

$$T_a - T_b = B \ln \frac{a}{b} - \frac{(a^2 - b^2)A_o}{4k} \tag{191}$$

The coefficient B can be determined from the boundary condition that there is no heat loss from the outside wall of the pipe (at radius = b)

$$\left.\frac{\partial T}{\partial r}\right|_{r=b} = 0 = \frac{\partial}{\partial r}\left(A + b \ln r - A_o r^2/4k\right)\Big|_{r=b} \tag{192}$$

$$0 = \frac{B}{b} - \frac{A_o b}{2k} \tag{193}$$

Therefore, B is given by

$$B = \frac{A_o b^2}{2k} \tag{194}$$

and the final result is

$$T_a - T_b = \frac{A_o b^2}{2k} \ln \frac{a}{b} - (a^2 - b^2)\frac{A_o}{4k} \tag{195}$$

This can be put into a more useful form by using the definition of the heat production per volume of material,

$$A_o = q \frac{2\pi \ a^2 \ L}{\pi \ (b^2 - a^2) \ L} = \frac{2 \ a \ q}{b^2 - a^2} \tag{196}$$

Making this substitution, we find that

$$T_b - T_a = \frac{a \ q}{k \ (b^2 - a^2)} \left[\frac{a^2 - b^2}{2} + b^2 \ \ln \frac{b}{a} \right] \tag{197}$$

where q is the heat flux.

For the apparatus used in this work, the inside diameter, a, equals 1.87 inches, and the outside diameter, b, equals two inches. These values give the result that:

$$T_a - T_b = 0.002676 \ q/k \tag{198}$$

Therefore, the predicted temperature drops through the wall for the three heat fluxes used are as follows, using a value of 9.4 Btu/hr ft^2°F for k given by Peckner and Bernstein (92):

Heat Flux	Temperature Drop
22,000 Btu/hr ft^2	6.3°F
16,500 Btu/hr ft^2	4.7°F
11,500 Btu/hr ft^2	3.3°F

With A.C. heating, there will be a fluctuation in the heat flux with time that follows the voltage fluctuation. The oscillation in the wall temperature resulting from this heat flux variation could be serious under certain conditions. Jeglic (100) set up and solved this rather complicated problem. Using his graphs,

the magnitude of the temperature fluctuation expected for the 22000 Btu/hr ft^2 heat flux case is calculated to be only 0.05°F peak-to-valley. This is insignificant, and justifies the use of the steady heat flux assumption in the above derivation.

APPENDIX III

ANALOG-DIGITAL CONVERSION PROGRAM FOR FIBER OPTICS SIGNALS

```
LIST

  5  REM  VOID FRACTION ANALYZER
 10  REM  HUGH P. LAVERY SEPT 1979
 20  REM  DATA LOGGER FOLLOWS, W A YOUNG WROTE IT
 50  DIM N[2],A[3],R[3],G[3,20],H[3,20]
 51  DIM S[3]
 52  CALL 1,97,15+4096  A1-2,A3-4 DISPLAY
 54  CALL 5             REFRESH
 56  CALL 4,4           CLEAR
 65  CALL 1,97,3+1024+2048+4096  A1-2,B-34 DISPLAY
 67  CALL 5             REFRESH
 70  CALL 4,4           CLEAR
 75  CALL 1,98,32768    PUSH "NEGATE" BUTTON
 80  IF  LCN (99)&(256+512+1024)=256 GOTO 90 IS PERIPHERAL SET TO "MAG"?
 85  PRINT "SET PERIPHERAL TO MAG"
 90  PRINT "ARITHMETIC MODE: ADD  SET PRESET WEEPS  PREPARE TAPE"
100  INPUT N[ 0]
105  PRINT
106  PRINT "NUMBER OF SAMPLES TO BE PROCESSED";
107  INPUT J4
108  PRINT
109  FOR J3=1 to J4
110    FOR J=1 to N[ 0]
111      CALL 9, 0,2,49, 0          ┐
112      CALL 1,96,15& LCN (97)     │ THESE PUSH "ACQUIRE DATA" BUTTON
113      CALL 5                     ┘
115      FOR I= 0 TO 2047
120        IF  DTA (I)<> 0 GOTO  145
130        FOR K=1 TO 4  ┐
135          CALL 5      │ DELAY
140        NEXT K        ┘
145        CALL 1, LCN (115)+I, DTA (I)  COPY MEMORY CHANNEL I
150        CALL 3,I, 0                   ZERO MEMORY CHANNEL I
155      NEXT I
160      CALL 4,7     OUTPUT TO MAGNETIC TAPE
165      CALL 5       ┐
170      PRINT "X":   │ DELAY
175    NEXT J
200    IF N[ 0]<> 0 GOTO  215
205    PRINT "NUMBER OF MEMORY HALVES AVAILABLE"
210    INPUT N[ 0]
215    PRINT
216  NEXT J3
230  CALL 1,229,0  TURN OFF ORANGE AND SELECT OPTION BUTTONS
235  CALL 5        TURN OFF BLUE BUTTONS
240  CALL 1,98, 0
250  CALL 1,97,15+4096  A1-4 DISPLAY
255  CALL 5             REFRESH
260  CALL 4,4           CLEAR
```

APPENDIX IV

COMPUTER PROGRAM FOR FIBER-OPTICS SIGNAL PROCESSING

```
265  REM  END OF DATA LOGGER. START PROGRAM
270  PRINT
280  PRINT "SAMPLE ID";
300  INPUT I2
320  PRINT
340  PRINT "NUMBER OF MEMORY HALVES TO BE SCANNED";
360  INPUT N
380  PRINT
400  PRINT "VERTICL BUG READING FOR THRESHOLD";
420  INPUT T
421  PRINT
422  PRINT "NUMBER OF SAMPLES TO BE PROCESSED";
423  INPUT J2
424  PRINT
425  FOR J1=1 TO J2
430    LET M=1
445    LET M2=5
450    LET D=5
454    PRINT
455    DIM G[3,20],H[3,20]
460    FOR J=1 TO 2
470      LET A[J]= 0
475      LET S[J]= 0
480      LET R[J]= 0
485      FOR K=1 TO 15   INITIALIZE VARIABLES
490        LET H[J,K]= 0
495        LET G[J,K[= 0
500      NEXT K
510    NEXT J
520    GOSUB  2999  READ IN FIRST MEMORY HALF FROM MAGNETIC TAPE STORAGE
560    LET TO=1
580    LET X= DTA (IO)  READ FIRST CHANNEL OF FIRST MEMORY HALF
600    IF X>T GOTO 700  IS IT ABOVE THE THRESHOLD?
620    LET I=2          IF NOT, CONTENTS ARE LIQUID
640    GOTO  800
700    LET I=1          IF SO, CONTENTS ARE VAPOR
720    GOTO  800
800    LET R[I]=R[I]+1
820    LET IO=IO+1      NEXT MEMORY CHANNEL
840    IF IO<=2047 GOTO  900   IS CHANNEL NUMBER WITHIN THE MEMORY BOUNDS?
860    LET M=M+1               IF NOT, CONSIDER NEXT MEMORY HALF
862    LET A[I]=A[I]+R[I]
864    GOSUB  3999
866    LET R[1]=0
868    LET R[2]=0
880    IF M>N GOTO  5515       HAVE WE READ THE LAST MEMORY HALF FOR THIS SAMPLE?
885    GOTO  520               IF NOT, LOOP BACK AND READ NEXT MEMORY HALF
900    LET X+ DTA (IO)         READ FIRST CHANNEL OF NEXT MEMORY HALF
```

```
 920    IF X>T GOTO  1100        IS IT ABOVE THE THRESHOLD?
 940    IF I=2 GOTO  800         WAS THE PREVIOUS CHANNEL "LIQUID"?
 960    LET A[1]=A[1]+RC[1]      IF NOT, CONCLUDE THE ACCUMULATION PROCESS IN "VAPOR"
                                 VARIABLES
 980    GOSUB  3999         SORTING SUBROUTINE
1000    LET R[2]= 0           RESET PULSE LENGTH ACCUMULATOR
1020    LET I=2               CURRENT CONTENTS ARE "LIQUID" (SEE 940)
1040    LET R[1]= 0           RESET PULSE LENGTH ACCUMULATOR
1060    GOTO  800             ADD 1 TO LIQUID PULSE LENGTH ACCUMULATOR, CONTINUE
1100    IF I=1 GOTO  800      CURRENTLY "VAPOR"; WAS PREVIOUS CHANNEL "VAPOR"/
1120    LET A[2]=A[2]+R[2]    IF NOT, CONCLUDE THE ACCUMULATION PROCESS IN THE
1140    GOSUB  3999           "LIQUID" VARIABLES
1160    LET R[1]= 0
1180    LET R[2]= 0      RESET PULSE LENGTH ACCUMULATORS
1200    LET I=1       CURRENT CONTENTS "VAPOR"
1220    GOTO  800     ADD 1 TO VAPOR PULSE LENGTH ACCUMULATOR & CONTINUE....
2999    REM  INPUT ROUTINE  SUBROUTINE TO GET DATA FROM TAPE INTO MEMORY
3000    CALL 1,97,3+256+512+4096  A1-2,B1-2,DISPLAY
3020    CALL 5                    REFRESH
3040    CALL 4,6                  PUSH "IN" BUTTON
3060    RETURN
3999    REM  SORTING ROUTINE
4000    IF R[I]<M2 GOTO  5000
4010    IF R[I]<(M2+D)  GOTO  5050     THIS SUBROUTINE SORTS THE PULSE LENGTH
4020    IF R[I]<(M2+2*D)  GOTO  5100   ACCUMULATOR, R(I) OUT ACCORDING TO LENGTH
4030    IF R[I]<(M2+3*D)  GOTO  5150
4040    IF R[I]<(M2+4*D)  GOTO  5200
4050    IF R[I]<(M2+5*D)  GOTO  5250
4060    IF R[I]<(M2+6*D)  GOTO  5300
4070    IF R[I]<(M2+7*D)  GOTO  5350
4080    IF R[I]<(M2+8*D)  GOTO  5400
4090    IF R[I]<(M2+9*D)  GOTO  5450
4095    GOTO  5500
5000    LET H[I,1]=H[I,1]+1     H(I,J) ACCUMULATES PULSE COUNTS
5005    LET G[I,1]=G[I,1]+R[I]  G(I,J) ACCUMULATES PULSE DURATION
5010    GOTO  6000
5050    LET H[I,2]=H[I,2]+1
5055    LET G[I,2]=G[I,2]+R[I]
5060    GOTO  6000
5100    LET H[I,3]=H[I,3]+1
5105    LET G[I,3]=G[I,3]+R[I]
5110    GOTO  6000
5150    LET H[I,4]=H[I,4]+1
5155    LET G[I,4]=G[I,4]+R[I]
5160    GOTO  6000
5200    LET H[I,5]=H[I,5]+1
5205    LET G[I,5]=G[I,5]+R[I]
5210    GOTO  6000
5250    LET H[I,6]=H[I,6]+1
```

```
5255    LET G[I,6]-G[I,6]+R[I]
5260    GOTO  6000
5300    LET H[I,7]=H[I,7]+1
5305    LET G[I,7]=G[I,7]+R[I]
5310    GOTO  6000
5350    LET H[I,8]=H[I,8]+1
5355    LET G[I,8]=G[I,8]+R[I]
5360    GOTO  6000
5400    LET H[I,9]=H[I,9]+1
5405    LET G[I,9]=G[I,9]+R[I]
5410    GOTO  6000
5450    LET H[I,10]=H[I,10]+1
5455    LET G[I,10]=G[I,10]+R[I]
5460    GOTO  6000
5500    LET H[I,11]=H[I,11]+1
5505    LET G[I,11]=G[I,11]+R[I]
5510    GOTO  6000
5515  REM  NORMALIZE TO PCT. TOTAL COUNTS
5518  LET X= 0
5520  LET Y= 0
5530  LET Z= 0
5540  FOR K=1 TO 11
5545    LET X=G[1,K]+G[2,K]+X      TOTAL TIME
5550    LET Y=H[1,K]+Y             TOTAL VAPOR COUNTS (NUMBER OF PULSES)
5560    LET Z=Z+H[2,K]             TOTAL LIQUID COUNTS
5570  NEXT K
5580  FOR K=1 TO 11
5582    LET G[1,K]= INT (((G[1,K]/X)*100)+.5)
5584    LET G[2,K]= INT (((G[2,K]/X)*100)+.5)
5590    LET H[1,K]= INT (((H[1,K]/Y)*100)+.5)
5600    LET H[2,K]= INT (((H[2,K]/Z)*100)+.5)
5610  NEXT K
5620  GOTO  7000
6000  LET S[I]=S[I]+(R[I]*R[I])     ACCUMULATES SUM OF (PULSE LENGTH)2
6010  RETURN
7000  REM  EXIT STATEMENTS
7002  LET S1= SQR (((4*S[1])-((A[1]*A[1]*4)/Y))/(Y-1)) CALCULATE STD. DEVIATIONS
7004  LET S2= SQR (((4*S[2])-((A[2]*A[2]*4)/Z))/(Z-1)) (FACTOR OF 4 IS NEEDED TO
7010  PRINT                                            CONVERT TIME TO MILLISCECONDS
7020  PRINT
7030  PRINT "TOTAL VOID COUNTS";A[1]
7040  PRINT "TOTAL LIQ. COUNTS";A[2]
7041  PRINT
7050  PRINT "VOID FRACTION";(A[1]/(A[1]+A[2])
7051  PRINT
7052  PRINT "VOID AVG. DURATION, MS/PULSE";2*(A[1]/Y)
7053  PRINT "VOID STD. DEV.";S+
7054  PRINT "LIQUID AVG. DURATION, MS/PULSE";2*(A[2]/Z)
7055  PRINT "LIQUID STD. DEV.";S2
7060  PRINT
7070  PRINT "HISTOGRAM OF VAPOR DURATION"
7075  PRINT "TOP LINE:  MILLISECONDS  BOTTOM LINE:  PERCENT OF COUNT"
7080  PRINT "     10  20  30  40  50  60  70  80  90  100 >100"
7090  FOR I=1 TO 11
7100    PRINT  TAB (4*I);H[1,I];
```

FINAL PRINTOUT

```
7101  NEXT I
7102  PRINT
7103  PRINT "TOTAL VAPOR PULSE COUNT";Y
7150  PRINT
7155  PRINT
7160  PRINT "HISTOGRAM OF LIQUID DURATION"
7165  PRINT "TOP LINE:  MILLISECONDS  BOTTOM LINE:  PERCENT OF COUNT"
7170  PRINT "     10  20  30  40  50  60  70  80  90  100  >100"
7180  FOR I=1 TO 11
7190    PRINT  TAB (4*I);H[2,I];
7200  NEXT I
7201  PRINT
7202  PRINT "TOTAL LIQUID PULSE COUNT";Z
7300  PRINT
7400  PRINT
7410  PRINT "LIQUID AND VAPOR PULSE DURATION AS PCT. OF TOTAL TIME"
7420  PRINT "TOP LINE:  MILLISECONDS  BOTTOM LINES:  PCT. OF TOTAL TIME
7430  PRINT "     10  20  30  40  50  60  70  80  90  100 >100"
7440  PRINT "VAPOR"
7460  FOR I=1 TO 11
7470    PRINT  TAB (4*I);G[1,I];
7480  NEXT I
7490  PRINT
7500  PRINT "LIQUID"
7510  FOR I=1 TO 11
7520    PRINT  TAB (4*I);G[2,I];
7530  NEXT I
7540  PRINT
7550  PRINT
7560  PRINT "TOTAL TIME";X
7570  PRINT
7580  PRINT
7585  NEXT J1
*
```

FINAL PRINTOUT CONTINUED

APPENDIX V

FIBER OPTICS SIGNAL PROCESSING PROGRAM CALIBRATION-SAMPLE OUTPUT

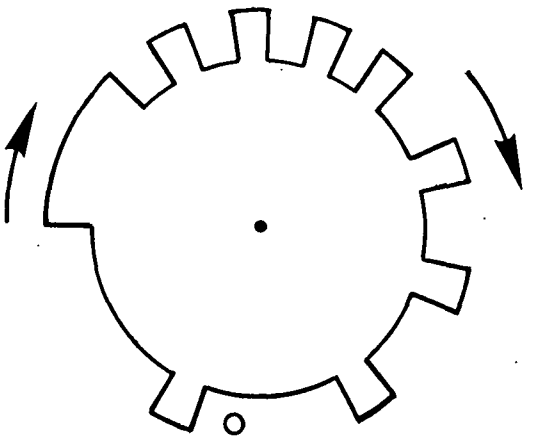

"DISK 3"

TOTAL VOID COUNTS 18801
TOTAL LIQ. COUNTS 11904

	PREDICTED RESULTS
VOID FRACTION .612311	0.62
VOID AVG. DURATION, MS/PULSE 46.4222	44.4
VOID STD. DEV. 30.6294	28.1
LIQUID AVG. DURATION, MS/PULSE 29.5385	27.2
LIQUID STD. DEV. 19.43	19.6

HISTOGRAM OF VAPOR DURATION

TOP LINE: MILLISECONDS BOTTOM LINE: PERCENT OF COUNT

10	20[a]	30	40	50	60	70	80	90	100	>100
1	2	42	0	22	0	11	0	11	0	10

TOTAL VAPOR PULSE COUNT 810

HISTOGRAM OF LIQUID DURATION

TOP LINE: MILLISECONDS BOTTOM LINE: PERCENT OF COUNT

10	20	30	40	50	60	70	80	90	100	>100
0	0	89	0	0	0	0	0	11	0	0

TOTAL LIQUID PULSE COUNT 806

	ms.	%
	20	44
	40	22
	60	11
	80	11
	100	11
	20	88
	80	12

LIQUID AND VAPOR PULSE DURATION AS PCT. OF TOTAL TIME

TOP LINE: MILLISECONDS BOTTOM LINES: PCT. OF TOTAL TIME

	10	20	30	40	50	60	70	80	90	100	>100
VAPOR	0	0	11	0	12	0	9	0	12	0	15
LIQUID	0	0	27	0	0	0	0	0	12	0	0

TOTAL TIME 30705 x 2=61410 seconds

RESULTS OF RUN USING "DISK 3", 93.75 RPM. THE SLIGHT DISCREPANCIES BETWEEN MEASURED AND PREDICTED RESULTS ARE PROBABLY DUE TO VARIATIONS IN THE RPM OF THE DISK.

[a]"20" means the interval 10 to 19, etc.

APPENDIX VI

TABULATED DATA

Heat transfer data. Series B

Material: Distilled water

Heat Flux	11,500			16,500			22,000 Btu/hr ft^2			
Flow Rate	1/2	1	2	1/2	1	2	1/2	1	2	gpm
TC No.										
10	--[a]	--[a]	--[a]	--[a]	--[a]	--[a]	--[a]	--[a]	--[a]	
9	1670	1670	1720	1570	1570	1630	1520	1520	1580	
8	1580	1580	1619	1540	1540	1540	1520	1550	1560	
7	1620	1670	1720	1630	1570	1630	1580	1630	1610	
6	1530	1530	1620	1460	1490	1540	1480	1480	1460	
5	1580	1670	1670	1490	1510	1570	1480	1480	1500	
4	1720	1720	1720	1570	1600	1670	1580	1580	1580	
3	--[a]	--[a]	--[a]	--[a]	--[a]	--[a]	--[a]	--[a]	--[a]	
2	1770	1770	1830	1570	1600	1700	1560	1540	1540	
1	1320	1210	1140	1200	1190	1170	1630	1140	1150	

[a]Thermocouples 10 and 3 were not reading during this series.

Heat transfer data. Series B replicates

Material: Water

Heat Flux	11,500			16,500			22,000 Btu/hr ft^2			
Flow Rate	1/2	1	2	1/2	1	2	1/2	1	2	gpm
TC No.										
10	1670	1670		1570	1570		1520			
9	1670	1670		1600	1600		1520			
8	1620	1670		1540	1600		1520			
7	1620	1670		1500	1600		1520			
6	1530	1620		1540	1510		1480			
5	1620	1670		1600	1570		1500			
4	1720	1720		1630	1600		1560			
3	--[a]	--[a]		--[a]	--[a]		--[a]			
2	1950	1670		1700	1630		1560			
1	1290	1210		1220	1260		1240			

[a]Thermocouple 3 was not reading during this series.

Replicate done before series:

E H 0 G 0

The two runs done before series 0 were <u>not</u> deaerated and were Appleton city water straight from the tap.

Heat transfer data. Series B replicates

Material: Water

Heat Flux	11,500			16,500			22,000 Btu/hr ft^2			
Flow Rate	1/2	1	2	1/2	1	2	1/2	1	2	gpm
TC No.										
10	1620			1460			1500			
9	1620			1460			1500			
8	1620			1460			1480			
7	1670			1460			1440			
6	1670			1460			1420			
5	1720			1490			1440			
4	1770			1540			1560			
3	--[a]			--[a]			--[a]			
2	1770			1570			1500			
1	1210			1150			1090			

[a]Thermocouple 3 was not reading during this series.

Replicate done before series:

Q	Q	Q

Heat transfer data. Series C

Material: 12.5% potassium carbonate solution

Heat Flux	11,500			16,500			22,000 Btu/hr ft^2		
Flow Rate	1/2	1	2	1/2	1	2	1/2	1	2 gpm
TC No.									
10	1090		1890				1610		2320
9	1830		1950				1420		1760
8	1620		1830				1440		1710
7	1720		1950				1440		1760
6	1620		1830				1420		1610
5	1670		1950				1460		1630
4	1670		2090				1610		1760
3	--[a]		--[a]				--[a]		--[a]
2	1830		2020				1520		1790
1	1240		1770				1190		1500

[a]Thermocouple 3 was not reading during this series.

Heat transfer data. Series D

Material: 35% potassium carbonate solution

Heat Flux	11,500			16,500			22,000 Btu/hr ft^2		
Flow Rate	1/2	1	2	1/2	1	2	1/2	1	2 gpm
TC No.									
10	1350	1350	1460				1050	1200	1260
9	1290	1320	1420				944	1200	1200
8	1350	1210	1290				920	1180	1230
7	1420	1320	1390				920	1200	1260
6	1240	1240	1290				900	1150	1190
5	1320	1260	1350				900	1140	1240
4	1350	1390	1420				920	1200	1290
3	--[a]	--[a]	--[a]				--[a]	--[a]	--[a]
2	1390	1460	1670				990	1220	1300
1	950	950	600				800	790	1050

[a]Thermocouple 3 was not reading during this series.

Heat transfer data. Series E

Material: 100 ppm Igepal 610 (surfactant) in water.

Heat Flux	11,500			16,500			22,000 Btu/hr ft^2			
Flow Rate	1/2	1	2	1/2	1	2	1/2	1	2	gpm
TC No.										
10	2090	2950	3480	1813	2260	2620	1680	2060	2420	
9	1950	2950	3290	1813	2260	2700	1680	2060	2320	
8	1830	2800	3290	1900	2390	2700	1630	2060	2270	
7	1830	3110	3710	1900	2320	3000	1680	2060	2470	
6	2020	2950	3480	2090	2390	2890	1650	2220	2320	
5	2250	3710	3970	2390	2620	3510	1680	2420	2370	
4	2950	3710	4260	2620	3000	3660	1700	2780	2590	
3	--[a]	--[a]	--[a]	--[a]	--[a]	--[a]	--[a]	--[a]	--[a]	
2	2800	3710	3290	2800	3100	3370	1700	2590	2590	
1	1620	1950	2020	1850	1990	1810	1480	1820	1540	

[a]Thermocouple 3 was not reading during this series.

Heat transfer data. Series F

Material: 100 ppm Deriphat 160 (surfactant) in water

Heat Flux	11,500			16,500			22,000 Btu/hr ft^2		
Flow Rate	1/2	1	2	1/2	1	2	1/2	1	2 gpm
TC No.									
10	4600	8850	8850	3110	5000	6600	2780	3190	4310
9	4260	8850	10450	3110	4460	6600	2780	3190	4490
8	3970	6050	6760	3240	4230	6110	2780	3490	4680
7	3970	6760	8850	3370	4460	6600	2860	3610	4890
6	4600	6760	6760	3676	4714	6110	3010	4000	4890
5	6770	8850	8850	4460	6110	6600	3280	4680	4890
4	6770	8850	7670	5320	6600	7170	4490	5370	5640
3	--[a]	--[a]	--[a]	--[a]	--[a]	--[a]	--[a]	--[a]	--[a]
2	7670	10450	8850	5690	6600	6600	4680	5120	5950
1	3480	3480	3480	3000	3240	3240	2720	3010	3010

[a]Thermocouple 3 was not reading during this series.

Heat transfer data. Series G

Material: 1.25% cornstarch in water (viscosity = 1.96 lb/hr ft)

Heat Flux	11,500			16,500			22,000 Btu/hr ft^2			
Flow Rate	1/2	1	2	1/2	1	2	1/2	1	2	gpm
TC No.										
10	1670	1950	2250	1390	1600	1810	1290	1460	1680	
9	1670	1950	2350	1410	1630	1810	1300	1480	1680	
8	1670	2020	2350	1460	1670	1900	1320	1460	1650	
7	1720	2020	2350	1510	1670	1990	1370	1500	1710	
6	1890	2090	2500	1570	1700	1990	1400	1610	1790	
5	2170	2170	2350	1740	1900	2090	1540	1650	1790	
4	2250	2250	2670	1940	1990	2200	1650	1820	1850	
3	--[a]	--[a]	--[a]	--[a]	--[a]	--[a]	--[a]	--[a]	--[a]	
2	1950	11770	1490	1540	1670	1540	1610	1650	1710	
1	1260	1350	1490	1280	1090	1200	1180	1140	1030	

[a]Thermocouple 3 was not reading during this series.

Heat transfer data. Series H

Material: 0.15% NaCMC (viscosity = 2.24 lb/hr ft)

Heat Flux	11,500			16,500			22,000 Btu/hr ft^2		
Flow Rate	1/2	1	2	1/2	1	2	1/2	1	2 gpm
TC No.									
10	1190	1160	--[a]	--[a]	1040	1190	860	980	1150
9	1190	1160	1260	950	1040	1190	860	980	1160
8	1190	1160	1260	950	1050	1190	860	980	1150
7	1210	1160	1260	980	1050	1190	870	980	1160
6	1240	1190	1240	1000	1060	1170	890	970	1160
5	1260	1240	1260	1060	1110	1220	890	970	1150
4	1320	1320	1320	1150	1200	1280	970	1070	1220
3	--[a]	--[a]	--[a]	--[a]	--[a]	--[a]	--[a]	--[a]	--[a]
2	1260	1260	1290	1190	1150	1140	1090	1140	1200
1	880	950	950	870	860	900	910	920	940

[a]Thermocouples 10 and 3 were not reading during this series.

Heat transfer data. Series I

Material: 0.19% NaCMC (viscosity = 2.78 lb/hr ft)

Heat Flux	11,500			16,500			22,000 Btu/hr ft^2			
Flow Rate	1/2	1	2	1/2	1	2	1/2	1	2	gpm
TC No.										
10	1040	1040	1120	830	920	1040	790	860	990	
9	1040	1040	1140	830	920	1040	790	860	990	
8	1020	1060	1100	830	930	1040	780	860	980	
7	1020	1060	1100	850	930	1040	780	860	970	
6	1020	1060	1070	850	930	1040	790	860	960	
5	1120	1100	1140	890	960	1090	790	870	990	
4	1190	1160	1140	980	1040	1150	840	880	1050	
3	--[a]	--[a]	--[a]	--[a]	--[a]	--[a]	--[a]	--[a]	--[a]	
2	1100	1100	1120	1050	1060	1080	940	1010	1060	
1	800	840	820	810	820	840	790	810	860	

[a]Thermocouple 3 was not reading during this series.

Heat transfer data. Series J

Material: 0.10% NaCMC (viscosity = 1.36 lb/hr ft)

Heat Flux	11,500			16,500			22,000 Btu/hr ft^2		
Flow Rate	1/2	1	2	1/2	1	2	1/2	1	2 gpm
TC No.									
10	1260		1390				920		1220
9	1260		1390				910		1220
8	1240		1320				910		1190
7	1240		1320				910		1190
6	1240		1320				910		1190
5	1290		1390				910		1180
4	1320		1420				990		1220
3	--[a]		--[a]				--[a]		--[a]
2	1320		1210				1050		1230
1	910		950				940		950

[a]Thermocouple 3 was not reading during this series.

Heat transfer data. Series K

Material: 0.06% NaCMC (viscosity = 1.15 lb/hr ft)

Heat Flux	11,500			16,500			22,000 Btu/hr ft^2			
Flow Rate	1/2	1	2	1/2	1	2	1/2	1	2	gpm
TC No.										
10	1390						1290			
9	1420						1290			
8	1460						1290			
7	1460						1270			
6	1420						1290			
5	1460						1290			
4	1530						1400			
3	--[a]						--[a]			
2	1460						1320			
1	1100						1030			

[a]Thermocouple 3 was not reading during this series.

Heat transfer data. Series L

Material: 25% solids black liquor

Heat Flux	11,500			16,500			22,000 Btu/hr ft^2			
Flow Rate	1/2	1.44	2.2	1/2	1.44	2.2	1/2	1.44	2.2	gpm
TC No.										
10	3480	6050	5480	2540	4460	4710	1910	3380	3730	
9	3290	6050	5480	2540	4230	4710	1910	3380	3730	
8	2950	5000	4260	2540	4230	4560	1980	3380	3610	
7	2800	5000	4260	2540	3840	4230	2020	3190	3490	
6	2670	4260	4260	2460	3510	4020	2020	3190	3380	
5	3290	5480	5000	2460	3670	4230	2140	3190	3380	
4	3290	5000	5000	2540	3840	4460	2320	3280	3730	
3	--[a]	--[a]	--[a]	--[a]	--[a]	--[a]	--[a]	--[a]	--[a]	
2	2800	4600	5000	2390	3510	3840	2140	3010	3280	
1	1950	2800	2260	1670	2320	2320	2140	2020	2060	

Flow Rate	1/2	1.7	2	1/2	1.7	2	1/2	1.7	2	gpm
TC No.										
10	5000						3190			
9	4260						3190			
8	3710						3190			
7	3710						3010			
6	3710						2860			
5	3970						2780			
4	3970						2990			
3	--[a]						--[a]			
2	3480						2530			
1	2120						1820			

[a]Thermocouple 3 was not reading during this series.

Heat transfer data. Series M

Material: 35% solids black liquor

Heat Flux	11,500			16,500			22,000 Btu/hr ft^2			
Flow Rate	1/2	1	2	1/2	1	2	1/2	1	2	gpm
TC No.										
10	1120	2090	2800	690	1430	2040	760	1140	1850	
9	1100	2090	2800	680	1430	2040	740	1140	1880	
8	1100	1950	2350	760	1460	2040	730	1200	1910	
7	1100	1950	2170	790	1460	2040	770	1240	1910	
6	1320	1950	2170	860	1460	2040	800	1260	1880	
5	1490	1950	2250	1040	1540	2040	890	1320	1910	
4	1620	2090	2350	1190	1670	2200	1090	1400	2020	
3	--[a]	--[a]	--[a]	--[a]	--[a]	--[a]	--[a]	--[a]	--[a]	
2	1580	2170	2350	1300	1630	2200	1090	1440	1910	
1	1140	1490	1580	1040	1270	1490	930	1150	1460	

[a]Thermocouple 3 was not reading during this series.

Heat transfer data. Series N

Material: 45% solids black liquor

Heat Flux	11,500			16,500			22,000 Btu/hr ft^2			
Flow Rate	1/2	1	2	1/2	1	2	1/2	1	2	gpm
TC No.										
10	550	1120	880	500	900	780	¢[a]	710	710	
9	540	1120	890	490	900	780		720	710	
8	550	1120	860	540	900	790		740	730	
7	750	1160	860	580	950	800		790	730	
6	800	1210	860	650	990	800		820	740	
5	860	1210	860	720	1060	850		860	760	
4	910	1210	840	820	1190	900		990	810	
3	--[b]	--[b]	--[b]	--[b]	--[b]	--[b]		--[b]	--[b]	
2	1070	1390	640	1040	1200	920		1000	780	
1	850	1020	470	780	940	650		870	610	

[a] ¢ = Heat transfer for this run was so poor that overheating caused the equipment to shut down.

[b] Thermocouple 3 was not reading during this series.

Heat transfer data. Series O

Material: 12% potassium carbonate in water

Heat Flux	11,500			16,500			22,000 Btu/hr ft^2			
Flow Rate	1/2	1	2	1/2	1	2	1/2	1	2	gpm
TC No.										
10	1950	2020	3110	1600	1940	1940	1460	1760	2650	
9	1950	2020	3110	1600	1940	1940	1460	1790	2650	
8	1770	1950	2450	1630	1940	2040	1440	1790	2470	
7	1770	1830	2560	1630	1990	2090	1450	1820	2590	
6	1720	1770	2670	1630	1990	2140	1520	1880	2590	
5	1720	1770	2950	1630	2040	2320	1540	1950	2650	
4	1770	1770	3110	1630	2140	2460	1630	2220	2860	
3	--[a]	--[a]	--[a]	--[a]	--[a]	--[a]	--[a]	--[a]	--[a]	
2	1770	1770	3110	1570	2140	2140	1560	2220	2420	
1	1160	1620	2020	1190	1460	1570	1220	1540	1580	

[a]Thermocouple 3 was not reading during this series.

Heat transfer data. Series P

Material: 12% potassium carbonate in water

Heat Flux	11,500			16,500			22,000 Btu/hr ft^2			
Flow Rate	1/2	1	2	1/2	1	2	1/2	1	2	gpm
TC No.										
10	7670	8850	12780	6110	5690	8680	4890	5370	4490	
9	9710	8850	12780	5320	6110	8680	4490	5370	4490	
8	5000	6760	7670	4230	5320	6600	4000	4680	4150	
7	4600	6050	6050	4020	4710	6110	3860	4680	3860	
6	4600	5480	5000	4020	4710	5690	3610	4313	3730	
5	5480	7670	5480	4230	5000	5690	3730	4490	3730	
4	5000	5480	4600	4230	5000	5320	3730	4313	3860	
3	--[a]	--[a]	--[a]	--[a]	--[a]	--[a]	--[a]	--[a]	--[a]	
2	3110	3480	4600	3240	3840	3240	3190	3190	2420	
1	2350	2670	2950	1900	2140	2540	1730	1710	1910	

[a]Thermocouple 3 was not reading during this series.

The next series, series Q, was rejected because of excessive degradation of the CMC over the course of the run. This sample of CMC was also rejected (Hercules type 7M).

Heat transfer data. Series R

Material: 0.25% Guar gum (viscosity = 3.35 lb/hr ft)

Heat Flux	11,500			16,500			22,000 Btu/hr ft^2		
Flow Rate	1/2	1	2	1/2	1	2	1/2	1	2 gpm
TC No.									
10	950	1040	1120	830	930	1040	1000	960	970
9	950	1040	1120	830	930	1040	1010	960	970
8	950	1040	1070	830	930	1040	1000	960	970
7	950	1040	1070	830	930	1020	1000	960	970
6	950	1020	1060	830	940	1010	860	950	970
5	970	1020	1070	840	980	1010	880	940	970
4	980	1070	1100	930	1000	1020	900	950	1040
3	--[a]	--[a]	--[a]	--[a]	--[a]	--[a]	--[a]	--[a]	--[a]
2	1020	1020	1040	930	1020	1020	910	960	990
1	760	790	760	750	820	560	740	770	810

[a]Thermocouple 3 was not reading during this series.

Heat transfer data. Series S

Material: 0.46% Guar gum (viscosity = 9.46 lb/hr ft)

Heat Flux	11,500			16,500			22,000 Btu/hr ft^2			
Flow Rate	1/2	1	2	1/2	1	2	1/2	1	2	gpm
TC No.										
10	610	690	710	800	730	750	1160	960	970	
9	610	690	710	800	730	750	1150	970	970	
8	610	690	700	800	750	730	1080	910	910	
7	610	690	700	750	720	720	1020	860	840	
6	610	680	680	670	700	710	940	840	780	
5	640	710	690	660	690	730	860	830	880	
4	670	710	710	660	700	730	880	840	830	
3	--[a]	--[a]	--[a]	--[a]	--[a]	--[a]	--[a]	--[a]	--[a]	
2	690	710	660	700	710	710	880	750	790	
1	560	560	620	600	610	600	760	630	720	

[a]Thermocouple 3 was not reading during this series.

Heat transfer data. Series T

Material: 100 ppm Deriphat 160C plus Guar gum, viscosity = 7.7 lb/hr ft

Heat Flux	11,500			16,500			22,000 Btu/hr ft^2		
Flow Rate	1/2	1	2	1/2	1	2	1/2	1	2 gpm
TC No.									
10	930		920				1400		1020
9	920		930				1400		1020
8	880		970				1400		1020
7	860		980				1300		1000
6	890		1020				1200		990
5	1020		1190				1140		1020
4	1260		1240				1070		1150
3	--[a]		--[a]				--[a]		--[a]
2	1830		1070				1070		1130
1	1240		1100				1040		860

[a]Thermocouple 3 was not reading during this series.

Heat transfer data. Series U

Material: 100 ppm Deriphat 160C plus Guar gum, viscosity = 3.62 lb/hr ft

Heat Flux	11,500			16,500			22,000 Btu/hr ft^2		
Flow Rate	1/2	1	2	1/2	1	2	1/2	1	2 gpm
TC No.									
10	1210		1420				1270		1240
9	1210		1420				1270		1260
8	1210		1490				1270		1230
7	1190		1670				1220		1300
6	1190		1950				1190		1370
5	1580		2250				1180		1500
4	1890		2560				1460		1910
3	--[a]		--[a]				--[a]		--[a]
2	2670		1580				1910		1980
1	1670		1460				1580		1480

[a]Thermocouple 3 was not reading during this series.

Heat transfer data. Series V

Material: 100 ppm Deriphat 160C plus Guar gum, viscosity = 1.81 lb/hr ft

Heat Flux	11,500			16,500			22,000 Btu/hr ft^2		
Flow Rate	1/2	1	2	1/2	1	2	1/2	1	2 gpm
TC No.									
10	1670		2350				1580		1630
9	1670		2350				1580		1650
8	1620		2560				1540		1730
7	1720		2670				1520		1910
6	1830		2670				1500		2020
5	2350		3290				1500		2270
4	2670		3290				1880		2720
3	--[a]		--[a]				--[a]		--[a]
2	3110		2170				2270		2780
1	2170		1770				1790		1520

[a]Thermocouple 3 was not reading during this series.

APPENDIX VII

FIBER-OPTICAL FLOW PATTERN DATA FOR WATER

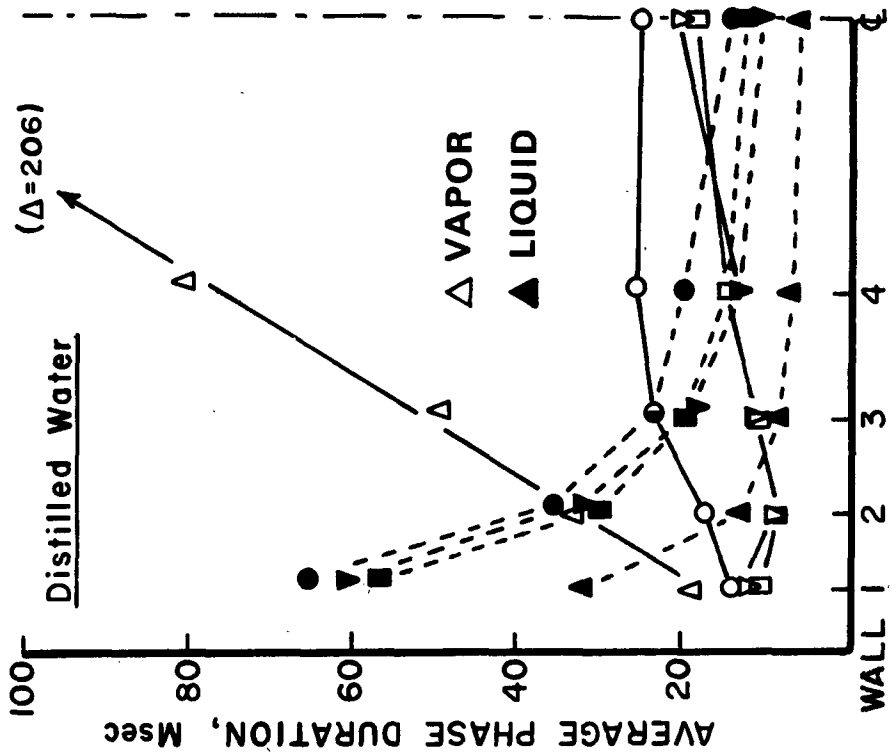

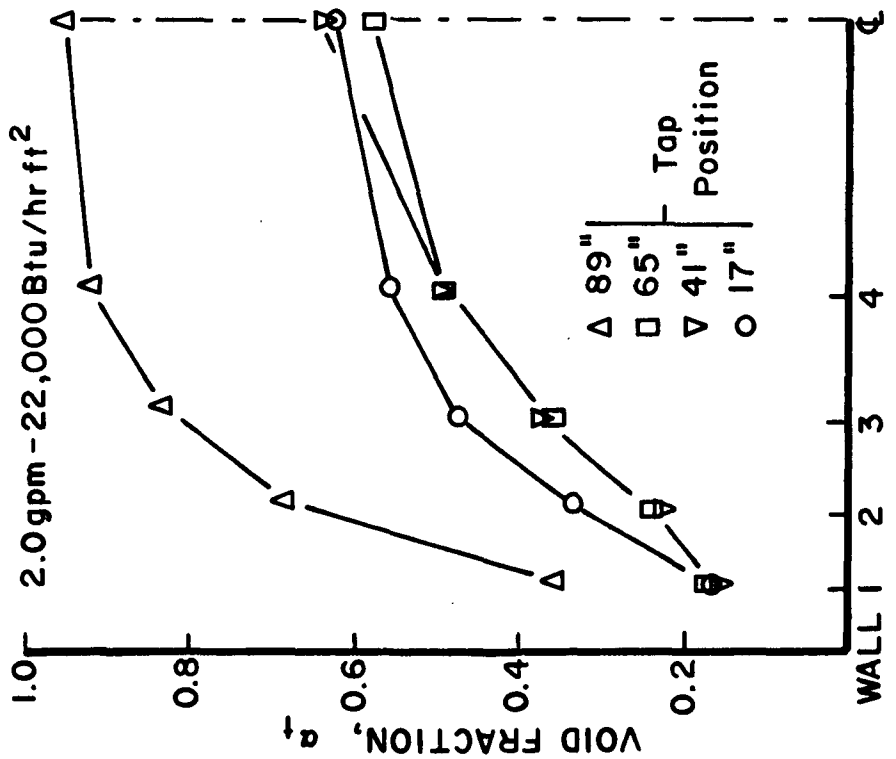

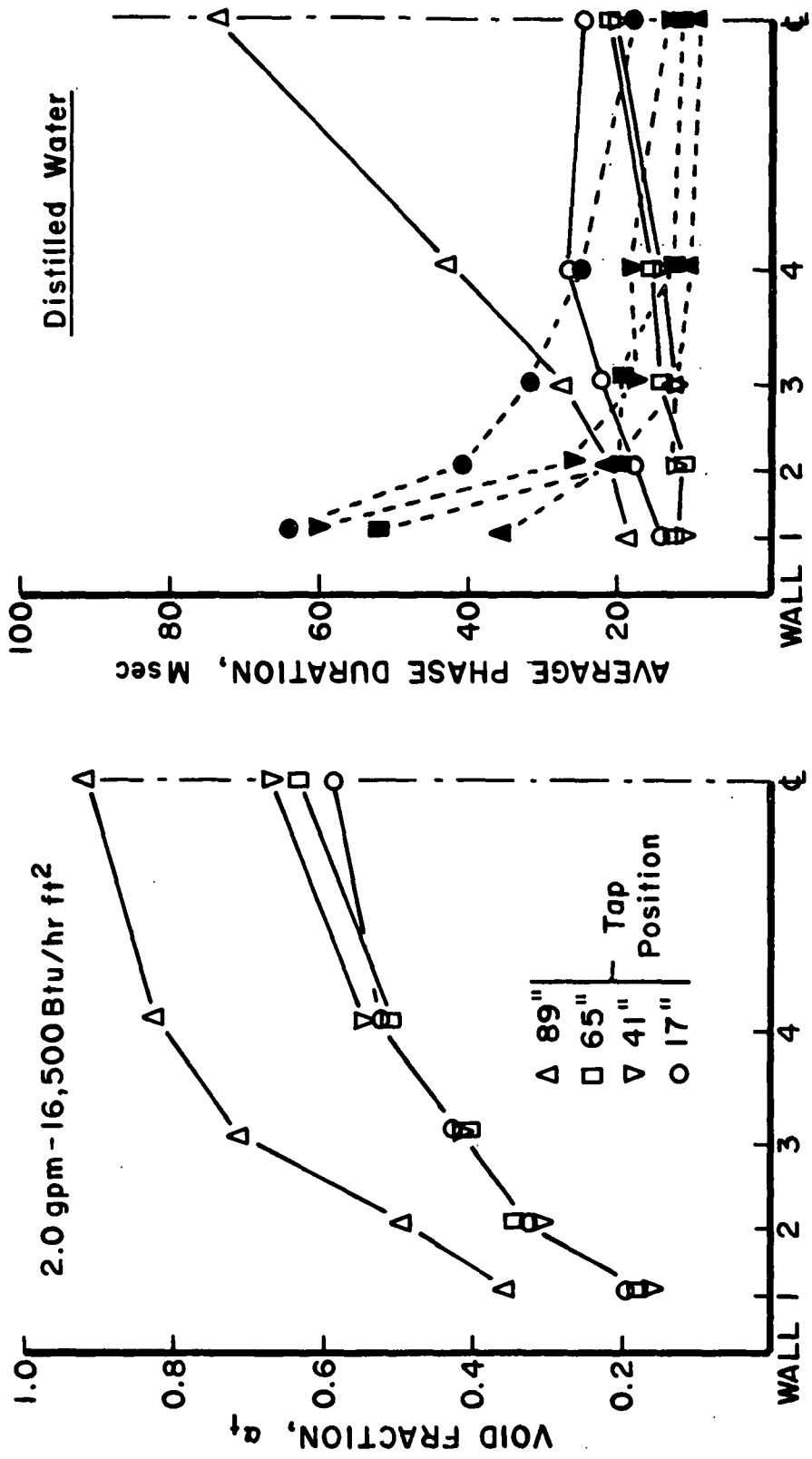
Distilled Water
AVERAGE PHASE DURATION, Msec
100
80
60
40
20
WALL 1
2
3
4
℄
2.0 gpm - 16,500 Btu/hr ft²
VOID FRACTION, α_t
1.0
0.8
0.6
0.4
0.2
Tap Position
Δ 89"
□ 65"
▽ 41"
○ 17"

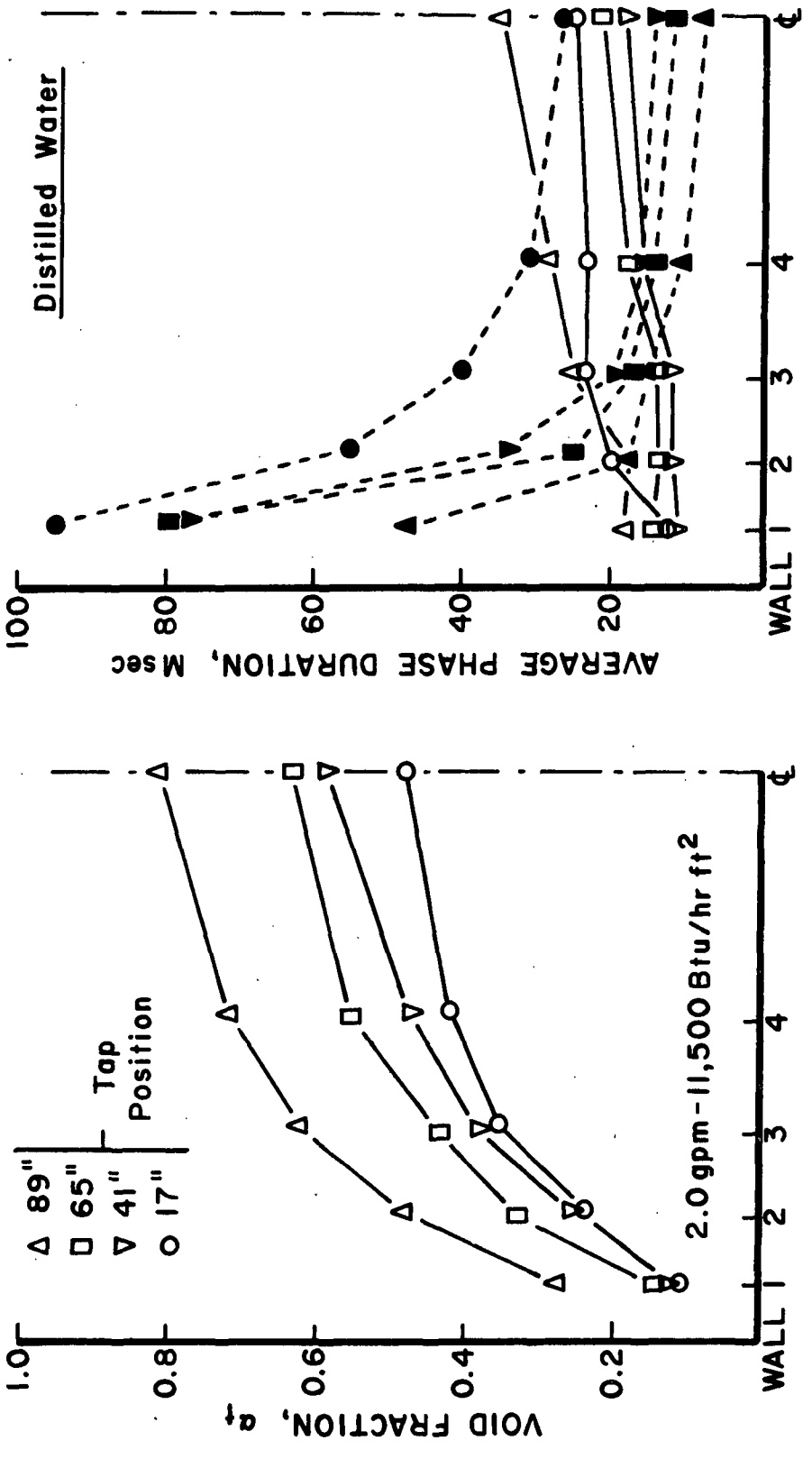
Distilled Water
AVERAGE PHASE DURATION, Msec
100
80
60
40
20
WALL
1
2
3
4
℄
VOID FRACTION, α_t
1.0
0.8
0.6
0.4
0.2
2.0 gpm - 11,500 Btu/hr ft²
Tap Position
Δ 89"
□ 65"
▽ 41"
○ 17"

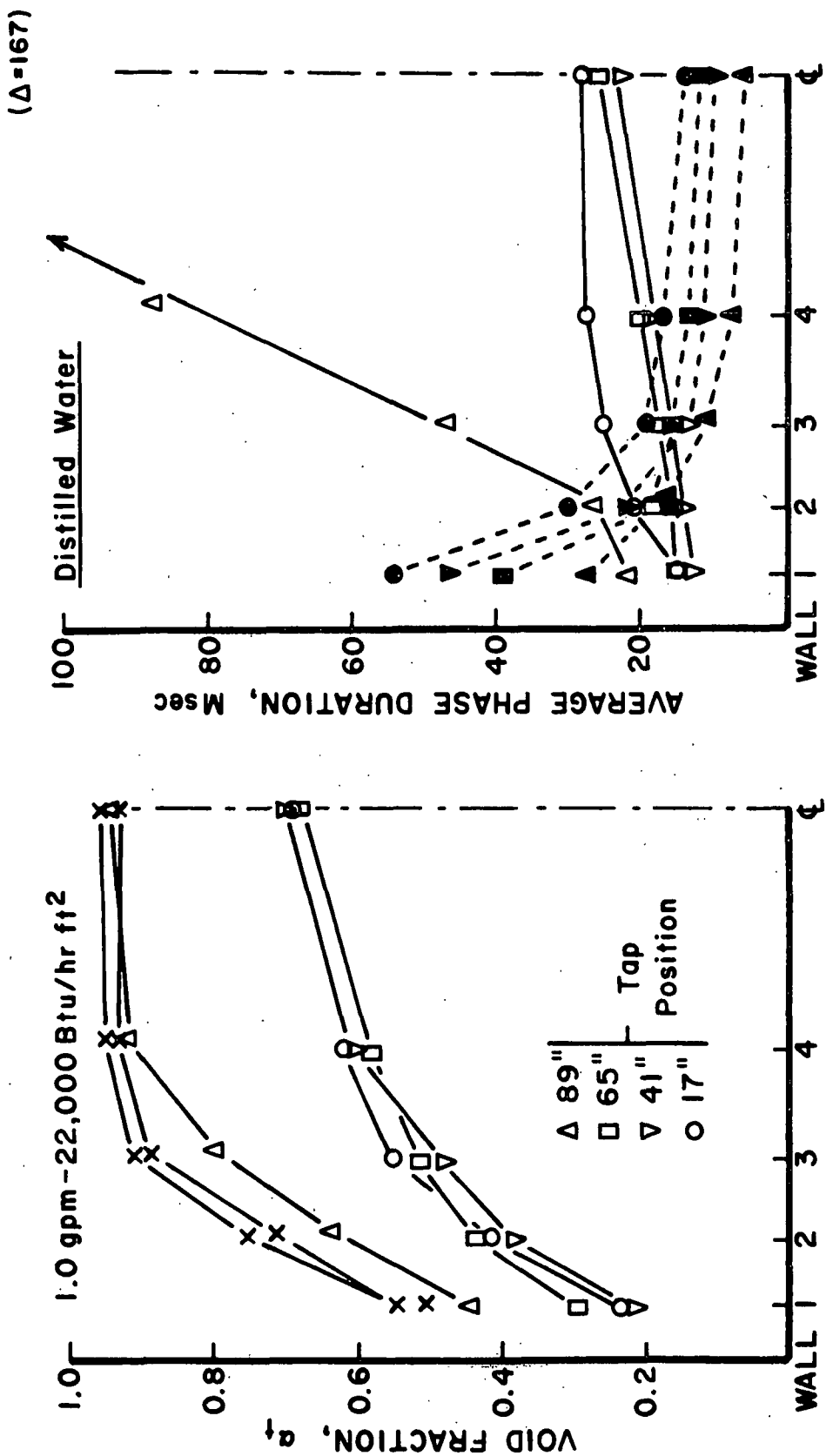

x's = Fong, et al., 1 gal/min, 20,000 Btu/hr, 90 inches and 10 inches.

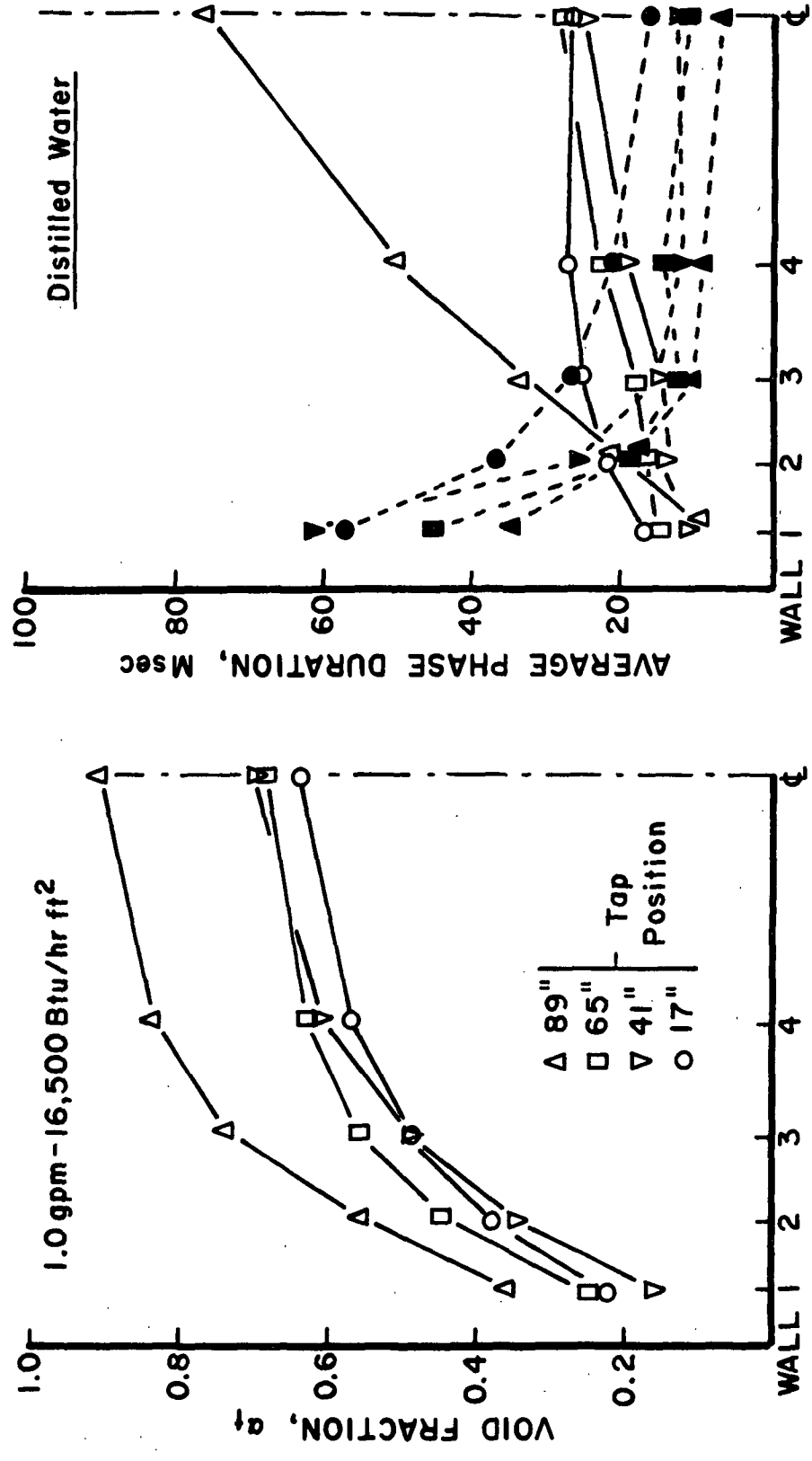
Distilled Water
AVERAGE PHASE DURATION, Msec
100
80
60
40
20
WALL
1
2
3
4
℄
1.0 gpm - 16,500 Btu/hr ft²
VOID FRACTION, α_f
1.0
0.8
0.6
0.4
0.2
Tap Position
Δ 89"
□ 65"
▽ 41"
○ 17"

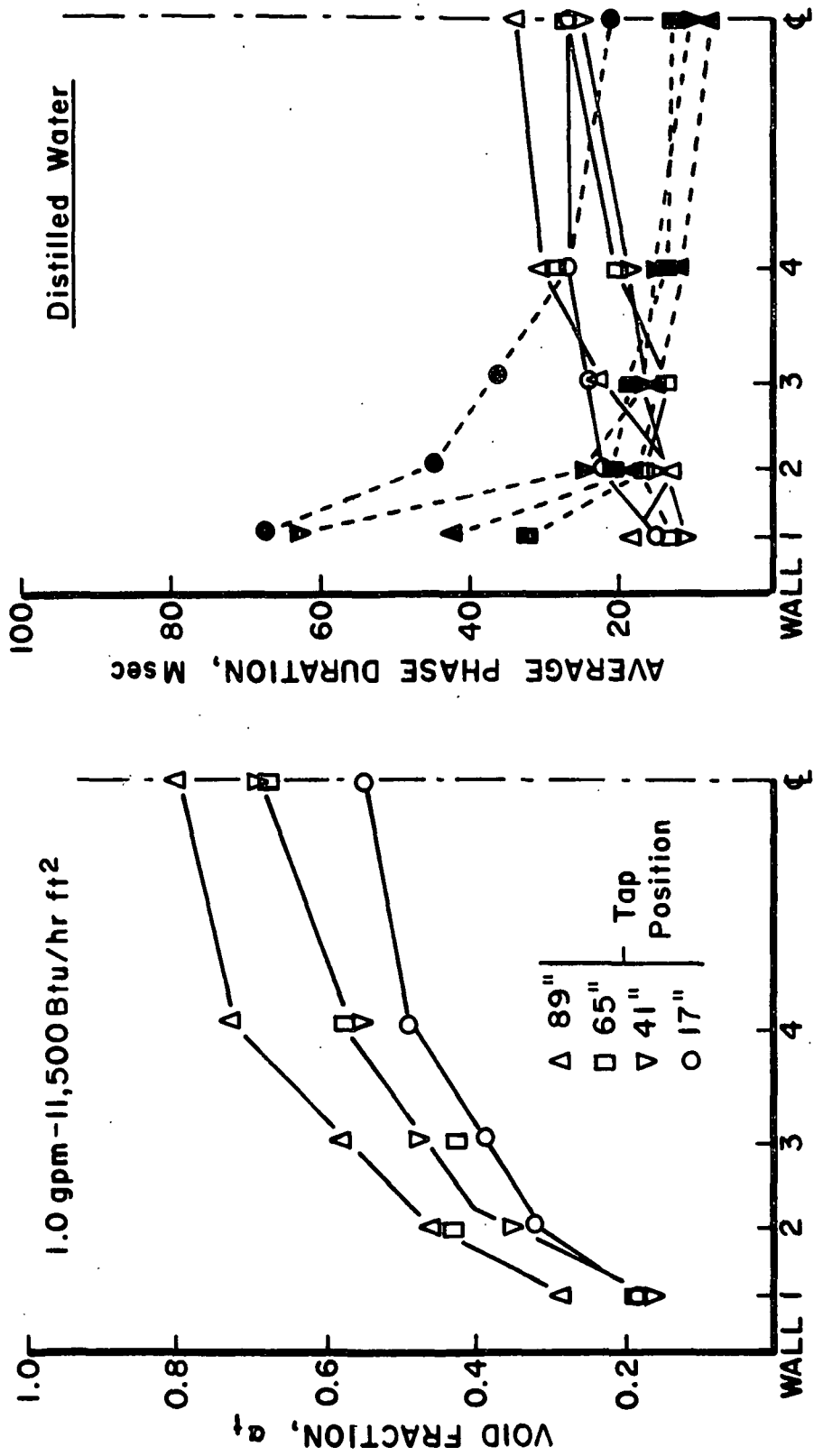
Distilled Water
AVERAGE PHASE DURATION, M sec
100
80
60
40
20
WALL 1
2
3
4
℄
1.0 gpm-11,500 Btu/hr ft2
VOID FRACTION, α_f
1.0
0.8
0.6
0.4
0.2
Tap Position
Δ 89"
□ 65"
▽ 41"
○ 17"

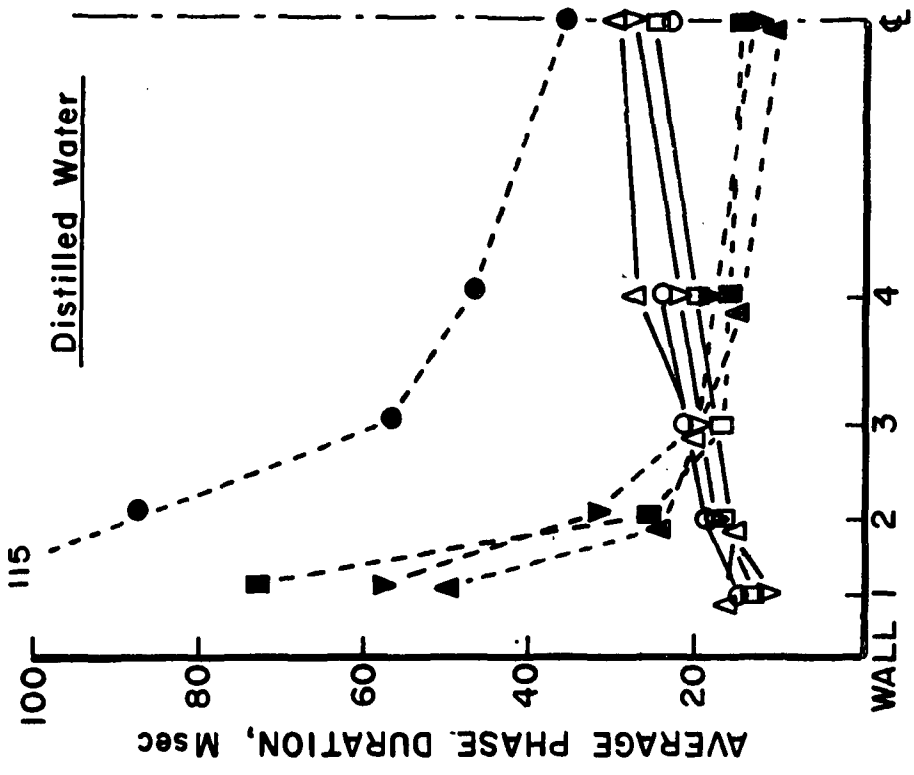
Distilled Water
115
100
80
60
40
20
AVERAGE PHASE DURATION, Msec
WALL
1
2
3
4
℄

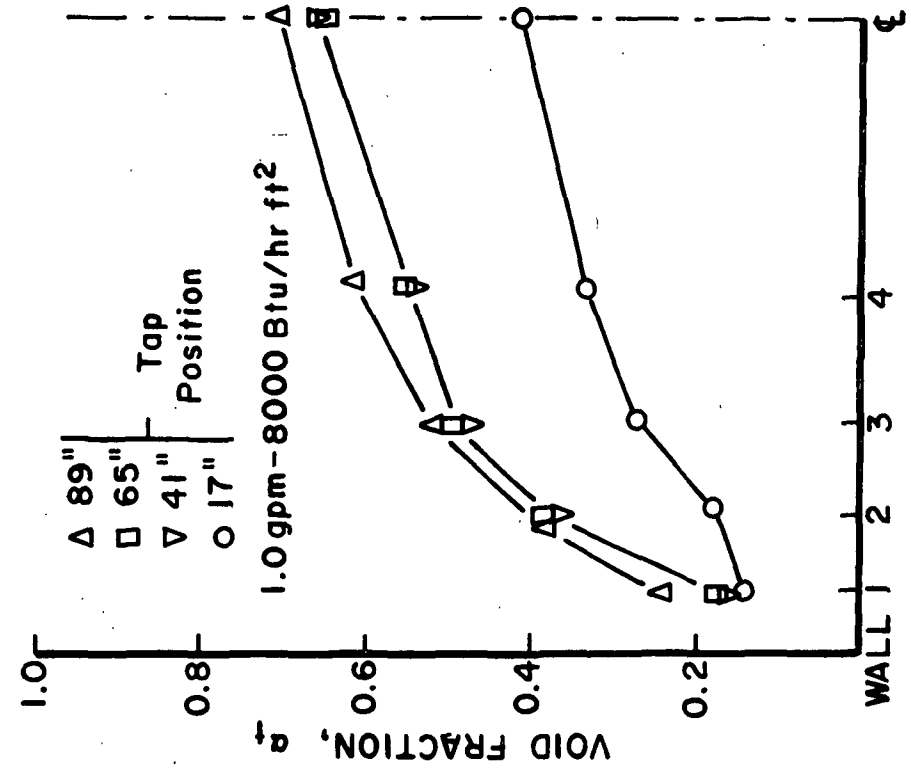
1.0
0.8
0.6
0.4
0.2
VOID FRACTION, α_t
WALL
1
2
3
4
℄
1.0 gpm-8000 Btu/hr ft²
Tap Position
△ 89"
□ 65"
▽ 41"
○ 17"

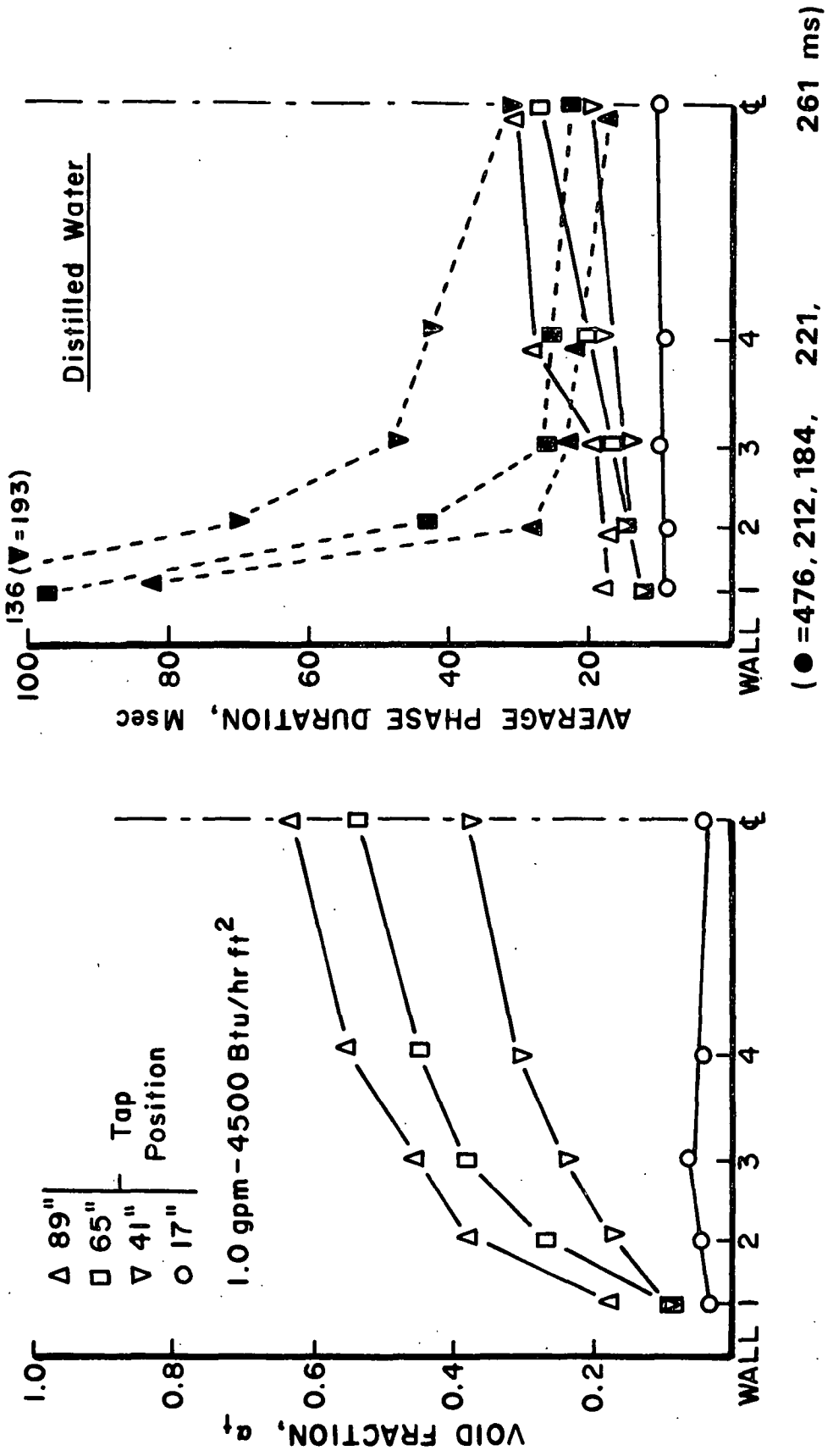
Distilled Water
136 (▼=193)
AVERAGE PHASE DURATION, Msec
100
80
60
40
20
WALL 1 2 3 4 ℄
(● =476, 212, 184, 221, 261 ms)
VOID FRACTION, α_1
1.0
0.8
0.6
0.4
0.2
WALL 1 2 3 4 ℄
1.0 gpm – 4500 Btu/hr ft^2
Tap Position
Δ 89"
□ 65"
▽ 41"
○ 17"

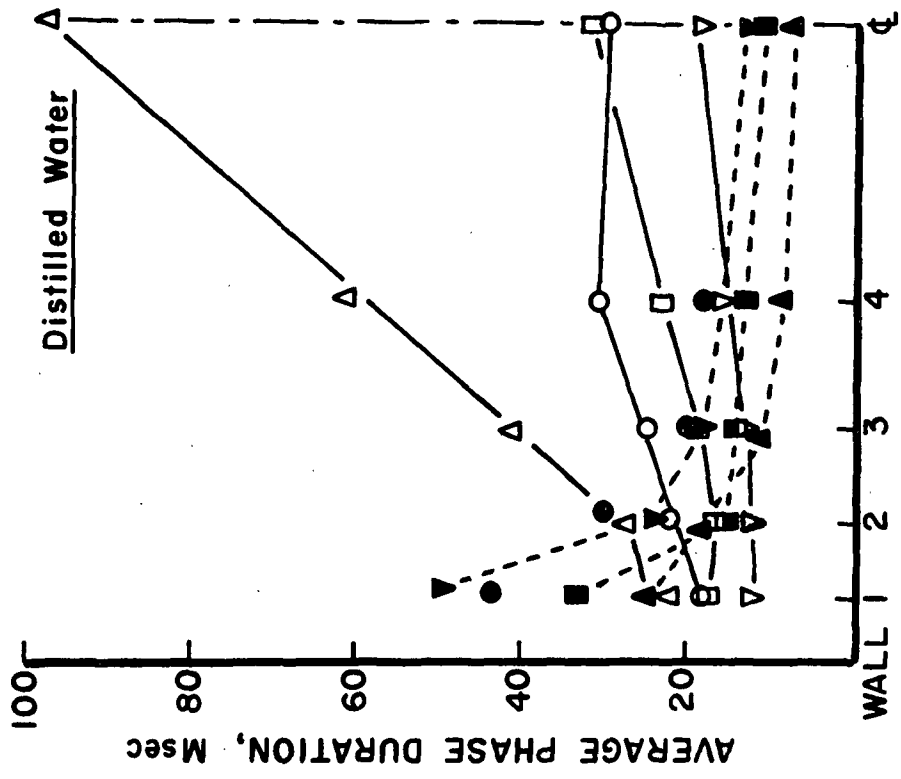
Distilled Water
AVERAGE PHASE DURATION, Msec
100
80
60
40
20
WALL 1
2
3
4
℄

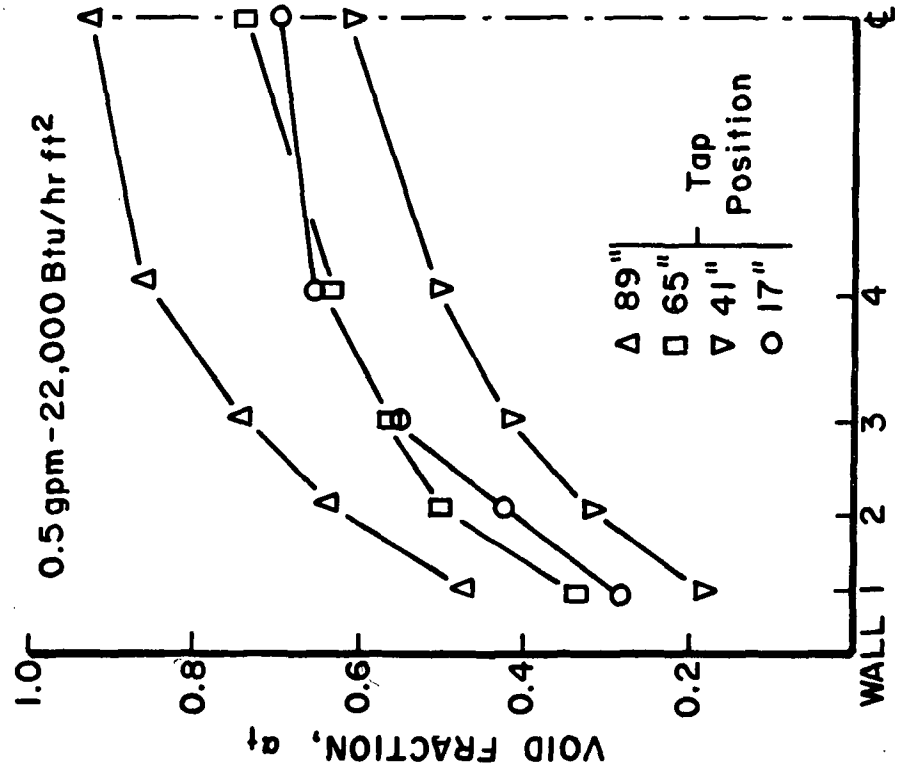
0.5 gpm - 22,000 Btu/hr ft²
VOID FRACTION, α₁
1.0
0.8
0.6
0.4
0.2
WALL 1
2
3
4
℄
Tap Position
Δ 89"
□ 65"
▽ 41"
○ 17"

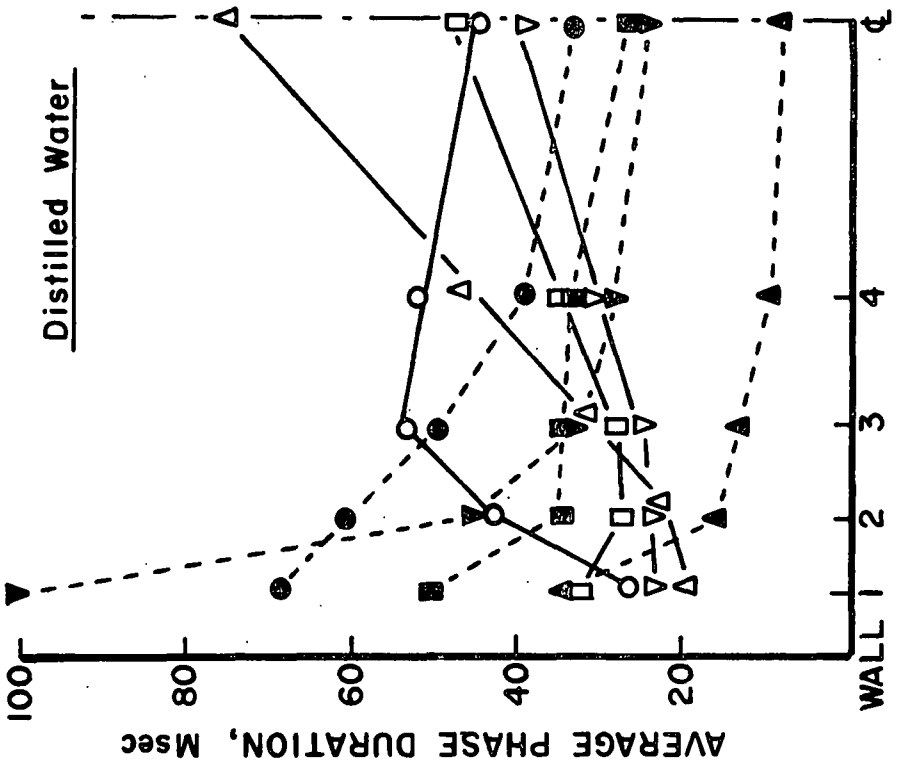
Distilled Water
AVERAGE PHASE DURATION, Msec
100
80
60
40
20
WALL
1
2
3
4
℄

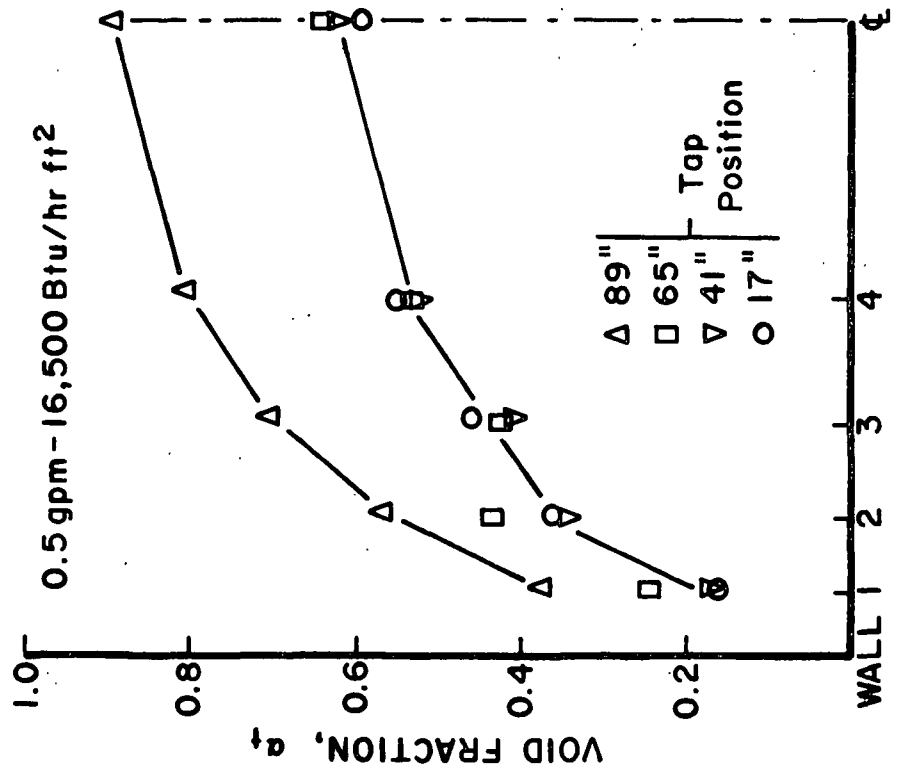
0.5 gpm - 16,500 Btu/hr ft²
VOID FRACTION, α_f
1.0
0.8
0.6
0.4
0.2
WALL
1
2
3
4
℄
Tap Position
Δ 89"
□ 65"
▽ 41"
○ 17"

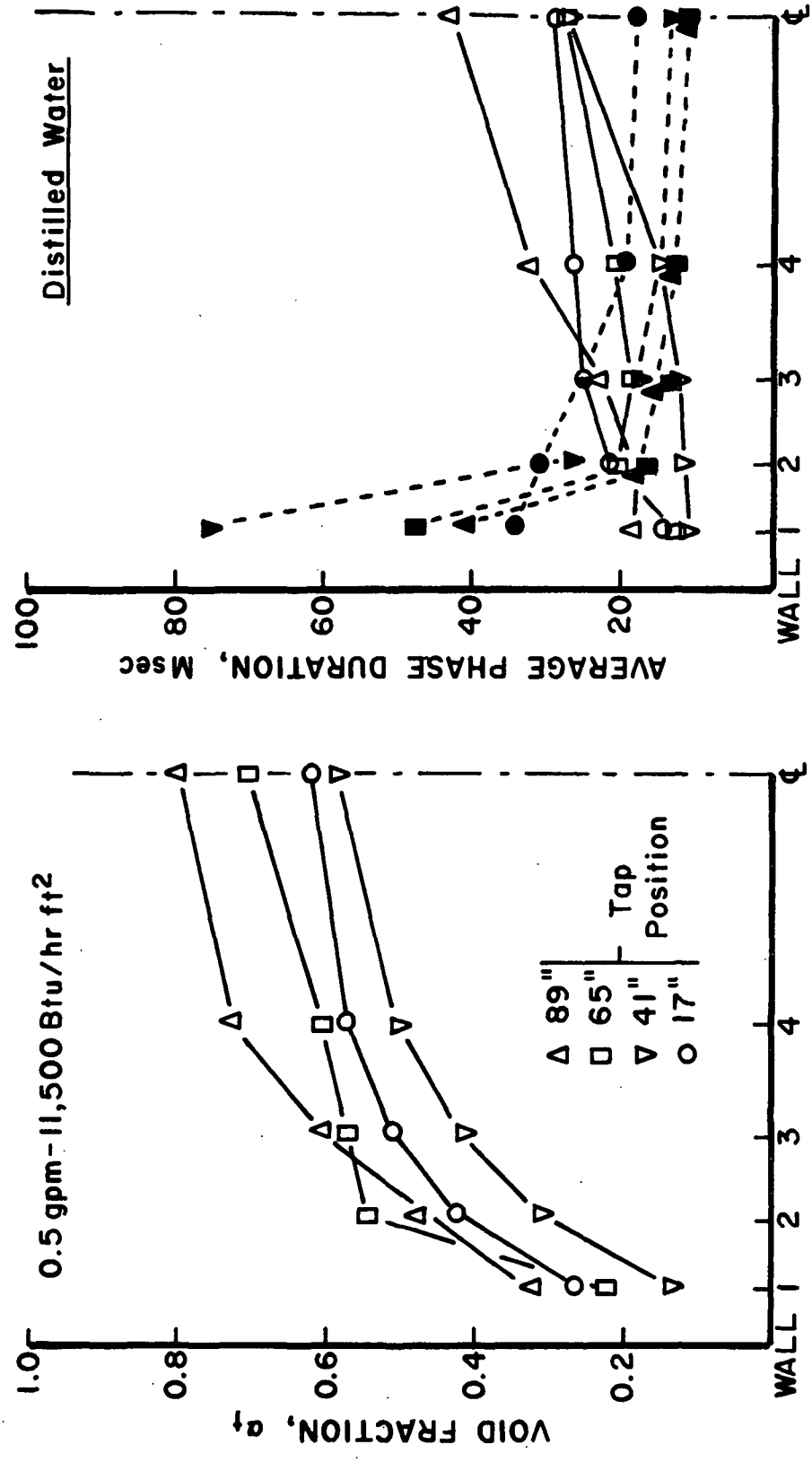
Distilled Water
AVERAGE PHASE DURATION, Msec
100
80
60
40
20
WALL
1
2
3
4
℄
0.5 gpm - 11,500 Btu/hr ft²
VOID FRACTION, α_f
1.0
0.8
0.6
0.4
0.2
Tap Position
89"
65"
41"
17"

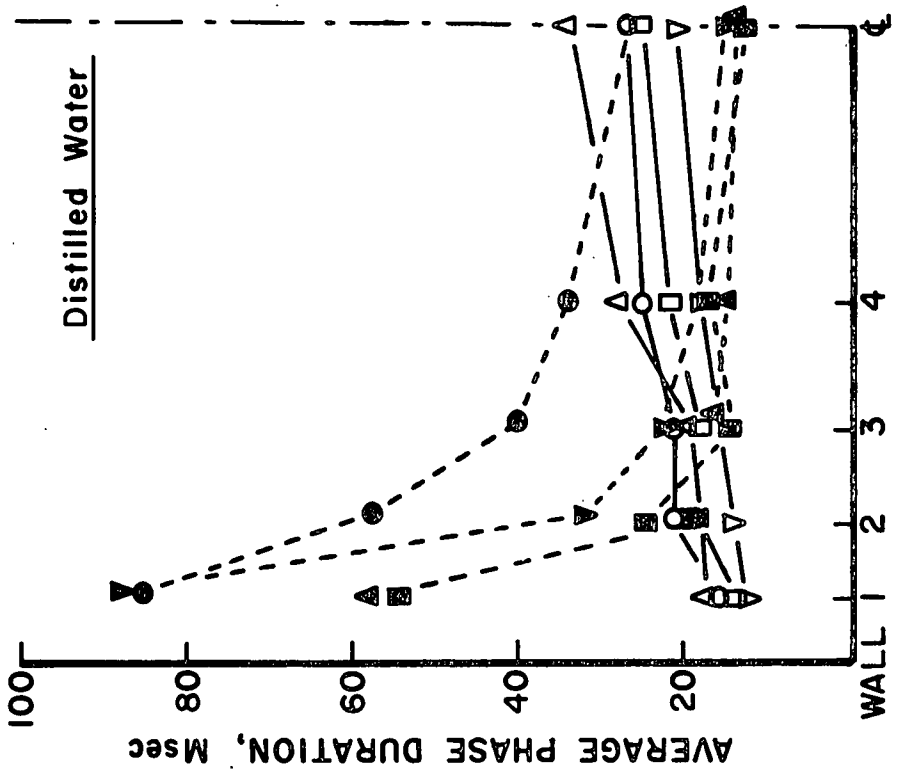
Distilled Water
AVERAGE PHASE DURATION, Msec
100
80
60
40
20
WALL 1
2
3
4
℄

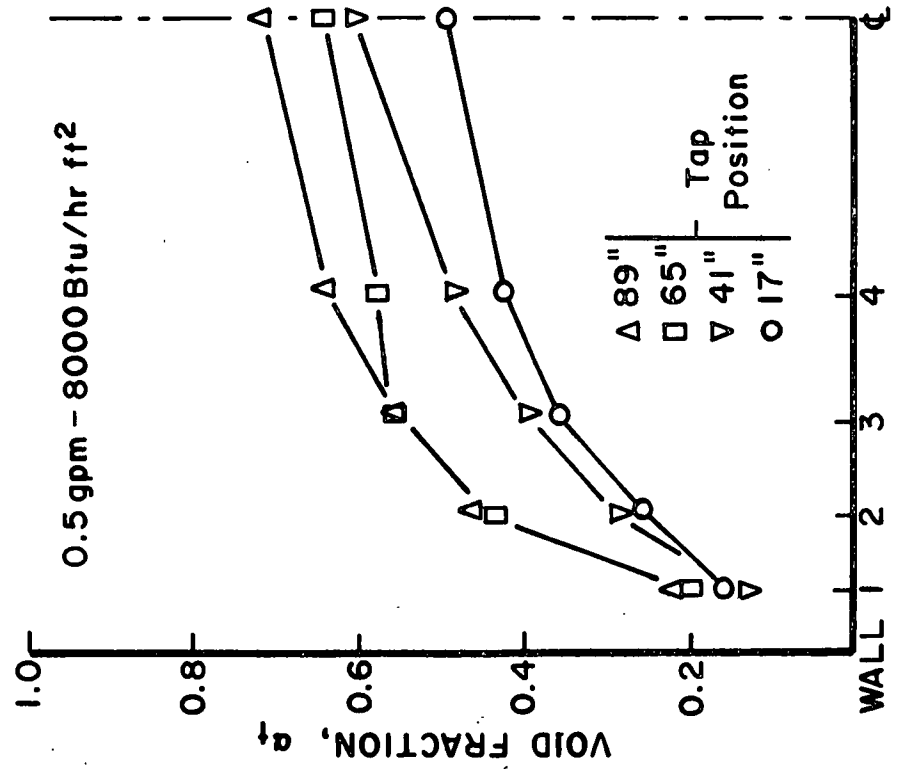
0.5 gpm - 8000 Btu/hr ft²
VOID FRACTION, α_1
1.0
0.8
0.6
0.4
0.2
WALL 1
2
3
4
℄
Tap Position
Δ 89"
□ 65"
▽ 41"
○ 17"

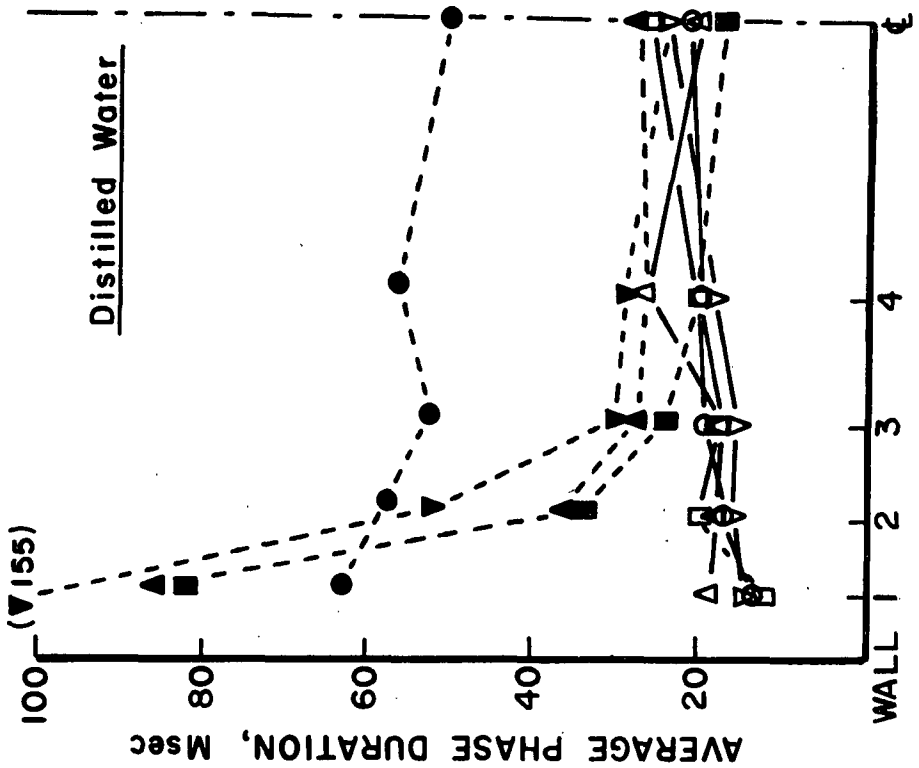
Distilled Water
(▼155)
100
80
60
40
20
AVERAGE PHASE DURATION, Msec
WALL
1
2
3
4
℄

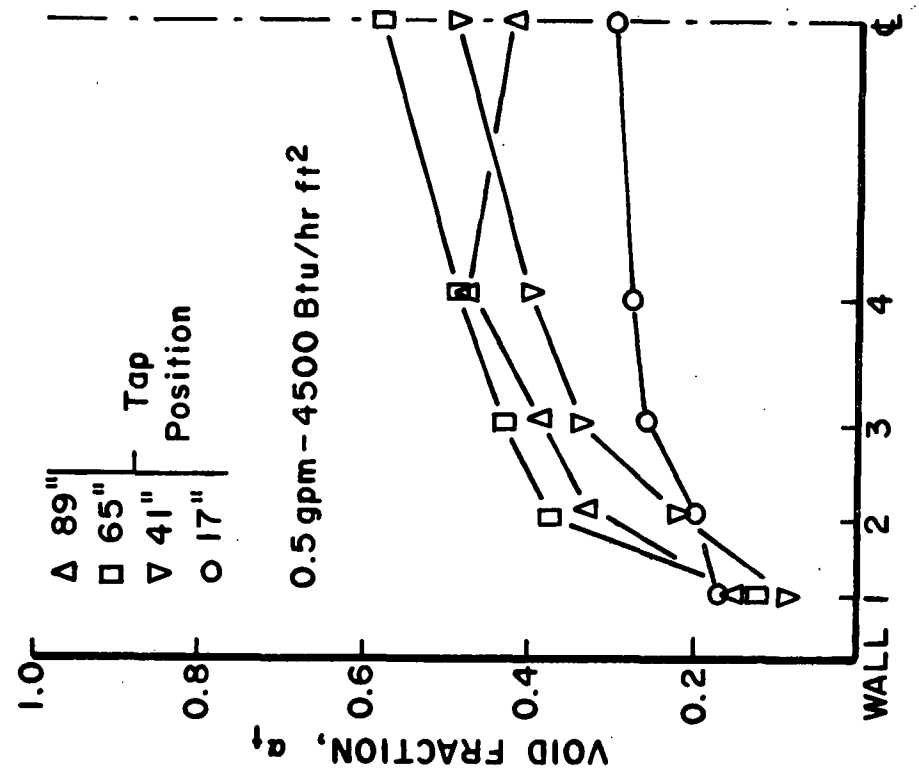
0.5 gpm - 4500 Btu/hr ft²
Tap Position
Δ 89"
□ 65"
▽ 41"
○ 17"
1.0
0.8
0.6
0.4
0.2
VOID FRACTION, α
WALL
1
2
3
4
℄

APPENDIX VIII

FIBER-OPTICAL FLOW PATTERN DATA FOR 12% POTASSIUM CARBONATE SOLUTIONS

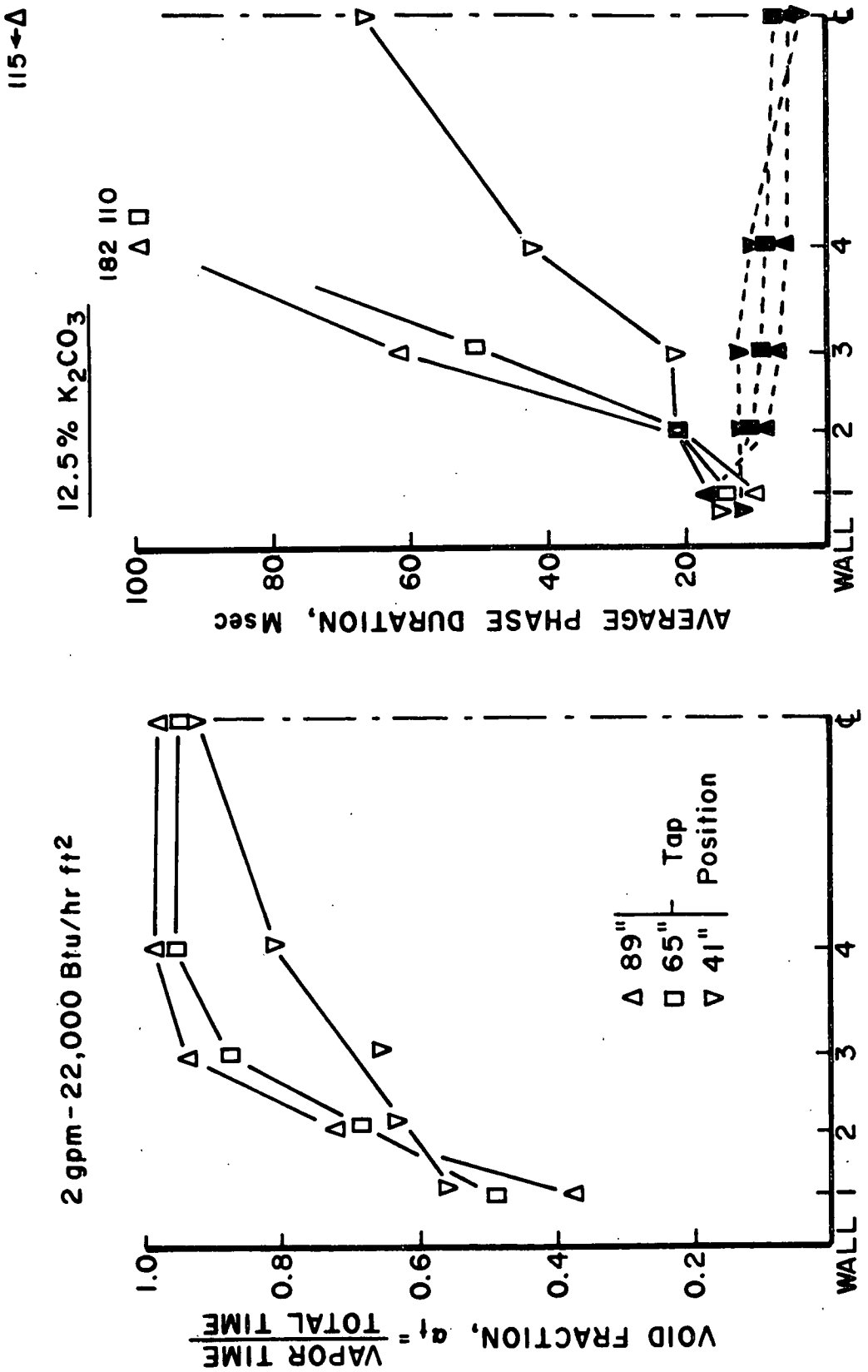

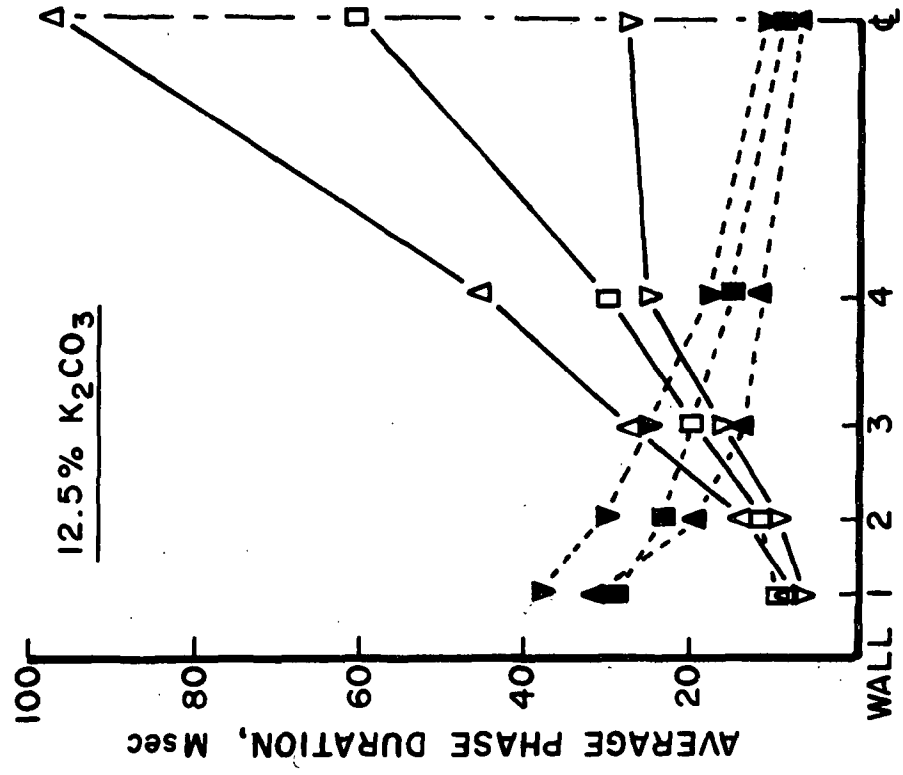
12.5% K_2CO_3
AVERAGE PHASE DURATION, Msec
100
80
60
40
20
WALL
1
2
3
4
℄

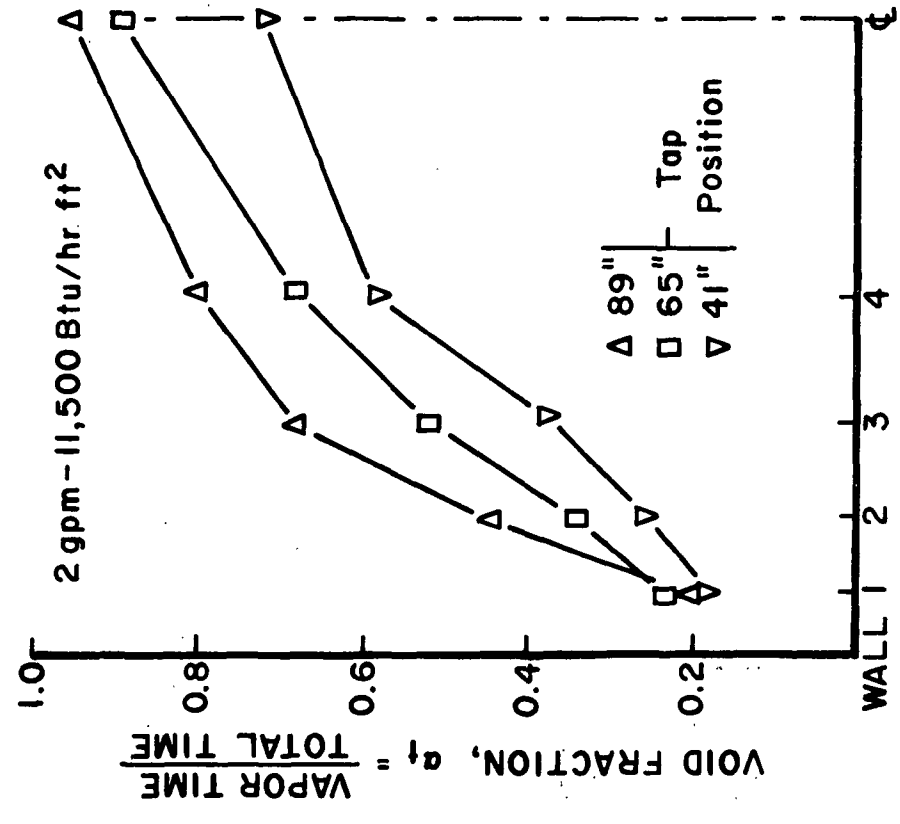
2 gpm – 11,500 Btu/hr ft²
VOID FRACTION, $\alpha_1 = \frac{\text{VAPOR TIME}}{\text{TOTAL TIME}}$
1.0
0.8
0.6
0.4
0.2
WALL
1
2
3
4
℄
Tap Position
Δ 89"
□ 65"
▽ 41"

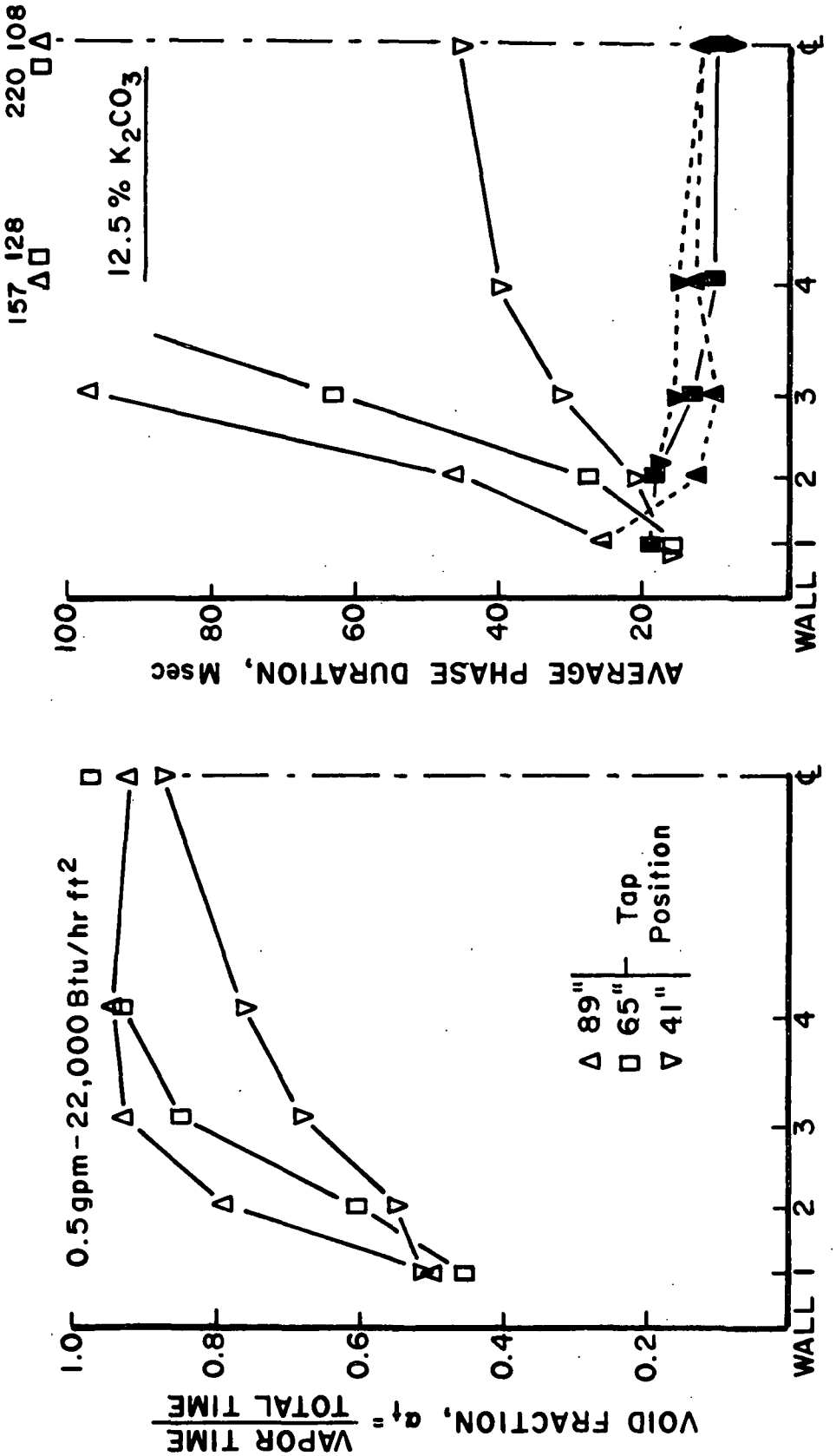
AVERAGE PHASE DURATION, Msec
100
80
60
40
20
WALL 1
2
3
4
℄
12.5% K_2CO_3
157 128
220 108
VOID FRACTION, $\alpha_i = \frac{\text{VAPOR TIME}}{\text{TOTAL TIME}}$
1.0
0.8
0.6
0.4
0.2
0.5gpm-22,000 Btu/hr ft²
Tap Position
89"
65"
41"

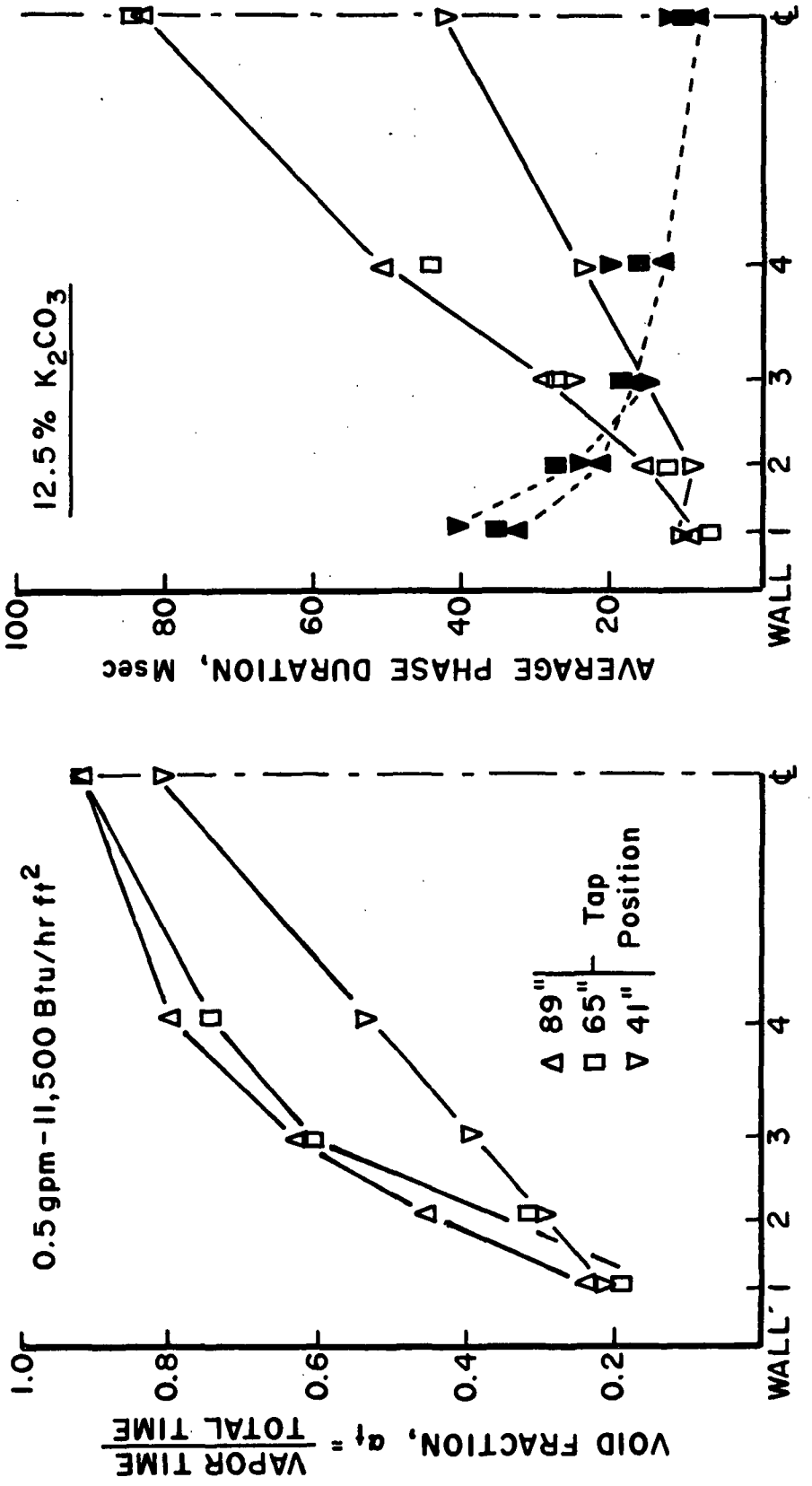
AVERAGE PHASE DURATION, Msec
100
80
60
40
20
12.5% K_2CO_3
WALL
1
2
3
4
℄
VOID FRACTION, $\alpha_i = \frac{\text{VAPOR TIME}}{\text{TOTAL TIME}}$
1.0
0.8
0.6
0.4
0.2
0.5 gpm - 11,500 Btu/hr ft^2
Tap Position
89"
65"
41"